Low Carbon Economy: Addressing Technical Challenges Spanning the Electricity and Steel Sectors

by

Nicole A. Ryan

A dissertation submitted in partial fulfillment
of requirements or the degree of
Doctor of Philosophy
(Natural Resources and Environment, and Mechanical Engineering)
in the University of Michigan
2020

Doctoral Committee:

Associate Professor Shelie A. Miller, Co-Chair
Professor Steven J. Skerlos, Co-Chair
Assistant Professor Daniel R. Cooper
Associate Professor Jeremiah X. Johnson, North Carolina State University

Nicole A. Ryan

naryan@umich.edu

ORCID iD: 0000-0003-4448-998X

ACKNOWLEDGMENTS

This dissertation would not have been possible without the help and guidance of so many amazing people.

First and foremost, I want to thank my advisors, Professor Shelie Miller and Professor Steven Skerlos, as well as, my committee members, Professor Jeremiah Johnson and Professor Daniel Cooper. Each of you provided me guidance and support when I needed it most, all while giving me the freedom to pursue my own path within academia. I have learned so much from each of you. I also want to thank my Masters advisor Professor Gregory Keoleian, without whom I may not have begun to pursue research.

Throughout my dissertation, I have had a number of wonderful co-authors who contributed significantly to this work for whom I would like to thank, Professor Johanna Mathieu, Dr. Yashen Lin, and Noah Mitchell-Ward.

I would also like to thank my colleges at the National Renewable Energy Laboratory for all they taught me, especially Dr. Paul Denholm for his help and guidance on my third chapter and Josh Novacheck for providing me the opportunity to work at the national lab in the first place.

I have also had so many wonderful lab mates at University of Michigan spanning each of my committee members' lab groups, as well as, the wonderful PhD community in School for Environment and Sustainability. I want to thank each of you for inspiring me with your work and motivating me with my own. Especially, those in the Center for Sustainable Systems (CSS), which became my home at University of Michigan and was a constant throughout my time at University of Michigan. I would especially like to thank Helaine Hunscher and Dr. Geoffery Lewis for working to make it a supportive and welcoming environment.

I meet many of my closest friends in CSS and through my involvement in student organizations, including Sustainability without Borders, MUSE, and Climate Blue. Some of my most cherished experiences throughout my PhD were during my participation in these organizations and that is due to the amazing people that contribute to them, without whom this experience would not have been the same.

Most importantly, I want to thank my family and friends near and far, for without their love and support I would not have been able to complete this dissertation. What I will remember most about this experience will not be the late nights and missed deadlines, but the coffee breaks, happy hours, game nights, dinners, and all the adventures.

I would like to acknowledge the National Science Foundation Environmental Sustainability Program (#1510788), Rackham Graduate School, and the School of Environment and Sustainability for providing financial support.

TABLE OF CONTENTS

LIST OF TABLES

LIST OF FIGURES

ABSTRACT

The Intergovernmental Panel on Climate Change states that in order to reduce the most extreme consequences of climate change we must reduce global greenhouse gas (GHG) emissions by 41-72% by 2050 from 2010 levels.[1] For this to happen, all sectors must be included in the effort to decarbonize. Two major sources of anthropogenic emissions are the electricity and industrial sectors, combined accounting for 49% of 2018 U.S. anthropogenic GHG emission.[2] This dissertation addresses challenges with decarbonization in the electricity sector and outlines potential decarbonization pathways in the U.S. steel sector. The steel industry accounts for 25% of industrial sector CO_2 emissions globaly.[3]

This dissertation addresses two electricity sector challenges, which stem from the inherent variability and uncertainty of wind and solar generation, which we specify as variable renewable energy (VRE). The first is the need for sustainable frequency regulation resources, which increase with the addition of VRE. Energy storage, specifically lithium ion batteries, are an attractive option. However, their systems environmental impacts were unknown. In order to quantify potential environmental impacts Chapter 2 employs a life cycle assessment (LCA) framework, which couples cradle-to-gate and end-of-life LCA data on lithium ion batteries with a unit commitment and dispatch model run on a 9-bus power system with lithium ion batteries used for frequency regulation. Chapter 2 finds that the sustainability of lithium ion batteries in this application depends on the grid mix and that the constant charging and discharging required for frequency regulation does not increase the upstream and end-of-life impacts beyond the use-phase.

The second challenge with the addition of VRE this dissertation addresses is the need to improve day-ahead generator scheduling to prevent unplanned startups and shutdowns (i.e., commitment error) caused by the increased variability in net load. Chapter 3 uses a regression

model to quantify the relationship between net load shape, VRE generation, and commitment error with the goal of predicting commitment error in order to improve the day-ahead schedules and reduce system inefficiency. Chapter 3 finds statistically significant relationships between net load, ramp rate, portion VRE generation, and commitment error. Using these relationships, the regression models were able to explain 21-57% of the variability in commitment error.

This dissertation also analyzes options for U.S. steel sector decarbonization. Steel use spans almost all sectors and its use is correlated to economic growth. However, its production is carbon intensive. Through examination of available and developing production technologies in combination with steel flow modeling Chapter 4 outlines potential pathways for U.S. to cut emissions allocated to its steel consumption 70% by 2050 from 2010 levels. There are a number of steps the U.S. steel sector could take to reduce CO_2 emissions, however, Chapter 4's results indicate that, given available technologies, steel stocks per capita, in turn demand, must be reduced in the near term to have a chance of cutting CO_2 emissions 70%.

The challenges in decarbonizing the electricity sector are focused on supply side measures, while this dissertation recommends demand side changes for the steel sector. This is a result of the stark difference in availability of low carbon technologies. Although there remain outstanding challenges with electricity decarbonization they are technological or market based both being easier to address than the demand changes required in the steel sector, which will likely require top down regulation and incentives to achieve.

CHAPTER 1

Introduction

To prevent the most extreme consequences of climate change, all processes within the economy will need to significantly reduce their carbon output (i.e., decarbonize).[4] Based on the Intergovernmental Panel on Climate Change's (IPCC) representative emissions pathways, the world may even need to reach negative carbon emissions, meaning carbon will need to be sequestered at a greater rate than it is emitted.[5] Therefore, society must decarbonize in every sector. In 2017, carbon dioxide accounted for 82% of global greenhouse gas (GHG) emissions.[6] Electricity production and materials production are two major contributors.

Globally, 28% of GHG emissions are from the electricity sector.[2] However, technologies exist today that produce virtually zero carbon electricity (e.g., wind and solar) and there has been extensive research assessing the feasibility of a 100% renewable electricity grid.[7–12] Therefore, a number of sectors are turning to electrification to decarbonize. However, there are still some outstanding technical challenges related to the transition to, and operation of, an electricity grid composed of variable renewable energy (VRE) sources like wind and solar.[13] Challenges stem from a greater need for grid flexibility with the increased uncertainty and variability from VRE generation.[14] Wind and solar generation are dependent on local weather conditions,[13] resulting in variability and uncertainty of their output on short time scales (i.e., minute & seconds), large anticipated variations throughout the day (e.g., the sun does not shine at night), and seasonal variations throughout the year. For the electricity supply to remain reliable (i.e., meeting demand in real time), the grid must be flexible enough to accommodate these rapid and/or significant changes in electricity output from VRE. Davis et al. (2018) calls out that even a well-integrated grid will still need dispatchable electricity sources to remain reliable either from dispatchable

generators, energy storage, or demand response.[15] Chapters 2 and 3 examine two challenges that arise with VRE dominated electricity grids. Chapter 2 addresses the need for more sustainable frequency regulation and Chapter 3 addressed the difficulty in scheduling dispatchable generation.

Unlike the electricity sector, there are other polluting sectors where zero carbon technology options are not yet commercially available. Globally, 22% of GHG emissions are from the industrial sector and, of those, cement and steel are two of the largest emitting and most challenging to decarbonize. Chapter 4 will focus on steel production, which accounts for 25% of the global industrial sector CO_2 emissions[3] and nearly one-fifth of the CO_2 emitted by the most challenging to decarbonize sectors.[15] Steel use is central to all product sectors. It is in construction, transportation, and machinery, as well as smaller scale products like kitchen appliances. Historically its usage has been an indicator of economic growth and its demand is anticipated double by 2050,[16] making research on its decarbonization imperative to overall economic decarbonization.

1.1. **Background Chapter 2:**

Use-Phase Drives Lithium-Ion Battery Life Cycle Environmental Impacts When Used for Frequency Regulation

Reliable grid operation requires supply and demand to be equal in real time. Electricity systems have created a number of services (e.g., electricity reserves) that operate across a range of time scales (e.g., hours to seconds) to ensure this matching. With the addition of a greater percentage of VRE generation, including solar and wind power, these services can become strained as the grid is required to become more flexible. This means that the delivery or method of financial compensation, or lack thereof, for these services may need to be revisited to ensure they are supplied in adequate quantities. One such service is frequency regulation, the focus of Chapter 2. Frequency regulation reserves ensure supply and demand match on the basis of seconds, the shortest time scale of any reserve product. Frequency regulation is the first reserve service to respond to an imbalance. Prior to significant shares of VRE on our power systems, this service was supplied in adequate quantities, with minimal intervention, by conventional power plants that use large scale synchronous generators (e.g., steam turbine, coal, gas and nuclear). The small divergences between demand and supply on the second to second basis was made up by extracting or adding energy to the mechanical inertia of the electricity grid's rotating machines (i.e., it

synchronous generators). This extraction or addition causes the generators' speed to change, in turn, changing their frequency. Therefore, the greater the capacity of rotating machines on the electricity grid, i.e., conventional power plants, the greater the grid's ability to absorb the differences between demand and supply,[13] increasing its flexibility. However, there is a limit to the variation in frequency each generator can handle. Errors are usually only in the range of 0.01% of the stable system frequency.[17] In the U.S. the stable system frequency is 60 Hz.

With the additional VRE, the capacity of frequency regulation suppliers on the grid decreases and the quantity required increases. In an effort to address this from a market perspective, PJM and other regional transmission organizations (RTOs) have developed a regulation market to monetize frequency regulation as an ancillary service to incentive its production. PJM's market has two regulation signals; Regulation D, which requires an almost instantaneous response by a provider, and Regulation A, which is slower and is intended to handle longer fluctuations in system conditions.

This new market design and the increased need for frequency regulation reserves has motivated the development of alternative methods of supplying frequency regulation reserves. Wind can provide synthetic inertia with specific controls by extracting energy from the rotating blades and photovoltaic inverters can provide synthetic inertia when curtailed if installed with appropriate controls.[13] However, these are not currently used in the PJM regulation market.[18] Other alternative technologies include demand response and energy storage,[18] both of which are deployed in PJM's regulation market. Chapter 2 models energy storage, specifically lithium ion batteries as a source of Regulation D frequency regulation.

Energy storage is an attractive option for suppling frequency regulation,[19–21] specifically lithium ion batteries given their fast response time, high energy and power densities, high cycle efficiency, long cycle life, scale flexibility and decreasing cost.[21–24] Additionally they have already been widely applied for frequency regulation in PJM[25] and past studies have found them as a best fit for frequency regulation.[26]

Although energy storage is technologically capable of supplying frequency regulation, the environmental implications of lithium ion batteries use in this application has not been thoroughly analyzed. Operating a battery to provide Regulation D services requires rapid and frequent battery cycling, more quickly degrading the battery and reducing its lifetime. This would potentially

increase the upstream environmental burdens of the device and raise questions about the overall environmental impact of using batteries in this manner.

1.1.1. Research Aims/Questions

Chapter 2 aims to address this gap in the literature by quantifying the life cycle environmental impacts of using lithium ion batteries for frequency regulation. This is achieved by modeling lithium ion batteries in a test grid system (i.e., IEEE 9-bus test case) using a unit commitment and optimal power flow (UCED) model. The UCED determines the changes in the operation of the test system's generators from the addition of batteries for frequency regulation, from which the use-phase environmental impacts are calculated. The degradation of the battery is modeled based on its use profile, from PJM's Regulation D signal. The resulting lifetime is combined with the environmental impacts from battery manufacturing, material production, and disposal to calculate the battery's upstream and end-of-life environmental impacts. The life cycle environmental impacts are the sum of the use-phase and these upstream and end-of-life impacts. The paper presented in Chapter 2 offers the first comprehensive life cycle assessment of lithium ion batteries for frequency regulation. Our use of a simple test system in this chapter allows us to model extremes and examine individual generator reactions to the addition of the lithium ion battery system.

1.2. **Background Chapter 3:**

The Impact of Forecasted Net Load on Real-Time Generator Operation

A change in infrastructure is not always required to address grid flexibility limitations. In certain cases, supply-side resources (i.e., generators) are technologically capable of meeting demand but an electricity market's financial incentives may not be aligned to motivate it or market structures may prevent it. For example, without the flexible ramp product in California Independent System Operator (CAISO), electricity generators with the capacity to change output rapidly did not have an incentive to hold generation for when rapid changes in net load occurred, limiting the system's ability to match supply and demand.

Day-ahead and real-time markets are used to schedule least cost operation of dispatchable electricity generators to ensure that supply meets demand. The day-ahead market uses security

constrained unit commitment to determine which units will be on during each hour of the next day (commitments) and their prices and schedules, which are based on forecasted load, physical grid constraints, generator bid information, and ancillary service requirements.[27] The real-time market determines the optimal output of committed generators in real time. Currently, day-ahead markets operate on an hourly time scale, i.e., generator on/off decisions are made hourly. However, with increasing penetrations of VRE, there is increasing variability and uncertainty within hours and across hours; simply planning for the average generation level of an hour may not result in the most efficient operation of generators. Over-scheduling or under-scheduling can occur, which can cause curtailment of VRE, unplanned imports or exports, and unplanned startups and shutdowns in the real-time market, reducing the overall efficiency of the market and potentially increasing costs and emissions.

Dispatchable generation needs to be able to increase or decrease generation rapidly during hours with large net load changes to ensure that supply and demand are equal in real-time. However, traditional generators have a minimum number of hours for start-up and shutdown, as well as, a specific operating ranges, and ramp rates, inhibiting their flexibility to respond to net load. These constraints make scheduling generators that much more important and difficult. Chapter 3 focuses on improving generator scheduling to more efficiently match supply and demand.

It is hypothesized that hours with large ramp rates and higher levels of VRE generation cause these system inefficiencies, however, research has not been completed to determine the significance of these relationships. If these inefficiencies can be identified, there is the potential that market corrections can be designed in the day-ahead market.

1.2.1. Research Aims/Questions

Chapter 3 investigates the impacts of both net load characteristics and VRE generation on real-time system inefficiencies, specifically unplanned generator startups and shutdowns. If such impacts can be identified, can the unplanned startups and shutdowns be predicted? A production cost model (PCM) of the Western Interconnection is used to model the day-ahead and real-time markets and a regression model is used to relate the net load characteristics and VRE generation to the unplanned startups and shutdowns that occurred in the real-time market of the PCM. The use of a PCM allows for VRE penetrations that are not yet realized in existing U.S. grid systems,

which provides greater insights into the system response with a grid mix that more aggressively challenges the system. Chapter 3 is the first analysis to quantify the statistical relationship between commitment error and VRE generation, and net load in an effort to develop a predictive model. The results have the potential to improve day-ahead generator scheduling to reduce system costs and improve efficiency.

1.3. **Background Chapter 4:**

Reducing CO_2 emissions from U.S. steel consumption by 70% by 2050

The majority of global decarbonization pathways provide limited details on how to reduce emissions in the industrial sector and even less on steel specifically, despite its large carbon footprint.[4,28] Steel accounts for 25% of global industrial sector CO_2 emissions[3] and he International Energy Agency predicts global steel demand to double by 2050 from 2012 levels,[16] making steel production an important industry to address in order to reduce global CO_2 emissions. Wesseling et al. (2017) asserts that energy-intensive processing industries will need to have zero emissions before 2070 to meet the "well below 2C" goal.[28]

Decarbonization pathways likely include limited information on the steel industry because there are few technological options for reducing GHG emissions from production. The bulk of GHG emissions in the production of steel products occurs in the conversion of iron ore to steel (primary production).[16] Currently, this is almost exclusively done in a blast furnace (BF). The primary GHG from this process is CO_2. Therefore, BF emissions must be significantly reduced or the process replaced in order to make any significant strides in reducing steel production emissions. However, given the financial advantage of reducing energy consumption, steel producers have already identified most of the efficiency improvements that can be made to the BF processes. Some alternative technologies are operating at commercial scale (e.g., natural gas direct reduction). However, these technologies do not provide the drastic emissions reductions required to meet the IPCC goal. Steel electrolysis and hydrogen direct reduction, operated with zero carbon electricity, have the potential to reduce emissions compared to the BF by almost 100%, but they are believed to be 20[29] to 30[30] years away from reaching commercialization.

The other alternative to reduce steel sector emissions is to produce less steel from iron ore. This means either reducing overall steel demand or using recycled steel. Steel is primarily recycled in the electric arc furnace (EAF), which produces one quarter of the CO_2 emissions as the BF [31,32]

and if operated with zero carbon electricity, would produce about 10% of BF emissions. However, there are limits to recycling including the availability and quality of the scrap. The other option is simply to reduce demand. Extending product lifetimes, increasing material efficiency, and reducing per capita stocks can all contribute to demand reduction.

Extensive literature exists on novel steel production technologies[33,34] and select studies model future steel flows.[35–37] However, few model future steel sector emissions[3,38,37] and none model future steel sector emissions in the United States. The CO_2 emissions attributed to U.S. steel consumption represent as significant portion of global steel sector CO_2 emissions. The U.S. was the world's largest steel importer, importing 14.4 Mt[39] and the second-largest steel consumer behind China, consuming 122 Mt in 2017,[40] making the U.S. an important market to consider when striving to reduce steel sector emissions.

1.3.1. Research Aims/Questions

Chapter 4 determines pathways for reducing CO_2 emissions attributed to U.S. consumption 70% by 2050 to remain in line with the IPCC's recommended emissions reductions.[1] This work seeks to fill the gap in existing literature by modeling mechanisms with the potential to reduce steel sector CO_2 emissions and assessing their realized impacts on emissions and industry in the U.S. Each pathway defined in this analysis is a unique combination of scenarios and parameter values that, together, represent a comprehensive review of the potential levers that could be adjusted to reduce future steel sector emissions, including both technology options and demand reduction options. Chapter 4 is the first U.S. specific analysis that quantifies potential future U.S. steel sector CO_2 emissions and outlines the requirements of reaching an emissions reduction target. If the U.S. decides to take action on steel sector decarbonization Chapter 4's pathways could provide valuable guidance.

CHAPTER 2

Use-phase Drives Lithium Ion Battery Life Cycle Environmental Impacts when Used for Frequency Regulation

This chapter was published in its entirety in *Environmental Science and Technology*.

Nicole A. Ryan, Yashen Lin, Noah Mitchell-Ward, Johanna L. Mathieu, and Jeremiah X. Johnson;
Environmental Science & Technology **2018** *52* (17), 10163-10174
DOI: 10.1021/acs.est.8b02171

Abstract

Battery storage systems are attractive alternatives to conventional generators for frequency regulation, due to their fast response time, high cycle efficiency, flexible scale, and decreasing cost. However, their implementation does not consistently reduce environmental impacts. In order to assess these impacts, we employ a life cycle assessment (LCA) framework. Our framework couples cradle-to-gate and end-of-life LCA data on lithium ion batteries with a unit commitment and dispatch model. The model is run on a 9-bus power system with energy storage used for frequency regulation. The addition of energy storage changes generator commitment and dispatch causing changes in the quantities of each fuel type consumed. This results in increased environmental impacts in most scenarios. The impacts caused by the changes in the power system operation (i.e., use-phase impacts), outweigh upstream and end-of-life impacts in the majority of scenarios analyzed with the magnitude most influenced by electricity mix and fuel price. Of parameters specific to the battery, round trip efficiency has the greatest effect.

2.1. Introduction

Safe and reliable operation of the power system requires generation to match demand in real time. When they do not, the system frequency deviates from its nominal value (60 Hz in the U.S.). To correct the frequency, conventional generators (e.g., coal, gas, and nuclear) provide frequency response (also referred to as droop control or primary frequency control) and frequency regulation (also referred to as secondary frequency control) via automatic generation control. While the former is required of all conventional power plants in the U.S., the latter is a service procured through the balancing reserve market. Generators contracted to provide frequency regulation receive commands from the system operator every four seconds to increase/decrease their consumption continuously, helping the system balance supply and demand. With the addition of variable renewable energy (e.g., wind and solar), the need for frequency regulation increases,[41] as the frequency and magnitude of supply and demand differentials increase. Generator use for frequency regulation can reduce generator efficiency, and increase associated emissions.[42,43] Wind turbines can provide frequency regulation but it is often uneconomical since wind power production must be curtailed.[44]

An attractive option to managing the increasing need for frequency regulation is energy storage.[19–21] Energy storage devices, such as lithium ion (Li-ion) batteries, are promising alternatives because such technologies respond quickly[19] and are available at increasingly competitive costs.[45] The first use of grid battery storage systems was for frequency regulation and spinning reserves.[24] We focus on Li-ion batteries in this work as they have become the predominant battery type for frequency regulation.[25] They have high energy and power densities, fast response time, high cycle efficiency, long cycle life, scale, flexibility, and decreasing cost.[21–24] Li-ion batteries have already been widely applied for frequency regulation in PJM[25] and past studies have found them as a best fit for frequency regulation.[26] PJM's pay-for-performance regulation market, designed to reward a resource's accuracy and quality, has incentivized an increase in battery energy storage capacity. Battery energy storage capacity in PJM has increased from 0 MW in 2005 to 280 MW (41% of regulation procurement capacity) in 2017.[46] Additionally, second-use applications of Li-ion batteries, previously used in electric vehicles (EVs), are increasingly appealing.[47] Studies have demonstrated the potential economic benefits of re-use,[48] environmental

trade-offs,[47] use to support rural electrification,[49] and the potential to facilitate the integration of variable renewables.[50]

With low or no direct emissions during operation, it is a commonly held conception that the implementation of energy storage will have an environmentally positive outcome. The California Energy Storage Mandate states that "Use of energy storage systems to provide the ancillary services otherwise provided by fossil-fueled generating facilities will reduce emissions of carbon dioxide and criteria pollutants."[51] However, recent research has shown that the introduction of energy storage may not always benefit the environment.[52–55] In current U.S. electricity markets, only the energy and reserve costs of the system are minimized, while the emissions impacts are not explicitly considered (though in some parts of the country some emissions are priced; for example, SO_x is limited through a cap and trade program and CO_2 can be priced through carbon markets). A number of dispatch algorithms that consider environmental impacts have been proposed[56,57] including algorithms that incorporate emissions cost or constraints. Arbabzadeh et al.[58] also developed principles for using energy storage sustainably. However, these algorithms and principles are not widely adopted in electricity markets. As a result, although adding energy storage to the system could reduce the cost of operating the system, the environmental outcome may not necessarily improve.

A significant body of research exists on the environmental impacts of Li-ion batteries. Many studies focus on vehicular applications and cradle-to-gate system boundaries,[59–64] providing detailed examinations of the environmental impacts from Li-ion materials, manufacturing, and end-of-life (EOL) for automotive applications. However, there are far fewer studies that examine the same for stationary power system applications and many use inventory data from automotive vehicles.[65–69] Stroe et al.,[21] Swiersczynski et al.[44] and Xu et al.[46] all model Li-ion batteries for frequency regulation, but the focus of these papers is not environmental impacts. In one such study, Hiremath et al.[22] evaluated Li-ion, lead-acid, sodium-sulfur, and vanadium redox flow batteries used for six stationary applications, including "Area and Frequency Regulation." The study found that the use-phase dominates the environmental impacts and that cradle-to-gate analyses are misleading when comparing environmental performance.[22] However, it assumed that the batteries were charged by the average German electricity mix from the Ecoinvent database.[22] Koj et al.[70] performed a comparative life cycle assessment (LCA) of providing primary frequency

control using either Li-ion batteries or coal power plants, Oliveira et al.[71] tested different electricity mixes on environmental outcomes, and Arbabzadeh et al.[72] examined the use of vanadium redox flow batteries to reduce wind curtailment on a microgrid. While these studies demonstrate the importance of the electricity mix, assuming a certain mix or a single plant type obscures the true environmental impacts due to the complex nature of power systems and their operation. Ryan et al.[73] emphasizes the need to incorporate temporal variability in electricity mix when estimating emissions from temporally varying changes to electricity load, as is the case with energy storage. Changes in generator commitment and dispatch are also important factors that affect how energy storage is used and its associated environmental impacts.[74]

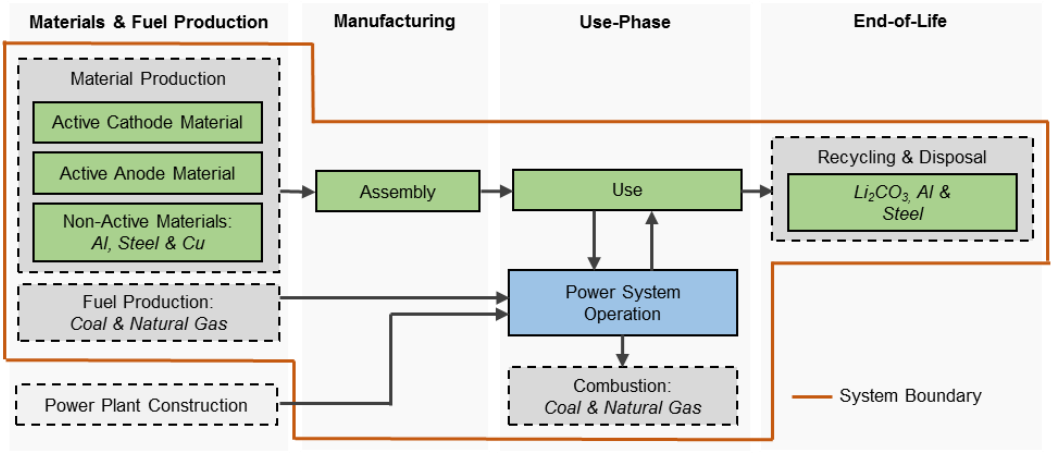

Figure 2 - 1, System boundary from upstream to end-of-life stages. Green boxes indicated battery phases and components

In this work we investigate the life cycle environmental impact of using energy storage, namely Li-ion battery systems, for frequency regulation. We solve a unit commitment and dispatch problem on a 9-bus power system for eight different electricity mixes and couple the results with a cradle-to-grave LCA of Li-ion batteries. Figure 2-1 presents the system boundary. The study presented here differs from past work by investigating the impact of energy storage on the operation of a power system and its resources rather than making assumptions about electricity mixes. Our methods, like Lund et al.,[75] combine the use of LCA with a detailed energy system modeling; however, Lund et al.[75] used these methods to determine the environmental impacts of changes in demand by identifying the marginal generation technologies. Our results offer new insights into the direction and magnitude of environmental impacts, as well as the relative importance of battery materials and manufacturing.

2.2. **Methods**

2.2.1. System Boundary and Scenarios

To analyze the environmental impacts of deploying Li-ion battery systems for frequency regulation, we adopt an LCA framework. We compare the life cycle environmental impacts of a Li-ion battery system to the use of coal and natural gas power plants, for frequency regulation in a test grid system. For simplicity, we model one large battery system to represent the aggregation of a number of smaller battery systems. Figure 2-2 summarizes our study's modeling approach. It includes the key processes that we investigate for the energy storage system and the power system, data inputs and outputs and required models (i.e., energy storage degradation and power system models). The scope of this study includes the impacts of battery materials, manufacturing/assembly, use (which includes changes in power plant dispatch and battery degradation), and battery EOL.

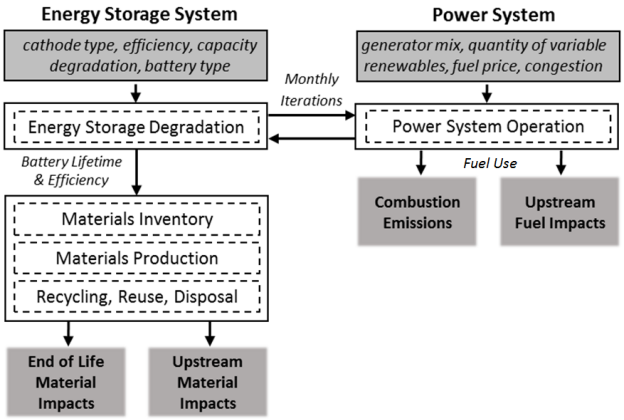

Figure 2 - 2, Methodology outline and system interactions. Energy storage and power system parameters (row one), models (row two), connections, and model outputs.

The functional unit for this study is the provision of 1 MW of symmetrical reserve capacity for one year (i.e., +/-1 MW-yr of frequency regulation). This functional unit is not a function of the energy that goes through the battery, but a measure of the capacity of regulation provided (i.e., the power bid into the market) over a defined period. Bids are placed into the regulation market based on capacity (i.e., power) rather than available energy. The grid frequency changes based on the increase or decrease in power output of generators (i.e., +/- MWs) meaning that conventional units of energy (e.g., MWhs) used in previous LCAs of energy storage are inappropriate to apply in this context. The functional unit incorporates a time component (i.e., 1 year of service) so that

the upstream and EOL impacts can be allocated appropriately based on the battery system's lifetime.

The battery use-phase impacts are dependent on the capacity and efficiency of the battery, both of which are impacted by the battery's degradation. The degradation is calculated monthly for the life of the battery and incorporated into the power system model. The energy storage degradation model also determines the lifetime of the battery, which also affects the upstream and EOL material impacts of providing 1 MW-yr of service since the upstream and EOL material impacts are distributed over the lifetime of the battery. The upstream impacts of thermal and renewable power plants are not included, due to the insignificance of emissions from natural gas or coal power plant construction and decommissioning.[76] Additionally, the upstream impacts of this infrastructure will not change with the addition of energy storage.

The overall impacts are calculated using LCA inventory outputs as well as three environmental impact categories: Global Warming Potential (GWP), Cumulative Energy Demand (CED), and Acidification. GWP, CED, and Acidification are commonly assessed impact categories in previous LCAs of energy storage and are dominate power system impacts. We recognize the selection of these impact categories limits our ability to make conclusions about water or land impacts such as eutrophication and land use, but lack of data availability prevented their inclusion.

To understand the role of key parameters on life cycle impacts, we conduct a series of parametric studies, which vary the assumptions for the Li-ion battery system characteristics and power grid characteristics. Section 3.3 summarizes the base case parameters and parametric studies.

2.2.2. Energy storage system material inventory, production and manufacturing

The main components of the battery are the anode and cathode, which account for the majority of the mass of the battery. Other components of the battery are the electrolyte, binder, battery housing, and the battery management system. The base case battery cathode material is $LiMn_2O_4$ (LMO). Kim et al.[24] describes it as stable, safe, abundant, easy to synthesis and environmentally friendly. Its drawbacks are a lower capacity and higher temperature sensitivity.[24] The parametric studies use $LiFePO_4$ (LFP), $LiNiMnCoO_2$ (NMC) and $LiNiCoAlO_2$ (NCA) batteries. LFP and NMC were selected due to their common use in grid applications. LFP is stable and low cost.[24]

NCA batteries are used in Telsa Model S vehicles,[77] the EV with the highest sales in 2016,[78] and therefore this cathode was modeled for the first-use and second-use EV batteries for grid energy storage. The battery anodes are graphite, as it is considered the most practical;[24] however, LTO is also becoming an attractive alternative.[20] Battery data and associated upstream and EOL environmental impacts are from Argonne National Laboratory's Battery Performance and Cost (BatPaC) model and "Greenhouse gases, Regulated Emissions, and Energy use in Transportation" (GREET) Vehicle-Cycle Model, as well as other existing literature on Li-ion LCA.[61,79–81] Figure A-7 in the Supporting Information (SI) contains a material flow diagram.

Argonne National Laboratory's Vehicle-Cycle Model contains detailed process level emissions data on components of conventional and advanced vehicle technologies, which includes cathode specific EV battery components.[82] The BatPaC model analyzes Li-ion battery packs, providing battery designs and associated costs based on user-defined parameters.[81] In this study, we use BatPaC to create a materials inventory for the Li-ion batteries. We convert our energy and power specifications into masses of the active materials. Masses and emissions for the production of each battery component were derived using GREET. Assumptions in Dunn et al.[79] for energy consumption in battery assembly were used along with GREET's assumptions for shares of process fuels to calculate impacts of battery assembly.[82] It is important to note the assumptions in Dunn et al. [79] are for LMO and these values can vary across literature and cathode types. The recycled content approach was used for this study.[83] Recycled components include Li_2CO_3 (for the LMO cathode) via hydrometallurgical recycling, and a percentage of steel and aluminum for all cathode types (Table A-8). The impacts of the battery management system (BMS) were calculated using GREET's inventory and impact assumptions on a per mass of BMS basis.[82] The mass of the BMS was calculated by using Dunn et al.'s[60] BEV battery assumption that 1.1% of battery mass is attributed to electronics. Additionally, we do not include the impacts of transportation of materials to/from site, installation, or decommissioning.

Using an inverter materials inventory from Mason et al.,[84] a study on photovoltaic LCA, we derive a Life Cycle Inventory (LCI) for an appropriately sized battery inverter using linear scaling. We input the mass of the materials in the LCI into the GREET model to determine the environmental impacts of the inverter.

Battery lifetime is a function of degradation, which depends on how the battery is cycled and utilized during the use-phase.[22] We assume EOL occurs when a battery reaches 50% capacity degradation, based on the assumption that stationary applications can tolerate more degradation before retirement than automotive applications. Upstream and EOL impacts are allocated over the life of the battery.

2.2.3. Power System Unit Commitment and Dispatch

2.2.3.1. *Problem formulation*

Results from the unit commitment and dispatch are important factors in determining the environmental impacts of Li-ion energy storage system in the use-phase.[74] Adding energy storage into the power system provides more options for the system operators to balance supply and demand on the grid, which can lead to changes in the operation of generators.

In this study, we use the IEEE 9-bus test system,[85] modified to include renewables (wind and/or solar), and a Li-ion battery system solely for frequency regulation. The unit commitment and dispatch problem determines the most cost-efficient commitment (i.e., which generating units will be turned on during which hours) in addition to the production levels and reserve capacities across the committed units, while ensuring that all power flow and engineering constraints are satisfied. We run simulations for each case with and without energy storage, attributing the change in each generator's output to the introduction of the energy storage. Based on the commitments and production levels, the quantity and type of fuel consumed is calculated. In bidirectional frequency regulation markets conventional generators must be able to increase or decrease their output based on the control signal. The partial load heat rates for the generators are reflected in the cost curves, meaning that generators that hold back capacity to provide reserves experience a loss of efficiency that is reflected in their costs. We formulate the problem as a mixed integer programing problem, detailed in Section 2.1 of the SI. The dispatch results also provide the committed reserve capacity of the battery system, which affects its degradation over time.

Battery capacity and efficiency degradation affect the optimal system dispatch. Capacity degradation, which represents the reduction in the energy the battery can store, is a function of both usage (charging/discharging cycle) and time. How quickly a battery degrades in response to the use-phase operations will affect upstream, downstream, and use-phase impacts. There are a number of models to estimate the capacity degradation of Li-ion batteries.[86–90] In this study, our

primary capacity degradation model is from Xu et al.[91] Xu et al.[91] models the degradation of a LMO battery in response to frequency regulation in the PJM system, which is consistent with our base case battery cathode and battery system application. In order to understand the impact of rapid degradation we perform parametric studies using the Wang et al.[86] and Fortenbacher et al.[89] models. Fortenbacher et al.[89] used synthetic data from an electrochemical battery model called DUALFOIL,[92] while Wang et al.[86] developed their model through experimental testing based on batteries for E-bikes and robotics. Wang et al.'s [86] model is consistent with the base case cathode, while Fortenbacher et al.'s[89] model is consistent with the battery system application. It is important to note that degradation is tied to battery chemistry; however, in order to maintain consistency across parametric studies the degradation models were not varied by cathode type. We apply the models to one year of PJM's dynamic regulation signal (RegD) from August 2015 to July 2016,[93] as detailed in Section 2.2 of the SI. Using the model from Xu et al.,[91] the batteries take 70 months to degrade to 50% capacity (our assumed EOL for stationary grid applications), while using the model from Fortenbacher et al.[89] and Wang et al.[86] the batteries take 23 months and 21 months, respectively, to degrade to 50% capacity. This value can vary significantly with different E/P ratios and slightly with allowable state of charge (SOC) range. Section 2.2 of the SI contains the calculations to reach these results.

The use-phase emissions are strongly tied to the battery efficiency, which determines the quantity of energy lost through storage. In this study, efficiency degradation, which represents the rate of increase in energy losses incurred from charging/discharging the battery, is based on the model developed in Cordoba-Arenas et al.[90] detailed in section 2.3 of the SI.

In this paper, we model the unit commitment and dispatch problem over a 24-hour period, with dispatch occurring in one-hour increments. Battery degradation is assessed on a monthly basis and the problem is re-solved each month with the degraded battery. We sized the energy storage system to ensure that the SOC does not limit the ability of the battery to meet the reference signal for reserves more than 5% of the time over the year, as detailed in section 2.2 of the SI.

2.2.3.2. *Test system*

Our modified IEEE 9-bus test system consists of four fossil fuel generators, totaling 800 MW of generation capacity, one 3.04 MWh / 8 MW energy storage device (E/P=0.38) at Bus 8, and a renewable generator (wind, solar or wind and solar) at Bus 8. Although, the energy storage and

renewable generator are located at the same bus, they are operated independently. The line constraints and system configuration align with those used in Lin et al.;[52] however, the size and primary fuel source at each bus are different. We modeled eight base case scenarios with different electricity mixes, summarized in Table 2-1. The scenarios consider two fossil fuel cases: 'Coal' (80% coal, 20% gas, based on capacity), 'Gas' (20% coal, 80% gas, based on capacity), and four renewable electricity mixes. In each scenario with renewable energy, it makes up 15% of the day's electricity demand, resulting in different installed capacities depending upon renewable generation type. The size and fuel consumed by the generators varies between the Coal and Gas case in order to maintain realistic generator sizing based on fuel type. All assumptions are listed in Section 1 of the SI and Tables A-2 and A-3.

Table 2 - 1, Summary of Base Case Scenarios

Base Case Scenarios	
Non-Renewable Generation	*Renewable Generation*
Coal	No Renewable Energy (R.E.)
	Wind
	Solar
	Wind & Solar
Gas	No Renewable Energy (R.E.)
	Wind
	Solar
	Wind & Solar

2.2.4. Electricity generation environmental impacts

For the use-phase, we compute environmental impacts associated with changes in power system operation caused by the introduction of 1 MW-yr of frequency regulation capacity. First we computed changes in fuel consumption by the conventional generators, as determined by the unit commitment and dispatch problem. Then, we calculated the environmental impacts of the change in fuel consumption using the impact factors found in the Table A-9. The changes in fuel consumption during the use-phase are also used to calculate upstream fuel impacts of the system. The impact factors for gas and coal production come from the GREET model and are listed in Table A-9.[94]

2.3. **Results and Discussion**

2.3.1. Base Case Impacts

Figure 2-3 shows changes in environmental impacts in three categories: Use-Phase, Upstream: Fuel, and Upstream/End-of-Life: Battery System. The use-phase accounts for the majority of environmental impacts from implementing the energy storage system. These impacts are the sum of net changes in individual generators' combustion emissions, caused by changes in generator electricity output, when energy storage was integrated into the system. Changes that were driven by three phenomena: changes in type of generators committed (i.e., coal or natural gas), changes in generator output (and subsequently, heat rates), and increases in generation requirements due to battery round-trip losses. These three phenomena also caused changes in the quantity and type of fuel consumed in the system, which in turn changed upstream fuel impacts. Under the base case assumptions presented in this section, all scenarios resulted in net increases in aggregate environmental impacts, as shown in Figure 2-3. This is due to the increase in net generation for all electricity mixes, resulting from the battery round-trip losses, and, in the Coal cases, an increase in coal and decrease in natural gas generation.

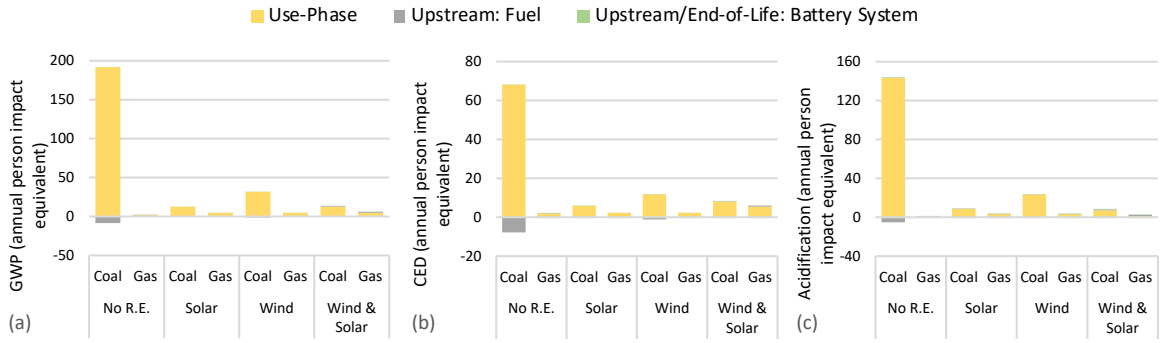

Figure 2 - 3, Changes in environmental impacts from using Li-ion battery systems for frequency regulation for each base case scenario normalized with the annual U.S. per-capita impacts in 2016, a) GWP (Global Warming Potential) b) CED (Cumulative Energy Demand) c) Acidification. Yellow bars are use-phase impacts resulting from changes in the quantity/efficiency of coal/gas, grey bars are upstream impacts resulting from changes in the quantity of coal/gas, and green bars are upstream/end-of-life impacts of the battery system. R.E. = Renewable Energy

The addition of energy storage reduces the need for generators to hold back capacity for reserves, changing the commitment and dispatch. Different electricity mixes produce different changes because the commitment/dispatch decisions are a function of energy costs, reserve costs, and generator parameters such as size and minimum production level, all of which differ across technologies. For example, different electricity mixes result in different "lumpiness" in

commitment decisions, i.e., we can achieve a better optimization result committing a large number of small generators than a small number of large generators.

There are confounding factors that cause the changes in generator commitment in the base case. In the base case, coal is less expensive than natural gas per MWh of generation (Figure A-2), so optimal operation will utilize minimal natural gas, all else equal. However, natural gas is less expensive than coal for frequency regulation and so, generally, a mix of coal and natural gas plants will be committed. Note that a generator cannot provide frequency regulation if it is not committed. With the addition of energy storage, conventional generators no longer need to provide as much frequency regulation and so some natural gas plants may not be committed, as their lower cost frequency regulation no longer compensates for their higher cost generation. This results in higher utilization of coal. For example, in the 'coal no renewable energy' base case, all generators are committed during the peak in order to provide sufficient frequency regulation (see Section 3.3.4), but with the addition of energy storage not all generators are required. More specifically, a coal unit that was providing frequency regulation can lower its supply of frequency regulation and increase its generation, and a natural gas unit no longer needs to be committed. This reduces the total natural gas output and increases the total coal output. The impacts from the increased coal consumption outweigh the reduction in impacts from reduced natural gas consumption. We explore the impact of dispatch in more depth in Section 3.3.4. It is important to note these specific commitment changes are particular to the Coal cases.

The only life cycle category in which we observed any decreases in environmental impacts in the base cases was 'Upstream: Fuel'. The cases with decreases are 'Coal; no renewable energy' and 'Coal; wind', in which there were decreases in cumulative energy demand and NO_x. Upstream fuel impact factors are higher for the production of natural gas than coal, and this difference was large enough to cause reductions in overall impacts even with a net increase in fuel consumption caused by battery round-trip losses.

Overall, the magnitude of the upstream and EOL impacts of the battery system were insignificant in comparison to those caused by the battery system's effect on power system operation, except for Acidification impacts in the 'Gas; no renewables' and the 'Gas; Wind & Solar' cases. The upstream impacts for the base case cathode LMO were 2,172 kg CO_{2eq}/MW-year or 33.1 kg CO_{2eq}/kWh. This value is the same across all base case scenarios and not far from the

range in the existing literature. Ellingsen et al.[95] found 38-145 kg CO_{2eq}/kWh, Kim et al.[64] found 39-63 kg CO_{2eq}/kWh, and Notter et al.[61] found 50 kg CO_{2eq}/kWh for LMO. Differences in results stem from differences in study assumptions and data sources.

2.3.2. Curtailment Impacts

Although six of the base cases scenarios have 15% renewable generation, there was less than 1% renewable curtailment in each scenario. In order to assess the effects of renewable curtailment on the overall results, the share of generation from renewables was increased until the system reached 10% curtailment without energy storage. The required increases in renewable generation capacity varied for each scenario due to differences in system flexibility and renewable generation profiles as shown in Table A-15. Congestion was the primary driver of curtailment at these high penetrations; the reserve requirement also led to curtailment. It is important to note that since energy storage is only used for frequency regulation it does not directly mitigate curtailment caused by congestion. It simply provides more options for the dispatch. Across all cases it only mitigated 1.5% of the total curtailment on average. The emissions impacts in the curtailment scenarios showed the opposite trends as the base case for almost all scenarios (Figure 2 - 4, Changes in environmental impacts from using Li-ion battery systems for frequency regulation for each curtailment scenario normalized with the annual U.S. per-capita impacts in 2016, a) GWP (Global Warming Potential) b) CED (Cumulative Energy Demand) c) Acidification. Yellow bars are use-phase impacts resulting from changes in the quantity/efficiency of coal/gas, grey bars are upstream impacts resulting from changes in the quantity of coal/gas, and green bars are upstream/end-of-life impacts of the battery system. R.E. = Renewable Energy

2-4), i.e., the addition of energy storage decreased emissions. Moreover, the decreases are, in general, significantly larger than the increases in the base case. In all curtailment cases, there was a reduction in overall fuel required because there was more realized renewable generation (i.e., less curtailment). The percent penetration of renewables and their generation profiles had a larger effect on overall environmental impacts than any factor investigated in our parametric studies.

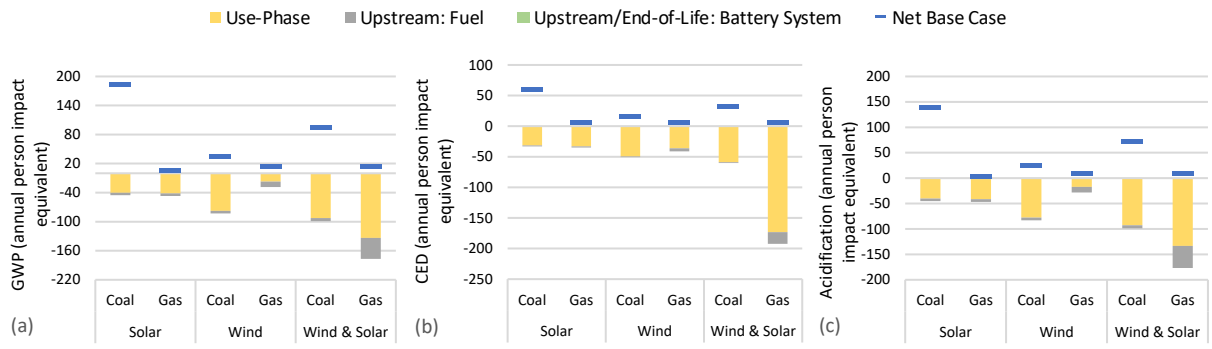

Figure 2 - 4, Changes in environmental impacts from using Li-ion battery systems for frequency regulation for each curtailment scenario normalized with the annual U.S. per-capita impacts in 2016, a) GWP (Global Warming Potential) b) CED (Cumulative Energy Demand) c) Acidification. Yellow bars are use-phase impacts resulting from changes in the quantity/efficiency of coal/gas, grey bars are upstream impacts resulting from changes in the quantity of coal/gas, and green bars are upstream/end-of-life impacts of the battery system. R.E. = Renewable Energy

The addition of energy storage to the 'Gas; wind and solar' case caused the most changes in unit commitment out of all curtailment cases, and subsequently the greatest reduction in environmental impacts. The combination of wind and solar in the 'Gas; wind and solar' case creates a smoother renewable generation profile than when the wind and solar are operated independently. Additionally, in the Gas cases the generators are all of similar size, so it is easier to effect the unit commitment than in the Coal case. Additionally, in this scenario, energy storage helped mitigate 4.7% of curtailment.

2.3.3. Parametric Studies

In order to better understand the drivers for overall environmental performance we tested key parameters relating to the battery composition and the power system. The parameters tested include fuel costs for conventional generation (i.e., coal and gas), alternative battery degradation models, alternative battery efficiency, induced congestion, different cathode materials, and use of EV batteries, both new and second-use. Table 2-2 outlines these parameters.

Table 2 - 2, Base case parameters and parametric studies

Parameter	*Base Case*	*Parametric Studies*	
		Name	Description
Cathode material	$LiMn_2O_4$	Cathode (LFP)	$LiFePO_4$ (LFP) cathode
		Cathode (NMC)	$LiNiMnCoO_2$ (NMC) cathode
Battery Type	Commercial stationary battery	New Car Battery	$LiNiCoAlO_2$ (NCA) cathode
		2nd Use Car Battery	$LiNiCoAlO_2$ (NCA) cathode with 80% starting capacity
Capacity Degradation	Xu et al.[91]	Capacity Degradation (Fortenbacher et al.)	Alternative battery capacity degradation model with faster degradation (Fortenbacher et al.[89])
		Capacity Degradation (Wang et al.)	Alternative battery capacity degradation model with faster degradation (Wang et al.[86])
Starting Efficiency	90%[22]	Eff 100%	Modeling a 100% efficient battery with no efficiency degradation
Fuel Costs	2014 Average[96]	Price Swap	Switching 2014 gas price to coal and vice versa: natural gas $2.37/MMBtu and coal $5.00/MMBtu
		Fuel Prices	2017 Fuel Prices: coal $2.22/MMBtu and natural gas $3.67/MMBtu
Congestion	1000 MW line limits	Congestion	200 MW line limit (coal) 170 MW line limit (gas)

Of the parameters tested, those related to fuel price, battery efficiency, and transmission congestion yielded the largest changes in environmental impact, though the electricity mix had a larger impact on overall environmental outcomes than any of these parameters. As seen in Figure 2-5, the trends for GWP emissions are similar across parameters for each electricity mix. It is important to note that the Coal cases use the left axis and Gas cases the right. The difference in magnitude of these axes is significant. In nearly all of the Coal cases, the addition of energy storage caused coal consumption to increase, due mainly to changes in unit commitment and, in part, to battery round-trip efficiency losses. However, in the Gas cases the increase in coal consumption was smaller and less consistent, leading to the lower impacts. This is because, in the Gas cases, coal operates near its maximum output except during a few hours when wind and solar are operating at full capacity. Figure A-14 shows other impact categories.

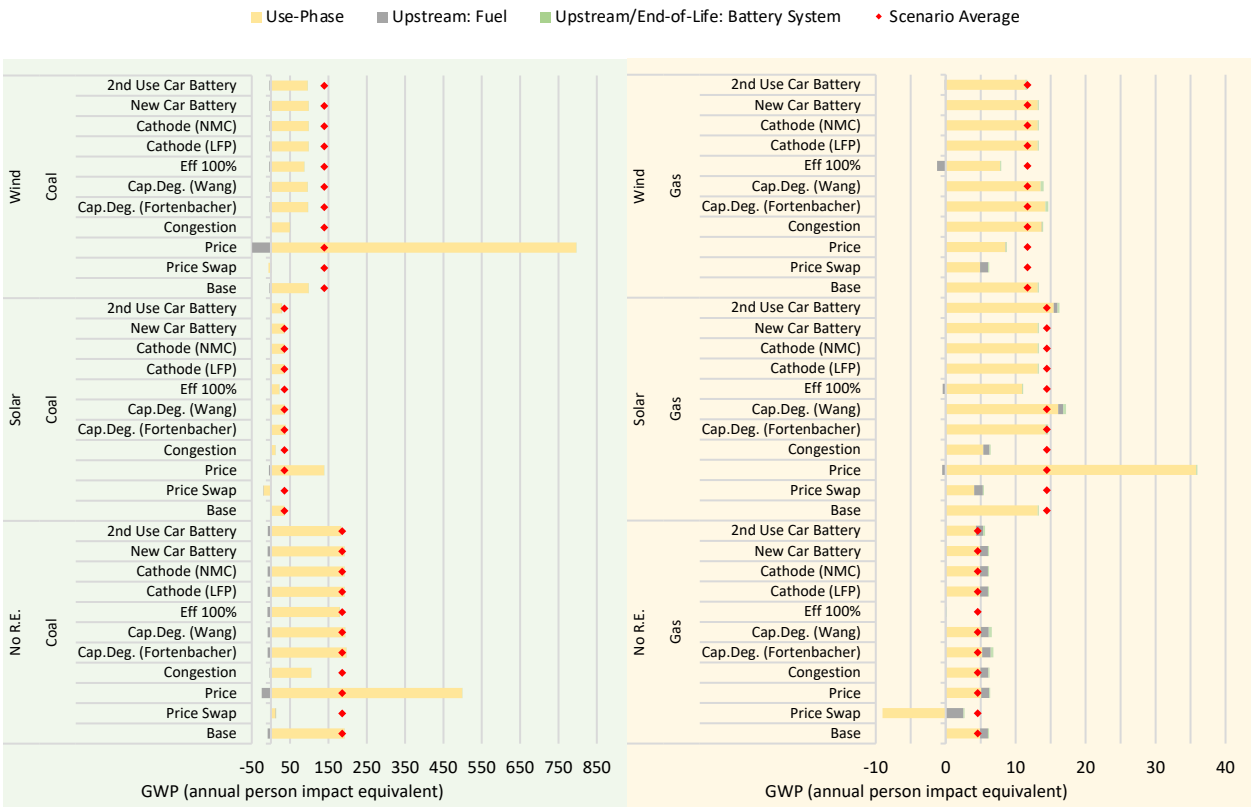

Figure 2 - 5, Changes in global warming potential (GWP) emissions for each parametric study under each scenario listed in Table 2-1 due to the addition of 1 MW-yr of reserve capacity provided by Li-ion battery systems normalized based on per-capita impacts in the U.S. in 2016. The red dots represent the average value across parametric studies for each scenario. Coal cases correspond to the left axes and Gas cases correspond to the right axis. Note the difference in scale between the two axes. Reference Table 2-2 for details on parametric studies. Yellow bars are use-phase impacts resulting from changes in the quantity/efficiency of coal/gas generation, grey bars are upstream fuel impacts resulting from changes in the quantity of coal/gas, and green bars are upstream/end-of-life impacts of the battery system. R.E. = Renewable Energy

2.3.3.1. *Cathode type impacts*

We tested four battery configurations different from the base case (which used a grid scale battery system with a LMO cathode): a grid scale battery system with different cathodes (NMC & LFP), a system with new EV batteries (NCA), and a system with second-use EV batteries starting at 80% capacity (NCA). Although the battery types have different round trip efficiencies, they were all modeled at 90% efficiency so that the parametric study could focus on the impacts solely related to battery materials and capacity changes. Impacts of efficiency were addressed in a separate parametric study. As the battery configuration does not affect the grid model, the reasons for differences in commitment/dispatch resulting from different electricity mixes are the same as for the base case.

We assume an allocation of the upstream and EOL impacts proportionally based on capacity degradation. The battery is modeled to reach end of life after 50% capacity degradation, where vehicle use degrades 20% of the battery's capacity and the grid use degrades 30%. This means that the vehicle use was responsible for 40% of the degradation (i.e., 0.2/0.5=0.4) and the grid use was responsible for 60% of the degradation (i.e., 0.3/0.5=0.6). Therefore, 60% of upstream and EOL battery impacts were allocated to the grid application. Note that we did not consider the impacts from additional material requirements to aggregate EV batteries.

There were not significant differences in GWP and CED between the four cathodes, as seen in Figure A-18. However, the differences were a result of differences between cathodes in production impacts and the quantity of aluminum required in the battery. NMC production produces the most CO_2 and LFP the least; however, the amount of aluminum required in LFP production increases its overall impacts. The drastic differences in cathode production-related SO_x emissions causes the large differences in acidification. The total GWP impacts were 33.5 CO_{2eq}/kWh for LFP, 35.9 kg CO_{2eq}/kWh for NCA, and 40.1 kg CO_{2eq}/kWh for NMC. These values are lower than ranges reported in existing literature,[64,95] driven in part by assembly values. However, even if our results mirrored the high end of ranges in existing literature our conclusions would remain the same in regard to the overall upstream battery impacts in comparison to use-phase impacts. Additionally, metals recycling rates do not strongly influence these results. Assuming no recycling increased emissions by 1.1% or less for each battery type.

2.3.3.2. *Capacity degradation impacts*

The rate of capacity degradation affects the upstream and EOL emissions. The shorter the battery life the larger the percent of impacts allocated to the one-year timeframe of the functional unit. However, because upstream and EOL impacts are small, the difference in battery life had little effect on overall system environmental impacts. On average, Fortenbacher et al.'s[89] model results for total impacts only varied 9% from the base case and Wang et al.'s[86] model results only varied 10% from the base case. Faster capacity degradation does affect generator dispatch but the differences were small and scenario specific, yielding results similar to the base case.

As discussed previously, degradation rates will vary for different cathodes. For example, Xu et al.[91] estimate that LFP batteries with E/P of 0.25 will degrade 0.75% in the first month while similarly sized NCM batteries will degrade 1.56%. In order to maintain consistency

across parametric studies, we have not varied the degradation models by cathode type, which would be required to obtain precise estimates of the impacts of different battery/cathode types. However, we have shown that differences of this magnitude would not change our paper's central finding, specifically, the limited significance of battery upstream impacts.

2.3.3.3. *Efficiency and efficiency degradation impacts*

To determine the share of environmental impacts attributable to battery round-trip losses , we compared our results to using a 'perfect' battery (100% round trip efficiency and no efficiency degradation). Our base case system utilizes a battery with 90% initial round trip efficiency, and 0.4% efficiency degradation annually, and 0.76% efficiency degradation over the battery's lifetime. In reality, LMO can reach efficiencies close to 100% while NMC's efficiency is 90% or less.[24] Therefore, this study also presents the impacts of efficiency differences between cathodes.

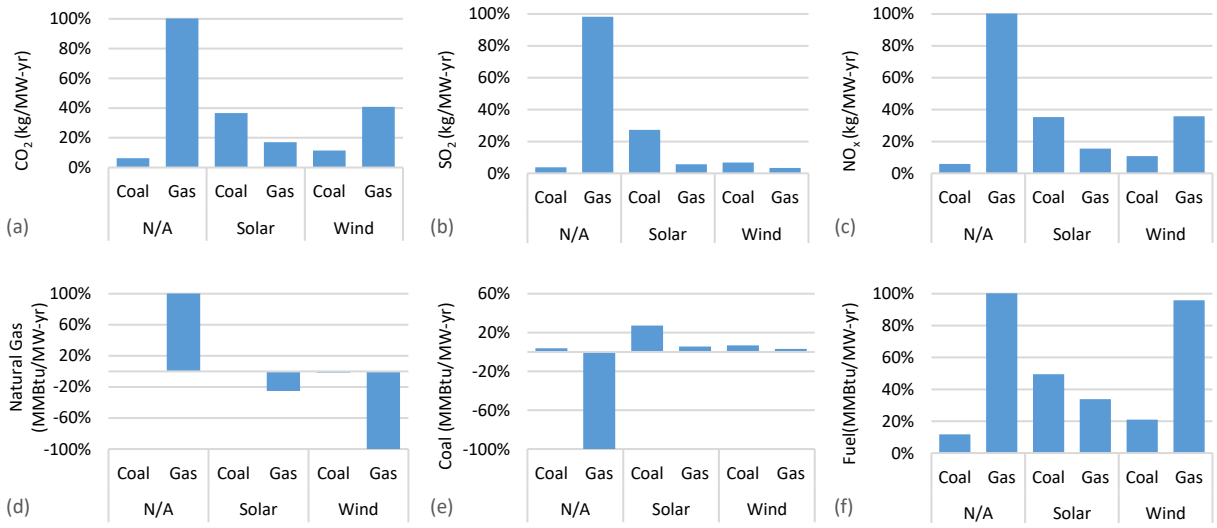

Figure 2 - 6, Percent of change in impacts caused by battery efficiency and efficiency degradation a) CO_2, b) SO_x, c) NO_x, d) natural gas consumption, e) coal consumption, f) net fuel consumption. R.E. = Renewable Energy

Use of the perfect battery reduced fuel consumption and, subsequently, environmental impacts. However, the percent of changes in impacts caused by battery efficiency and efficiency degradation was heavily dependent on the magnitude of the change in the dispatch caused by the energy storage system (Figure 2-4). In the 'Coal; no renewable energy' base case, the fuel consumption changes from adding energy storage were significantly larger than any other scenario, with the 'Coal; wind' case having the second largest changes, resulting in the lowest percentage change in impacts due to battery efficiency (Figure 2-6). We see the opposite for the 'Gas; no

renewable energy' case where the addition of energy storage had no effect on the dispatch and all impacts in the use-phase were a result of the additional electricity required due to battery inefficiency and efficiency degradation (Figure 2-6). These are the two extremes, but in many of the cases, environmental impacts from efficiency and efficiency degradation represent a significant proportion of overall impacts. However, although the percentage of impacts from efficiency is greatly dependent on the magnitude of impacts caused by changes in dispatch in the base case, it is also depended on system electricity mix, as seen in Figure A-17.

2.3.3.4. *Fuel costs impacts*

Fuel price was the most influential driver of generator commitment and dispatch, in turn, having drastic impacts on the battery system's environmental impacts (Figure 2-5). The first fuel cost parametric study uses fuel prices from U.S. Energy Information Administration's (EIA) Short Term Energy Outlook for 2017 ($2.22/MMBtu coal and $3.67/MMBtu natural gas), which is a slight decrease from 2014 coal prices ($2.37/MMBtu) and a considerable decrease from 2014 natural gas prices ($5.00/MMBtu) as used in the base case analysis. Impacts increased in each scenario, except the 'Gas; wind' scenario (Figure 2-5).

Figure 2-7 gives intuition for this result. In both price cases all generators are committed during the peak when energy storage is unavailable, but with energy storage, Generator 4 (G4, natural gas) is not committed and coal consumption increases. The difference between 2017 coal and natural gas fuel prices is smaller than in 2014 (see Figures A-3 and A-4), and small enough that the cost reductions from providing frequency regulation from natural gas generators is greater than the increased cost of natural gas generation at certain load levels. This causes natural gas generation to be committed for a greater number of hours in comparison to the base case. Therefore, with 2017 prices, the impact of not committing Generator 4 is larger. Note that, at equal loading during different hours of the day, unit commitment and dispatch schedules are not always equal. This is a result of the time coupling constraints (e.g., minimum startup and shutdown times) used in the 24-hour unit commitment and dispatch problem.

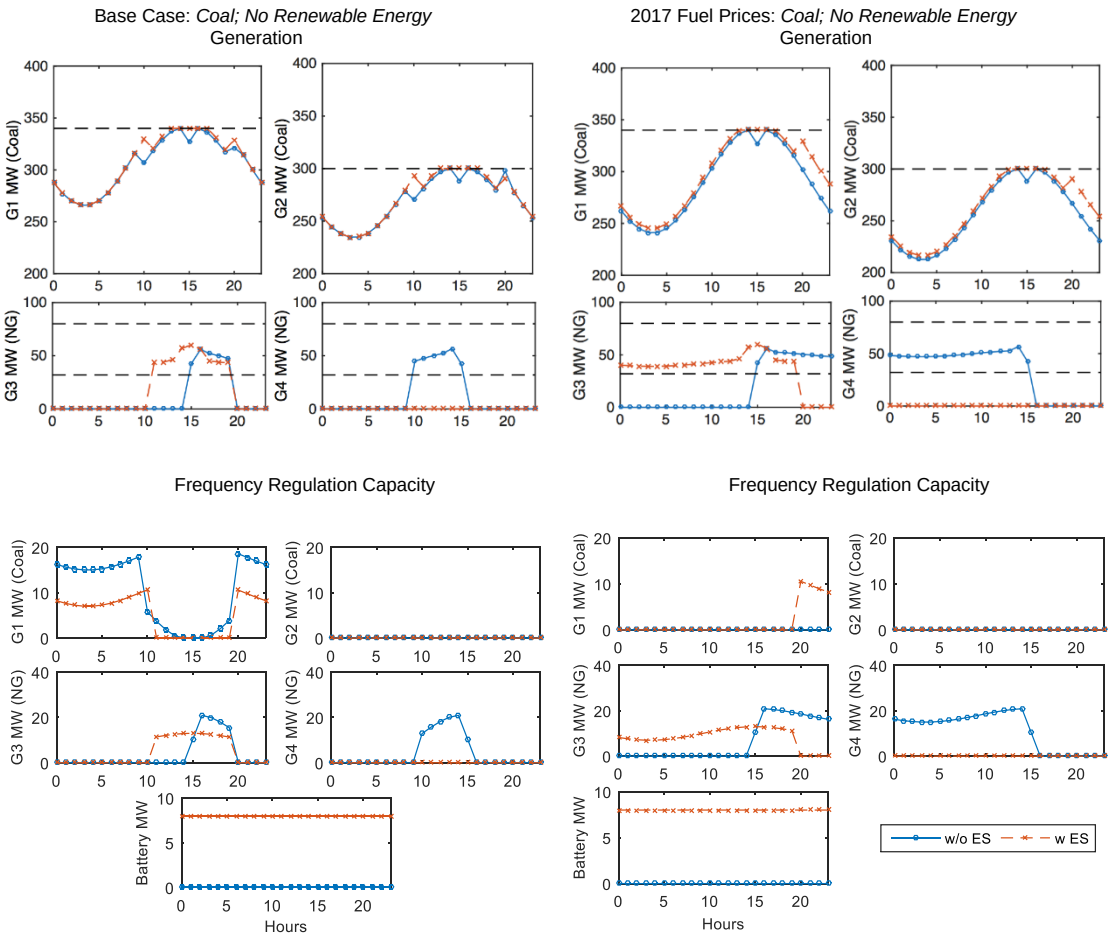

Figure 2 - 7, Dispatch and reserve results for the 'Coal; no renewable energy' base case (left) and parametric study with Energy Outlook 2017 fuel prices (right). The top eight figures are the generation from each generator over a 24-hour period. The horizontal dashed lines in the top eight figures are the minimum and maximum limits of the generators when they are committed. The bottom ten figures are the frequency regulation capacity provided by each of the generators and the battery over the same 24-hour period. ES = Energy Storage

To test the impacts of more extreme changes in fuel price, the second fuel cost parameter study swaps 2014 natural gas and coal prices. This had a significant change in the commitment/dispatch in each case. In this parametric study, natural gas is less expensive than coal for both frequency regulation and generation, shifting the dispatch priority from coal to natural gas. This, in turn, changed the way the energy storage system affected generator dispatch. When energy storage was introduced, natural gas generators, rather than coal, increased their generation in each scenario other than 'Coal; no renewable energy' and 'Gas; wind'. However, the impact of the decrease in coal was not always large enough to offset the impacts from increasing natural gas consumption (Figure 2-5).

The addition of energy storage does not change the dispatch in the 'Coal; no renewable energy' or the 'Gas; wind' case. In the 'Coal; no renewable energy' case, natural gas plants are at maximum generation in each hour and both coal plants are dispatched. The savings from reduced cost natural gas generation are greater than the increased cost from frequency regulation provided by coal, meaning, the coal plants provide frequency regulation. Therefore, with the addition of energy storage, the dispatch does not change; the coal units just reduce the amount of frequency regulation they provide. In these cases, the increased fuel consumption (i.e., increase impacts) in these cases is from battery round-trip losses.

2.3.3.5. *Congestion impacts*

Transmission congestion was added to the Coal cases by reducing the line limits from 1000 MW to 200 MW and to the Gas cases by reducing the line limits to 170 MW, in all lines other than those connecting generators to the system (i.e., 1-4, 3-6, and 8-2). The difference in limits is a function of the generator sizes. The addition of congestion caused changes in environmental impacts from the base case in all six scenarios. However, we cannot make generalizations about the effects of congestion because, in practice, results would be strongly dependent on grid topology and parameters, generator sizing and location, and so on. Overall, we can say the impacts of adding energy storage are affected by congestion, but to determine exactly how on a particular system would require detailed information on and analysis relating to the grid parameters and topology.

2.3.4. General Impacts

Changes in generator commitment and dispatch caused by the addition of energy storage were the most significant contributors to the energy storage system's environmental impact, meaning that the use-phase denominated. These changes resulted in changes in combustion emissions and upstream fuel impacts. The magnitude of the upstream and EOL impacts of the battery system were small in comparison. In the base case, net increases in environmental impacts were observed for each electricity mix. In the Coal cases, the impacts were much larger than those in the Gas cases as there was a significant switch from natural gas generation to coal generation since coal generators no longer needed to provide frequency regulation.

The parameters most affecting the impacts of the energy storage system were grid characteristics. The electricity mix had the largest impact on the magnitude of the environmental impacts of the addition of energy storage. Specifically, as seen in the curtailment case, the percent

penetration of renewables and their generation profiles changed the commitment and dispatch of generators significantly reducing emissions. Fuel price, congestion and battery round trip efficiency had the next largest effects on net environmental impacts.

CHAPTER 3

The Impact of Forecasted Net Load on Real-Time Power Generator Operation

Abstract

Wind and solar electricity generation is anticipated to be a key contributor to mitigating electricity sector emissions. However, wind and solar are inherently variable and uncertain, resulting in increased intra-hourly variability in net load (i.e., load minus wind and solar generation), making it more challenging for dispatchable generators to match supply and demand. If scheduled generators cannot adjust their output to match net load changes in the real-time market it could result in system inefficiencies like wind and solar curtailment, reducing the overall carbon-free electricity supplied to the grid, or unplanned generator start-ups and shut-downs.

Although literature assumes these inefficiencies occur in hours with large changes in net load and high levels of wind and solar generation, there has been limited statistical analysis. This chapter quantifies these relationships with a regression model whose independent variables are day-ahead net load characteristics (e.g., ramp rate, percent wind and solar generation) and whose dependent variables are unplanned shut-downs and start-ups. The day-ahead and real-time markets are modeled for the U.S. western interconnection in a production cost model.

As illustrated with a test case, the regression model results show that a substantial share of the variability in unplanned generator start-ups and shut-downs can be explained by net load characteristics. Net load, fraction wind and solar, ramp rate, and hour had the greatest impact on the predictability of the model. These results indicate that there is potential to use day-ahead net load characteristics to predict real-time system inefficiencies. Day-ahead generator scheduling could be adjusted based on these predictions, to improve system efficiency and reliability.

3.1. **Introduction**

Electricity generation from wind and solar power is anticipated to be, and in some regions already is, a key contributor to mitigating emissions in the electricity sector. It offers the potential to supply a significant share of U.S. electricity demand while producing zero direct emissions and causing minimal environmental impacts. Currently, wind and solar represent a modest percentage of total electricity generation in the U.S, providing a combined 8.3% in 2018.[97] However, with decreasing installation costs, minimal operational costs, and zero direct emissions, their installed capacities are anticipated to grow rapidly.[98] However, challenges remain with integrating high percentages of variable renewable energy (VRE) into the electricity grid while maintaining reliability. The purpose of this study is to present an operation strategy, informed by statistical analysis, which has the potential to improve generator scheduling; mitigating certain challenges with operating a high percent VRE grid.

A high VRE penetration grid is challenging to manage because of the rapid changes in available generation from VRE and the limited predictability of VRE generation, which requires additional efforts to balance supply and demand in real-time.[99] With increasing penetrations of these resources, electricity supply uncertainty and variability increase considerably.[14] Therefore, for the system to remain reliable, it must be able to react quickly to changes in both demand and supply,[100,101] requiring increasing flexibility [102,103]. Despite this need, many existing power systems are not currently operated in a way that allows for the degree of flexibility required for high VRE penetration and operation; planning practices are beginning to be viewed as inadequate.[104] Insufficient ramp rates, minimum generation levels, congestion, limited storage, and limited demand response can all constrain the flexibility of grid operations.[14,105,106]

This study investigates the implications of the inflexibility caused by existing dispatchable generators' limited ramping capabilities (i.e., their feasible rate of change of generation) and operating ranges (i.e., minimum generating levels). These limitations can inhibit the system's ability to meet large ramp events, which will likely increase under higher VRE penetrations.[107] In this study, we calculate the ramp rate based on a region's net load, defined as the total load minus non-dispatchable generation (narrowed to include only wind and solar generation). VRE increases system ramp rates needed from dispatchable generators when the change in load and the change in VRE generation are trending in opposite directions, which is a common occurrence. For

example, solar's peak generation typically occurs in the middle of the day (i.e., near solar noon), while peak electricity demand in many regions occurs in the evening. Therefore, when solar generation is subtracted from load, the rate of change for net load often increases, resulting in the need for additional ramping from flexible generators. When existing dispatchable generators cannot adjust rapidly enough to these changes in net load and neighboring regions cannot shift imports or exports to balance the system, the renewable energy must be curtailed.[108] Such curtailment potentially reduces the overall carbon-free electricity supplied to the grid and adds to system costs. The inability to meet ramping requirements is an important cause of power balance violations and high scarcity prices.[109]

Large ramp rates can pose a challenge to operators when their magnitudes are known in advance, but they can be an even greater challenge when their magnitudes are unknown in advance. Uncertainty exists due to day-ahead VRE forecasts, which can cause inefficient scheduling of generators in the day-ahead market resulting in under-scheduling or over-scheduling.[110,111] When insufficient power capacity is scheduled, flexible dispatchable resources with shorter startup times and higher ramping capability are prioritized in the real-time market to make up the shortfall.[108,112] These are typically less efficient units, so their use can increase overall system costs and emissions. Over-scheduling generators can also introduce power system inefficiencies by requiring less efficient low load operation or renewable curtailment in the real-time market.[108,110] This uncertainty is compounded by the fact that most day-ahead scheduling is done on the hourly time scale so even if there is no forecast error, the inter-hour variability in the real time could case inefficient commitments.

These new challenges are unlikely to be mitigated by adjustments in the real time market alone, meaning that some of the burden will fall on ancillary services [99] or grid-scale storage. In the case of a large unexpected up ramp event, potentially caused by a sudden drop in VRE generation, reserves may be required.[113] Some large unexpected down or up ramp events can cause power balance violations,[109] in which case real-time energy price is no longer a function of economic bids but of penalty prices, impacting market efficiency.[114] Therefore, to ensure reliability, more reserves are held for VRE,[115] increasing VRE's associated costs and potentially hampering the adoption of VRE power sources or reducing their environmental and economic benefits. Moreover, calculating the optimal capacity to hold in reserve is not straightforward and

a standard method is not universally accepted. Different regions calculate and classify reserves differently.[115] This is in part due to the diversity of generating resources and grid configurations across the country.[115] Studies have used a number of methods, mostly based on statistical approaches.[111] Simple approaches calculate a constant reserve requirement, which results in overly-conservative standards, holding more reserves than needed and further increasing costs.[111,115] It is more challenging to dynamically calculate reserves such that they respond to improved forecasts and changes in renewable energy penetration.[111] or are responsive to not just the level of demand and VRE supply but also the resulting net load's rate of change (i.e., ramp rate).

One approach to this challenge is to improve the day-ahead predictions of the ramp events caused by rapid wind and solar generation changes, enabling operators to improve scheduling (see, for example, Kamath 2010; Cui et al. 2017; Sevlian and Rajagopal 2012; Cui and Zhang 2018). However, these studies, that look to improve ramp event predictions, have not investigated the system impacts or cost impacts of these events. A number of studies attempt to quantify additional system costs incurred from integrating cost of VRE, but they assess costs related to the system with and without VRE,[99,108,118,119] and costs are often a result of increased ramp, but there are a larger number of factors impacting costs with addition of VRE. Additionally, such studies are commonly motivated by the assumption that hours with high ramp rates require additional system flexibility and that higher percentages of VRE generation require increased reserves, but there has been limited statistical analysis of these assumptions. A second approach to mitigate the impacts from large ramp events is to more effectively schedule units in the day ahead market by improving how the unit commitment problem is solved. The literature on novel optimization methods to improve the unit commitment problem is extensive (for example, Abujarad, Mustafa, and Jamian 2017). However, the disadvantage of many novel methods is their increased computational complexity and execution time.[104]

Driven by these known research gaps, in this study we investigate the significance of the relationships between forecasted net load characteristics across time (e.g., ramp rate, percent of capacity) and realized system operations on an hourly basis (e.g., generation costs, generator commitment errors) through detailed power system and statistical modeling. Specifically, we investigate if, given forecasted net load and VRE generation, we can determine when the system

inefficiently committed generators. Inefficiencies are evident when generators are forced to startup or shutdown unexpectedly, which we define in our methods as commitment error. By focusing on the net load changes over time and controlling for other system characteristics (e.g., forecast error), we isolate relationships between forecasted net load shapes and real-time system impacts. These relationships are broadly applicable to other power systems given they are based on variables which can be calculated in any power system with a real-time and day-ahead market.

If the relationships between net-load characteristics and real-time system impacts are significant, they could be used to predict real-time system reactions to the day-ahead net-load. This would enable operators to prevent system inefficiencies by adjusting the optimized generator commitments from the day-ahead market, and improve reserve requirement calculations by enabling them to be responsive to conditions in a given system. These improvements have the potential to reduce system-wide emissions and cost by reducing curtailment and improving generator efficiencies, as well as improving system reliability under higher shares of VRE generation.

The organization of this chapter is as follows: the methods section first describes the power system model, followed by the statistical analysis of the power system model outputs. The results section present trends between the weeks modeled and the relationships found between net load shape and commitment error. In the discussion, we explore the robustness of the results, why the relationships exist, and their potential applications.

3.2. **Methods**

3.2.1. Power system representation

We simulated electricity grid operation with a highly detailed production cost model (PCM) which minimizes system operational cost subject to system constraints (e.g., transmission limits, generator ramp rates). Appendix B contains the mathematical formulation. This approach effectively captures grid operations and enabled us to explore the implications of changing electricity markets and infrastructure by modify grid characteristics (such as the minimum generation levels by generator type). By analyzing levels of flexibility and VRE penetrations that are yet to be realized in any existing U.S. grid system, our results have broad applicability and offer insights beyond the region that we investigated.

The focus of our study is the balancing regions operated by California Independent System Operator (CAISO), which includes much of the California's power system. California's facilities generate the largest amount of VRE of any state in the U.S., as of 2017, and they are seventh in terms of annual share of generation served by wind and solar, with a greater percent solar than any other state.[120] This high penetration of variable renewables offers an ideal case to build upon and explore the potential impacts of variability and uncertainty in their regional net load. Because California's electricity grid is not isolated and its generators and utilities participate in the Energy Imbalance Market, which spans multiple western states, we modeled the entire Western Interconnection (WI) to capture the impacts associated with changing imports and exports from the CAISO system. WI is one of three interconnections in the United States, which spans the western region of the country. There is limited trade between the interconnections but significant trade within them.

Our WI model is modified from NREL's Low Carbon Grid Study, which was built on the Transmission Expansion Planning Policy Committee (TEPPC) 2024 Common Case.[121,122] Details on the WI model and modifications from previous studies is included in Appendix B. Western Electricity Cooperation Council (WECC)'s Transmission Expansion Planning department, with input from TEPPC stakeholders, develops the Common Cases.[122] The cases represent the ten-year trajectory of WECC transmission based on planning information at the time of development.

The Common Cases themselves are PCMs developed as a foundation for TEPPC's ten-year studies.[122] The Common Case separates WI is into 40 subregions, which are representative of balancing authorities or load serving regions, Figure 3-1.[122] We modeled the transmission constraints between each of these subregions, as well as the transmission limits *within* the California subregions (i.e., using a nodal representation of CIPV, CIPB, CISC, and CISO). In order to more accurately model the impacts of load shape and VRE generation it is important to consider the region's transmission constraints. Modeling all of the WI with a nodal representation would not provide significant additional insight into CAISO's modeling results but would be much more computationally intensive.

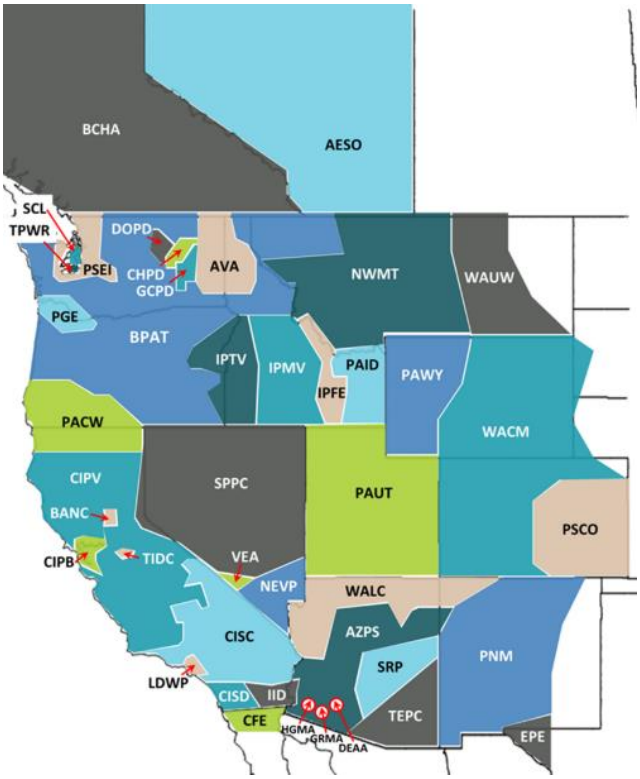

Figure 3 - 1, Transmission Expansion Planning Policy Committee 2024 Common Case regions used in Western Electricity Cooperation Council production cost model [122]

The results from the original 2024 model had 13% VRE generation across the WI. To improve our understanding of the impact of deep decarbonization in the power sector, we modified the power system representation, greatly expanding (by a factor of four) the system VRE capacity in all of the WI. This allows us to determine the commitment and dispatch response with a grid mix that is more challenging for power system operations. Our method of increasing VRE penetration is similar to Martinez-Anido et al. (2016)'s when examining the impacts of forecast error in the Independent System Operator New England[123] and similar in approach with other studies examining the impacts of deep decarbonization (e.g., Arbabzadeh et al. 2019). Figure B-1 contains the final grid mix.

We modeled WECC using the commercial PCM software PLEXOS, which solves the unit commitment and economic dispatch problem using a mixed integer linear optimization. PLEXOS has been used in a number of grid studies.[121,125–127] Details of how each scenario was built and executed in PLEXOS are included in the Appendix B-1.

For each scenario, we simulated the day-ahead market on an hourly time scale and the real-time market on a five-minute time scale, both consistent with current CAISO operation. CAISO also changes commitments in the Residual Unit Commitment, which occurs after the day-ahead market is complete, in the Short-Term Unit Commitment, with is part of the real-time process and extends three hours beyond the trading hour, and in the Real-Time Unit Commitment, which is run every 15 minutes.[128] However, rather than explicitly modeling CAISO's additional markets (which would increase the complexity of the model), we simulated improved or degraded VRE forecasts, ranging from -25% (i.e., forecast error is increased 25%) to +100% error (i.e., forecast error is decreased 100%). Improved forecasts offer insights similar to these nearer term commitment changes as well as potential futures where VRE forecasting capabilities have improved.

Similar to CAISO's operation, we only allow certain units with short cycle times to have unscheduled changes in commitment status in the real-time market. Minimum up and down times are defined by unit type and size (details in Table B-1), with combustion turbines having the shortest times. Given the operational constraints associated with other types of the fossil units, only combustion turbines are sufficiently responsive to have unscheduled shutdowns and startups in the real-time market. In addition, batteries and pumped hydro storage are also not constrained to their day-ahead schedules.

Daily net load shapes vary significantly across the year. In order to understand important relationships without modeling the entire year, which would be highly computationally intensive, we modeled the weeks in which we expected to observe the largest and smallest system impacts from the net load shapes. As such, we considered four weeks: the weeks with the greatest and least ramping, as well as the weeks with the greatest and least inter-hour variability. We calculated the ramp for a week as the sum of the absolute value of the difference in net load and the beginning and end of each hour. We calculated the variability for a week as the sum of the difference between the maximum and minimum values in each hour of the real-time net load. Appendix B-1.2 contains the calculations used to select these weeks.

3.2.2. Statistical methods to evaluate commitment changes

A key PCM result that we analyzed is the generator commitments for the day-ahead simulation and the real-time operational decisions. When a generator's commitment status changes between the day-ahead and the real-time results, we categorize this as a commitment error (i.e., an unscheduled generator shutdown or startup). In this section, we use day-ahead grid system model inputs (e.g., forecasted load and VRE generation) to create a regression model with the goal of predicting the commitment error. We hypothesize that the net load shape in a given hour and the four hours leading up to a given hour will impact the commitment error within that hour. This four-hour window corresponds to the four hour recommitment window used in CAISO's short-term unit commitment. However, our regression model could be applied to the output of the day-ahead unit commitment schedule or the four-hour ahead commitment schedule to modify generator commitments. We selected a linear regression model, to better understand the drivers for commitment error. Given that the regression is an additional modeling step that would need to be deployed during day-ahead market decisions, we selected a method with minimal computation time.

The commitment error is calculated as follows for each hour, t, and generator, i,

$$CE_t = \sum_{i=0}^{n} \alpha_i \left(\frac{1}{12} \left(\sum_{k=1}^{12} C_{RT,i,k,t} \right) - C_{DA,i,t} \right), \quad (1)$$

where *t*, is the hour for which the commitment error is being calculated, *k* is the five minute interval within hour *t* used in the real-time market, *n* is the number of generators available to change commitment status, α_i is the maximum capacity for generator i, and $C_{RT,i}$ and $C_{DA,i}$ are the on/off binary commitment operators for generator i, in each time increment in the real-time (*RT*) and day-ahead (*DA*) markets. The day-ahead market operates on an hourly basis and the real time operates on a five-minute basis, thus requiring twelve time increments to determine the real-time commitment status over an hour.

Model Variables

We characterize the net load shape using five variables and VRE generation as a fraction of generation. See Table 3-1 for each variable's description and associated equation. We calculated each variable for CAISO and WECC. The dataset contains 4,032 observations for each variable, given we ran four weeks under six levels of forecast error. Each variable is modeled

across a span of hours leading up to a given hour, *t*, (Value across hours, Table 3-1) and/or for each individual hour leading up to a given hour, *t*, (Values in each hour, Table 3-1).

Table 3 - 1, Regression model variable definitions

Name	Value in each hour *(n=0…4)*		Value across hours *(n=0…4)*		Model Equation Type
Net Load	ρ_t	(2)	*N/A*		$\beta_1\rho_t + \beta_2{\rho_t}^2$
Relative Net Load	$R\rho_t = \frac{\rho_t}{\rho_{max,daily}}$	(3)	*N/A*		$\beta_1\rho_t + \beta_2{\rho_t}^2$
Ramp Rate	$\varepsilon_{t-n} = \rho_{t-n} - \rho_{t-n-1}$	(4)	$\varepsilon_{t0-n} = \rho_t - \rho_{t-n-1}$	(5)	$\beta_1\varepsilon_t$
Relative Ramp Rate	$R\varepsilon_{t-n} = \frac{\rho_{t-n} - \rho_{t-n-1}}{\rho_{t-n-1}}$	(6)	$R\varepsilon_{t0-n} = \frac{\rho_t - \rho_{t-n-1}}{\rho_{t-n-1}}$	(7)	$\beta_1 R\varepsilon_t$
Variability	*N/A*		$\mu_{t0-n} = \sum_0^n \lvert\rho_{t-n} - \rho_{t-n-1}\rvert$	(8)	$\beta_1\mu_t$
Fraction VRE Generation	*N/A*		$g_{t0-n} = \frac{\omega_{t-n}}{\theta_{t-n}}$ $\omega = Forecast\ VRE$ $\theta = Load$	(9)	$\beta_1 g_t$

Note: t represents the hour of interest, n represents the number of hours prior to the hour of interest

Net Load, ρ_t, is defined as the total system demand minus solar and wind generation. We hypothesize that increased commitment error occurs during times of high ramp rates and high variability, which often correspond to median load levels. Meaning, we would expect median load levels to have higher commitment error. Therefore, we model the relationship between net load and commitment error as non-linear and more specifically as a second order quadratic. (eq. 2).

Additionally, the magnitude of the net load does not tell the whole story. The size of a power system region and the number of generators present may influence the magnitude of commitment errors. Therefore, it is important to evaluate the impact of where on the net load curve the hour falls. If it is near the peak or trough, there is likely less change than if the net load is in the middle where ramping occurs. To address this, we considered net load as a percentage of a region's peak net load ($R\rho$), modeled as a second order quadratic (eq. 3).

We assume a linear relationship for each of the four remaining variables; *VRE Forecasted*, g_t, *Ramp Rate*, ε_t, *Relative Ramp Rate*, $R\varepsilon_t$, and *Variability*, μ_t. We hypothesize that the fraction of load supplied by *VRE Forecasted*, g_t, will have a positive linear relationship with commitment

error (eq. 9). The greater the fraction of VRE, the greater the unplanned generator shutdowns and vice versa. We also consider that a high rate of change (i.e., ramp rate) will cause more commitment error (eq. 4 & 5). However, the errors are also related to how many generators are already committed. There is inherently greater down flexibility on the system when there are a larger number of generators committed and greater up flexibility when fewer generators are committed but the system is restricted in the opposite directions so we also modeled the relative ramp rate (eq. 6 & 7). The Relative Ramp Rate was calculated as the change in net load across a time interval relative to the load at the beginning of the time interval. Another potential predictor is the net load variability across and within hours. Given in the day-ahead we are using hourly data and, thus, we have no inter hour variability, we therefore calculate intra hour variability, μ_t, by taking the absolute value of the change in net load across an hour (i.e., absolute value of the net load ramp) (eq. 8).

Along with the net load shape, we hypothesize that the hour of the day will be a predictor of the commitment error. However, given that hours at the beginning and the end of the day (i.e, night) have the least variable net load and the morning and evening hours have the largest changes in net load, we modeled the hour variable with a third order quadratic relationship. This captures our hypothesis that in the morning there will be greater unplanned generator shutdowns and in the evening, there will be greater unplanned generator startups.

Additionally we model the week as a confounding variable, as it could influence the commitment error.

We ran a separate model for each level of forecast error to determine the impact forecast error would have on the predictability of our input variables.

Selecting Model Variables

In order to test the model's predictability, prevent overfitting, and determine the importance of each variable, we used the k-fold cross validation method, with five folds.[129] The k-fold validation method randomly splits the data into k sets or folds. We specified five folds given the number of variables and observations. The method runs the model five times, each time with a different fold acting as the test set and the remaining acting as the training set. We completed the k-fold cross validation method three times to remove impacts of data partitioning. All R^2 values

discussed in the paper represent the average of the k-fold method test set R^2 values. The average R^2 of the k-fold tests represents the predictability of the model. This process is repeated three times to average across different data partitioning. The k-fold test was also repeated with each variable removed (n-1). The average R^2 value of the test sets with a variable removed offers insights into its importance as a predictor. After running the model with each variable removed any results with an average test set R^2 equal to or greater than the test set R^2 with all variables included was removed from the model, as this indicates the variable does not contribute to the model's predictability.

The above process is conducted for each forecast error scenario and region (CAISO and WECC) separately. This results in 12 models, each potentially having different variables and coefficients, with each model having 672 observations of each variable

3.3. **Results and Discussion**

We begin analyzing the results of the twelve regression models, one for each level of forecast error and regional boundary, by comparing the predictive power of each model.

3.3.1. Model Predictive Power

We find that 21-57% of the variability in commitment error can be explained by the forecasted load and VRE generation variables, Table 3-1, based on the average R^2 values (Figure 3-2). All references to R^2 values in the results and discussion reference the average R^2 values calculated using the k-fold method on the final regression models after the removal of the variables that did not increase the R^2 value. On average, the predictability of the regression model increases with a reduction in forecast error. We also see that the model's predictability improves with the broader geographical area; its performance is better for WECC than for CAISO. We examine how the commitment error varies between regions and levels of forecast error to better understand differences in the predictive power of the models

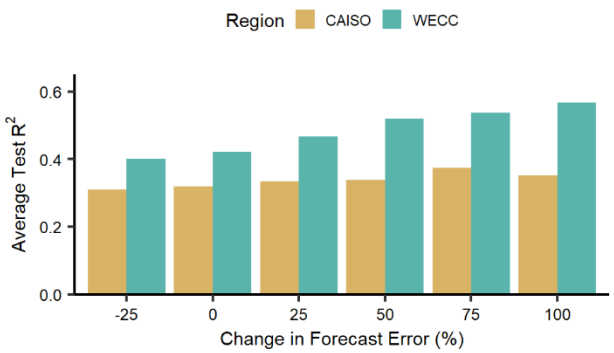

Figure 3 - 2, Strength of model predictions. Average R^2 values are the average values from preforming the k-fold method on the individual regression models developed for the forecast scenarios and regions.

3.3.1.1. *Influence of Region Size*

Overall, the model's predictive power is consistently better in WECC than CAISO. Figure 3-3 shows the distribution of commitment error for WECC and CAISO. Both are normally distributed, however, CAISO's median is negative, meaning there were more unplanned startups, and WECC's is positive, meaning there were more unplanned shutdowns. There is also greater variation in WECC's commitment error compared to CAISO's. The skewed nature of the data in WECC is a result of how the hydro generation (non-pumped storage) was modeled. A limit was placed on the hydro generation in the day-head to ensure that units did not exceed a monthly maximum generation. However, this constraint was removed in the real-time. Without the constraint, hydro units operated at full capacity in each hour reducing the generation required from combustion turbines causing them to de-commit. There is a greater amount of hydro in WECC than CAISO, causing WECC commitment error to be skewed positively toward de-commitment. Investigation of the modeling results showed this to be a limitation to the test case, as the hydro generation would not be unconstrained in a realistic real time market. While this deviation from realistic hydropower operation adversely impacts the magnitude of the PCM results in this study, we are still able to demonstrate the novelty of the method on this test case.

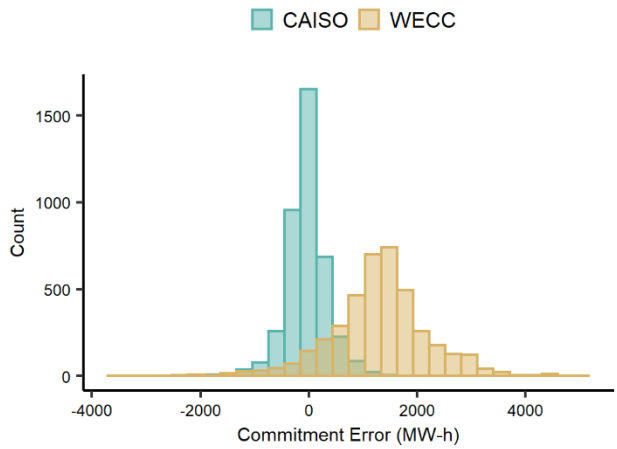

Figure 3 - 3, Histogram of hourly commitment error for WECC and CAISO for all forecast errors, and weeks histogram of hourly commitment error for WECC and CAISO

The skew in commitment error in WECC is likely not the primary reason for the WECC models to be more predictive as this error operates in a similar manner to the forecast error, which does not have a major impact on the model's ability to predict commitment error. In a larger region (WECC), the step function nature of commitment changes are averaged over a larger number of generators, in turn, better fitting a linear model. Additionally, because WECC (outside of CAISO) is modeled with less transmission detail, commitment changes are less likely to be driven by congestion, which may be challenging to predict from net load shape alone. Given the interconnectedness of the system, we can infer that generators outside of CAISO are also responding to VRE integration, with shifting imports and exports, further complicating the ability to predict commitment changes on CAISO. On average, net imports meet 6% of CAISO's load across the four weeks with a standard deviation of 9%. We do know that the difference in commitment predictability does not relate to a difference in the capacity that is able to change commitment in the real-time, given this capacity, relative to peak load across the four weeks, is similar in CAISO and WECC 26% and 22% respectively.

Even though the regression model is less predictive on a smaller region, if the regression model were to be used to inform and change commitment decisions, it should be utilized at the same regional scale at which the day-ahead market is operated. This would enable the operators to more accurately select the units to commit or de-commit in response to the model results, which are likely to be the marginal generator/s. Selecting the marginal generators would mean that energy price was still a function of economic bids.

3.3.1.2. *Influence of Forecast Error*

Figure 3-4 shows the impact of forecast error on the average commitment error as a percentage of average load (termed "relative commitment error"). The relative commitment error does decrease with improved forecast, decreasing 3.3% for WECC and 5.2% for CAISO when comparing a -25% and 100% reduction in renewable forecast error. Although modest in magnitude, these reductions illustrate that improved forecasts can reduce commitment error. When the regression model is run on the commitment error after subtracting out the error in the perfect forecast error case, the R^2 value never exceeds 0.1. This implies that the model performs well in predicting the relationship between net load characteristics and commitment error, but it is not successful at predicting the additional commitment error caused by forecast error, reducing the model's predictive power with greater forecast error. It is important to note that even with a perfect renewable forecast, there are still commitment errors in the real-time market given the intra-hour variability not captured in the hourly day-ahead market.

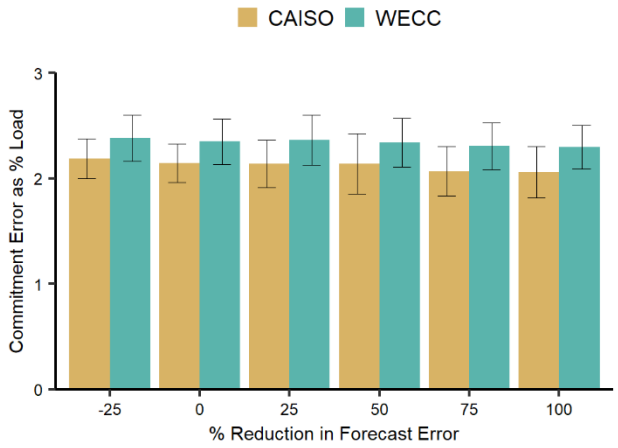

Figure 3 - 4, Impact of week and forecast error on the average commitment relative to the average load for WECC and CAISO. Error bars represent the standard deviation of each value across forecast error scenarios when the x-axis is weeks and across weeks when the x-axis is forecast error (V=Variability, R=Ramp)

3.3.2. Predictive Potential of Independent Variables

The initial regression model contained 34 variables, which describe the forecast load and VRE generation, with 672 observations each. After selecting for predictive variables for each level of forecast error and region, the models contained between 15 and 24 variables. Table 3-3 shows

the relative importance of each variable to the model's predictability in reference to their impact on the R^2 value of the model. The more the removal of the variable reduces the R^2 of the model, the greater its importance. If the boxes in Table 3-3 are patterned, the corresponding variable had no impact on the results.

Based on the results in Table 3-3, Fraction VRE (g_t), Ramp Rate (ε_t), and Week (h) contribute most to predicting commitment error in WECC and Net Load (ρ_t), Relative Net Load ($R\rho_t$), and Hour (h) contribute most to predicting commitment error in CAISO. Order of importance of these variables varies by level of forecast error. In general, removing variables in the CAISO models had a greater impact of the R^2 value. This could be a function of the, the level of constraint in the system, or the overall predictability of the model.

Table 3 - 2, Percent decrease in R^2 value of removing each variable from the regression model and running the k-fold test. All values with zero had no impact of the R^2 or their removal increased the predictability of the model

Variable	Hour (t or t-n)	WECC						CAISO					
		Improvement in Forecast Error (%)											
		-25	0	25	50	75	100	-25	0	25	50	75	100
Net Load (ρ_t), B_1	0												
Net Load (ρ_t), B_2	0												
Relative Net Load ($R\rho_t$), B_1	0												
Relative Net Load ($R\rho_t$), B_2	0												
Fraction VRE (g_t)	0												
	1												
	2												
	3												
	4												
Ramp Rate (ε_t)	0												
	0-1												
	0-2												
	0-3												
	0-4												
Relative Ramp Rate ($R\varepsilon_t$)	0												
	1												
	2												
	3												
	4												
	0-1												
	0-2												
	0-3												
	0-4												
Variability (μ_t)	0-1												
	0-2												
	0-3												
	0-4												
Hour (h), B_1	0												
Hour (h), B_2	0												
Hour (h), B_3	0												
Controls													
Week	0												

Just as CAISO and WECC have different variables that contribute most to the prediction of commitment error, it is likely that other regions will as well. Therefore, after modeling only one region of the country we cannot assume the variables we found most predictive would be most predictive in other grid regions. However, it would be useful for grid operators to understand the grid characteristics that are most likely to lead to greater errors in commitment in their own region making it important to run the regression on a regional basis.

Additionally, it is important to know the directionality of the relationships between variables and commitment error. The values in Table 3-2 provide information on each variable's

contribution to the predictability of the model, but does not provide information on the directionality of the relationships between variables and commitment error. Table 3-3 shows the value of each variables' regression model coefficient (i.e., the directionality of each relationship). The coefficients in Table 3-3 are for the final model after the k-fold test was used to subset the predictive variables.

Table 3 - 3, Correlation coefficients for each level of forecast error and region's final regression model. All values are on a log scale.

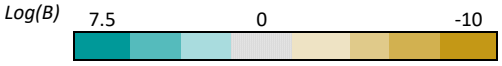

Variable	Hour (t or t-n)	WECC						CAISO					
		Improvement in Forecast Error (%)											
		-25	0	25	50	75	100	-25	0	25	50	75	100
Net Load (ρ_t), B_1	0												
Net Load (ρ_t), B_2	0												
Relative Net Load ($R\rho_t$), B_1	0												
Relative Net Load ($R\rho_t$), B_2	0												
Fraction VRE (g_t)	0												
	1												
	2												
	3												
	4												
Ramp Rate (ε_t)	0												
	0-1												
	0-2												
	0-3												
	0-4												
Relative Ramp Rate ($R\varepsilon_t$)	0												
	1												
	2												
	3												
	4												
	0-1												
	0-2												
	0-3												
	0-4												
Variability (μ_t)	0-1												
	0-2												
	0-3												
	0-4												
Hour (h), B_1	0												
Hour (h), B_2	0												
Hour (h), B_3	0												
Controls													
Week (HighVar)	0												
Week (LowRamp)	0												
Week (LowV)	0												

We discuss a few illustrative examples of the relationships found in WECC and CAISO for the most predictive variables. Again, the results in Table 3-3 are specific to modeling assumptions used in the PCM and should not be assumed to hold outside of this analysis.

The average coefficients across levels of forecast error for Net Load (ρ_t), and Relative Net Load's ($R\rho_t$), both important variables in predicting commitment error in CAISO, result in functions that are concave down with vertexes when the Net Load or Relative Net Load ($R\rho_t$) are very close to zero. This means that larger values for Net Load and Relative Net Load ($R\rho_t$) yield greater unplanned startups in the real-time. In a smaller region, the load is likely a stronger indicator of generator activity given that changes in load are distributed over a smaller number of generators. The Relative Net Load ($R\rho_t$) coefficients are more consistent across the two regions than actual Net Load (ρ_t). The Relative Net Load ($R\rho_t$), which is based on the net load relative to the day's peak load, could be an indicator of time of day, which has a strong influence on model predictability or ramp rate. For example, if the Relative Net Load is close to one, there is likely going to be a decrease in load in the future, which is more likely associated with unplanned shutdowns. The Net Load (ρ_t) variable does not capture this information as well, given the magnitude of the peak load is different between days.

The hour (*h*), a strong predictor of commitment error in CAISO, has coefficients that result in a function with peak in the morning hours and a trough in the evening hours. This is consistent with our hypothesis that the morning hours will have more unplanned shutdowns, due to rapid net load reductions, and evening hours will have more unplanned startups, due to rapid net load increases. Figure 3-5 illustrates this trend for CAISO but not for WECC. If an hourly trend exists in WECC the unplanned shutdowns caused by the hydro modeling are likely overshadowing it. In general, the significance of the hour variables could indicate a predictable trend in commitment error in certain hours of the day. If a consistent hourly trend exists this would be extremely helpful to improve generator scheduling. It would be relatively simple to overcommit the same hours each day if hours the model predicts unplanned startups.

When significant, Fraction VRE (g_t) and Ramp Rate (ε_t), both important predictors in WECC, have (near) consistent directional trends across levels of forecast error and region with the sign of the relationship alternating between hours. Fraction VRE (g_t), was the best predictor in hour four with a positive relationship, meaning the greater the percent VRE the more shutdowns.

For Ramp Rate (ε_t), the time between zero and three had the largest relative importance, with a negative relationship, indicating when ramp is large and positive there are more unplanned startups. This is the logical relationship; however, when examining the ramp across different time spans leading up to a given hour, the directionality of the correlation alternates. We believe that this result is driven by the minimum cycle times of the combustion turbine units. If a combustion turbine is committed, it must operate for at least two hours and if it is de-committed, it must remain off for at least two hours. In our model, the day-ahead and real-time commitments are optimized across the entire day. Therefore, commitment changes will happen with anticipation of future load levels resulting in the delayed correlations. Knowing the time increments that have the strongest impact of commitment error are extremely important to understanding how to improve generator schedules. It is important to note that the Fraction VRE (g_t) values are only within the hour (t-n) while the Ramp Rate (ε_t) spans hours (t to (t-n)).

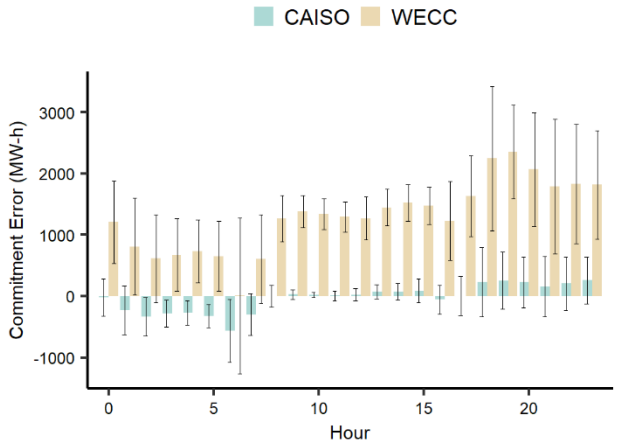

Figure 3 - 5, Average commitment-error in each hour for WECC and CAISO for all forecast errors and weeks. Error bars represent the standard deviation.

The week is also a significant predictor of commitment error, especially in WECC. The quantity of commitment error itself varies between the weeks, as seen in Figure 3-6.

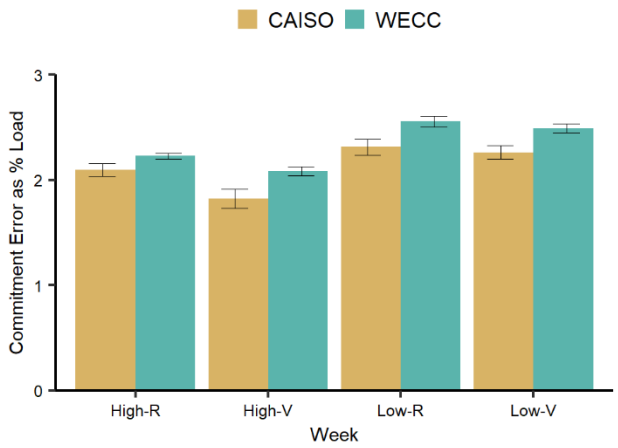

Figure 3 - 6, Impact of week on the average commitment relative to the average load for WECC and CAISO. Error bars represent the standard deviation of each value across forecast error scenarios when the x-axis is weeks and across weeks when the x-axis is forecast error (V=Variability, R=Ramp)

Given the *Low Ramp* (Low-R) and *Low Variability* (Low-V) weeks have greater commitment errors as a percent of load other factors are likely contributing to the weekly difference in commitment error, for example the percent of load supplied by VRE. As shown in Figure 3-7, *High Ramp* (High-R) and *High Variability* (High-V) weeks have larger loads and higher percentages VRE generation than the *Low Ramp* and *Low Variability* weeks. The relative differences between weeks illustrated are similar in CAISO and WECC; however, CAISO's percent of generation from VRE ranges from 39 to 56% where WECC's ranges from 26% to 36%. The week could also be representative of an underlying seasonal trend. If there is a seasonal skew in commitment error this could be additional knowledge to further improve scheduling.

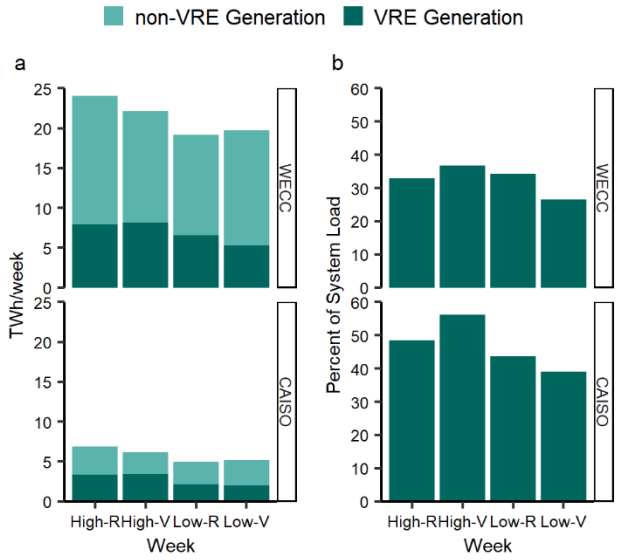

Figure 3 - 7, a) WECC and CAISO non-VRE generation and VRE generation post-curtailment and b) percent of load served by VRE. Generation is averaged over the forecast error cases. (VRE=variable renewable energy, V=variability, R=ramp)

We address these intra-hour ranges with the *Variability* (μ_t) variable, which had a constantly positive coefficient in the hour of interest, indicating that increased *Variability* (μ_t) correlates to an increase in unplanned shutdowns and a decrease in unplanned startups. The *Variability* (μ_t) coefficients in other time increments did not have consistent signs and were often insignificant. This is not surprising considering the logical relationship would be a correlation between the absolute value of commitment error and *Variability* (μ_t).

We did not find significant consistent relationships between *Relative Ramp Rate* ($R\varepsilon_t$) and commitment error. Although certain *Relative Ramp Rate* (εR_t) variables improved predictions, the direction of their relationship was not consistent across regions and levels of forecast error nor was their significance.

3.3.3. Model System Impacts

Given the results in this paper are specific to not only the regions modeled but how they were modeled, we cannot use the correlations found between specific variables and commitment error to make generalizations. However, we can say that the regression models were able to predict between 21-57% of commitment error in our test case, which suggests that this approach could be deployed in a manner that improves generator scheduling. However, in order to understand how successful the regression models are at reducing commitment error and improving operational

efficiency the PCM would need to be re-run with a modified commitment schedule based on the regression model output. This is an ideal area for future work. Given the incremental nature of commitment, small improvements in day-ahead commitment decisions will not mean equivalent improvements in real time dispatch. Additionally, there is much more complexity that could be added to this model. We could employ time series forecasting methods, like time series decomposition, exponential smoothing, or ARIMA models but we cannot say whether this added complexity would be worth the computational time without first testing the simple case in an updated PCM model.

CHAPTER 4

Reducing CO_2 emissions from U.S. steel consumption by 70% by 2050

Abstract

The steel sector emits 25% of global industrial greenhouse gases and the U.S. is the world's second-largest steel consumer. In this article, we determine how CO_2 emissions attributable to U.S. steel consumption can be cut by 70% by 2050. We vary four key steel flow parameters (U.S. steel stocks per capita, recycling rate, product lifespan, and manufacturing yield) in a dynamic material flow analysis to determine annual steel demand and the scrap available for recycling. We combine these data with steelmaking technology and trade scenarios to calculate potential U.S. steel sector emissions in each year to 2050. Only 20% of the pathways we modeled for the U.S. steel sector achieved the emissions target. Emissions in 2050 are most sensitive to the CO_2 released per kilogram of steel produced and the steel stocks per capita. Deployment of emerging low carbon steelmaking technology alone is insufficient to achieve the emissions cut; conversely, reducing stocks per capita from the current ~11 tons/capita toward levels in the U.K. and France, ~8 tons/capita, would enable the emissions cut to be achieved under a range of foreseeable steelmaking technology scenarios and steel flow parameters. If action to reduce per capita steel stocks is delayed by more than five years then it is likely infeasible for the U.S. steel sector to stay within its 2050 CO_2 budget because of the increased demand for emissions-intensive steel made from iron ore.

4.1. Introduction

All sectors of the economy will need to decarbonize significantly in order to stabilize the global temperature and prevent the most extreme consequences of climate change.[4] The Intergovernmental Panel on Climate Change (IPCC) recommends a cut in greenhouse gas (GHG) emissions of 41-72% by 2050 from 2010 levels in order to 'likely' stay below a 2°C temperature increase.[1] In 2017, the industrial sector, which produces materials, products, fuels and chemicals, accounted for 21% of the world's anthropogenic GHG emissions.[5] This percentage has likely shifted slightly since 2017 and has the potential to shift with changing economies. The production of a few key materials makeup the majority of industry emissions. Steel production alone accounted for 25% of global industry emissions in 2017,[3] and global steel demand is projected to double by 2050.[16] Wesseling et al. (2017) assert that energy-intensive processing industries, like steel, will need to have zero emissions before 2070 to meet the "well below 2°C" target.[28] However, despite industry's significant contribution to global GHG emissions, most decarbonization roadmaps (e.g., Rockström et al. (2017)) present little guidance for the industrial sector, and even less for the steel sector specifically, on how to achieve the necessary emissions cut.[4,28,130,131] Supekar and Skerlos (2017) outline how the U.S. could meet IPCC goals in the automotive and energy sectors,[132] but no analysis has been completed for the U.S. steel sector. This work seeks to fill that gap by determining pathways that reduce U.S. steel sector emissions by combining options to deploy emerging steelmaking technology with options for reducing steel demand. The U.S. is the world's second-largest consumer of steel behind China.[133] Therefore, the emissions attributable to the U.S. steel sector account for a significant portion of global steel sector emissions.

Steel sector emissions predominantly depend on the mass of steel consumed and the emissions released per kilogram of steel produced, which we term the emissions intensity (EI) of production. Several studies have sought to predict the mass of future steel flows. Yin and Chen (2013) use a stock-based dynamic material flow analysis model with stock forecasts based on relationships such as floor space per capita versus GDP.[35] Toi and Sato (1998), Hatayama et al. (2010), and Pauliuk (2012, 2013a) also predict future flows using stock-driven dynamic material flow analysis models. They model stock saturation by extrapolating logistic curves fitted to historical data of stocks per capita against time or GDP for select sectors.[36,37,134,135] Pauliuk et al.

(2013a)'s global steel demand prediction (2008-2018) had only a 6% error in annual demand and a 1% error in cumulative demand when compared to recorded World Steel Association values.[37,40] These papers make strides in predicting steel demand and highlight the use of stock-driven predictions of future steel flows. However, none of the above articles focus on the U.S. nor do they discuss the emissions implications of the predicted flows, which requires knowing what the production EIs are now and what they could be in the future.

The energy intensities of widely used steelmaking technologies are well documented in seminal works such as Cairns et al. (1998) and Worrell et al. (2007). Both include detailed data on the current process energy consumption of commercialized steelmaking technologies as well as potential reductions through best available technologies.[33,34] These energy intensities have been converted to EIs that can be found in academic publications[136–139] and grey literature.[33,140,141] Currently, there are no economically competitive low carbon primary steelmaking technologies. The technologies that show the greatest potential to reduce CO_2 emissions (e.g., electrolysis and hydrogen direct reduction) rely on expensive electrical energy and are currently 4 to 6 times more electricity intensive than the electric arc furnaces used to recycle scrap steel (Appendix C Section 4).

A few researchers have combined estimates of future steel flows (e.g., demand) and steelmaking EIs to predict future steel sector emissions; however, none have conducted a parametric study that reveals the options for how the sector needs to evolve over time in order to meet an emissions goal. Most studies do not consider potential changes to the demand trajectory,[138,142–147] and only a small subset consider changes to steelmaking technology.[3,38] Milford et al. (2013)'s global analysis is the most comprehensive found in the literature. Their analysis includes both supply (e.g., electrolysis deployment) and demand (e.g., more intense material use) emission reduction options. Globally, the effect on emissions of improving supply-side technology is negated by increasing demand for emissions-intensive primary steel to build-up societal stocks in the developing world. Subsequently, Milford et al. find that even aggressive deployment of supply-side efficiency measures can only reduce global steel sector emissions by 20% by 2050.[137] In contrast, U.S. steel consumption per capita has plateaued since the 1980s.[148] Without a U.S. focused study, it is unclear whether supply-side measures alone are sufficient for the U.S. steel sector to meet the emissions target.

4.1.1. Scope of this Work

The goal of this study is to define pathways that cut CO_2 emissions attributable to U.S. steel consumption by 70% from a 2010 baseline by 2050, which is close to the maximum reduction recommended by the IPCC.[1] We focus on CO_2 emissions because it accounts for 93% of the GHG emissions from primary and secondary steel production.[149]

Each pathway defined in this analysis is a unique combination of *steelmaking technology scenarios*, *trade scenarios*, and *steel flow parameters*, together representing a comprehensive suite of options for reducing emissions. Therefore, this analysis informs an evaluation of the efficacies and trade-offs between a supply-side technology driven and/or demand driven emissions reduction strategy for the steel sector. The *steelmaking technology scenarios* determine the EI of primary and secondary steelmaking in the U.S. and the rest of the world (ROW). The *trade scenarios* determine the percentage of U.S. steel consumption that is produced overseas. This analysis focuses on emissions attributable to U.S. steel consumption and therefore includes emissions released outside of the U.S. in order to make steel for U.S. consumption. The four *steel flow parameters* (U.S. steel *stocks per capita*, *recycling rate*, *steel lifespan*, and *manufacturing yield*) determine future steel demand and the availability of scrap for recycling. Policy interventions (e.g., to increase *recycling rates*) could be made, or societal or commercial shifts (e.g., towards longer product *lifespans*) could be realized that reduce future steel demand. Therefore, a range of values is modeled for each steel flow parameter in 2050. A business as usual (BAU) pathway is defined as equal to the base case *steelmaking technology* and *trade scenario* and base case set of *steel flow parameters* (see *Methodology*).

This article is intended to be useful to a broad audience, including industry, policymakers, and researchers. Each of these stakeholders has the potential to take action that could shift the steel sector towards a lower emissions pathway.

4.2. **Methods**

The methods section explains how the annual and cumulative CO_2 emissions were calculated for each simulated pathway of the future U.S. steel sector (4.2.1), and how the *steelmaking technology scenarios* (4.2.2), *trade scenarios* (4.2.3), and *steel flow parameters* (4.2.3) were defined and combined.

4.2.1. Calculating U.S. steel sector emissions and targets

The annual CO_2 emissions attributable to U.S steel consumption, $Annual\ emissions_{t,i}$ in year *t* (2020-2050) under simulated pathway *i*, were calculated using eqn. 1:

$$Annual\ emissions_{t,i} = \sum_{tech}\left(prod^{U.S.}_{t,i,tech} \times EI^{U.S.}_{t,i,tech}\right) + \sum_{tech}\left(prod^{ROW}_{t,i,tech} \times EI^{ROW}_{t,i,tech}\right), \quad (1)$$

where $prod^{U.S.}_{t,i,tech}$ and $prod^{ROW}_{t,i,tech}$ are the masses of steel produced for U.S. consumption by each steelmaking technology in the U.S and the ROW respectively; and, $EI^{U.S.}_{t,i,tech}$, and $EI^{ROW}_{t,i,tech}$ are the EIs of those steelmaking technologies in the U.S. and the ROW respectively. This research focused on emissions released from steelmaking (i.e., the conversion of iron ore to steel or the melting of scrap), which accounts for 70-77% of the CO_2 emissions released during the production of a steel part.[149] The majority of the remaining emissions are indirect emissions from the generation of electricity used to power manufacturing processes.[150]

The IPCC emissions targets are in reference to 2010. As with pathway emissions (eqn. 1), 2010 emissions are dependent on steel flows (collected from World Steel Statistical Yearbook)[40] and production EIs (Appendix C Section 6).

4.2.2. The emissions intensity of production: Steelmaking technology scenarios

Four *steelmaking technology scenarios* determine the EIs used in eqn. 1. Each scenario defines the mix of primary and secondary steelmaking technologies and the EI of the electricity grid for each year (2020-2050) in the U.S. and the ROW. The scenarios were defined by identifying emerging steelmaking technologies (section 2.2.1); calculating the EI of the steelmaking technologies (section 2.2.2); and, then determining their feasible market share by 2050 (section 2.2.3). All the *steelmaking technology scenarios* are equal in 2020. After 2020, they begin to

diverge as the market share of emerging technologies increases at a constant rate ultimately matching the unique scenario values in 2050.

4.2.2.1. *Identifying emerging steelmaking technologies*

Most primary steelmaking facilities in the U.S. and the ROW currently include a **Blast Furnace** (BF) that converts iron ore, coke and sinter to pig iron, and a **Basic Oxygen Furnace** (BOF) that converts pig iron to raw steel. The BF is the most emissions intensive step in conventional primary steelmaking, driven by indirect emissions from the coking process and direct emissions from fuel burning and reduction of the iron ore. Therefore, for the EI of primary steelmaking to reduce significantly the conventional BF must be improved or superseded. Alternative commercial and emerging steelmaking technologies were identified through a literature review[29,151–154] and interviews with industry experts.[155–157]

An adaptation of the conventional BF that lowers the EI is **BF top-gas recycling** where the CO from the BF off gases is fed back into the furnace. The returned CO acts as a reductant and displaces the use of coke. Direct reduction (DR) can decrease emissions further by reducing iron ore to direct reduced iron (DRI) without the emissions intensive coking process. DRI is a sponge iron that must go through an EAF or a BOF to produce steel. DR can use a variety of fuels. **Coal-DR** and **NG-DR** (natural gas-DR) are commercialized steelmaking technologies, but globally produce less than 5% of all primary steel. **H-DR** (hydrogen-DR) is an emerging steelmaking technology and could release near to zero emissions if the hydrogen were produced using electrolysis powered by a renewable electricity source. **Smelt reduction** (SR) and **steel electrolysis** are both emerging primary steelmaking technologies that also eliminate the coking process. SR reduces pelletized iron ore or fines in a two-step process with coal gasification. Steel electrolysis is electricity intensive (2,692 kWh/t steel) but could greatly reduce the EI of steelmaking if powered by decarbonized electricity (Appendix C Section 4).

Recycling steel scrap in the U.S. and the ROW currently occurs either in an **EAF** (secondary steelmaking) or in the BOF, where it cools the molten pig iron. For secondary steelmaking, we identified no rival technologies to the EAF. Approximately 73% of EAF emissions are from electricity generation (Appendix C Section 4); however, some direct emissions

are released from burning natural gas within the furnace, which provides up to 30% of the energy.[158]

Other steelmaking processes considered in this study but excluded from the *steelmaking technology scenarios* include the paired straight hearth furnace (**PSH**), hydrogen flash ironmaking technology (**FIT**), and carbon capture and storage (**CCS**) (Appendix C Section 4). PSH is an emerging technology that uses coal to produce DRI but is more emissions intensive than commercially available NG-DR. FIT is an emerging steelmaking technology similar to DR but requires almost twice as much hydrogen as H-DR.[136,159] CCS could remove CO_2 from the BF exhaust gas but has a limited potential to reduce emissions: a European Steel Association analysis found that equipping all BFs in the E.U. with CCS by 2050 would lower annual emissions by only 60% compared to 1990.[160] CCS is also expensive (200 to 500 USD/tCO_2),[3] and it is unproven at an industrial scale.[160]

4.2.2.2. *Calculating the emissions intensity of steelmaking technology*

Figure 4-1 shows the EIs of the steelmaking technologies included in the *steelmaking technology scenarios* at different electricity EIs. The EI of each steelmaking technology includes the direct emissions from burning fuels (e.g., coke in the BF), and indirect emissions from electricity generation and the production of feedstocks (e.g., sinter in smelt reduction). For most commercial steelmaking technologies, direct emissions, feedstock and electricity requirements were found in academic publications[136–139] and grey literature.[33,143,160] However, the EIs of emerging steelmaking technologies, which have yet to see commercial use (e.g., electrolysis), are less well reported. They were derived from data sources that publish anticipated reductions in emissions compared to existing technologies; e.g., the European Steel Associations Low Carbon Roadmap (2013) reported that making steel using electrolysis can reduce CO_2 emissions by 98% compared to using a BF (Appendix C Section 4).[160,161]

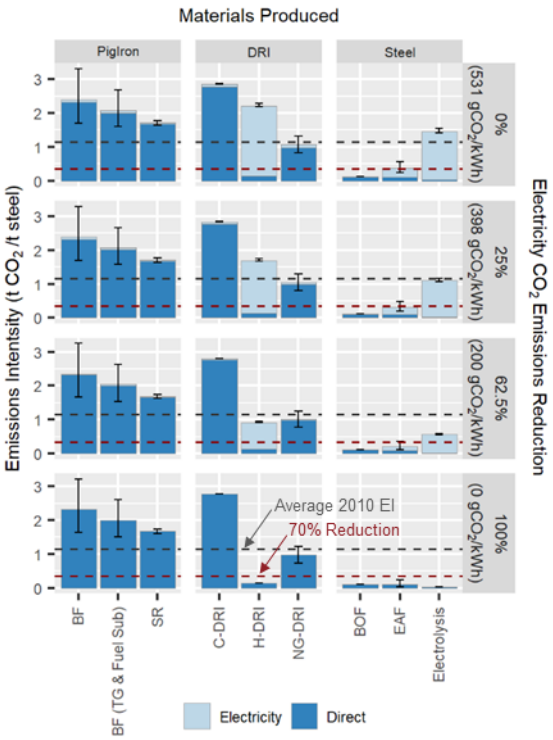

Figure 4 - 1, Steelmaking technology CO_2 emissions intensity (EI) at different levels of electricity decarbonization. Pig Iron and direct reduced iron (DRI) must also go through either the BOF or the EAF to become steel. 2010 U.S. electricity EI = 531 gCO_2/kWh. BF = blast furnace, TG = top gas recycling, SR = smelt reduction, C = coal, H = hydrogen, NG = natural gas, EAF = electric arc furnace

4.2.2.3. *Market share of low carbon technology by 2050*

Table 4-1 defines the four *steelmaking technology scenarios* used in this analysis. In the base case scenario (highest emissions), the market share of each steelmaking technology and the EI of the electricity grid is the same in 2050 as it was in 2020 (421 g CO_2/kWh). The three other *scenarios* represent increasingly aggressive steelmaking decarbonization (decreasing EIs).

Figure 4-1 shows that the greatest potential to reduce steelmaking emissions is rapid deployment of H-DR and steel electrolysis coupled with a decarbonizing electricity grid. However, Fischedick et al. (2014) and Wyns et al. (2016), in comprehensive reviews of the potential for deep decarbonization in primary steelmaking, predict that H-DR and steel electrolysis will not be fully commercialized until 2030 and 2040 respectively because they are uneconomical at current electricity prices without subsidies.[29,30] Therefore, even in the low emissions *steelmaking*

technology scenario, H-DR and steel electrolysis were limited to a 20% and 15% market share by 2050 respectively (Appendix C Section 4).

SR is also not anticipated to be fully commercialized until 2030 or later[152,160] and has a limited potential to reduce emissions compared to the BF (Figure 4-1) and was therefore kept at a 5% market share by 2050 in each scenario.

NG-DR is already used at a commercial scale; therefore, it is expected that its market share could grow significantly by 2050. However, because the EI of NG-DR is still greater than 50% of the BF/BOF route, NG-DR was limited in the scenarios to a 40% market share to leave a share for cleaner technologies (e.g., steel electrolysis).

The BF remains a significant source of primary steel in all the scenarios. BF top gas recycling and fuel substitution only offers a small reduction in the BF EI. However, BF top gas recycling and fuel substitution is assumed to be widely deployed by 2050 in the high, medium, and low *steelmaking technology scenarios* because it is a (relatively simple) retrofit to existing BF facilities (Table 4-1).

The EI of the electricity grid was varied across the *steelmaking technology scenarios*, because it has a significant effect on the overall steelmaking EI (Figure 4-1). In 2018, electricity generation from low carbon resources accounted for only 17% of the supply in the U.S.[162] and 26% globally.[163] Many studies have shown that 80-100% renewable grids are feasible.[8–10,12] Therefore, in the low emissions *steelmaking technology scenario*, a 100% reduction in electricity emissions is assumed by 2050 (Table 4-1).

Table 4 - 1, Parameter values for each technology scenario

	Technology Scenarios				
	Base Case (highest) Emissions (2020-2050)		High Emissions (2050)	Medium Emissions (2050)	Low Emissions (2050)
Primary EI					
U.S. (t CO_2/t steel)	2.25		1.77	1.40	0.970
ROW (t CO_2/t steel)	2.31		1.81	1.42	0.970
Secondary EI					
U.S. (t CO_2/t steel)	0.313		0.260	0.180	0.100
ROW (t CO_2/t steel)	0.346		0.285	0.192	0.100
Electricity Grid Emissions					
% Electricity Emissions Reduction	0%		25%	62.5%	100%
U.S. Electricity EI (g CO_2/kWh)	421[164]		316	158	0.00
ROW Electricity EI (g CO_2/kWh)	485[164]		364	182	0.00
Primary Steelmaking Market Share 2050	**U.S.**[40,165,166]	**ROW**[40,166]	**U.S. & ROW**		
Electrolysis	0%	0%	10%	12.5%	15%
Coal-DR	0%	1%	0%	0%	0%
NG-DR	10%	6%	20%	30%	40%
H-DR	0%	0%	5%	12.5%	20%
Smelt Reduction	0%	<1%	5%	5%	5%
Blast Furnace	90%	93%	60%	40%	20%
Top Gas Recycling as fuel substitution % of BFs in 2050	0%[167]	0%[167]	80%	90%	100%
Secondary Steelmaking Market Share					
EAF	100%		100%	100%	100%

4.2.3. Mass of steel produced by each steelmaking technology

The mass of steel produced each year by each steelmaking technology in the U.S. and the ROW (needed in eqn. 1) was calculated by:

- First, using the *steel flow parameters* to determine the annual steel demand and scrap available for secondary steelmaking (section 2.3.1);
- Second, using the *trade scenario* to determine the amount of that steel demand that will be produced in the ROW and the amount of scrap that will be exported (section 2.3.2);
- Third, using an annual mass flow analysis to combine the steel demand, available scrap, imports/exports, and steelmaking technology mix to calculate the annual mass of steel produced by each steelmaking technology (section 2.3.3).

4.2.3.1. *Calculating U.S. steel demand and scrap availability*

Annual steel demand and scrap availability depend on the *steel flow parameters*: the quantity of steel *stocks per capita* needed to provide material services (e.g., infrastructure); the *lifespan* of steel that determines how often it needs to be replaced; the *recycling rate* that determines the percentage of available scrap from discarded products collected for U.S. recycling or export; and, the *manufacturing process yield* that determines the steel required per kilogram of finished steel product. This analysis simulated changes to the *steel flow parameters* at a constant rate from their values in 2020 to a range of feasible values in 2050 (Table C-1).

A dynamic material flow analysis (DMFA) was used to calculate the annual scrap availability and steel consumption. Based on when a material enters use (i.e., stock), a DMFA uses a *lifespan* distribution to predict when it leaves use as scrap. Not all steel products have the same *lifespan*; therefore, steel flows were disaggregated into four demand sectors (construction, transport, machinery, and products) and assigned unique *lifespan* distributions taken from the literature (Table C-6).[164–167] The annual scrap availability, $Scrap_{t,s,i}$, in demand sector *s* under simulated pathway *i*, was calculated using eqn. 2 for *t* = 2020, 2021, ..., 2050:

$$Scrap_{t,s,i} = \sum_{t_o=1880}^{t} Consumption_{t_o,s,i}\, L_{t-t_o}\left(\mu_{t_o,s,i}, \sigma_{t_o,s,i}\right), \quad (2)$$

where $Consumption_{t_o,s,i}$ is the annual consumption of steel products in demand sector *s* in year t_o (dating back to 1880) under pathway *i*, and L_{t-t_o} is the discrete *lifespan* normal distribution of steel with a mean *lifespan* of μ years and a standard deviation of σ years. L_{t-t_o}determines the probability that steel entering use in year t_0 will leave use as scrap in year *t*. Increasing the product *lifespan* delays when a product will be scrapped, reducing annual scrap availability (eqn. 2), replacement rate, and consumption (eqn. 3). Steel sector pathways were simulated for steel *lifespans* (μ and σ) that in 2050 are +/- 30% of the 2020 values (Table C-6). Base case *lifespans* are kept at 2020 values. One set of analyses simulated the effect of changing the *lifespan* of only new products (non retrofit case; eqn. 2), and another set of analyses simulated

the effect of changing the *lifespan* of both new and existing products (retrofit case; Appendix C Section 2.3). The base case simulated unchanged product *lifespans* between 2020 and 2050.

The annual steel consumption ($Consumption_{t,s,i}$) in demand sector *s* in future year *t* was calculated using eqn. 3 (a stock-driven DMFA).

$$Consumption_{t,s,i} = \left(STC_{t,s,i}Pop_{t,i} - STC_{t-1,s,i}Pop_{t-1,i}\right) + Scrap_{t,s,i}, \quad (3)$$

where $STC_{t,s,i}$ is the *stocks per capita* in demand sector *s* in year *t* under pathway *i*, and $Pop_{t,i}$ is the U.S. population in year *t*. Consumption is modeled as a function of stocks because it is the demand for material services (e.g., commercial real estate) provided by the in-use stock that drives the material cycle for materials with long product *lifespans* (e.g., steel).[168,169] By connecting stocks and consumption, we can begin to understand how the design and use of steel products will have to change in order to reduce consumption.

The U.S. steel *stock per capita* in 2020 was estimated to be 10.7 tons/capita using methods from Cooper et al. (2020) (Appendix C Section 2.1).[148] The range of simulated *stocks per capita* values in 2050 was based on the range of *stocks per capita* saturation values found in the literature for developed countries (8-14 tons/capita).[170] In the BAU pathway, the *stocks per capita* followed a logistic saturation curve as a function of time (Appendix C Section 2.3.1), rising from 10.7 tons/capita in 2020 to 11.4 tons/capita in 2050. Otherwise, the *stocks per capita* was simulated at a constant rate of change between 2020 and 2050. The base case U.S. population is modeled at 331 million in 2020 and 389 million in 2050, as predicted by the U.S. Census Bureau.[171] In order to account for the uncertainty in this population projection (eqn. 3), we modeled steel emissions for a range of population growth rates (Table C-1); from no population growth to a population of 452 million by 2050 (similar to the U.S. Census Bureau's high migration scenario).[172]

The DMFA calculated the future annual U.S. steel consumption of finished goods. However, this is not equal to the quantity of steel that must be produced (the steel demand) because scrap is generated in manufacturing between the production of intermediate steel goods (e.g., slabs) and finished steel components (e.g., car doors). The ratio by mass of finished to intermediate goods is called the *manufacturing process yield* and was used to calculate the annual steel demand.

Globally, the mean *manufacturing process yield* is 78%.[16] Many researchers have advocated improving this yield,[16] which could reduce manufacturers' material costs.[16] Therefore, alongside a base case process yield value of 78% (unchanged between 2020-2050), we also simulated the case of *manufacturing process yields* increasing at a constant rate from 78% in 2020 to 88% in 2050.

The DMFA calculated the future annual generation of scrap from discarded products but not all of the scrap produced is recycled (secondary production). The percentage of this scrap collected for domestic recycling or export is equal to the *recycling rate*. The aggregate recycling rate in 2020 was 79% (Table C-7).[147,173,174] In the base case, *recycling rates* remained unchanged between 2020 and 2050. There is scope for *recycling rates* to increase but there are also pressures that could reduce *recycling rates* (e.g., due to a decrease in demand for low quality recycled steel products (Cooper et al. 2020)); therefore, we modeled a range of *recycling rates* in 2050 that are +/-10% compared to the 2020 values.

4.2.3.2. *Calculating steel imports and scrap exports: Trade Scenarios*

International trade of steel and steel scrap must be tracked because the U.S. and the ROW currently use different steelmaking technology, have a different ratio of primary to secondary steelmaking, and have different electricity EIs. Three *trade scenarios* (high, medium, zero; Table C-8) were simulated in this analysis to encompass the range of possible foreign policy effects on iron ore, steel, and scrap trade. The scenarios define the percentage of U.S. steel consumption provided by imports and the percentage of collected U.S. scrap that is exported. All the trade scenarios model a constant rate of change over time from 2020 to 2050. The highest trade scenario reflects an extension of the free trade seen before the imposition of the 2018 U.S. steel import tariffs.[175] The base case is the medium *trade scenario*.

This study used the recycled content method[176] to account for emissions attributable to trade. No credit (i.e., negative emissions) was assigned to U.S. scrap exports but the recycled content of imports was included in the EI of the ROW steelmaking.

4.2.3.3. *Annual mass flow analysis: calculating production routes*

An annual mass flow analysis was used to calculate the mass of steel produced by each steelmaking technology in the U.S. and ROW in each year of the simulated steel sector pathways.

The annual mass flow analysis combined the simulated steel demand, scrap collection, steel imports, and scrap exports with the steelmaking technology mix. The mass flow (Figure C-30) was made determinant by using a linear optimization, with the masses of steel produced by domestic steelmaking technologies as decision variables. The optimization minimized domestic primary steelmaking subject to scrap supply and steel demand constraints. In turn, this maximized the use of scrap in secondary steelmaking. The optimization objective function is reflective of real-world practice because secondary steelmaking is cheaper than primary steelmaking.

The mass of steel produced using each steelmaking technology in the ROW was determined by the U.S. steel consumption, the *trade scenario*, the predicted ratio of primary to secondary steelmaking in the ROW 2020-2050 from Pauliuk et al. (2013),[37] and the technology mix in each simulated *steelmaking technology scenario* (Table 4-1).

4.3. **Results and Discussion**

In this analysis, we simulated 329,284 distinct pathways for the future of the U.S. steel sector (Table C-1). The BAU pathway results in annual emissions of 129 Mt CO_2 in 2050 and 3.4 Gt of cumulative CO_2 emissions (2020-2050): 278% and 58% above the annual, 34 Mt, and cumulative, 1.7 Gt, emissions target respectively. Only 1 in 5 of the pathways successfully meet the requirement that CO_2 emissions attributable to U.S. steel consumption are reduced by 70% by 2050. Figure 4-2 illustrates the sensitivity of meeting the CO_2 emissions targets to the *steelmaking technology scenario*, *trade scenario*, and *steel flow parameters*. Figure 4-2 shows how the percentage of pathways that meet the targets changes when switching between extreme scenarios and 2050 *steel flow parameter* values.

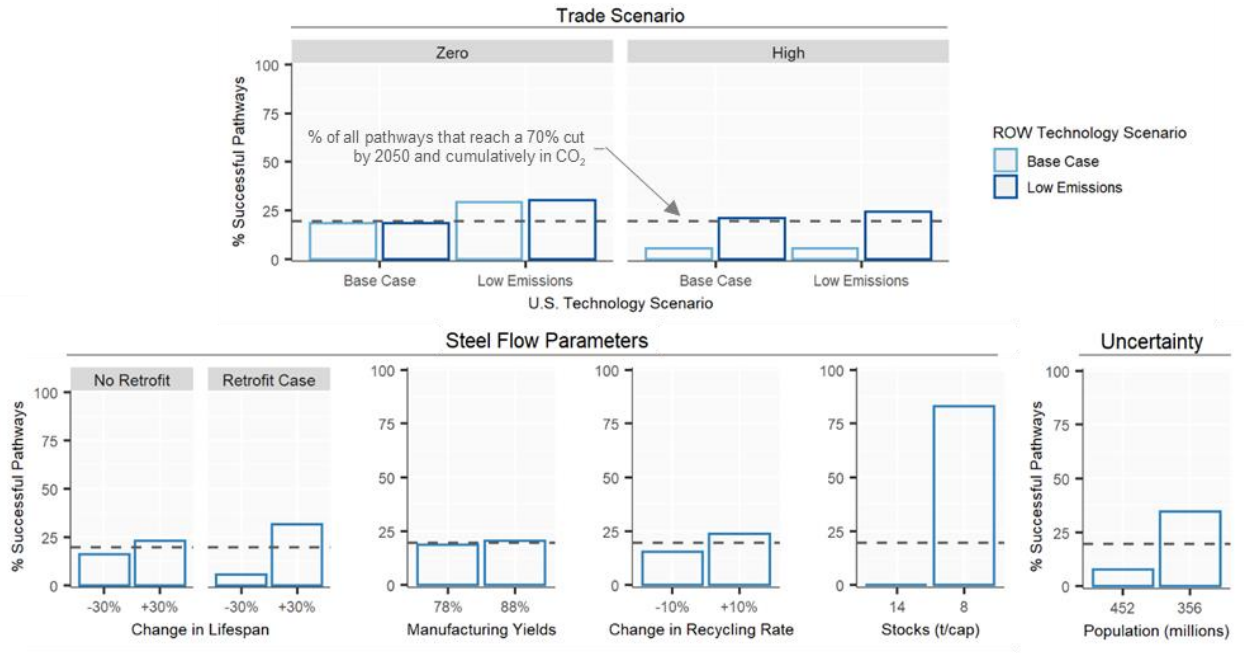

Figure 4 - 2, The percentage of pathways that meet the 2050 annual and cumulative CO_2 emissions targets (i.e., a successful pathway) for extreme trade scenarios (top), steelmaking technology scenarios (top), steel flow parameters in 2050 (bottom), and values for the U.S. population in 2050 (bottom-right). The Base Case steelmaking technology scenario (Table 4-1) is the highest emissions steelmaking scenario. The percentage changes in recycling rate and lifespan represent changes from the base case values listed in Table C-7 and Table C-4. ROW = Rest of World

Figure 4-2 shows that U.S. emissions are most sensitive to the *steelmaking technology scenario*, *stocks per capita*, *product lifespan*, and *population*. Figure 4-3 shows how these *steelmaking technology scenarios* and *steel flow parameters* combine to determine the annual emissions in 2050, and which combinations stay within the emissions limits. Appendix C Section 8 includes results figures for all 329,284 simulated pathways.

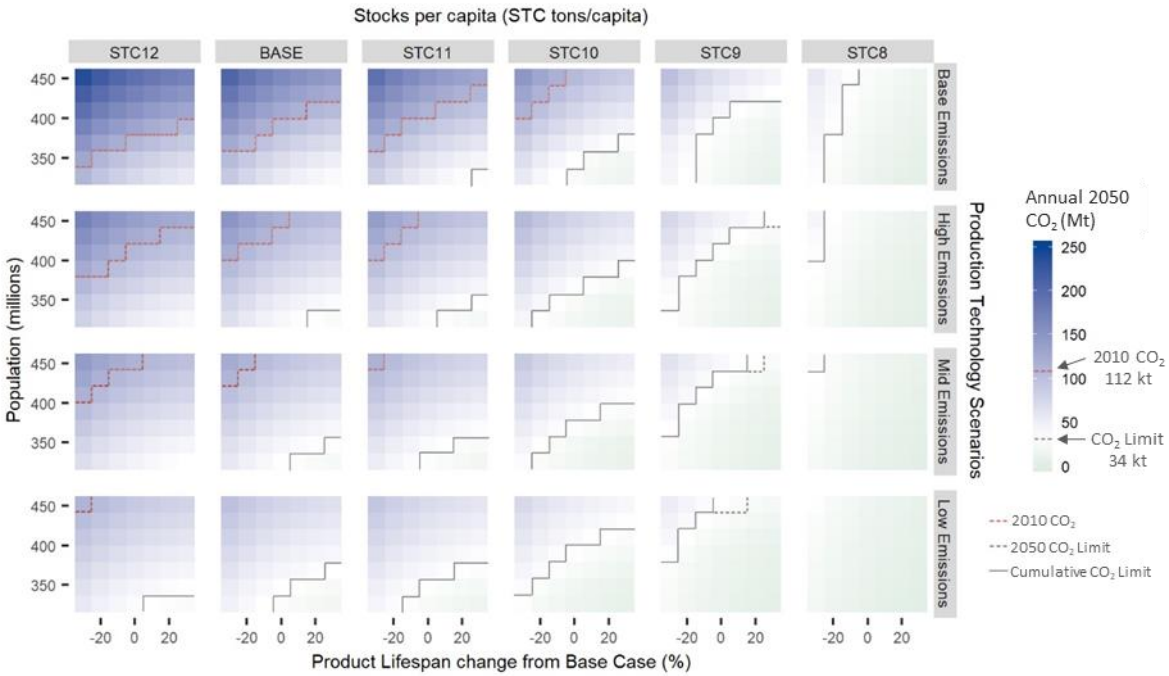

Figure 4 - 3, Annual emissions attributable to U.S. steel consumption in 2050. The gray lines mark the divisions between pathways that do (green) and do not (blue) achieve the emission targets. Results generated for the base case *trade scenario*, *recycling rate*, *manufacturing process yield*, and product *lifespan* under the retrofit case. The expected U.S. population in 2050 is 389 million people (middle row in each facet)

All of the pathways that meet the emissions targets represent a significant departure from BAU steelmaking and steel demand; extraordinary action is likely required by industry and government to sufficiently reduce emissions. Figure 4-3 shows that reducing the EIs of steel production and the steel *stocks per capita* will have the greatest impact on emissions, and are discussed in sections 3.1 and 3.2 respectively. Section 3.3 discusses the effect on emissions of varying product *lifespans*, *recycling rates*, and the *manufacturing process yield*. Section 3.4 addresses the effect of delaying action on the feasibility of meeting the cumulative CO_2 emissions target.

4.3.1. Changes Needed in Steelmaking Technology

If the steel sector continues to use its current technology, then it is highly unlikely that the emissions targets will be met. Figure 4-3 shows that only 4% of pathways with the base case *steelmaking technology scenario* stay within the CO_2 emissions limits. This 4% of pathways represented an average reduction in domestic primary production of 94% between 2019 and 2050. Additionally, Figure 4-3 shows that even under the lowest emissions *steelmaking technology scenario*, the emissions targets can only be met if there has also been a reduction in *stocks per*

capita, a reduction in expected *population* growth, or an increase in *product lifespans* by 2050. Meaning, less carbon intensive steelmaking does not guarantee that the emissions targets will be met.

Decarbonization will likely require a reduction in *stocks per capita* (Figure 4-3). Figure 4-4 shows the relationship between reductions in *stocks per capita* and the deployment of low carbon steelmaking technologies. For any level of *stocks per capita* in 2050, there exists a theoretical range (shaded in green) of primary and secondary steelmaking EIs that would allow the U.S. to succeed in meeting the 2050 annual emissions cut. However, even under the low emissions steelmaking *technology scenario*, the *stocks per capita* must be reduced to at least 10 tons/capita by 2050 for the emissions targets to be achieved.

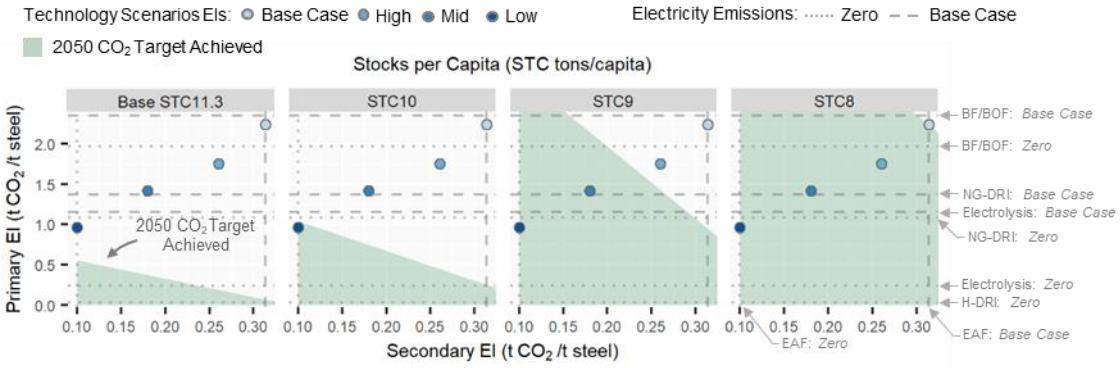

Figure 4 - 4, Primary and secondary steelmaking EIs needed by 2050 to achieve a 70% cut in annual emissions from 2010 levels under varying *stocks per capita* (STC) values in 2050 (green regions) compared to *technology scenario* emissions intensities (EIs). The data plotted is for the base case *trade scenario*, *recycling rate*, and *manufacturing process yield*

The primary steelmaking EI is the main barrier to the emissions targets being met (Figure 4-4). Unfortunately, low carbon primary steelmaking technologies (H-DRI and electrolysis) are not expected to be fully commercialized for another 10 to 20 years. Furthermore, Figure 4-4 shows the importance of a decarbonized grid in the development of low carbon steelmaking: the emissions target is unachievable with today's electricity EI irrespective of the steelmaking technology if not accompanied by a reduction in *stocks per capita* to at least 9 tons/capita.

Hazardous Air Pollutant standards,[177] which exclude GHGs, are currently the only air emissions regulations on U.S. steelmaking plants. The U.S. government could attempt to motivate the development of H-DRI and electrolysis by introducing GHG regulations; however, given low

carbon technologies are currently uneconomical the increased costs could cause a shift to greater international production. The U.S. government could also provide research and development grants aimed at reducing the operation costs of H-DRI and electrolysis, and production and investment tax credits to motivate the construction of low emissions steelmaking plants in the U.S. However, given the short time frame for action, these actions would likely be insufficient to meet the emissions target. Additionally, Figure 4-2 shows that high levels of trade limit the ability to decarbonize U.S. consumption through domestic action alone. This is because imported steel has a lower recycled content than domestically sourced steel. The U.S. could try to use the advancement of low emissions technologies and foreign policy to help motivate a shift to using low emissions steelmaking technology in the ROW.

4.3.2. Options to reduce U.S. steel stocks per capita

Of the *steel flow parameters*, changing the *stocks per capita* has the greatest effect on emissions. Figure 4-2 shows that a reduction to 8 tons/capita by 2050 increases the percentage of pathways that stay within the emissions limits to above 83%. Figure 4-4 shows that at 8 tons/capita the emissions targets are likely to be achieved even without a change in steelmaking technology. 8 tons/capita is equal to the saturated *stocks per capita* in the U.K. and France,[168] illustrating that a high standard of living can be maintained at a lower *stocks per capita* value.

U.S. *stocks per capita* can be reduced by either decreasing steel consumption (i.e., any additions to stock) or prematurely discarding, recycling, and not replacing existing steel products (e.g., demolishing a functioning building). Given 64% of the steel stocks that will exist in 2050 have yet to be built (Figure C-39), there is significant scope for reducing *stocks per capita* by reducing additions to stock and there is no need to discard steel prematurely in order to reduce in-use stocks. If all new U.S. steel consumption 2020-2050 is used at an intensity of 8 tons/capita then aggregate U.S. stocks by 2050 will have reduced to 9.7 tons/capita; thus, enabling the emissions targets to be met without extreme steelmaking decarbonization (Figure C-39).

Reducing additions to stock can be achieved by making products that contain less steel (i.e., lightweighting) or by making fewer products. The first option (lightweighting) is perhaps the most attractive politically as its effects are largely invisible to the final user. Carruth et al. (2011) found that most new steel products could be 30% lighter[178] without a loss in performance. If all steel products made between 2020 and 2050 are 30% lighter than equivalent products today then

aggregate U.S. stocks will be 9.9 tons/capita by 2050. The second option, making fewer steel products, could occur without government intervention if the U.S. economy continues to shift toward online shopping and remote working. If the expected steel demand (2020-2050) for new office buildings, commercial real estate, and transport is halved then aggregate U.S. stocks will be 9.3 tons/capita by 2050.

This transition to lower *stocks per capita* could be supported by incorporating steel utilization targets[179] into green building rating systems (e.g., LEED)[180], mandating that new infrastructure be bikeable and walkable, and increased funding for public transportation. Government could also act as an exemplar in the construction of new lightweight government buildings and remote working practices. Examining the connection between societal characteristics (e.g., population density, transportation infrastructure, location of commercial areas etc.) and steel stocks (particularly in the U.K. and France versus U.S.) could reveal other methods of reducing U.S. steel *stocks per capita*.

Reducing *stocks per capita* decreases the annual steel consumption. For the pathways simulated in this study that successfully meet the emissions requirement, the average quantity of steel produced domestically in 2050 by primary and secondary steelmaking is 3.2 Mt and 58 Mt respectively. Compared to 2019, this represents an 86% cut in primary steelmaking but only a 6.4% cut secondary steelmaking. This means that most of the eight BF facilities currently operating in the U.S. would likely need to close by 2050.[181,182] The consequent job losses could have significant impacts due to the concentration of BFs in the Midwest.

4.3.3. Product lifespans, Recycling rates, and Process yields

Of the other *steel flow parameters*, changing the *lifespan* (retrofit case) has the greatest impact on emissions. However, increasing the *lifespan* of only new products (Figure 4-2: product lifespan non-retrofit), potentially through more durable or modular designs, will result in a negligible decrease in emissions across 2020-2050 because the mean steel product lifespan is already 44 years (Figure 4-2). On the other hand, increasing the lifespan of both new and existing products by 30% (Figure 4-3: product lifespans, retrofit case) increases the number of pathways that meet the emissions requirement by 25%. Lifespan extension could be promoted by reducing value added taxes on repairs and remanufacturing, as implemented by Sweden in 2016.[183]

Figure 4-2 shows that increasing the *recycling rate* or the *manufacturing process yield* causes a minimal increase to the percentage of pathways that achieve the emissions targets. Increasing the recycling rate changes the ratio of primary to secondary steelmaking but does not affect the aggregate steel demand. The effect of generating manufacturing process scrap is only to add an industry recycling loop, which generates minimal emissions. Additionally, improving process yields can reduce a manufacturer's material costs, meaning that the profit motive alone should increase yields.

4.3.4. Time frame for action

Immediate and significant action is required to meet the emissions targets. These actions, shifting towards low carbon steelmaking and reducing *stocks per capita*, will take time to implement. However, the U.S. does not have long before the cumulative target is no longer feasible. Figure 4-5 shows that if no action is taken (BAU) then the cumulative U.S. steel sector CO_2 budget 2020-2050 will run out in 2031. If action to reduce *stocks per capita* and steelmaking *emissions* is delayed by more than 5 years then it is likely infeasible for the U.S. steel sector to stay within the budget. However, immediate action towards low carbon steelmaking and a reduction in *stocks per capita* towards 8 tons/capita by 2050 will achieve the emissions target with over one-fifth of the emissions budget remaining in 2050.

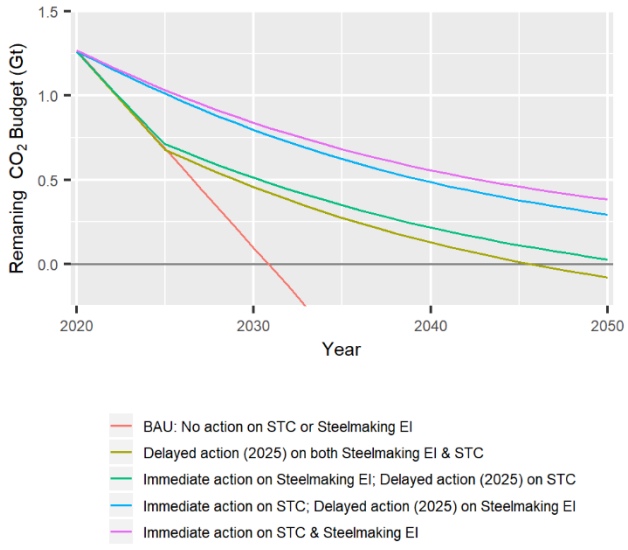

Figure 4 - 5, The remaining U.S. steel sector cumulative CO_2 budget 2020-2050 under different pathways. Modeled for the base case *trade scenario*, steel *lifespans*, *manufacturing yield*, *recycling rate*, and expected population. Action on STC: a constant decrease in STC at -0.11 t/cap/year. If not delayed, would reach 8 t/cap in 2050. Action on steelmaking EI: a constant decrease in primary (-46 $kgCO_2$/t steel/year) and secondary steelmaking EI (9 $kgCO_2$/t steel/year). If not delayed, would reach the values for the low emissions technology scenario (Table 4-1) by 2050.

CHAPTER 5

Conclusion

Each chapter of this dissertation addresses decarbonization challenges in different sectors and at different levels of specificity, with the goal of producing guidance or implementable methods to address the challenges presented. To achieve the emissions reductions necessary to reach IPCC targets all sectors and all challenges, small or large, must be addressed and rapidly. The research topics within this dissertation were selected because they are challenges that needed to be addressed to achieve successful decarbonization and there was a lack of focus or sufficient analysis in the space. In the electricity sector, economic zero carbon technologies exist and are being deployed, therefore, the challenges addressed in Chapter 2 and 3 are more specific. They focus on the increases in flexibility needed to continue VRE deployment. However, Chapter 4 encompasses a larger systems perspective because there is a much less defined path forward to achieve decarbonization in the steel sector. There will be more specific challenges, as new technologies develop, but they are currently decades away.

5.1. **Summary Chapter 2:**

Use-Phase Drives Lithium-Ion Battery Life Cycle Environmental Impacts When Used for Frequency Regulation

Chapter 2 addresses a very specific challenge associated with grid decarbonization. The need for a sustainable alternative sources of frequency regulation. By modeling, a simplified grid system Chapter 2 was able to quantify a range of potential life cycle environmental impacts of lithium ion batteries for frequency regulation and show that grid system characteristics, specifically fuel mix, had the largest influence on environmental impacts. Even with the shortened

battery lifetime from increased cycling for frequency regulation use-phase impacts significantly outweighed upstream and end-of-life environmental impacts. Although, the environmental impacts increased for many of the grid system configurations analyzed in Chapter 2 from the addition of a lithium ion battery system for frequency regulation, the battery system's use does not inherently mean environmental impacts will increase. Utilities will need to examine their existing and projected fuel mix, dispatch order, and level of congestion to make this determination.

5.1.1. Future Work

Since the publication of Chapter 2 there have been a number of studies analyzing the emissions impacts of grid scale energy storage for frequency regulation and energy arbitrage[184] and the costs they need to reach for various applications to be economical.[124,185,186] However, there is limited work on the life cycle environmental impacts for applications beyond frequency regulation and energy arbitrage.[184] It is important to continue to assess grid-scale battery storage using a life cycle approach, especially as storage technologies and grid infrastructure evolve. However, the research should focus beyond the energy storage systems themselves.

Battery costs are continuing to decrease. In 2018 battery energy storage systems ranged from 700-260 $/kWh and are anticipated to reach 482-189 $/kWh by 2025, reducing cost barriers.[187] Regulation and market mechanisms are also changing. FERC order 841 removes regulatory barriers to energy storage participating in the capacity, energy, and ancillary service markets.[188] All motivating and allowing for the continued increase in the installed capacity of battery energy storage from 850 MW in 2018 to a projected 2,500 MW by 2023.[189] Given battery energy storage is already being integrated into the grid and research has been completed on the environmental impacts of battery production future research's scope should be focused beyond the battery. Researchers should ask how the environmental impacts from an existing grid system as a whole could be reduced, with the use of battery energy storage technology as just one tool of many that could be implemented.

5.2. **Summary Chapter 3:**

The Impact of Forecasted Net Load on Real-Time Generator Operation

Chapter 3 examines a more general challenge with VRE generation by working to improve market operation, day-ahead commitment, by using statistical regression, which can be applied, to

most markets to try and predict inefficiencies. The regression was able to predict 21-57% of the variance in commitment error and its results indicated significant relationships between net load, fraction VRE, ramp rate and commitment error confirming some of existing literature's assumptions. However, it was not able to confirm definitively the relationship between variability and commitment error across all scenarios. Chapter 3 represents a positive first step in a developing a simple method of reducing commitment error and improving grid system efficiency.

5.2.1. Future Work

Chapter 3 addresses an intermittent challenge with integrating VRE generation into the electricity grid. At a certain point even with perfect scheduling, net load changes will be too great for traditional generators (e.g., coal and gas) to ensure supply and demand match in real time. However, there are a number of other technologies and operating strategies that are able to increase grid flexibility and enable reliable electricity supply with a majority VRE grid. These include but are not limited to demand response, energy storage, small scale nuclear, pumped storage, thermal storage, hydrogen, EV storage, expanded transmission, micogrids, etc. Which technologies minimize costs and emissions depends on market rules, generation resources, load profiles, and transmission restrictions. Therefore, research that examines options for a specific region to transition to a low carbon grid is required to develop a clear path forward.

Although, there are still challenges to be addressed before a high VRE generation grid can be implemented. The research is leaps ahead of the current VRE capacity, i.e., we do not need to wait for additional research before pushing for the development of significantly more VRE generation. Additionally, there is not a major gap in the technologies needed. There are technologies in development that could be useful tools in grid decarbonization (e.g., long duration storage, small scale nuclear), but again there is significant capacity to expand VRE generation beyond existing levels without these technologies. Therefore, understanding what mechanisms are most effective at incentivizing economic VRE development also crucial to a rapid transition to a low carbon grid.

5.3. **Summary Chapter 4:**

Reducing CO_2 emissions from U.S. steel consumption by 70% by 2050

Chapter 4 asks the broadest question. How can the U.S. reach a CO_2 reduction goal in the steel sector? Its results provide guidance on actions the U.S. could take to reach that goal. Although, there are still outstanding questions in regards to how to operationalize some of Chapter 4's recommendations they are clear. Near term, reductions in U.S. stocks per capita are required to cut U.S. steel sector emission 70% by 2050.

5.3.1. Future Work

The results of Chapter 4 illustrate what the steel industry needs to look like in order to reach the emissions reduction goal. However, this is only part of the story; determining the most effective actions to change the industry is predicated on knowing their cost and being able to minimizing it. Therefore, an expansion of the research in Chapter 4 would be to model the economic impacts of the pathways defined in Chapter 4 that meet the emissions reduction target.

Using less steel does not always equal an economic benefit and depending on the means of reduction, the economic impacts will be borne by different groups. For example, increasing beam loading could increase construction costs, due to the added complexity of design. Who would bear these increased costs will depend on a number of factors, including whether tenants are willing to pay a premium for the change. In contrast, increasing work from home, reducing office space requirements and commute costs will likely reduce costs for individuals and companies. Understanding cost implications can help educate more efficient policies and regulations to incentivize the use of less steel.

There is also an economic impact of producing less steel. Almost all of the scenarios that meet the emissions reduction goal required a significant reduction in primary steel production. This will likely result in communities losing a major employer and steel producers losing a major revenue source. A firm understanding of the economic impacts of these losses is required to mitigate them.

Along with reducing steel consumption, it is important to reduce the EI of steelmaking. Reducing secondary steelmaking EI only requires a reduction in electricity EI; however, reducing primary steelmaking EI requires the development and deployment of new steelmaking technologies. An understanding of the costs associated with this development and deployment is

required to create policies that will economically incentivize the transition to low carbon steel production.

5.4. **General Conclusions**

The decarbonization of the electricity sector is paramount to economic decarbonization given the number of sectors that will depend on it to decarbonize themselves, steel included. Decarbonization of the electricity sector, on its surface, seems simple given the availability of economic zero carbon resources, wind and solar. However, this dissertation illuminates just two of the imbedded challenges associated generating electricity from VRE. One is addressed in chapter 2 through a technological advancement, lithium ion batteries, and the other in chapter 3 through improved modeling. Continued advancement in technology will be required to managing the increasing variability and uncertainty driven by increased generation from VRE, however, electricity markets will also have to advance to incentivize their use, and modeling will need to improve to assess their impacts on system costs and reliability.

The challenges related to decarbonization discussed for the electricity sector are focused on the supply side, while this dissertation recommends demand side changes for the steel sector. This is a result of the stark difference in availability of technologies for decarbonization. Although outstanding challenges remain with electricity decarbonization they are technological or market based, both being easier to address than required demand changes. The only currently available low carbon option to produced steel is by recycling scrap, which is limited by scrap availability and quality. Additionally, this process along with those in development (H-DRI and electrolysis) are all dependent on decarbonization of the electricity sector to significantly reduce emissions. The lack of alternative technology options resulted in the need to reduce near term steel demand. In this case, decarbonization would require a change of behavior, given technological options to reduce primary steel demand, improved recycling rate, and improved material efficiency were alone not sufficient to reduce sector emissions. Steel use per-capita needs to be reduced and product lifetime extended to make a significant impact on decarbonization. Further research is required on how to effectively achieve these goals without hindering economic growth, but regulation and financial incentives will likely be required. Although there is still space for further research and outstanding challenges on the topics explored in each chapter of this dissertation, their results could aid in the ability of the electricity and steel sectors to decarbonize reliably.

APPENDCIES

Appendix A:

Use-phase Drives Lithium Ion Battery Life Cycle Environmental Impacts when Used for Frequency Regulation

1. System Assumptions and Parameters

This power system model is based on an IEEE 9-bus test system.[85] It consists of four conventional generators, totaling 800 MW, a Li-ion battery storage system totaling 3.04 MWh, and renewable generation totaling 15% of the day's electricity demand. The renewable generation type and capacity vary by case, as does the fossil fuel mix. The test system uses the same parameters as Lin et al.[2] unless otherwise noted in the body of the paper or supporting information.[52]

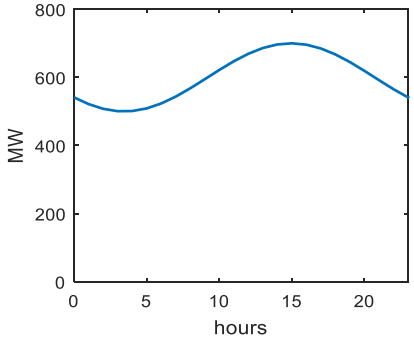

Figure A - 1 Aggregated system load curve

Figure A-1 illustrates the aggregated system load, which is distributed to buses 5, 7 and 9. The daily load profile is modeled as a sinusoidal curve with a minimum load at 500 MW and a maximum load at 700 MW. The load shape remains constant across the year and across the three load buses but the magnitude at each bus is scaled based on minimum and maximum loads found in Table A-1. The frequency regulation requirements for the system vary hourly depending on the

load and renewable forecast. The total frequency regulation requirement is the sum of 3% of the load and 5% of the renewable energy production.

Table A - 1. Bus Base Loads

Bus Number	Min Load	Max Load
5	143	200
7	159	223
9	198	277
Total	**500**	**700**

1.1. Fossil Generators

Table A-2 contains the sizes and locations of the fossil units for the Coal and Gas scenarios. The generator sizes were selected with the goal of supplying the appropriate percentage of coal or natural gas, as defined by the scenario, while maintaining realistic generator sizes and not causing congestion in the base case. Table A-3 contains the list of detailed assumptions about each generator type and Figure A-2 to A-4 show each generator's cost curve for the base case and the two fuel price parametric studies. Coal unit cost curves, Figure A-2, were derived from Hunters Point 3 and gas unit cost curves were derived from Moss Landing 3 as in Lin et al.[52] The curves were scaled by the generator maximum capacity for the units in the test case based on equations 12-15 in Lin et al.[52]

Table A - 2, Fossil generator sizing by scenario

		Coal *(20% Gas, 80% Coal)*			**Gas *(80% Gas, 20% Coal)***		
	Bus	**Fuel Type**	P^g_{max}	P^g_{min}	**Fuel Type**	P^g_{max}	P^g_{min}
G1	1	Coal	*340*	*136*	Gas	*250*	*100*
G2	2	Coal	*300*	*120*	Coal	*160*	*64*
G3	3	Gas	*80*	*32*	Gas	*240*	*96*
G4	6	Gas	*80*	*32*	Gas	*150*	*60*

Note: G1 refers to Generator 1, G2 refers to Generator 2, G3 refers to Generator 3, and G4 refers to Generator 4

Table A - 3, Fossil generator assumptions by fuel type

	Coal	**Natural Gas**
2014 Fuel Cost ($/MMBtu)	2.37[96]	5.00[96]
2017 Fuel Cost ($/MMBtu)	2.22[190]	3.67[190]
Minimum Up Time (hours)	12 (4 for <300 MW) [191]	4[191]
Minimum Down Time (hours)	12 (4 for <300 MW) [191]	4[191]
Startup Cost ($/MW)[a]	5.61 (4.58 for <300 MW) [191]	3.99[191]
Startup Fuel (MMBtu/MW)[a]	7.50 (5.00 for <300 MW) [191]	3.67[191]
Shutdown Cost ($/MW)[a]	5.61 (4.58 for <300 MW) [191]	3.99[191]
Frequency Regulation Cost ($/MW-h)	10/9[192]	4/5[192]

[a] *Corresponding values are for a hot start*

Hummon et al.[192] assume a reserve cost of $10/MWh for subcritical coal and $4 /MWh for gas steam. These values were used as a basis for the coal and gas test cases, though we vary them slightly to simulate a real system in which generators of the same type have unequal reserve costs. The Coal case consisted of G1 = $9/MWh, G2 = $10/MWh, G3 = $4MWh, G4 = $4/MWh. The Gas case consisted of G1 = $5/MWh, G2 = $10/MWh, G3 = $4MWh, G4 = $4/MWh.[192]

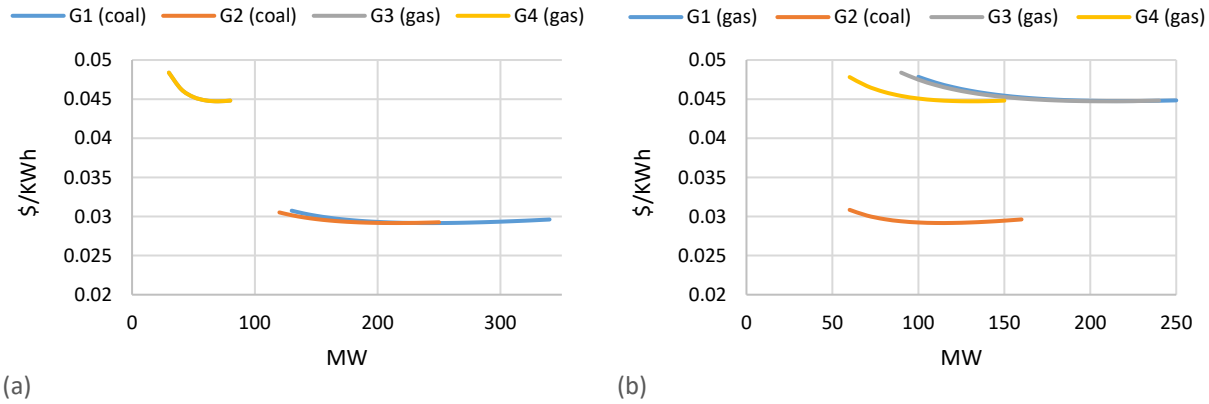

Figure A - 2, Fossil generator cost curves (a) Coal case and (b) Gas case

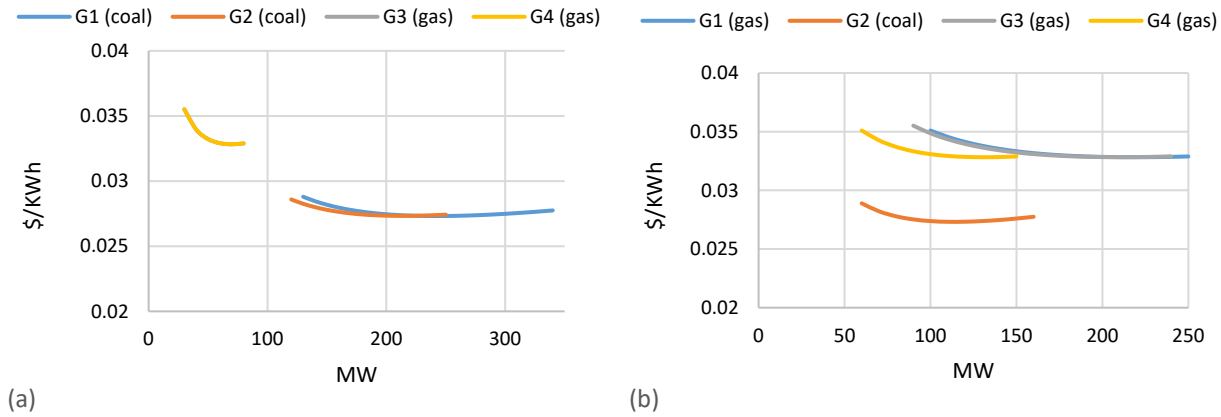

Figure A - 3, Fossil generator cost curves for fuel price parametric study (coal = 2.22 $/MMBtu & natural gas = 3.67 $/MMBtu) (a) Coal case and (b) Gas case

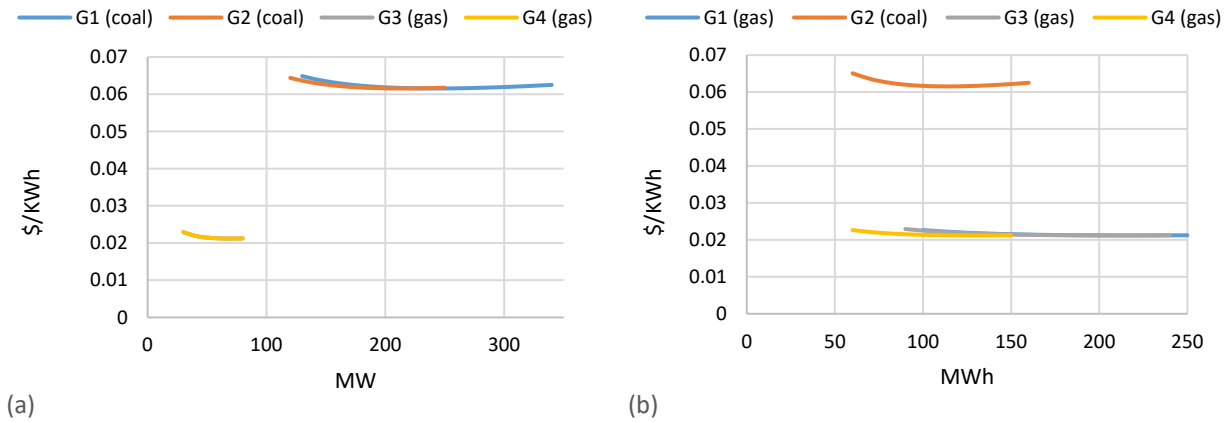

Figure A - 4, Fossil generator cost curves with price swap parametric study (coal = 5.00 $/MMBtu & natural gas = 2.37 $/MMBtu) (a) Coal case and (b) Gas case

1.2. *Renewable Generators*

The renewable generation assumptions are listed in Table A-4 and the generation profiles are in Figure A-5. The same data is used for each month of the year. The renewable generation is located at bus 8. The wind and solar profiles, Figure A-5, are based on real meteorological data from the National Renewable Energy Laboratory's (NREL) National Solar Radiation Database (NSRDB)[193] and Wind Integration National Dataset (WIND) Toolkit,[194] analyzed using the System Advisor Model (SAM) to calculate hourly generation.[195] Using power data from a whole year, we selected data from the days with median generation, for wind and solar independently (i.e., the data is taken from different days). The same data is used for each month of the year.

Table A - 4, Renewable generator assumptions

	Wind	Solar
Capacity	263 MW [a]	567 MW [a]
Technology Type	Vestas V90-1.8, 80m hub height	Fixed open rack fixed tilt at latitude, 14.08% losses
Representative Date	March 26	January 12
Representative Location	Wind Toolkit 41.04 N, -83.65 E	NSRDB 41.017 N, -83.667 E
Year	2011	TMY

[a] *Capacity selected so that total renewable generation in a 24-hour period would equal 15% of the load*

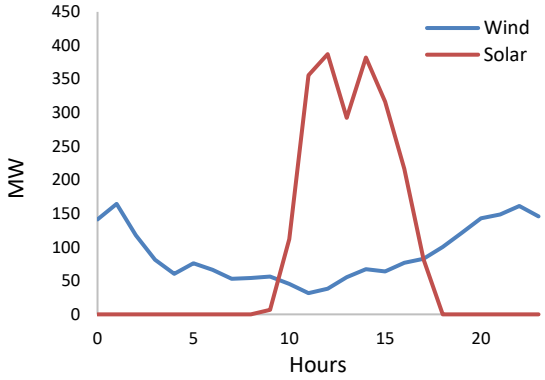

Figure A - 5, Wind and solar generation profiles[193,194]

1.3. Energy Storage System

The energy storage system characteristics are listed in Table A-5. We assume charging and discharging efficiencies are equal, end of life occurs when battery capacity degrades to 50%, and the allowable battery range is between 0.2 and 0.8 state of charge (SOC). The values for c-rate, energy-to-power ratio (E/P) and energy storage power are calculated in Section 2.2 and the remaining values are derived from the literature.

We determined the battery capacity based on the system frequency regulation requirement range throughout the day (15-40 MW). A size of 8 MW ensures that the battery size never exceeds the frequency regulation requirements, but that the battery will have an effect on the unit commitment and dispatch.

Table A - 5, Li-ion energy storage system assumptions

End of Life Capacity	50%
Starting Capacity	100%
Energy Storage Capacity	3.04 MWh
Energy Storage Power	8 MW
Energy SOC range	0.2-0.8
Initial Round Trip Efficiency	90%[22]
Initial Charging Efficiency	95%[46]
Initial Discharging Efficiency	95%[46]
C-rate (1/(E/P))	2.63
Energy-to-Power Ratio (E/P)	0.38
Temperature	25°C[26]

1.4. Emissions and Impact Assumptions

As discussed in the body of the paper the material inventory for the batteries was developed through BatPac, which represent the masses in Table A-6.[196] The emissions in Table A-6 were calculated from GREET.[82]

Table A - 6, Battery system life cycle inventory data[82,196]

Component	Total LMO	LMO						Total LFP	LFP					
		Cathode	Anode	Al	Steel	Au	BMS		Cathode	Anode	Al	Steel	Au	BMS
Mass (kg)	*2.5E+03*	*9.8E+02*	*3.3E+02*	*4.8E+02*	*3.6E+01*	*2.8E+02*	*2.8E+01*	*3.0E+03*	*7.9E+02*	*4.0E+02*	*5.6E+02*	*4.3E+01*	*3.2E+02*	*3.3E+01*
CO_2 (kg)	*9.8E+03*	3.2E+03	1.6E+03	3.3E+03	1.3E+02	8.3E+02	7.3E+02	*9.6E+03*	1.9E+03	1.9E+03	3.9E+03	1.5E+02	9.7E+02	8.6E+02
NO_x (kg)	*1.6E+01*	5.9E+00	4.5E+00	2.7E+00	1.3E-01	1.9E+00	5.9E-01	*1.7E+01*	5.5E+00	5.4E+00	3.2E+00	1.5E-01	2.2E+00	6.9E-01
SO_x (kg)	*8.5E+01*	3.1E+00	2.6E+01	1.3E+01	4.6E-01	4.0E+01	1.1E+00	*1.3E+02*	3.2E+01	3.2E+01	1.6E+01	5.4E-01	4.7E+01	1.2E+00
CH_4 (kg)	*2.4E+01*	7.9E+00	4.2E+00	7.2E+00	2.6E-01	2.0E+00	2.0E+00	*2.3E+01*	4.6E+00	5.1E+00	8.5E+00	3.0E-01	2.3E+00	2.3E+00
N_2O (kg)	*1.5E-01*	4.0E-02	2.5E-02	5.3E-02	1.5E-03	1.5E-02	1.4E-02	*1.6E-01*	2.8E-02	3.0E-02	6.2E-02	1.7E-03	1.8E-02	1.7E-02
Total Energy (MMBtu)	*1.5E+02*	3.8E+01	2.9E+01	5.9E+01	1.5E+00	1.2E+01	1.1E+01	*1.6E+02*	2.5E+01	3.5E+01	6.9E+01	1.8E+00	1.4E+01	1.3E+01
Component	**Total NCA**	**NCA**						**Total NMC**	**NMC**					
		Cathode	Anode	Al	Steel	Au	BMS		Cathode	Anode	Al	Steel	Au	BMS
Mass (kg)	*1.9E+03*	*5.3E+02*	*3.7E+02*	*3.6E+02*	*2.7E+01*	*2.1E+02*	*2.1E+01*	*2.2E+03*	*6.9E+02*	*3.7E+02*	*4.1E+02*	*3.2E+01*	*2.4E+02*	*2.4E+01*
CO_2 (kg)	*1.1E+04*	5.7E+03	1.8E+03	2.5E+03	9.6E+01	6.2E+02	5.4E+02	*1.2E+04*	6.1E+03	1.8E+03	2.9E+03	1.1E+02	7.2E+02	6.4E+02
NO_x (kg)	*2.6E+01*	1.7E+01	5.1E+00	2.0E+00	9.3E-02	1.4E+00	4.4E-01	*2.4E+01*	1.4E+01	5.1E+00	2.4E+00	1.1E-01	1.6E+00	5.1E-01
SO_x (kg)	*5.2E+02*	4.5E+02	3.0E+01	1.0E+01	3.4E-01	3.0E+01	7.9E-01	*4.3E+02*	3.5E+02	3.0E+01	1.2E+01	4.0E-01	3.5E+01	9.2E-01
CH_4 (kg)	*2.9E+01*	1.6E+01	4.7E+00	5.4E+00	1.9E-01	1.5E+00	1.5E+00	*3.1E+01*	1.7E+01	4.7E+00	6.3E+00	2.3E-01	1.7E+00	1.7E+00
N_2O (kg)	*2.1E-01*	1.2E-01	2.8E-02	3.9E-02	1.1E-03	1.1E-02	1.1E-02	*2.3E-01*	1.3E-01	2.8E-02	4.6E-02	1.3E-03	1.3E-02	1.2E-02
Total Energy (MMBtu)	*1.8E+02*	8.4E+01	3.2E+01	4.4E+01	1.1E+00	8.9E+00	8.2E+00	*1.9E+02*	8.8E+01	3.2E+01	5.1E+01	1.3E+00	1.0E+01	9.5E+00

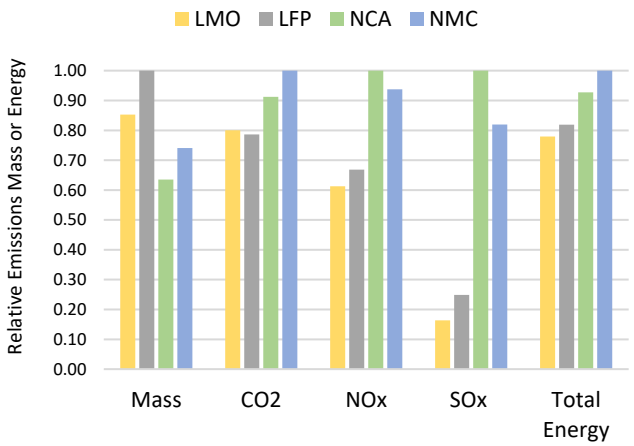

Figure A - 6, Battery system life cycle inventory comparison by battery type

Table A - 7, Inverter life cycle inventory data for 1 MW Battery Power Rating[84]

Component	Steel	Al	Au
Mass (kg)	*3040*	*894*	*625*
CO_2 (kg)	4270	1490	1870
NO_x (kg)	3.47	1.49	4.26
SO_x (kg)	7.64	2.84	91.1
CH_4 (kg)	10.74	4.76	4.52
N_2O (kg)	0.078	0.036	0.034
Coal (mmBTU)	24.0	3.97	8.79
NG Gas (mmBTU)	29.7	15.6	10.4

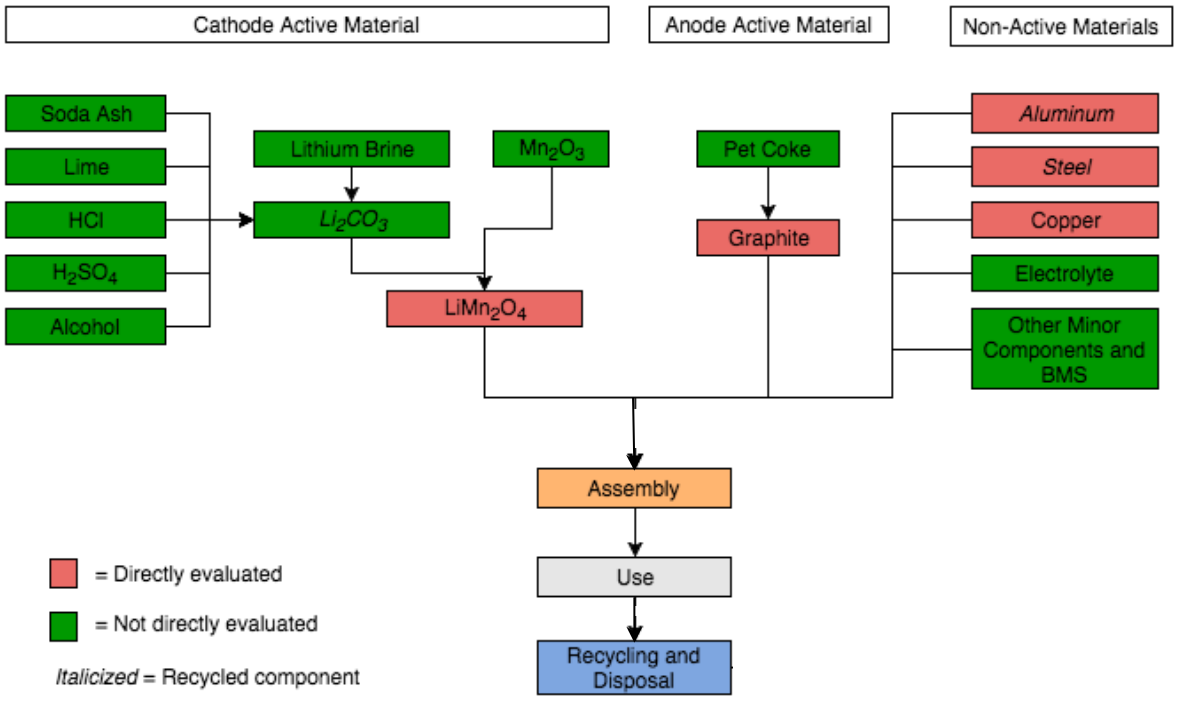

Figure A - 7, Materials and energy flow for the Li-ion battery in the power system, starting with raw materials and ending in battery end of life. This chart is a reduced version of the materials flow diagram in Dunn et al.[60] The dashed line denotes the system boundary line for upstream and downstream impacts, where recycling processes and impacts are incorporated into upstream results in our final impact calculations.

The energy of battery assembly is calculated from Dunn et al.'s [60] assumption of 2.7 MJ/kg battery for a LMO battery. The total battery masses for each battery type are given in Table A-6. Then GREET's assumptions for shares of process fuels for battery assembly (49% natural gas and 51% electricity) were used to calculate the emissions from battery assembly.[82]

Recycled content assumptions for steel and aluminum given in Table A-8 are GREET's default values. The recycling value for Li_2CO_3 is used in the base case only. No active materials are recycled in the parametric studies, which used different cathode types. Dunn et al.[80] notes that hydrometallurgical recycling processes are still under development, UNEP[197] estimated less than 1% recycling of lithium in 2011. The 2016 USGS Mineral Commodity Summary[198] does not have a specific recycling rate for lithium, but they discuss a facility in Canada and note funds have been allocated for a facility in the U.S. so lithium recycling is anticipated to grow. However, for this study we selected only 1% to remain in line with current values.

Table A - 8, Recycled Content Assumptions

	% Recycled Li2CO3	% Recycled Steel	% Recycled Aluminum
Base Case	1%	26.4%	11%

CO_2, NO_x, and SO_x emissions factors for coal were calculated from 2015 Air Markets Continuous Emissions Monitoring (CEM) unit level heat input and tons of emissions from scrubbed units.[199] NO_x and SO_x emission factors for natural gas were calculated from 2015 CEMs unit level heat input and tons of emissions for gas steam plants.[199] The CEMs data contains only SO_2, which we equated to SO_x, as only 0.7% of fuel sulfur is emitted as SO_3..[200] The CO_2 emissions factor for natural gas is from the EIA.[201] GWP was calculated using the CO_2, CH_4, and N_2O emissions factors with 100-year global warming potentials from the Environmental Protection Agency (EPA).[202] Acidification values were calculated using TRACI 2.1 impact factors for NO_x, and SO_x.[203]

Table A - 9, Fossil fuel inventory data

	Coal	Natural Gas
CO_2 Emissions Factor (kg/MMBtu)	93.6[199a]	53.2[201]
SO_x Emissions Factor (g/MMBtu)	71.4[199a]	0.45[199b]
NO_x Emissions Factor (g/MMBtu)	103[199c]	52.7[199c]
CH_4 Emissions Factor (g/MMBtu)	11[202]	1.6[202]
N_2O Emissions Factor (g/MMBtu)	1[202]	0.1[202]
CO_2 Upstream (g/MMBtu)	1,691[94]	5,968[94]
NO_x Upstream (g/MMBtu)	13.764[94]	29.758[94]
SO_x Upstream (g/MMBtu)	7.002[94]	11.464[94]
CH_4 Upstream (g/MMBtu)	148.92[94]	245.94[94]
N_2O Upstream (g/MMBtu)	0.033[94]	0.801[94]
Energy Upstream (Btu/MMBtu)	22,339[94]	96,195[94]

[a] *Values calculated from 2015 CEMS unit level heat input and tons of emissions for scrubbed units*
[b] *Values calculated from 2015 CEMS unit level heat input and tons of emissions*
[c] *Values based on average 2015 unit level Average NO_x rate*

Table A - 10, Life cycle impact category assumptions

Global Warming (kg CO_{2eq} / kg Substance)	
CH_4 100-yr GWP	25[204]
N_2O 100-yr GWP	298[204]
Acidification Air (kg SO_{2eq} / kg substance)	
NO_x	0.7[203]
SO_x	1[203]

Table A - 11, Per-Capita nominal U.S. impacts from 2016 used to normalize results

Impact Category	Per-capita (impact per person year)
Global Warming (kg CO_{2eq})	1.78E+04[205,206]
Acidification (kg SO_{2eq})	4.80E+01[205,207]
Fossil Fuel Depletion (MMBtu surplus)*	2.98E+07[205,208]

** Fossil Fuel Depletion value was used in equivalent to cumulative energy demand*

2. Mathematical Formulations

2.1. Unit Commitment and Dispatch

The unit commitment and dispatch problem is formulated as a mixed integer programing problem. Suppose we have n_g conventional generators, n_{gr} renewable generation plants, n_{es} energy storage devices, n_b buses, and n_l transmission lines in the system. Let $P_t^g \in \mathbb{R}^{n_g}$ be the power output of the conventional generators at time t, $P_t^{gr} \in \mathbb{R}^{n_{gr}}$ be the power output of the renewable generators at time t, $\Theta_t \in \mathbb{R}^{n_b}$ be the bus voltage angle at time t, $R_t^g \in \mathbb{R}^{n_g}$ be the frequency regulation capacity of the conventional generators at time t, and $R_t^{es} \in \mathbb{R}^{n_{es}}$ be the frequency regulation capacity of the energy storage at time t. Also, let U_t, V_t, and W_t be binary variables, where $U_t \in \mathbb{R}^{n_g}$ represents whether the conventional generators are committed at time t, $V_t \in \mathbb{R}^{n_g}$ represents whether the conventional generators are committed (turned on) at time t, and $W_t \in \mathbb{R}^{n_g}$ represents whether the conventional generators are uncommitted (turned off) at time t.

Let N be the number of time periods, the decision variables are:

$$X = [X_1^T, \dots, X_N^T]^T, \tag{1}$$

where the subscript is the time index and

$$X_t = \left[\left(P_t^g\right)^T, \left(P_t^{gr}\right)^T, \left(\Theta_t^l\right)^T, \left(R_t^g\right)^T, \left(R_t^{esl}\right)^T, \left(U_t^l\right)^T, \left(V_t^l\right)^T, \left(W_t^l\right)^T\right]^T. \tag{1}$$

The objective function is:

$$F_{cost} = \sum_{t=1}^{N}\left[f^g\left(P_t^g\right) + f^{gr}\left(P_t^{gr}\right) + f^r\left(R_t^g\right) + f^{es}(R_t^{es}) + f^{on}(V_t) + f^{off}(W_t)\right], \tag{2}$$

where f^g is the generation cost for conventional generators, which is modeled as a quadratic function:

$$f^g\left(P_t^g\right) = \left(P_t^g\right)^T A_g P_t^g + \left(B_g^l\right)^T P_t^g,$$

where A_g is a diagonal matrix of quadratic cost coefficients and B_g is a column vector of linear cost coefficients. The other costs are modeled as linear functions. Let B_* be the corresponding column vector of cost coefficients, then cost of renewable generation is:

$$f^{gr}\left(P_t^{gr}\right) = \left(B_{gr}\right)^T P_t^{gr},$$

the cost of frequency regulation from conventional generators is:

$$f^r\left(R_t^g\right) = (B_r^l)^T R_t^g,$$

the cost of frequency regulation from energy storage is:

$$f^{es}(R_t^{es}) = \left(B_{es}\right)^T R_t^{es},$$

and the commitment costs are:

$$f^{on}(V_t) = \left(B_{on}\right)^T V_t,$$

$$f^{off}(W_t) = \left(B_{off}\right)^T W_t.$$

The constraints include the standard optimal power flow (OPF) constraints and the unit commitment constraints. We first present the OPF constraints. At the beginning of the optimization horizon, we assume the SOC of the energy storage device is 50%. For the OPF, we assume the frequency regulation reference signal is zero mean and the SOC of the energy storage device returns to 50% at the start of each hour. The round trip loss is modeled as additional load at the bus where the energy storage is located:

$$P_t^{d,es} = \beta R_t^{es}, \tag{3}$$

where β is a parameter determined by the reference signal. The power balance equation can be written as: for $t = 1, 2, \dots, N$,

$$P_{b,t} = D_b \Theta_t, \tag{4}$$

$$P_{b,t} = C^g P_t^g + C^{gr} P_t^{gr} - C^d P_t^d - C^{es} P_t^{d,es}, \tag{5}$$

where $P_{b,t} \in \mathbb{R}^{n_b}$ is the power injection at each bus; $P_t^d \in \mathbb{R}^{n_b}$ is the load at each bus; matrix D_b (the imaginary part of the bus admittance matrix) describes the relationship between the bus voltage angle and the bus power injection; and C^g, C^{gr}, C^d, and C^{es} are grid topology matrices mapping conventional generators, renewable generators, loads, and energy storage to buses (the entry $C_{i,j}$ is one if unit j is connected to bus i and zero otherwise).

The transmission line power flow constraints can be written as: for $t = 1, 2, \dots, N$,

$$P_{f,t} = D_f \Theta_t, \tag{6}$$

$$P_{f,min} \preccurlyeq P_{f,t} \preccurlyeq P_{f,max}\,, \tag{7}$$

where $\succcurlyeq$ and $\preccurlyeq$ denote element-wise inequalities, $P_{f,t} \in \mathbb{R}^{n_l}$ is the power flow through each transmission line, matrix D_f describes the relationship between bus voltage angle and the line power flow ($P_{f,i,t} = \left(\Theta_{j,t} - \Theta_{k,t}\right)/X_{jk}$ where $P_{f,i,t}$ is the power flow on the ith line from bus j to bus k and X_{jk} is the susceptance of the line from bus j to bus k), and $P_{f,min} \in \mathbb{R}^{n_l}$ and $P_{f,max} \in \mathbb{R}^{n_l}$ are the lower and upper limits for the line power flow.

The generator limits can be written as: for $t = 1, 2, \dots, N$,

$$P_t^g - R_t^g \succcurlyeq P_{min}^g \otimes U_t, \tag{8}$$

$$P_t^g + R_t^g \preccurlyeq P_{max}^g \otimes U_t, \tag{9}$$

$$R_t^g \succcurlyeq \mathbf{0}, \tag{10}$$

where $\otimes$ denotes element-wise multiplication, $P_{min}^g \in \mathbb{R}^{n_g}$ and $P_{max}^g \in \mathbb{R}^{n_g}$ are the lower and upper power limits of the conventional generators, and $\mathbf{0}$ is a column vector of zeros with appropriate dimension.

The limits for the renewable generation can be written as: for $t = 1, 2, \dots, N$,

$$\mathbf{0} \preccurlyeq P_t^{gr} \preccurlyeq P_{f,t}^{gr}, \tag{11}$$

where $P_{f,t}^{gr}$ is the forecast capacity of renewable generation.

The regulation requirement can be written as: for $t = 1, 2, \dots, N$,

$$1^T R_t^g + 1^T R_t^{es} \geq r_{req}, \tag{12}$$

$$R_{min}^{es} \preccurlyeq R_t^{es} \preccurlyeq R_{max}^{es}, \tag{13}$$

where $1^T$is a vector of ones of appropriate dimension, r_{req} is the frequency regulation capacity required by the power system, and $R_{min}^{es} \in \mathbb{R}^{n_{es}}$ and $R_{max}^{es} \in \mathbb{R}^{n_{es}}$ are the lower and upper limits for the energy storage frequency regulation capacity.

Next, we present the unit commitment constraints. Recall that U_t, V_t, and W_t are binary variables that take values of 0 or 1. The minimum up/down time constraints can be written as: for $t = 1, 2, \dots, N-1$ and $j = 1, 2, \dots, n_g$,

$$-U_{t-1}^j + U_t^j - U_{t+i}^j \leq 0, \forall i \in \left\{1, \dots, t_{on}^j - 1\right\} \cap \{i | t + i \leq N\}, \tag{14}$$

$$U_{t-1}^j - U_t^j + U_{t+i}^j \leq 1, \forall i \in \left\{1, \dots, t_{off}^j - 1\right\} \cap \{i | t + i \leq N\}, \tag{15}$$

where U_*^j is the jth element of U_* and t_{on}^j and t_{off}^j are the minimum up and down time for the jth generator, respectively. Equation (15) ensures that, if the unit is turned on at time t, it stays on for the next t_{on} steps; while equation (16) ensures that, if the unit is shut down at time t, it stays off for the next t_{off} steps.

The start-up and shut-down constraints are: for $t = 1, 2, \dots, N$,

$$-U_{t-1} + U_t - V_t \preccurlyeq 0^T \quad , \tag{16}$$

$$U_{t-1} - U_t + W_t \preccurlyeq 0^T. \tag{17}$$

Note that these constraints only ensures that $V_t = 1$ when the unit is turned on at time t and $W_t = 1$ when the unit is shut down at time t. The values of V_t and W_t are free otherwise. Since there are

costs associated with start-up and shut-down, the optimal V_t and W_t take value of zero when the unit is not started up or shut down.

The full optimization problem can be formulated as: find the variable *X* in equation (1), which minimizes the objective function, equation (3), while subject to the constraints, equations (4) to (18).

2.2. Capacity Degradation

2.2.1. Base Case

The base case capacity degradation model is based on Xu et al.'s[32] calendar aging and cycle aging model for LMO batteries.[91] The cycle aging is calculated using the average SOC in each cycle, depth of discharge (DOD) in each cycle, and temperature in each cycle.[91] The calendar aging is calculated using time, average SOC over all time, and average temperature over all time.[91] To obtain the average SOC and DOD we first compute the SOC time series based on the PJM RegD signal. Let P_t be the power injection/extraction of the energy storage at time t (we use positive P_t to denote discharging and negative P_t to denote charging). Let σ_t be the SOC at time t. The SOC time series can be calculated by:

$$\sigma_{t+1} = \begin{cases} \sigma_t - \eta_{ch} P_t \Delta t, & P_t < 0 \\ \sigma_t - \frac{1}{\eta_{dis}} P_t \Delta t, & P_t \geq 0 \end{cases} \tag{18}$$

where Δt is the time interval in seconds, and η_{ch} and η_{dis} are charging and discharging efficiencies. Recall that we assume the SOC returns to 0.5 at the start of each hour. In practice, this is usually achieved through other types of services. For example, the California Independent System Operator (CAISO) uses Regulation Energy Management to manage the SOC of non-generating resources through the real-time market.[209] In this paper, we used a year (August 2015 to July 2016) of PJM's dynamic regulation signal (RegD) from August 2015 to July 2016.[93] In reality, this signal may not be zero mean over the hour, causing the SOC to deviate from 0.5 at the end of the hour. To correct the SOC, we add an offset to the reference signal so that it becomes zero mean in each hour, emulating SOC management. To calculate the offset, we first calculate the SOC time series with the original reference signal $P_{o,t}$. Let $\sigma_{o,end}$ be the SOC at the end of the hour resulting from $P_{o,t}$. We define the offset as:

$$\delta P_t = \begin{cases} \frac{1}{\eta_{ch}}\left(\sigma_{o,end} - 0.5\right) / \left(\frac{1}{\Delta t}\right), & P_t < 0 \\ \eta_{dis}\left(\sigma_{o,end} - 0.5\right) / \left(\frac{1}{\Delta t}\right), & P_t \geq 0 \end{cases} \tag{19}$$

We calculate this offset for each hour in the year. Note that the offset does not change within an hour but varies across hours. The modified reference signal is:

$$P_t = P_{o,t} + \delta P. \tag{20}$$

The charging and discharging of the battery at time t are:

$$P_{ch,t} = -\min(P_t\,, 0), \tag{21}$$

$$P_{dis,t} = \max(P_t\,, 0). \tag{22}$$

The SOC with and without the offset are shown in Figure A-8 for three hours (the reference signal used in the figure is discussed in the following sections).

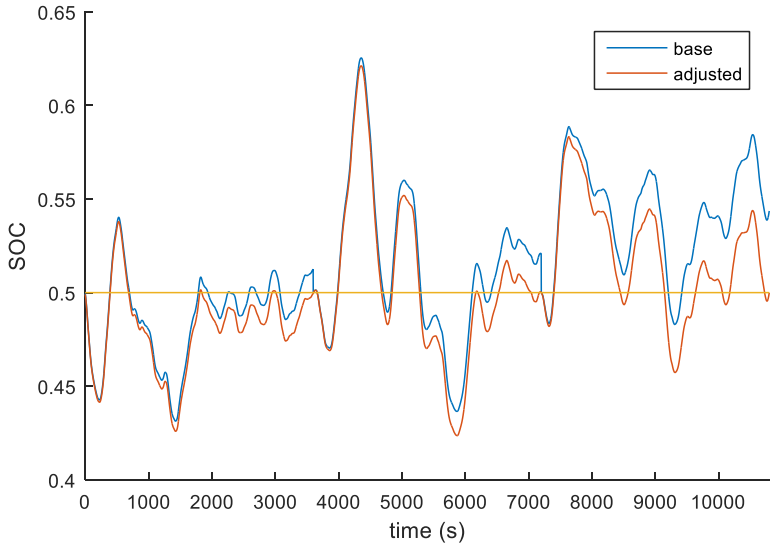

Figure A - 8, Three hours of the base state of charge (SOC), and the adjusted SOC (i.e., the SOC after it was adjusted to return to 0.5 at the end of each hour by the regulation signal offset). Time is in units of seconds and the signal changes every two seconds.

The PJM signal is normalized to [-1, 1]. The actual reference signal the participant needs to follow is scaled by its frequency regulation capacity. We use the signal to determine a reasonable energy to power ratio for the energy storage device. Denote the normalized PJM signal as P_{PJM}, the actual reference signal is $P_{o,t} = k_{ep}P_{PJM}$, where k_{ep} is the frequency regulation capacity. Suppose we have an energy storage device with energy capacity of one. Since the initial SOC in each hour is 0.5, the SOC will always remain within the storage energy limits when k_{ep} is less than 1. However, the magnitude of the signal P_{PJM} is usually much smaller than one and it

switches polarity often. Therefore, it is conservative to set k_{ep} to 1, and since frequency regulation providers do not need to perfectly track their reference signals, it makes more sense for the energy storage operator to bid $k_{ep} > 1$ into the market in order to earn higher profits. Note that k_{ep} is also the minimum power capacity for the energy storage, so the E/P is $1/k_{ep}$.

In this paper, we assume that the SOC needs to stay within [0.2, 0.8] for more than 95% of the time during the year. Through simulations, we determined that an E/P of 0.38 would achieve this, making k_{ep} 2.63. This estimate is within the range of previous literature. Swierczynski et al.[44] used a 0.25 E/P ratio for frequency regulation and Xu et al.[46] uses an E/P of 0.3. The effect of the energy to power ratio on the SOC can be seen in Figure A-9. The DOD is computed as 1-SOC.

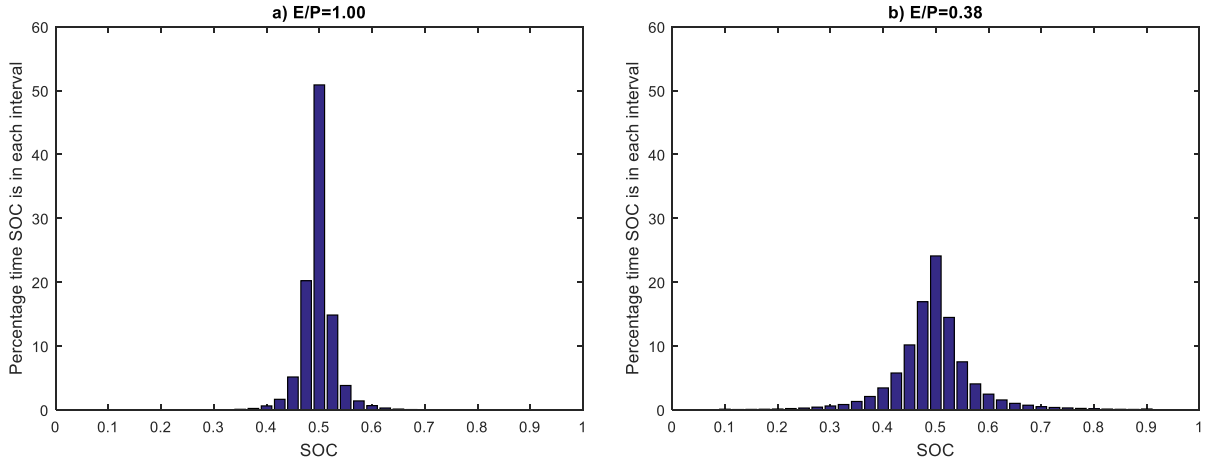

Figure A - 9, Histograms representing the frequency of state of charges (SOC) from 0 to 1 throughout the year for a) a battery with an E/P of 1 and b) a battery with an E/P of 0.38.

Xu et al.[32] calculates battery life (*L*) using:

$$L = 1 - \alpha_{sei} e^{-\beta_{sei} f_d} - (1 - \alpha_{sei}) e^{-f_{\mathrm{d}}}, \qquad \text{eq. 12 ref. 32}$$

where α_{sei} and β_{sei} are constants found in Table A-12, f_{d} is a function of the calendar and cycle aging:

$$f_{\mathrm{d}}(t, \delta, \sigma, T_c) = f_t(t, \bar{\sigma}, \bar{T}_c) + \sum_i^N n_i f_c(\delta_i, \sigma_i, T_{c,i}), \qquad \text{eq. 3 ref. 32}$$

where f_t is the calendar aging, f_c is the cycle aging, n_i indicates whether cycle *i* is a full or half cycle, t is the period of time, δ_i is the maximum DOD in cycle *i*, σ_i is the mean SOC in cycle *i*,

$T_{c,i}$ is the mean temperature in cycle *i*, *N* is the number of cycles, and a line over a variable indicates the mean over all time.[91] Xu et al.[32] define f_c as:

$$f_c(\delta_i, \sigma_i, T_{c,i}) = S_\delta(\delta_i) S_\sigma(\sigma_i) S_T(T_{c,i}), \qquad \text{eq. 18 ref 32}$$

where S_δ is the DOD stress, S_σ is the SOC stress, and S_T is the temperature stress, and each are defined for individual cycles. Xu et al.[32] define f_t as:

$$f_t(t, \bar{\sigma}, \bar{T}_c) = S_t(t) S_\sigma(\bar{\sigma}) S_T(\bar{T}_c)\,, \qquad \text{eq. 19 ref 32}$$

where S_t is the time stress. We assume the temperature stress S_T is one because we assume isothermal operation at the reference temperature. The remaining stresses are defined as:

$$S_\sigma(\sigma) = e^{k_\sigma(\sigma - \sigma_{ref})}\,, \qquad \text{eq. 25 ref. 32}$$

$$S_t(t) = k_t t\,, \qquad \text{eq. 27 ref. 32}$$

$$S_\delta(\delta) = (k_{\delta 1}\delta^{k_{\delta 2}} + k_{\delta 3})^{-1}\,, \qquad \text{eq. 32 ref. 32}$$

where k_σ, σ_{ref}, $k_{\delta 1}$, $k_{\delta 2}$, $k_{\delta 3}$, and k_t are constants found in Table A-12. When calculating the calendar aging, f_t, the SOC in equation (25 ref. 32) is the average over the battery life, $\bar{\sigma}$. When calculating the cycle aging the SOC in equation (25 ref. 32) is the average across an individual cycle, σ_i, and the DOD in equation (32 ref. 32) is the maximum across an individual cycle, δ_i.

Xu et al.[32] suggest applying the rainflow cycle-counting algorithm when the cycles are irregular. To do this we use the MATLAB functions SIG2EXT[36] and RAINFLOW.[36] SIG2EXT preprocesses the SOC time series and its output is the input to RAINFLOW, which outputs each cycle's amplitude (which is half of δ_i) , mean σ_i, and whether it is a full or a half cycle n_i.[210]

Table A - 12, Degradation parameters used in Xu et al.[91]

α_{sei}	5.75e-2
β_{sei}	121
k_{σ}	1.04
σ_{ref}	0.50
$k_{\delta 1}$	1.40e5
$k_{\delta 2}$	-5.01e-1
$k_{\delta 3}$	-1.23e5
k_t	4.14e-10/s

2.2.2. Capacity Degradation Parametric Studies

There is still a great deal of uncertainty surrounding capacity degradation. Therefore, we completed a parametric study using a two additional models Fortenbacher et al.[89] and Wang et al.[86] Fortenbacher et al.'s[37] degradation model is identified using synthetic data from an electrochemical battery mode called DUALFOIL. Equation (23 ref. 37) determines degradation using the SOC and the power injection/extraction.[89] Variables E_t, $P_{ch,t}$, and $P_{dis,t}$ are used in equation (23 ref. 37) to calculate the cost for the entire year, J_{bat}, which we then divided by an investment cost of 400 €/kwh used in Fortenbacher et al.[37] to determine the percent capacity degradation.

$$J_{bat} = b(E_t - a)^2 + cP_{ch,t} + dP_{dis,t} + eP_{dis,t}{}^2 \qquad \text{eq. 23 ref. 37}$$

Table A - 13, Degradation parameters used in Fortenbacher et al.[37] equation (23 ref. 37)

a	9.25e-4	C_{bat} h^{-1} $(kWh)^{-1}$
b	1.05e-3	$(kWh)^{-1}$
c	0	$(kWh)^{-1}$
d	1.25e-6	$(kWh)^{-1}$
e	1.5e-5	kWh $(kW)^{-2}$ h^{-1} $C_{bat}{}^{-1}$

The second model tested, Wang et al.[38] is dependent on temperature, which stems from its design for vehicle batteries, but for this analysis, we assumed the batteries will be in a temperature-controlled setting at 25°C. Modeling temperature fluctuations is an important area of future study. In equation (5 ref. 38) of their paper, $Q_{loss,\%}$, the percent capacity degradation based on the age of the battery in days, *t*, is:

$$Q_{loss,\%} = (aT^2 + bT + c)exp[(dT + e)I_{rate}]Ah_{throughput} + ft^{0.5}exp[-E_a/RT] \qquad \text{eq. 5 ref. 38}$$

Table A - 14, Degradation parameters used in Wang et al.[38] equation (5 ref. 38)

a	8.61e-6	1/Ah-K^2
b	-5.13e-3	1/Ah-K
c	7.63e-1	1/Ah
d	-6.7e-3	1/K-(C-rate)
e	2.35	1/(C-rate)
f	14,876	1/day$^{1/2}$
$\mathrm{I_{rate}}$	2.63	C-rate
t		Days
$\mathrm{E_a}$	24.5	kJ mol^{-1}
R	8.314	kJ mol^{-1} K^{-1}
T	298	K

In this model, degradation includes two components. One is due to cycling, which is determined by the total amount of charge delivered by the battery during cycling, denoted $Ah_{throughput}$; the other is standing degradation, which is determined by time. The model was developed through laboratory experiments. The $Ah_{throughput}$ is calculated by:

$$Ah_{throughput} = N_{cyc} * \mathrm{I_{rate}}, \tag{23}$$

where N_{cyc} is the average number of cycles per day. Again, the PJM data with offsets are used to evaluate the degradation. Figure A-10 shows the battery degradation due to providing frequency regulation (PJM signal with offsets) calculated from Xu et al.'s[32], Fortenbacher et al.'s[37], and Wang et al.'s[38] models.

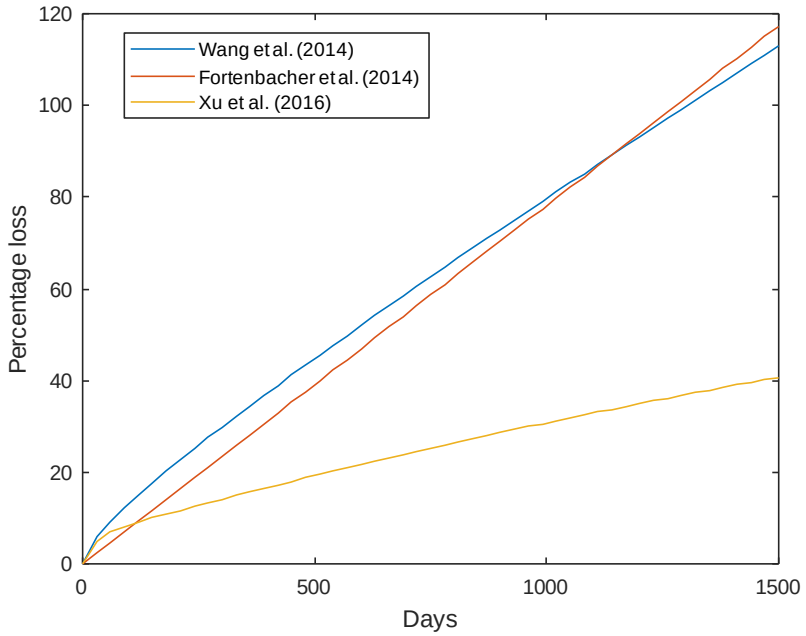

Figure A - 10, The rate battery capacity degradation for Xu et al.'s[32], Fortenbacher et al.'s[37], and Wang et al.'s[38] models.

2.3. Efficiency Degradation

Internal resistance, which can increase over time, has a significant impact on a battery's efficiency. Therefore, in order to model our battery system's rate of efficiency degradation, we first calculated its yearly increase in internal resistance, using data from Cordoba-Arenas et al.[90] Then, we computed the efficiency degradation from the resistance increase.

The main factors affecting resistive increase are $Ah_{throughput}$, the rate at which the battery is charged and discharged denoted, c_{rate}, temperature, and the minimum SOC, denoted SOC_{min}. Again, using the PJM data with offsets and the parameter values in Section 2.2, the $Ah_{throughput}$ per year is 7 kAh and the SOC_{min} is 0.2. Also, the c_{rate} of our battery system is 2.63, which is calculated from the E/P of 0.38. Based on these parameters, we estimate the percentage resistance increase per year, R_{inc}, to be 4% using the data in Figure 12 of Cordoba-Arenas et al. (2015).

Next we use R_{inc} to characterize the battery system's efficiency degradation. Let P be the battery system power assuming 100% efficiency, let P_{R_o} be the battery system power at the start of the year, and let P_R be the battery system power at the end of the year. Also, let n_o be the battery's initial efficiency at the start of the year and n_R be the battery system's efficiency at the end of one year. We have:

$$n_o = \frac{P - P_{R_o}}{P} = \frac{P - I^2 R_0}{P}, \tag{24}$$

$$n_R = \frac{P - P_R}{P} = \frac{P - I^2 R}{P}. \tag{25}$$

Note that the percentage resistance increase per year, R_{inc}, can be expressed as:

$$R_{inc} = \frac{R - R_o}{R_o}. \tag{26}$$

After some algebraic manipulation of Equations (24)-(26), we get:

$$n_R = 1 - (1 - n_o)(R_{inc} + 1), \tag{27}$$

which is used to calculate efficiency degradation.

3. Supplemental Results

3.1. *Base Case Scenario*

Figure A-11 shows the life cycle inventory data for NO_x, SO_x and CO_2 corresponding to the base case.

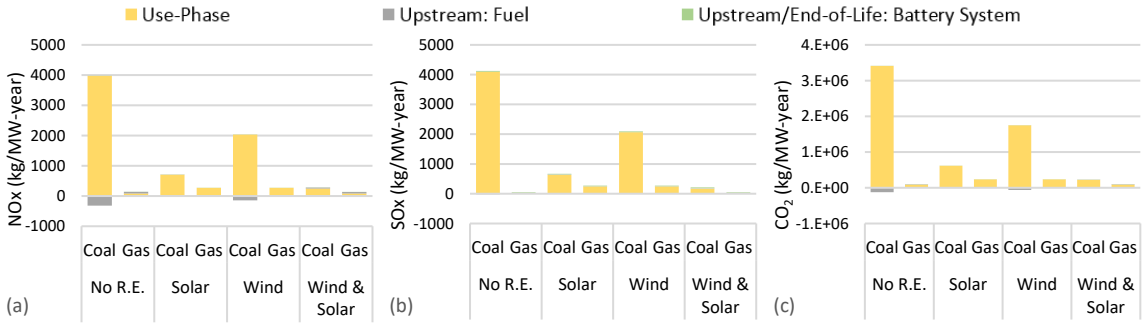

Figure A - 11, Changes in emissions from using Li-ion battery systems for frequency regulation for each base case scenario, a) NOx b) SOx and c) CO2. Yellow bars are use-phase impacts resulting from changes in the quantity/efficiency of coal/gas, grey bars are upstream impacts resulting from changes in the quantity of coal/gas, and green bars are upstream/end-of-life impacts of the battery system. R.E. = Renewable Energy

3.2. *Curtailment Scenario*

We determined the percent renewable capacity required to reach 10% curtailment (Table A-14) in each scenario using a brute force method. We used the renewable generation profile and the actual renewable energy generated after the first 24-hour time interval to calculate the percent curtailment of renewable generation for each scenario without energy storage. We increased the renewable energy generation by multiplying the load profile by a steadily increasing factor until the curtailment, after the first time interval, reached 10%.

Table A - 15, Percent wind and/or solar generation pre-curtailment to achieve 10% curtailment

Fuel	Renewable Resources	Percent Renewable Generation
Coal	Wind & Solar	40.5%
Coal	Solar	21.4%
Coal	Wind	43.5%
Gas	Wind & Solar	54.0%
Gas	Solar	29.4%
Gas	Wind	55.5%

Figure A-12 shows the life cycle inventory data for NO_x, SO_x and CO_2 corresponding to the curtailment case.

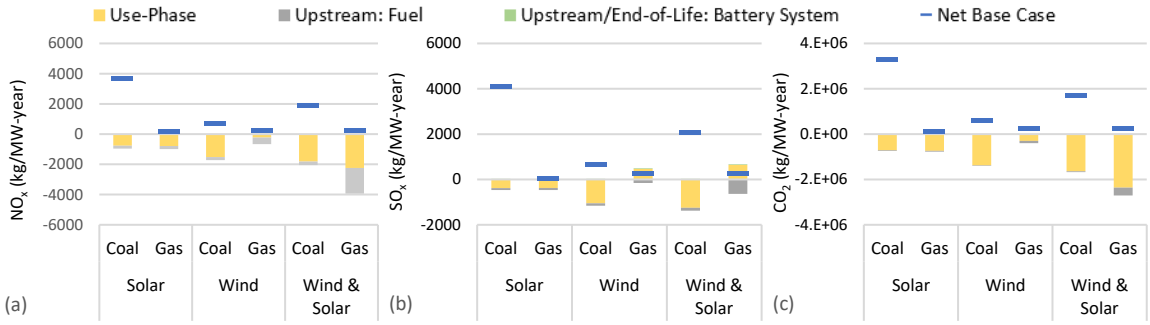

Figure A - 12, Change in environmental impacts from using Li-ion battery systems for power system frequency regulation for each curtailment scenario, a) NO_x, b) SO_x and c) CO_2. The blue lines are the net base case impacts. Yellow bars are use-phase impacts resulting from changes in the quantity/efficiency of coal/gas, grey bars are upstream impacts resulting from changes in the quantity of coal/gas, and green bars are upstream/end-of-life impacts of the battery system. R.E. = Renewable Energy

3.3. Complete Parametric Study Results

Figure A-13 shows the emissions and Figure A-14 shows the environmental impacts that were not included in the body of the paper for each parametric study.

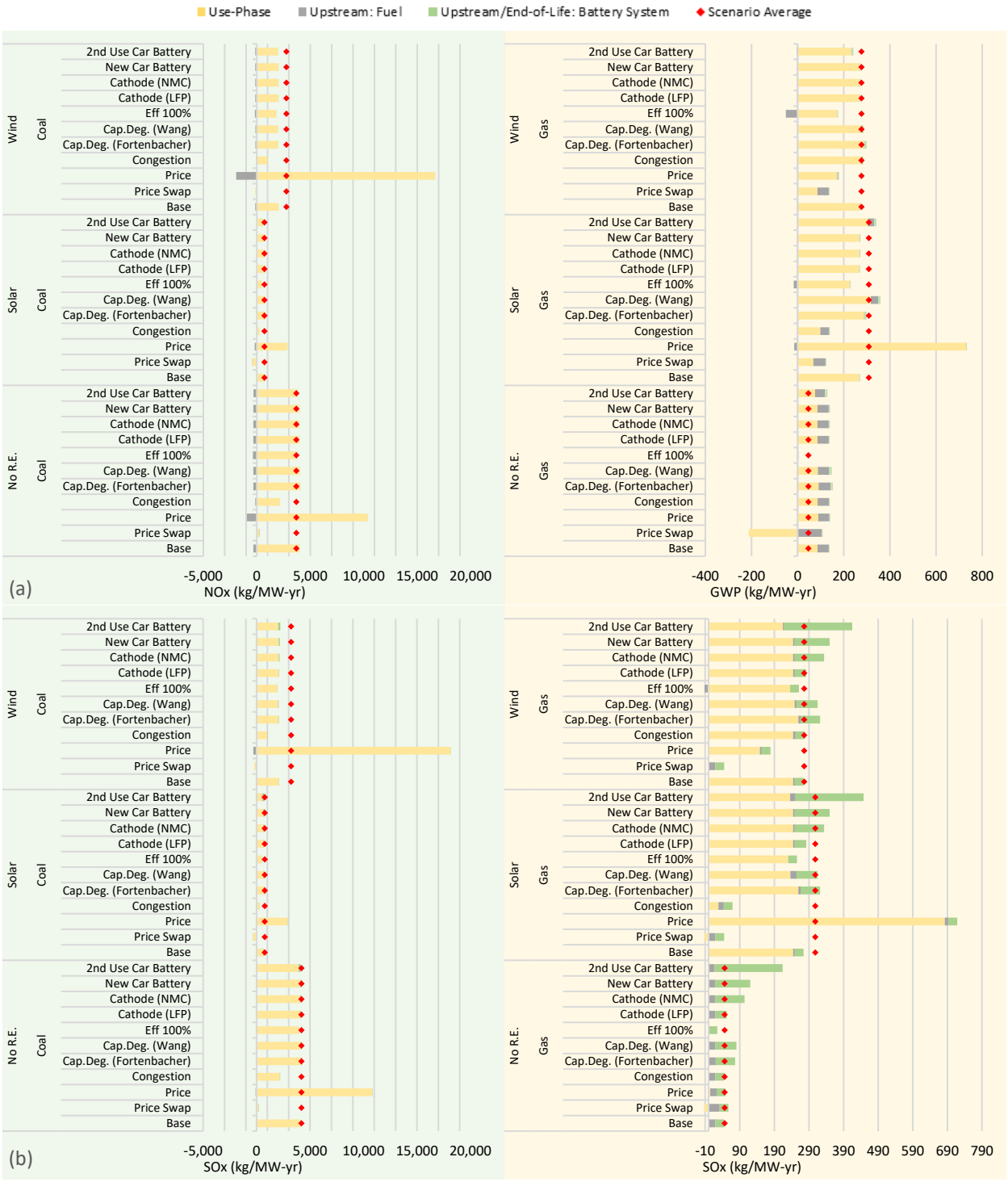

Figure A - 13, (a) NO_x, (b) SO_x for each parametric study under each scenario listed in Table 1 due to the addition of 1 MW-yr of frequency regulation capacity provided by Li-ion battery systems. The red dots represent the average value across parametric studies for each scenario. Coal cases correspond to the left axes and Gas cases correspond to the right axis. Note the difference in scale between the two axes. See Table 2 for details on parametric studies. Yellow bars are use-phase impacts resulting from changes in the quantity/efficiency of coal/gas generation, grey bars are upstream fuel impacts resulting from changes in the quantity of coal/gas, and green bars are upstream/end-of-life impacts of the battery system. R.E. = Renewable Energy

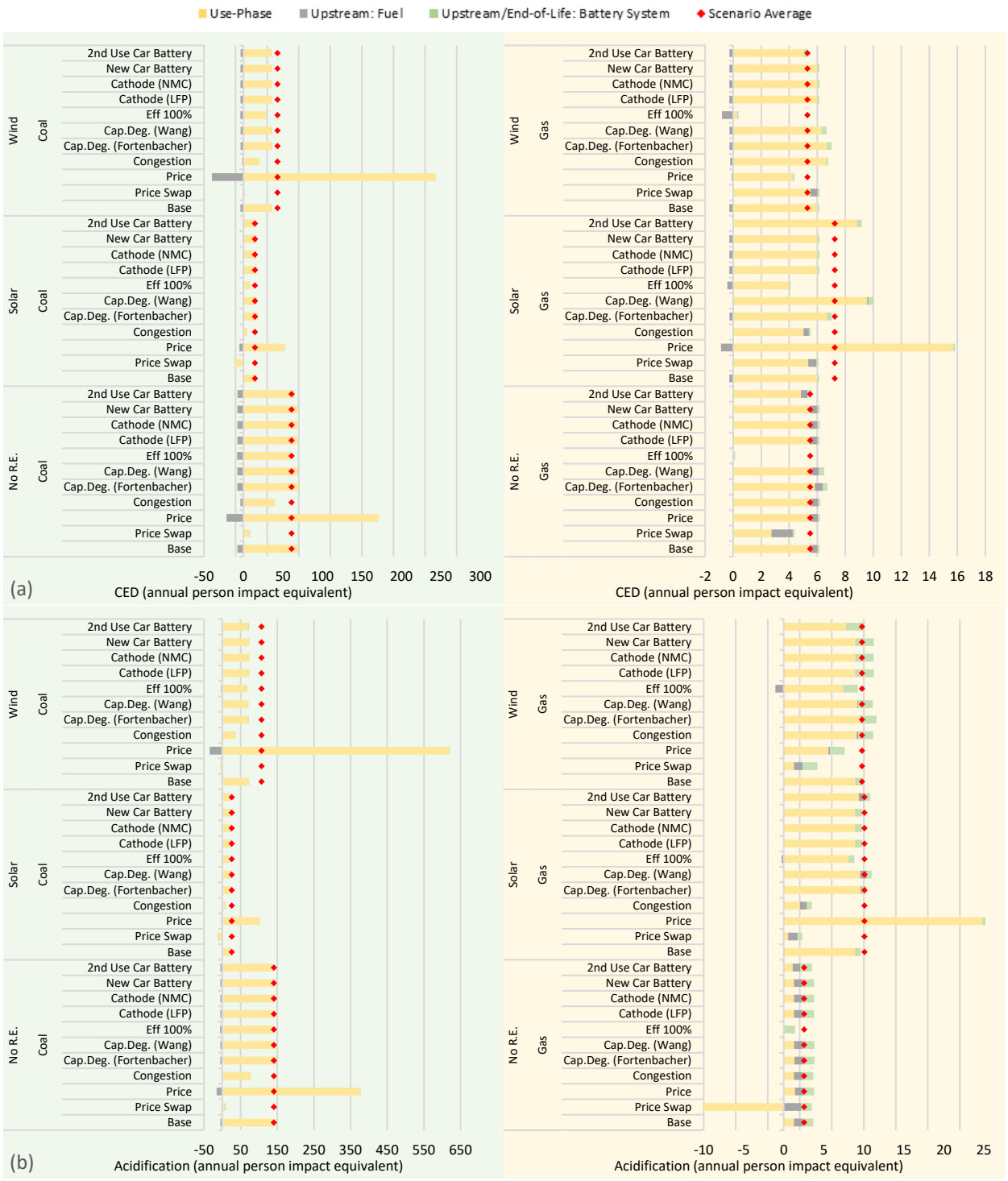

Figure A - 14, (a) Cumulative energy demand (CED) and (b) acidification impacts for each parametric study under each scenario listed in Table 1 due to the addition of 1 MW-yr of frequency regulation capacity provided by Li-ion battery systems normalized by average U.S. per-capita annual impacts. The red dots represent the average value across parametric studies for each scenario. Coal cases correspond to the left axes and Gas cases correspond to the right axis. Note the difference in scale between the two axes. See Table 2 for details on parametric studies. Yellow bars are use-phase impacts resulting from changes in the quantity/efficiency of coal/gas generation, grey bars are upstream fuel impacts resulting from changes in the quantity of coal/gas, and green bars are upstream/end-of-life impacts of the battery system. R.E. = Renewable Energy

3.3.1. Congestion Study

Transmission congestion was added to the Coal cases by reducing the line limits from 1000 MW to 200 MW and to the Gas cases by reducing the line limits to 170 MW in all lines other than those connecting generators to the system (i.e., 1-4, 3-6, and 8-2). Table A-15 details which lines were congested in each scenario with these line limits in place. Lines 7-8 and 8-9 connect the renewable generation and the energy storage bus to loads and lines 9-4 and 6-7 connect generator buses to loads

Table A - 16, Number of hours in the first day of the energy storage's life that a line is operating at its limit

Scenario	Line			
	6-7	7-8	8-9	9-4
Coal No R.E.	0	1	0	0
Coal Solar	0	9	1	0
Coal Wind	0	15	0	0
NG No R.E.	5	0	0	1
NG Solar	1	8	8	0
NG Wind	0	1	0	0

3.3.2. Capacity Degradation Study (Wang)

Figure A-15 shows emissions and Figure A-16 shows the environmental impacts of the Wang et al. capacity degradation model in comparison to the base case normalized based on average per-capita impacts for the U.S. in 2016.

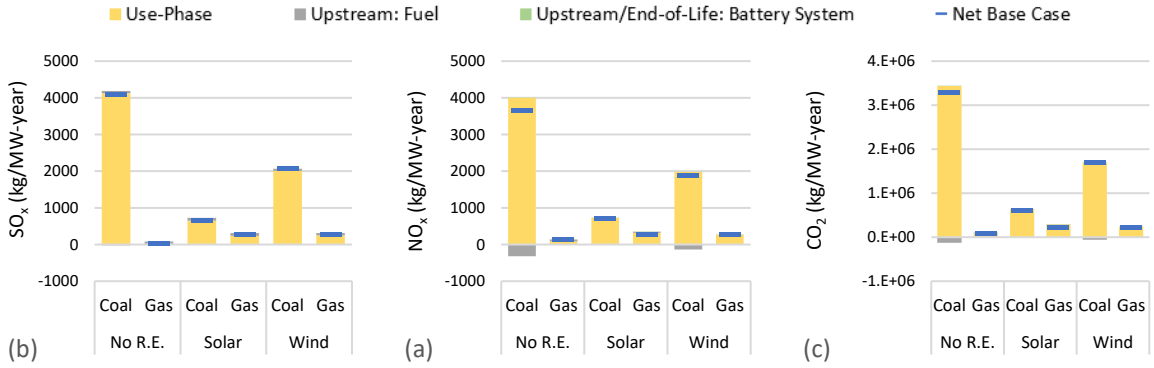

Figure A - 15, Change in emissions from using Li-ion energy storage for power system frequency regulation for each Wang capacity degradation scenario, a) NO_x, b) SO_x and c) CO_2 The blue lines are the net base case impacts. Yellow bars are use-phase impacts resulting from changes in the quantity/efficiency of coal/gas, grey bars are upstream impacts resulting from changes in the quantity of coal/gas, and green bars are upstream/end-of-life impacts of the battery system. R.E. = Renewable Energy

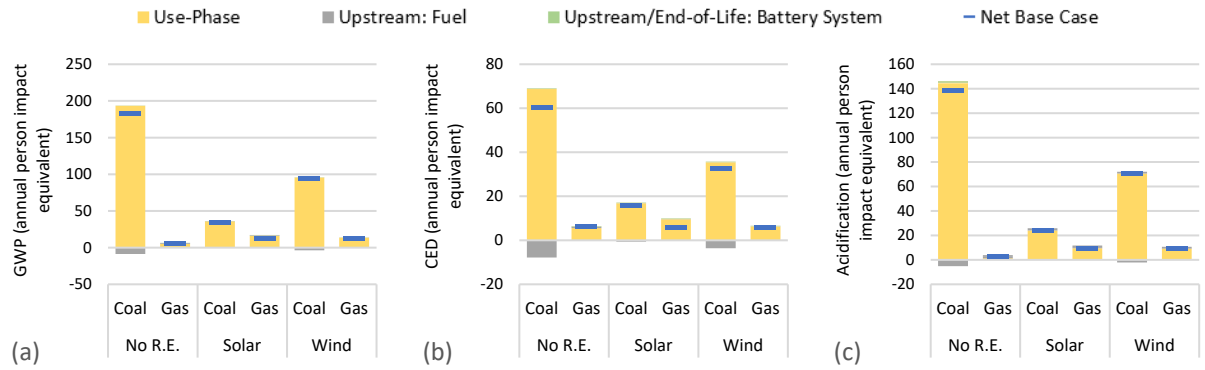

Figure A - 16, Change in environmental impacts from using Li-ion energy storage for power system frequency regulation for each Wang capacity degradation scenario, a) global warming potential (GWP), b) cumulative energy demand (CED) and c) acidification. The blue lines are the net base case impacts. Yellow bars are use-phase impacts resulting from changes in the quantity/efficiency of coal/gas, grey bars are upstream impacts resulting from changes in the quantity of coal/gas, and green bars are upstream/end-of-life impacts of the battery system. R.E. = Renewable Energy

3.3.3. Capacity Degradation Study (Fortenbacher)

Figure A-17 shows emissions and Figure A-18 shows the environmental impacts of the Wang et al. capacity degradation model in comparison to the base case normalized based on average per-capita impacts for the U.S. in 2016.

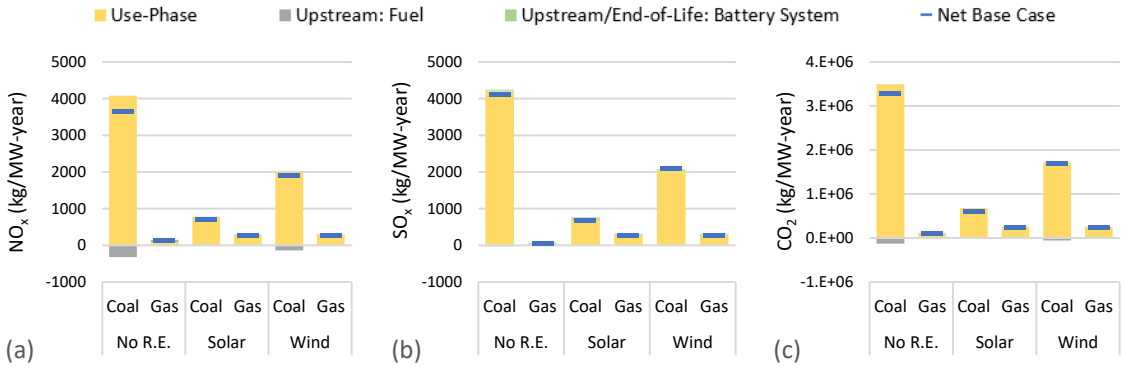

Figure A - 17, Change in emissions from using Li-ion energy storage for power system frequency regulation for each Fortenbacher capacity degradation scenario, a) NOx, b) SOx and c) CO2 The blue lines are the net base case impacts. Yellow bars are use-phase impacts resulting from changes in the quantity/efficiency of coal/gas, grey bars are upstream impacts resulting from changes in the quantity of coal/gas, and green bars are upstream/end-of-life impacts of the battery system. R.E. = Renewable Energy

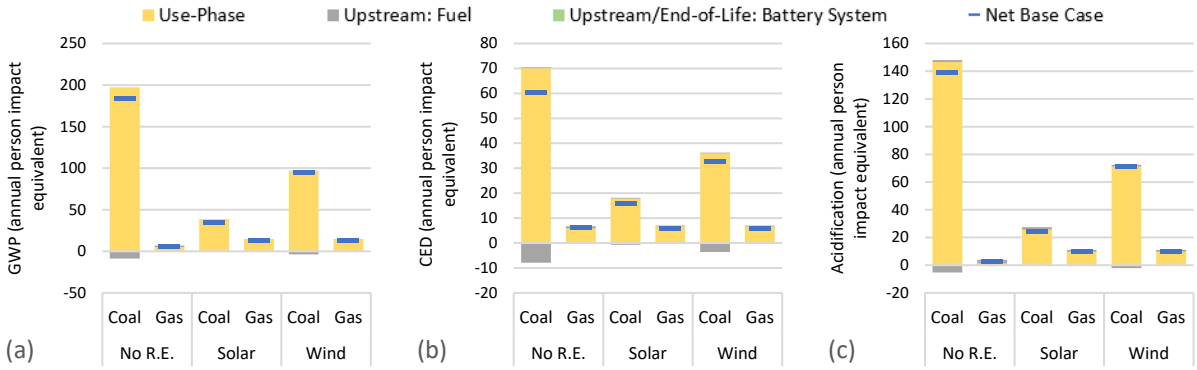

Figure A - 18, Change in environmental impacts from using Li-ion energy storage for power system frequency regulation for each Fortenbacher capacity degradation scenario, a) global warming potential (GWP), b) cumulative energy demand (CED) and c) acidification. The blue lines are the net base case impacts. Yellow bars are use-phase impacts resulting from changes in the quantity/efficiency of coal/gas, grey bars are upstream impacts resulting from changes in the quantity of coal/gas, and green bars are upstream/end-of-life impacts of the battery system. R.E. = Renewable Energy

3.3.4. Efficiency and Efficiency Degradation Study

Figure A-18 shows the environmental impacts of efficiency and efficiency degradation by showing the difference between net use-phase impacts in the base case and with a 100% efficient battery with no degradation.

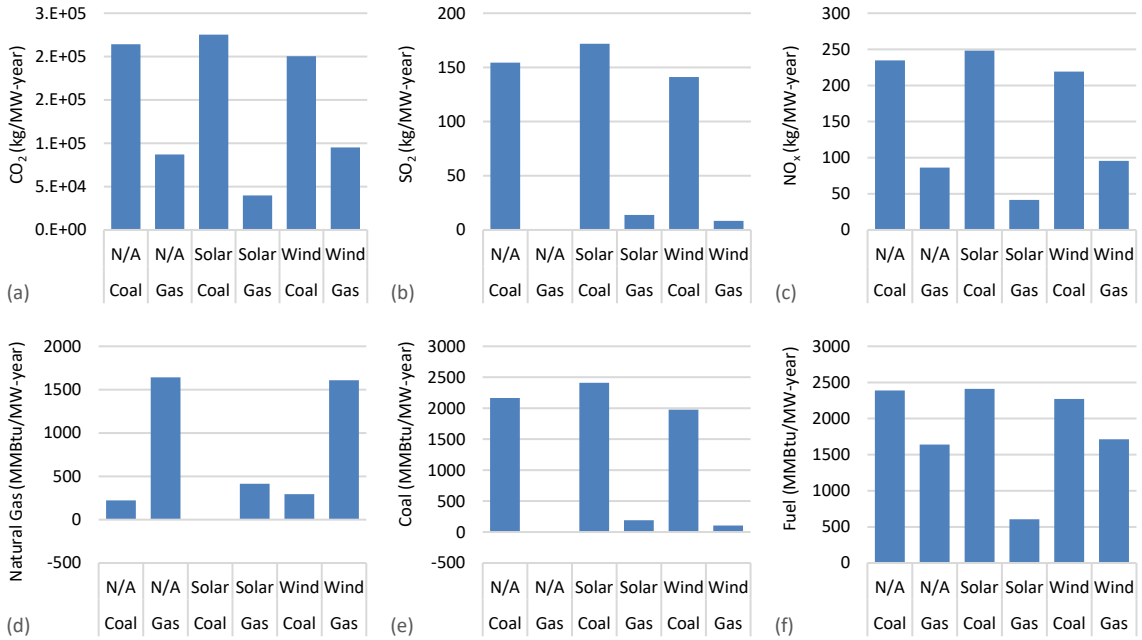

Figure A - 19, Difference in impacts between the base case and 100% efficient battery system a) CO_2, b) SO_x, c) NO_x, d) natural gas consumption, e) coal consumption, f) net fuel consumption. R.E. = Renewable Energy

3.3.5. Battery Type Study

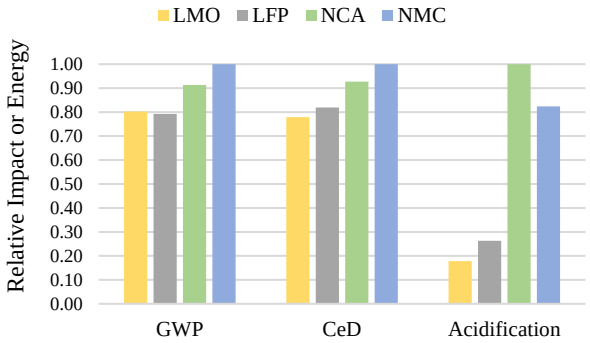

Figure A - 20, Relative environmental impacts from battery production (this figure does not include assembly). LiMn2O4 (LMO), LiFePO4 (LFP), LiNiMnCoO2 (NMC) and LiNiCoAlO2 (NCA).

4. Variables

Symbol	Description
	Unit Commitment and Dispatch
A_g	Diagonal matrix of quadratic cost coefficients for conventional generators
B_g	Column vector of linear cost coefficients for conventional generators
B_{gr}	Column vector of cost coefficients for renewable generation plants
B_r	Column vector of cost coefficients for frequency regulation
B_{es}	Column vector of cost coefficients for energy storage
B_{on}	Column vector of cost coefficients for start-up
B_{off}	Column vector of cost coefficients for shut-down
β	Parameter for additional load from energy storage-based frequency regulation
C^g	Grid topology matrix mapping conventional generators
C^{gr}	Grid topology matrix mapping renewable generators
C^d	Grid topology matrix of load
C^{es}	Grid topology matrix mapping energy storage
D_b	Matrix describes the relationship between bus voltage angle and bus power injection
D_f	Matrix describes the relationship between bus voltage angle and line power flow
η_{ch}	Energy storage charging efficiency
η_{dis}	Energy storage discharging efficiency
n_g	Number of conventional generators
n_{gr}	Number of renewable generation plants
n_{es}	Number of energy storage devices
n_b	Number of buses
n_l	Number of transmission lines
Θ_t	Bus voltage angle
P_t^g	Power output of the conventional generators
P_t^{gr}	Power output of renewable generation
$P_{b,t}$	Power injected at each bus
P_t^d	Load at each bus
$P_t^{d,es}$	Additional load at each bus due to round trip losses from energy storage
$P_{f,t}$	Power flow through each transmission line
$P_{f,t}^{gr}$	Forecast capacity of renewable generation

$P_{f,min}$	Lower limit for line flow
$P_{f,max}$	Upper limit for line flow
P_{min}^{g}	Lower bound of generator output
P_{max}^{g}	Upper bound of generator output
R_t^g	Frequency regulation capacity of the conventional generators
R_t^{es}	Frequency regulation capacity of energy storage
R_{min}^{es}	Lower limit for energy storage frequency regulation capacity
R_{max}^{es}	Upper limit for energy storage frequency regulation capacity
r_{req}	Frequency regulation capacity required by the power system
t_{on}^{j}	Minimum up time for the j^{th} conventional generator
t_{off}^{j}	Minimum down time for the j^{th} conventional generator
U_t	Binary decision variable for generator commitment
V_t	Binary variable for generator start-up
W_t	Binary variable for generator shut-down
	Capacity Degradation
Ah_{rated}	Rated battery current
$Ah_{throughput}$	The total current delivered by the battery during cycling
$E_{o,end}$	The SOC at the end of an hour resulting from $P_{o,t}$
E/P	Energy to power ratio
E_t	The SOC at time *t*
k_{ep}	Describes how aggressively the energy storage is bidding into the market, 1/(E/P)
N_{cyc}	Number of cycles
$P_{ch,t}$	Power injected into the battery
$P_{dis,t}$	Power extracted from the battery
$P_{o,t}$	The initial power injected/extracted prior to the addition of the offset
P_{PJM}	Actual reference signal from PJM
P_t	Power injected/extraction of the energy storage at time *t*
δP	Power offset
Δt	Time interval in hours
	Efficiency Degradation
I	Battery current
n_o	Initial battery efficiency
n	Battery efficiency after resistance increase
P	Battery power assuming 100% efficiency
P_{R_o}	Initial battery power with initial efficiency
P_R	Battery power after resistance increase
R_{inc}	Percent resistance increase
R_o	Initial battery resistance
R	Resistance after degradation

Appendix B:

The Impact of Forecasted Net Load on Real-Time Power Generator Operation

1. Power System Model

1.1. Input Data

1.1.1. Generators

The generator database is originally derived from the Transmission Expansion Planning Policy Committee (TEPPC) 2024 Common Case, and was modified for use in the National Renewable Energy Laboratory's Low Carbon Grid Study.[121,122] The primary modification for this chapter is the increase in variable renewable energy (VRE) discussed in section 1.1.3. Additionally, all local generation constraints were removed.

Given the focus of this study is generator scheduling it is important to understand each generator types' constraints, listed in Table B-1. Each unit type's flexibility varies significantly, with combustion turbines being the most flexible. They have the shortest minimum up and down times, as well as, the fastest ramp rate, which allows to be re-committed in the real-time. Nuclear is the least flexible, with a very low ramp rate. Its minimum up and down types are not applicable because these units are modeled such that they are not allowed to cycle, as this is how they are generally run.

Table B - 1, Generator constraints

Category	Combustion Turbine	Combined Cycle	Coal	Gas Boiler	Nuclear
Minimum Generation Level (% of Maximum Capacity)	45	55	40	15	50
Minimum Up Time (Hours)	2	8	24	12	NA
Minimum Down Time (Hours)	2	4	48	8	NA
Ramp Rate (% of Max Capacity per Min)	5.4	0.8	0.9	1.7	0.3

Each region of the U.S. has its own unique distribution of different generator types, making some more flexible than others. One of the major limits to a system's flexibility is generator minimum generation level. In an effort to examine the impact of a small change in flexibility of the system we decreased coal units' minimum generation level by 20%. This change is similar to the change Palchak and Denholm (2014) made to minimum generation levels when examining the impact of generator flexibility on cost. However, they reduced coal's minimum generation level from 60% of max capacity to 40% a more extreme change than the one we made, give coal's minimum generation level is already at 40% in this model. [211]

1.1.2. Day-ahead VRE Forecasts

The day-ahead wind and solar forecasts were originally developed for NREL's Interconnection SEAMs study.[212] The solar data used to develop the forecasts is from 1209 National Solar Radiation Database (NSRDB) sites.[213] The NSRDB irradiance data was converted to power data using the System Advisor Model (SAM).[214] The NSRDB data is only available on the half-hour time scale. The wind data used to develop the wind forecasts is from 223 of sites from the Wind Integration National Dataset (WIND) Toolkit, which as 5-min data.[215] Both sets of data are from 2012, as it is considered the most average power year of those avaliable.[212]

A range of forecast error scenarios was modeled to test the predictability of the regression as forecast error changes, providing insight into whether the model is better predictor of commitment error due to uncertainty or variability. It is also likely that forecasts will improve as technology advances. Additionally, we only model the day-ahead market, when additional markets exist that allow certain generators to be re-committed closer to the real-time when forecasts are likely better, for example CAISO's short-term unit commitment.

We modeled six levels of forecast error from an increase of 25% to a decrease of 100% i.e., no forecast error. It is unlikely that the forecasts will become less accurate therefore we only modeled one scenario with an increase in forecast error.

Each subregion and VRE generator has its own forecast. Prior to modifying the forecasts from the base case, they were multiplied by four to increase the VRE generation four times. This simple method was also employed by Martinez-Anido et al. when examining the impacts of forecast error in the Independent System Operator New England.[123]

The percent changes in forecast error are based on the error between the day-ahead forecast and the real-time generation. The day-ahead is hourly and the real-time is on a five minute basis however, error was calculated by only using the values in the real-time forecast that fall on the beginning of each hour. The initial error in each hour, *t*, is calculated as follows,

$$\epsilon W_{t,r} = W_{DA,t,r} - W_{RT,t,r}, \quad (1)$$

$$\epsilon S_{UPV,t,r} = S_{UPV.DA,t,r} - S_{UPV,RT,t,r}, \quad (2)$$

$$\epsilon S_{DPV,t,r} = S_{DPV.DA,t,r} - S_{DPV,RT,t,r}, \quad (3)$$

where, *r*, is the subregion, and *W*, is wind, *S* is solar, *D*, is distributed photovoltaics, and *U* is utility scale photovoltaics.

In order to create the new forecasts the error is multiplied by a factor, Δ, from 0.25 to -1, in increments of 0.25, depending on the scenario, and added to the original forecast to develop the new forecasts for each scenario, *i*.

$$W_{DA,t,r,i} = W_{DA,t,r,i} + (\Delta_i)\epsilon W_{t,r} \quad (4)$$

$$S_{U,DA,t,r,i} = S_{U,DA,t,r,i} + (\Delta_i)\epsilon S_{U,t,r} \quad (5)$$

$$S_{D,DA,t,r,i} = S_{D,DA,t,r,i} + (\Delta_i)\epsilon S_{D,t,r} \quad (6)$$

The new forecasts are verified by calculating their RMSE, table B-2. These values are calculated for the regional level forecasts.

Table B - 2, Root mean squared error for each forecast error scenario and variable renewable energy type. UPV = utility scale photovoltaics, DPV = distributed solar photovoltaics

Change in Error	Wind	UPV	DPV
+25%	134.7	29.9	14.3
Base Case	107.7	24.0	11.5
-25%	80.8	18.0	8.6
-50%	53.9	12.0	5.7
-75%	26.9	6.0	2.9
-100%	0.0	0.0	0.0

1.1.3. Reserves

This model contains one reserve product, which is combination of contingency and regulation reserves. The methods used to calculate these reserve products are outlined in Ibanez et al. (2012).[216] These methods have been used in a number of large grid studies executed in PLEXOS.[212] The reserve product calculations used the base case wind and solar forecasts and the real-time load, wind, and solar data, as well as, solar clear sky data.

1.2. Week Selection

Given the computational time required to run the real-time market for all of WECC and the number of forecast error scenarios, we only ran the weeks we anticipated having the most and least amount of commitment error i.e., the weeks with the most and least variability and ramping, Table B-3. We separated the two types of weeks to gain further insight into the impact the parameters had on commitment error. The base case net load, prior to any adjustments in forecast error or wind and solar generation is representative of the day-ahead net load, ρ_t, and the real-time net load, P_t, in the following calculations.

Table B - 3, Weeks selected based on analysis of variability and ramp rate

Week Type	Start Date	Week #
High Ramp	August 5, 2024	32
Low Ramp	Nov 18, 2024	47
High Variability	July 14, 2024	29
Low Variability	Nov 11, 2024	46

1.2.1. Calculating weekly ramp

The absolute value of the ramp rate, $A\epsilon_{t,r}$ in each hour, *t*, and each subregion, *r*, is calculated as follows across the year,

$$A\varepsilon_{t,r} = \left|\rho_{t,r} - \rho_{t-1,r}\right|. \quad (7)$$

The absolute value of the ramp was used so that the positive and negative values in different regions did not cancel each other out. This maintains the regional granularity of the ramp rate.

The weeks are compared based on the average of the sum of the ramp rate in each region, across each week, $T\varepsilon_w$,

$$T\varepsilon_w = \frac{\sum_0^{week}\sum_0^r A\varepsilon_{t,r}}{(7)*(24)}. \quad (8)$$

1.2.2. Calculating weekly variability

In order to calculate the intra-hour variability, $\mu_{t,r}$, the real-time net load, $P_{t,r,n}$, has to be used, given the day-ahead is on an hourly time scale, where *n* is the intra-hourly time increment and *t* is the hour.

$$\mu_{t,r} = \max_{0\ to\ n} P_{t,r,n} - \min_{0\ to\ n} P_{t,r,n}. \quad (9)$$

The variability is calculated for each week in the same way as the ramp, in eq. (9).

$$T\mu_w = \frac{\sum_0^{week}\sum_0^r \mu_{t,r}}{(7)*(24)}. \quad (10)$$

1.3. PLEXOS Modeling

1.3.1. Commitment Changes

We designed the production cost model to only allow certain generators change commitment in the real-time. The only fossil generation allowed is combustion turbines all other units are types of energy storage (pumped storage, batteries, and demand response) or VRE with the addition of hydro and concentrating solar power, whose commitments are uncontrollable unless they are curtailed. In order to model this behavior in PLEXOS we needed to pass the commitment data from the output of the day-ahead runs into the real-time runs. Therefore, we set the day-ahead runs to create a report, i.e., a csv file, for each generator's 'units generating' property. For the units

who are not allowed to change commitment in the real-time, the value for their 'commit' property is pointed to the 'units generating' property from the day-ahead and it is left free for those that can change commitment. This is similar to how the generator outage schedules are passed from the PASA to the day-ahead to the real-time.

1.3.2. Model Settings

PLEXOS has an array of model attributes that will change how the system is optimized. Table B - 4 includes some of the key attributes of the day-ahead runs and the real-time runs.

Table B - 5, Important PLEXOS model attributes for the day-ahead and real-time runs

Category		Day-ahead	Real-time
	Horizon Settings		
Time Interval		Hourly	5-min
Look ahead		none	none
	Production Settings		
Max Heat Rate Tranches		6	6
	Performance Settings		
Solver		2	2
MIP Relative Gap		0.01	0.001
Improve Start Gap		0	0
MIP Max Time		65000	65000
MIP Maximum Threads		4	4
	Transmission Settings		
OPF Method		1	1
Constraint Voltage Threshold		600	600
Max Loss Tranches		10	10

2. Power System Results

2.1. Generation

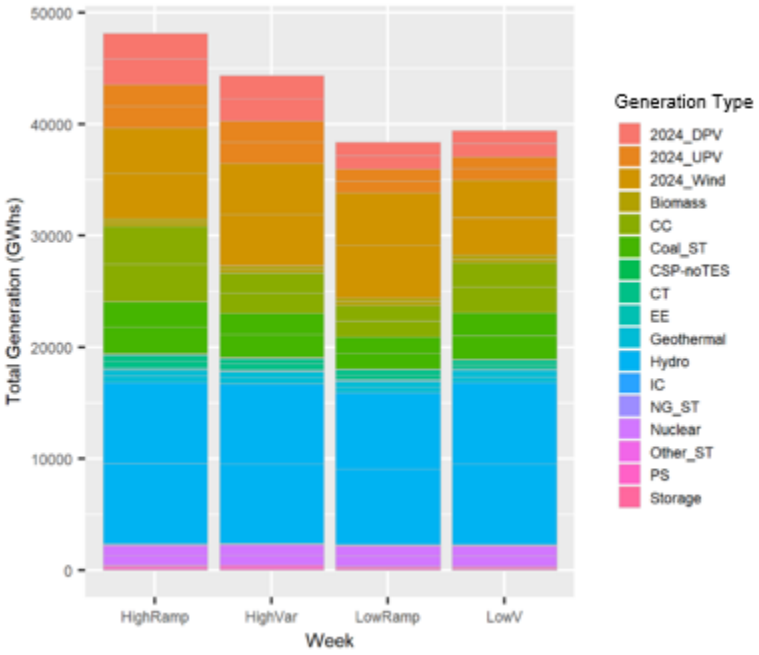

Figure B - 1, Total generation by type for each week for the base case level of forecast error

3. Statistical Results

Table B - 6, Variable P-values for each final model

0.001	***	0.01	**	0.05	*		not significant		not in model

Variables	*Hour (t or t-n)*	*WECC*						*CAISO*					
		Improvement in Forecast Error (%)											
		-25	*0*	*25*	*50*	*75*	*100*	*-25*	*0*	*25*	*50*	*75*	*100*
Net Load (ρ_t), B_1	0												
Net Load (ρ_t), B_2	0												
Relative Net Load ($R\rho_t$), B_1	0												
Relative Net Load ($R\rho_t$), B_2	0												
Fraction VRE (g_t)	0												
	1												
	2												
	3												
	4												
Ramp Rate (ε_t)	0												
	0-1												
	0-2												
	0-3												
	0-4												
Relative Ramp Rate ($R\varepsilon_t$)	0												
	1												
	2												
	3												
	4												
	0-1												
	0-2												
	0-3												
	0-4												
Variability (μ_t)	0-1												
	0-2												
	0-3												
	0-4												
Hour (h), B_1	0												
Hour (h), B_2	0												
Hour (h), B_3	0												
Controls													
Week (HighVar)	0												
Week (LowRamp)	0												
Week (LowV)	0												

Appendix C:

Reducing CO_2 emissions from U.S. steel consumption by 70% by 2050

1. Methods Outline

This work combines *steelmaking technology scenarios*, *trade scenarios*, and *steel flow parameters* resulting in 329,284 potential pathways the U.S. could take to reduce CO_2 emissions from steel consumption. The values for each parameter and scenario are outlined in Table C-1 and discussed in more detail in the proceeding sections of Appendix C.

Table C - 1, Different 2050 scenarios and steel flow parameter and population values simulated in the model. 16 x 3 x 7 x 14 x 5 x 2 x 7 = 329,280 U.S. steel industry pathways simulated in total

Steelmaking Technology scenarios	Trade scenarios	Steel flow parameters				Population (million)
		Stocks per capita (tons/cap)	Product lifespan	Recycling rate	Manufacturing process yield	
Basecase emissions (U.S.) & Basecase emissions (ROW)	Zero	8	Bascase - 30%*	Basecase - 10%	Basecase	328
Basecase emissions (U.S.) & High emissions (ROW)	Medium	9	Bascase - 20%*	Basecase - 5%	Basecase +10%	347
Basecase emissions (U.S.) & Mid emissions (ROW)	High	10	Bascase - 10%*	Basecase		368
Basecase emissions (U.S.) & Low emissions (ROW)		11	Bascase*	Basecase +5%		389
High emissions (U.S.) & Basecase emissions (ROW)		12	Bascase +10%*	Basecase +10%		410
High emissions (U.S.) & High emissions (ROW)		13	Bascase +20%*			431
High emissions (U.S.) & Mid emissions (ROW)		14	Bascase +30%*			452
High emissions (U.S.) & Low emissions (ROW)			Bascase - 30%**			
Mid emissions (U.S.) & Basecase emissions (ROW)			Bascase - 20%**			
Mid emissions (U.S.) & High emissions (ROW)			Bascase - 10%**			
Mid emissions (U.S.) & Mid emissions (ROW)			Bascase**			
Mid emissions (U.S.) & Low emissions (ROW)			Bascase +10%**			
Low emissions (U.S.) & Basecase emissions (ROW)			Bascase +20%**			
Low emissions (U.S.) & High emissions (ROW)			Bascase +30%**			
Low emissions (U.S.) & Mid emissions (ROW)						
Low emissions (U.S.) & Low emissions (ROW)						
Totals						
16	3	7	14	5	2	7

*Applied to both new and existing products
**Applied only to new products

Modeling each pathway required the use of existing data on steel production and consumption in the U.S. and globally, two dynamic material flow analysis (DFMA), and mass flow optimization. Figure C-1 depicts how each pathway is modeled and CO_2 emissions calculated. The SI complements the paper by providing more details on each step depicted in Figure C-1. The SI includes references for all input data, justification and references for each trade and technology

scenario, detailed calculations for all modeling steps, and results figures for each combination of scenarios and parameters not represented in the body of the paper.

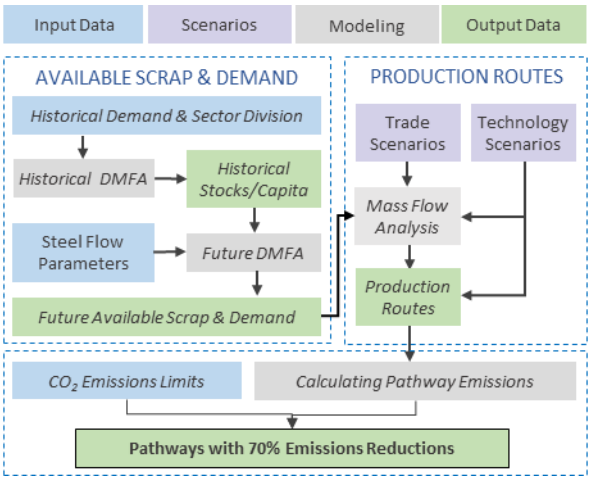

Figure C - 1, Schematic of methodology

2. Available Scrap & Demand

2.1. Historical Demand & Sector Division

Available data for historical steel demand in the U.S. have evolved and improved over the years. The American Iron and Steel Institute (AISI) published their first book of annual statistics in 1912 with data going back to 1810.[217] However, in order to estimate the quantity of in-use stocks and scrap produced in the U.S. the amount of final steel going into use, or consumption, is required. World Steel Yearbook estimated 'True Consumption' is currently the best estimate of consumption, however, this data only dates back to 2002 and has not been calculated for more recent years yet. Therefore, for all other years of data we used a combination of data on apparent consumption, production, yields, and indirect net imports in order to estimate true consumption dating back to 1880. 'True Consumption', as defined by the World Steel Yearbook as apparent steel use minus net indirect exports (i.e., apparent consumption does not include net indirect imports).[133] Apparent consumption is defined by USGS as steel shipments plus imports minus exports plus adjustments for industry stock changes minus semi-finished steel product imports.[218] Indirect net imports are the steel that is imbedded in final products like cars, washing machines, etc. As discussed earlier a large percentage of demand is supplied by imports, a value that has not been historically constant. These imports are a combination of net steel product imports and net indirect imports. Therefore, when 'True Consumption' values are not available but 'Apparent

Consumption' is available we use the United Nations Commodity Trade (Comtrade) database to estimate indirect imports (2017 & 2001-1962). From 1900 to 2015 United States Geological Survey (USGS) calculated the U.S. apparent.[219] These values were used for apparent consumption until 2002 when True consumption values are available from World Steel Yearbook. When imports and exports are no longer available production and process yield values are used to estimate consumption (1961-1880), table C-2. Muller et al. (2006) also ignored trade prior to 1950 as they assumed them to be negligible.[220] However, we are only excluding trade prior to 1940. Figure C-2 shows the resulting consumption for 1880-2017.

Table C - 2, Data sources and assumptions for historical demand

Years	Type	Source
2017	Apparent Consumption * + Indirect trade	United States Geological Survey
2016-2002	True Consumption	World Steel Yearbook
2001-1962	Apparent Consumption * + Indirect trade	United States Geological Survey
1961-1900**	Apparent Consumption *	United States Geological Survey
1899-1880**	(Production Steel Ingots & Casting) x Yield ***	American Iron and Steel Institute

*The apparent consumption was converted into the quantity of steel imbedded in products by multiplying by 0.84, based on Cullen et al.'s (2012) fabrication losses [16]
**Indirect trade is not included in true consumption estimates for these years as the net contribution is assumed to be negligible
*** Yield value of 0.78 used, based on Cullen et al.'s (2012) rolling/forming losses and fabrication losses [16]

Indirect trade is calculated from the Comtrade database by mapping the trade of 29 commodities which contain the highest cumulative global imports, totally over 1,000 Gg Fe/a globally.[221,222] These categories are a subset of the 220 categories Wang et al. (2007) used when characterizing iron cycles.[222] Table C-3 lists the commodity codes, part descriptions, percent iron and mass to value ratios. For 15 of the categories, the quantity (in kilograms) of the import and export category is reported and all other commodities listed are reported in U.S. dollar values. The quantity per U.S. dollar conversion factors, listed in table C-3, are from (Cooper 2019).

Table C - 3, Commodities mapped for indirect imports and exports[222]

SITC	STITC.1_Code	Parts or Final Product Descriptions	% Fe	Imports kg/$	Exports kg/$
S1	7321	Passenger motor cars, other than buses	0.65	0.05	0.04
S1	719	Machinery and appliances non electrical parts	0.75	0.11	0.13
S1	7328	Bodies & parts motor vehicles ex motorcycles	0.7	0.06	0.07
S1	698	Manufactures of metal	0.9	0.14	0.27
S1	729	Other electrical machinery and apparatus	0.55	0.03	0.03
S1	718	Machines for special industries	0.75	0.08	0.10
S1	7323	Lorries and trucks, including ambulances, etc.	0.8	0.10	0.11
S1	735	Ships and boats	0.9	0.12	0.15
S1	722	Electric power machinery and switchgear	0.55	0.03	0.02
S1	7250	Domestic electrical equipment	0.65	0.06	0.08
S1	69421	Nuts, bolts, screws, rivets, washers of iron/steel	0.98	0.20	0.32
S1	7115	Internal combustion engines, not for aircraft	0.5	0.03	0.03
S1	693	Wire products ex electric & fencing grills	0.9	0.19	0.30
S1	7333	Trailers & other vehicles not motorized, & parts	0.5	0.12	0.11
S1	861	Scientific, medical, & optical instruments	0.55	0.03	0.03
S3	8213	Metal furniture	0.7	0.16	0.15
S1	7316	Rail. &tram. cars ,not mechanically propelled	0.85	0.18	0.22
S1	69221	Casks, drums, etc. used for transport of iron/steel	0.96	0.25	0.28
S1	715	Metalworking machinery	0.65	0.06	0.06
S1	714	Office machines	0.22	0.02	0.02
S1	724	Telecommunications apparatus	0.25	0.02	0.02
S1	712	Agricultural machinery and implements	0.7	0.07	0.08
S1	894	Perambulators, toys, games and sporting goods	0.2	0.07	0.02
S1	695	Tools for use in the hand or in machines	0.85	0.23	0.05
S1	6291	Rubber tires & tubes for vehicles and aircraft	0.15	0.04	0.04
S1	717	Textile and leather machinery	0.65	0.06	0.06
S1	7325	Road tractors for tractor trailer combinations	0.8	0.13	0.17
S1	69721	Domestic utensils of iron or steel	0.95	0.24	0.16
S1	69411	Nails, tacks, staples, spikes, etc. of iron or steel	0.98	0.46	0.60

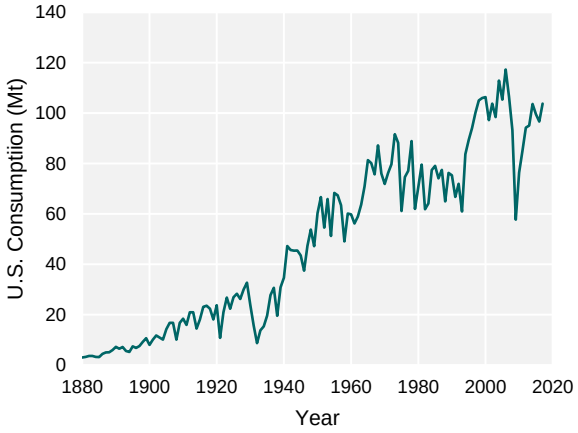

Figure C - 2, Historical United States Steel Consumption Estimate

We divided total consumption into four product sectors (construction, transportation, machinery and other/products), each having a different average lifespan and lifespan distributions. Meaning they are each modeled separately when estimating their in-use stock, end-of-life (EOL) scrap and future demand. A number of studies modeling the flow of steel use these four sectors.[37,173,220,223]

The percent of consumption attributed to each sector can potentially have a significant impact on the Dynamic Material Flow Analysis (DMFA) results (e.g., scrap) as it impacts stock and demand estimates. Pauliuk et al. (2013) found that the percent of demanded attributed to each sector has a similar impact on stock results as lifespan (i.e., it is one of the most influential parameters). However, calculating there percentages using primary data sources is challenging because a large percent of demand is classified as 'service centers' or 'other' in historic data.[173] Additionally, data sources are focused on domestic supply. Only the more recent data from AISI does not include the 'service center' classification. Therefore, we average AISI's estimated percentages from their yearly profiles for 2014 to 2017, found in table C-3. These values are kept constant across the modeling time frame, as done in Pauliuk et al. (2013), who also used AISI data sources for their sector splits.[173] We also assuming the sector split applies to domestic steel products, as well as, imports and exports as done in Muller et al. (2006).[220]

Table C - 4, Sector split used to estimate historical stock and future scrap and demand values[224–227]

Product Type	AISI (avg. 2014-2017)
Construction	42%
Transport	27%
Machinery	17%
Other	14%

2.2. Historical DMFA: to calculate in-use stocks

The input stocks are determined using a historical flow-driven DMFA. A flow-driven DMFA is used because the historical demand is known but historical stocks are unknown. We are not using values from existing literature for current in-use stocks due to the inconsistency in estimates, which range from 8 t/capita to 14.3 t/capita.[36,173,220,228]

A product's lifespan and its lifespan distribution determine the probability of a product leaving stock in a given year (i.e., becoming scrap). Different lifespan distributions have been used in previous DMFAs (e.g., beta, log-normal, normal, Weibull, Gaussian). Muller et al. (2014) discusses a number of existing literature studies that compare lifespan distribution functions and they either find no significant difference between lifespan distributions tested and their findings are most sensitive to mean lifespans themselves and not the distributions.[169] Muller et al. (2011) and Muller et al. (2006) also complete a sensitivity with normal, log-normal and Weibull finding little difference in results.[220,228] Our model, like Pauliuk et al. (2012), Muller et al. (2011), Muller et al. (2006) and Yin & Chen (2013), uses a normal lifespan distribution.[35,173,220,228] These are also the references used for the mean product lifespans and standard deviations used in our model (Table C-5).

The scrap produced in each sector, $Scrap_{t,s}$, is calculated as follows: for *t=1880, …, 2017,*

$$Scrap_{t,s} = \sum_{t_o=1880}^{t} Consumption_{t_o,s}\, L_{t-t_o}(\mu_s, \sigma_s), \quad (1)$$

where L_{t-t_o} is the probability distribution function,

$$L_{t-t_o} = \frac{1}{\sigma_s\sqrt{2\pi}} e^{-\frac{1}{2}\left(\frac{T-(t+\mu_S)}{\sigma_S}\right)^2}, \quad (2)$$

where μ_s is the lifespan of products in sector *s*, σ_s is the standard deviation of the lifespan for products in sector *s* and $Consumption_{t_o,s}$ is the consumption for products in sector *s* in year *t*. These calculations were implemented in R using their cumulative distribution function. Table C-5 lists the lifespans and standard deviations used. The product lifespan distributions are normal.

Table C - 5, Product lifespans and lifespan distribution standard deviations[35,173,220,228]

Product Category	Lifespan	Standard Deviation
Construction	75	25
Transport	20	6.7
Machinery	30	10
Other	15	5

The stocks per capita (STC) in each year for each sector, $STC_{t,s}$, is equivalent to the sum the consumption in each previous year minus the sum of the scrap produced in each previous year, which is calculated as follows: for *t=1900, …, 2017,*

$$STC_{t,s} = \frac{1}{pop_t}\left[\sum_{t_o=1880}^{t} Consumption_{t_o,s} - \sum_{t_o=1880}^{t} Scrap_{t_o,s}\right]. \quad (3)$$

In order to calculate the STC for each year *t* is the difference in consumption and scrap is divided by the population from the U.S. Census Bureau historical population data.[229]

Table C - 6, Stock per-Capita values in 2017 calculated from the historical stock analysis for each product lifespan scenario

Product Type	Stocks per-Capita (t/capita)		
	Short Lifespan	Average Lifespan	Long Lifespan
Construction	5.90	6.96	7.72
Transport	1.15	1.62	2.03
Machinery	1.06	1.44	1.79
Other	0.45	0.64	0.83
Total	8.27	10.7	12.4

The variations between the literature estimates and the analysis presented here could result from the use of different sector divisions or different methods of accounting for the steel imbedded in imports and exports of finished products (e.g., imported stoves) in demand estimates. Another source of variation could be the assumed historical product lifespan distributions across the four categories. As a sensitivity analysis, short and long product lifespans (±30% of the medium scenario) were simulated in the historical DMFA, resulting in STC in 2017 of 8.3 and 12.4 t/cap respectively. These short and long historical product lifespan scenarios result in unacceptable discontinuities between the recorded steel demand in 2017 and the subsequent steel demand

needed in 2018 to maintain STC levels, showing that the average lifespan was the closest to the real world lifespan and is therefore, used in the analysis of the rest of the paper.

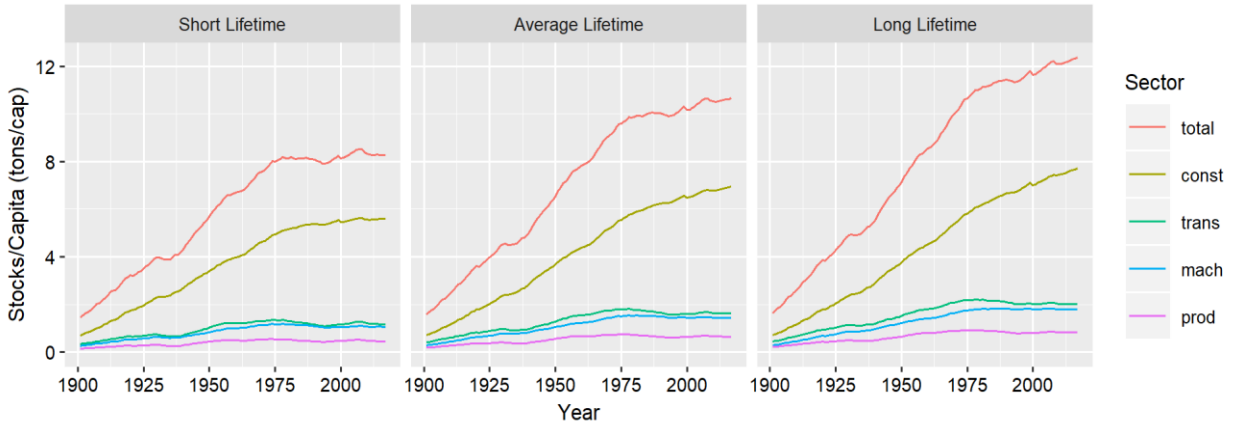

Figure C - 3, Historical per-capita stocks by sector in the United States

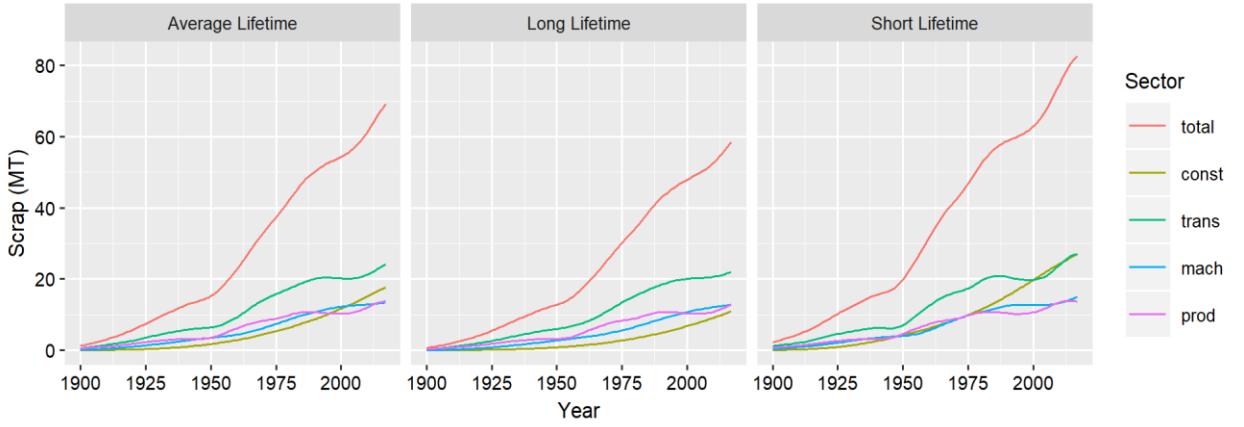

Figure C - 4, Historical scrap by sector in the United States

2.3. Future DMFA: to calculate future demand and available scrap

In order to estimate steel consumption and available scrap for 2018-2050, demand can be projected and in-use stock and scrap calculated through a flow-driven DMFA, or in-use stock can be projected and demand and scrap calculated though a stock-driven DMFA. Hatayama et al. (2010) and Pauliuk et al. (2013) use stock driven models to estimate future demand.[36,37] Muller et al. (2011) notes that stocks reflects demand more adequately than flows and patterns of in-use stocks are more robust than flow patterns because they have a physical meaning through the

services they provide.[228] This is particularly applicable when stocks are assumed to have saturated because there is less uncertainty in estimated stocks per-capita (STC) as they have remained constant over time wear as even after stocks saturate demand is still variable, as seen in the years since the U.S. stock plateaued in about 1980 (Figure C-2). Therefore, a stock-driven model was selected instead of a flow-driven model for estimating future scrap availability.

2.3.1. Future DMFA: 2018-2020

All interventions begin in 2020 therefore, the business as usual scrap values must be calculated for 2018-2020. A stock-driven DMFA estimates the steel flows from 2017 to 2020 as historical demand data was unavailable for these years. The values for product lifespan equal those used in the historical DMFA and the population values are calculated using a linear interpolation and the United States Census Bureau's estimate for the U.S.'s 2050 population, 388.992 million.[171] The STC values are calculated with a logistic model, using historical STC values calculated in section C-1.2 with the average lifespan assumption, figure C-5. The logistic growth model is derived from Cooper et al. (2019).[148] The resulting STC values are also used in the future DMFA for the business as usual scenario.

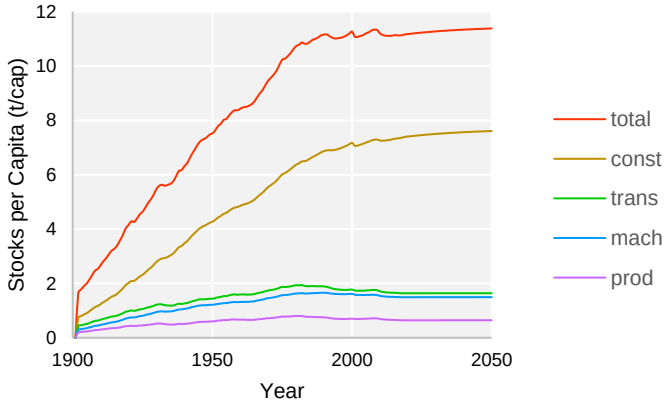

Figure C - 5, Business as usual stocks per capita projection

2.3.2. Future DMFA: 2021-2050

The values for population, in-use STC, and product lifespan in each year from 2021 to 2050 are calculated by linearly interpolating (eqn. 4-7) between the 2020 value and the 2050 value set in each scenario discussed below.

The population for each year is calculated as: for *t=2021… 2050,*

$$P_{t,i} = P_{2020} + \left(\frac{P_{2050,i} - P_{2020}}{2050-2020}\right)(t - 2020), \quad (4)$$

where $P_{t,i}$ is the U.S. population in year *t* for theoretical U.S. population value i, $P_{2050,i}$ in year 2050, P_{2020} is the U.S. population in year 2020 and *N* is the number of scenarios. The 2050 population estimates range from 328 million, zero population growth, to 452 million, divided into seven scenarios, *N*.

The stocks per-capita in each year for each sector, $STC_{t,i,s}$, is calculated as: for *t=2021 … 2050,*

$$STC_{t,i,s} = STC_{2020,s} + \left(\frac{STC_{2050,i,s} - STC_{2020,s}}{2050-2020}\right)(T - 2020), \quad (5)$$

where $STC_{2050,i,s}$ is the stocks per-capita in year 2050 for a given scenario i and sector *s*, and $STC_{2020,s}$ is the stocks per-capita in year 2020 for a given sector s calculated in section C-2.3.1. The minimum and maximum realistic stock values are based on minimum and maximum values for stock saturation found in existing literature for developed countries. Pauliuk et al. (2013) predicts average stock level for mature steel stocks to be 13.4 ±2 tons per-capita.[173] However, Muller et al. (2011) says that the average industrialized country stocks range from 8 to 12 tons per-capita.[228] Therefore, we set our minimum value at 8 tons per-capita, with a maximum value of 14 tons per-capita. Although none of the existing stocks per-capita analyzed in literature have shown a decrease in per-capita stocks we still modeled these scenarios as they would indicate a decoupling of steel demand and economic growth,[228] which could be necessary to ultimately reduce emissions to the required levels.

The average lifespan in each year for each sector and scenario, $\mu_{t,s,i}$, is calculated as: for *t=2021, …, 2050,*

$$\mu_{t,s,i} = \mu_{2020,s} + \left(\frac{\mu_{2050,i,s} - \mu_{2020,s}}{2050-2020}\right)(t - 2020), \quad (6)$$

Where $\mu_{2020,s}$ is the lifespan in 2020 for a given sector, *s*, and $\mu_{2050,i,s}$ is the lifespan in year 2050 for scenario i, and sector *s*. The minimum and maximum values are a +/- 30% of the average values in the base case. Pauliuk et al. (2013) completed their sensitivity analysis by

varying project lifespan by the same percentage.[173] Muller et al. (2011) also varied product lifespans by +/-33% except in the case of their high transportation lifespan scenario.[228]

The standard deviation in each year for each sector and each scenario, $\sigma_{t,s,i}$, is calculated as: for *t=2021, …, 2050,*

$$\sigma_{t,s,i} = \sigma_{2020,s} + \left(\frac{\sigma_{2050,i,s} - \sigma_{2020,,s}}{2050-2020}\right)(t - 2020), \quad (7)$$

Where $\sigma_{2020,s}$ is the standard deviation in 2020 for a given sector, *s*, and $\sigma_{2050,i,s}$ is the standard deviation in year 2050 for scenario i, and sector *s*.

As with the historical DMFA, a normal distribution is used to calculate the scrap each year. However, the distribution is not constant overtime. The lifespan and standard deviation are based on the current year *t*, as calculated in eqn. 6-7. We model lifespan shifts in two ways.

In one case we assume material that has not yet left use can be retrofitted (i.e., its lifespan can be extended or shorted based on the changing lifespan distributions between 2020 and 2050). In this case the lifespan and standard deviation calculated in eqn. 6-7, for a give year *T*, are applied to all remaining stock to calculate the scrap in leaving in *T*. However, in the case where there is no retrofitting the new lifespan and standard deviation calculated in eqn. 6-7 is only applied to the materials that went into stock after 2020.

2.3.3. Shifted Start Date

In order to investigate the impact of when interventions occur (i.e., deviations from the business as usual) in the lifespan, population, and STC we shift the starting value of *T* in five year increments in eqs. 4-7 for scenarios whose emissions remain below the cumulative and 2050 limit.

1.4. Future demand and available scrap

1.4.1. No Retrofit: Future demand and scrap

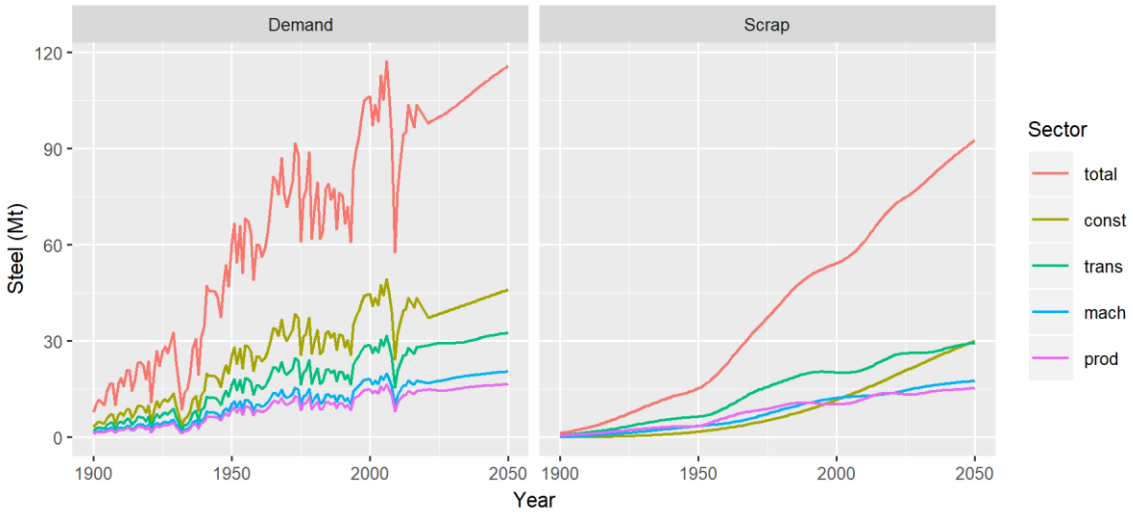

Figure C - 6, Total U.S. steel demand and scrap 1900 to 2050 for the business as usual scenario

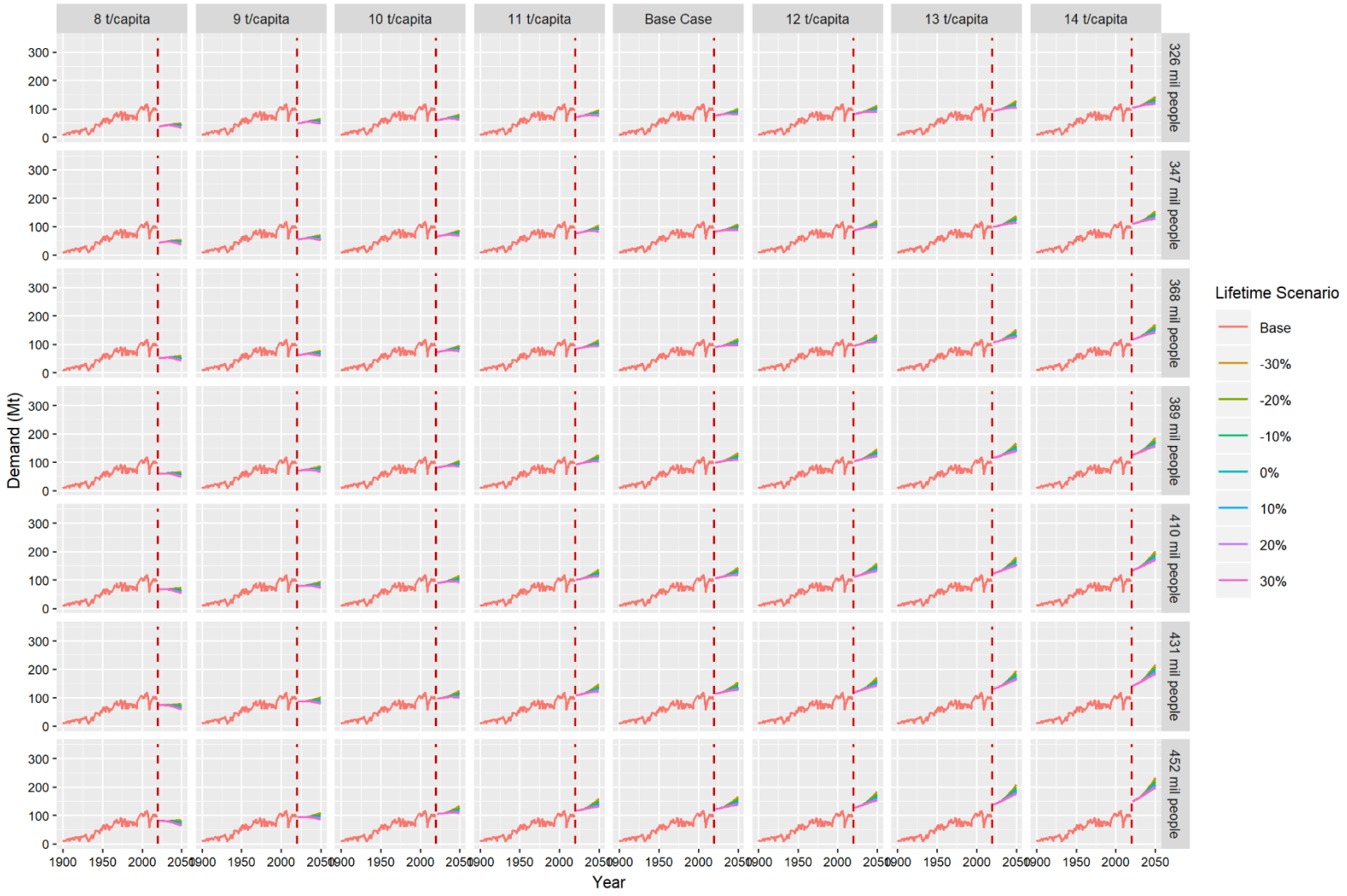

Figure C - 7, Total U.S. steel demand 1900 to 2050 for 2050: stocks per capita ranging from 8 tons/capita to 16 tons/capita (columns), population from 325 to 452 million people (rows), lifespan scenarios ranging from a -30% decrease from average to a 30% increase from average (line color)

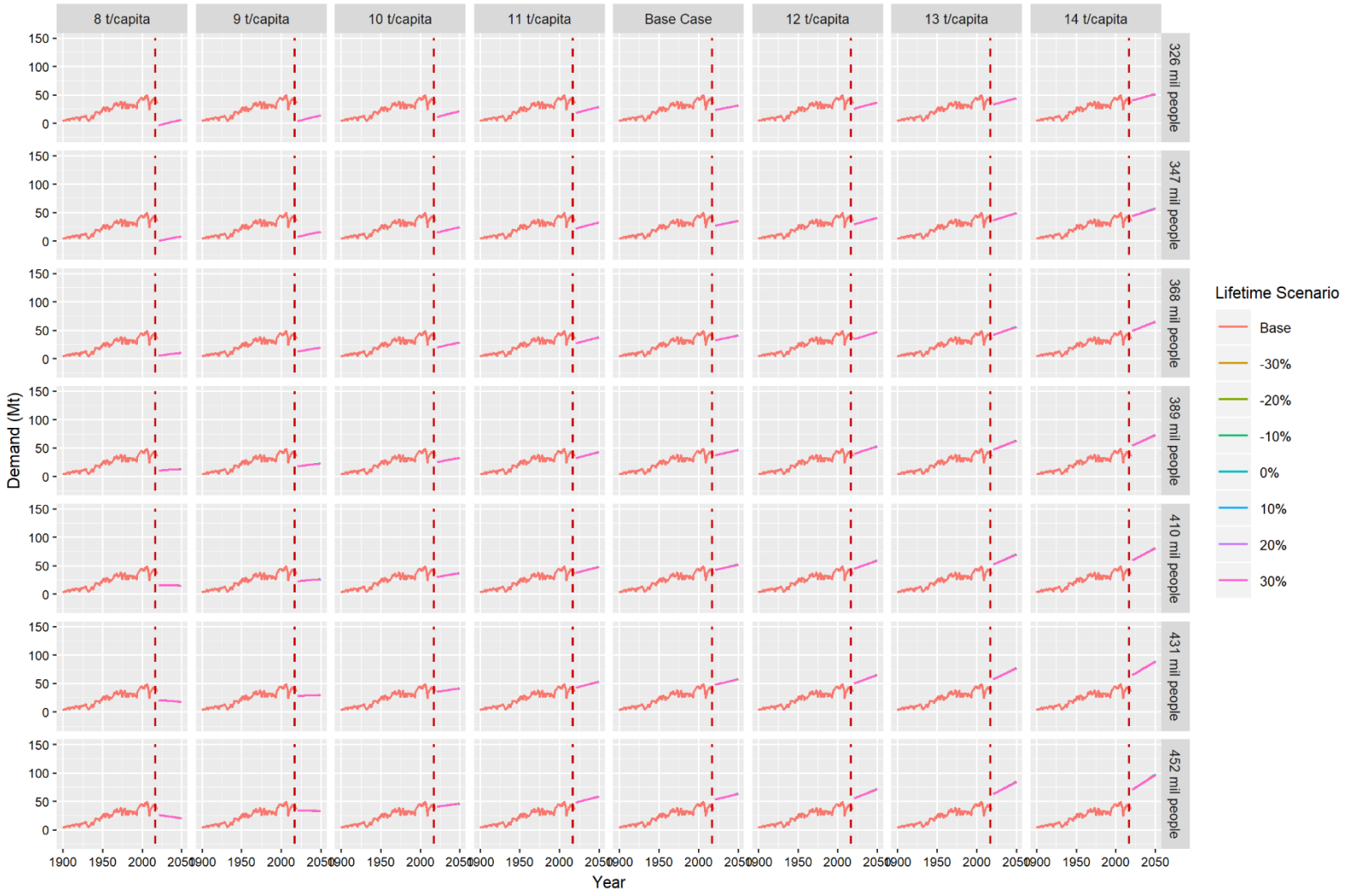

Figure C - 8, U.S. construction steel demand 1900 to 2050 for 2050: stocks per capita ranging from 8 tons/capita to 16 tons/capita (columns), population from 325 to 452 million people (rows), lifespan scenarios ranging from a -30% decrease from average to a 30% increase from average (line color)

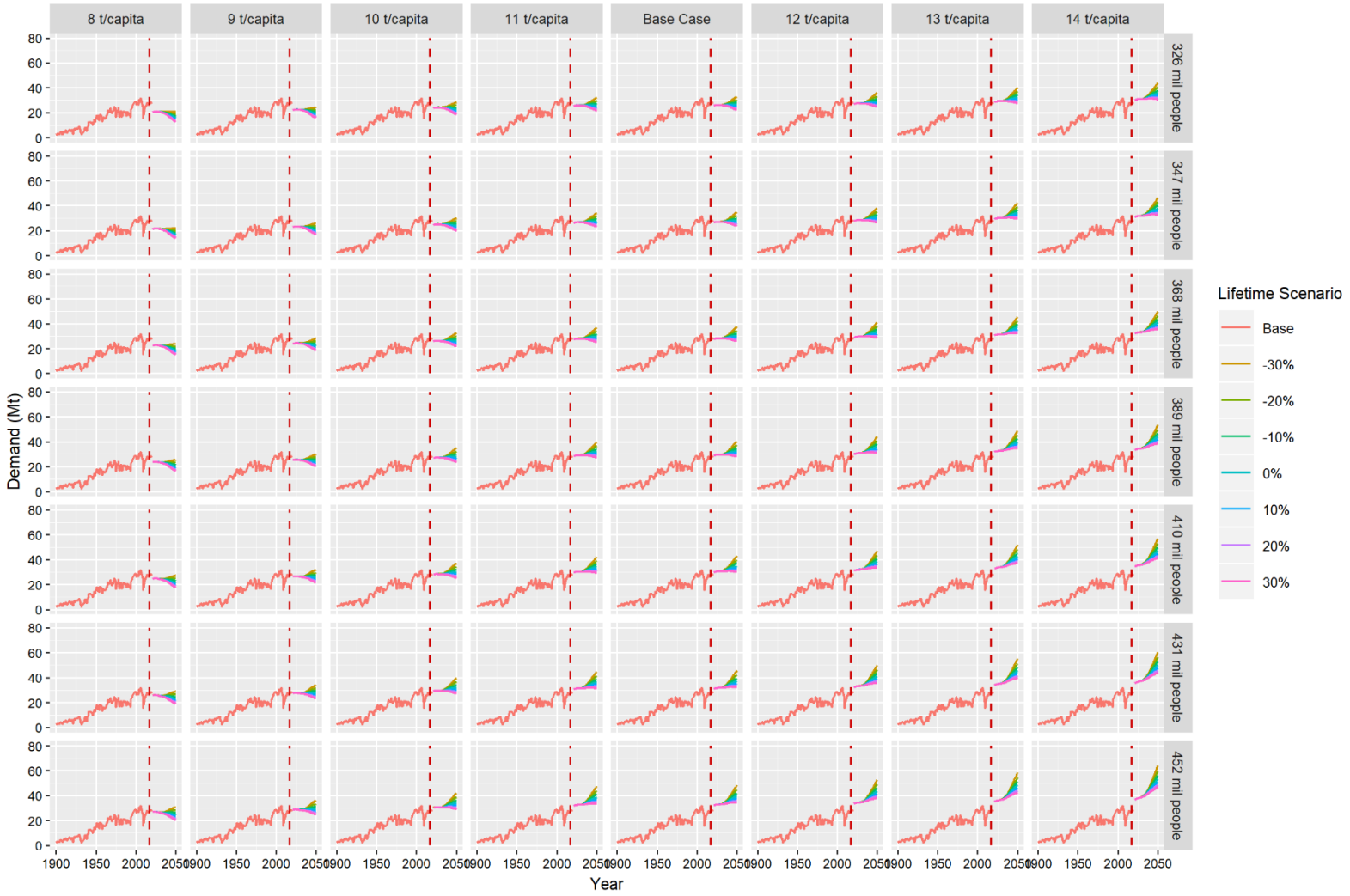

Figure C - 9, U.S. transportation steel demand 1900 to 2050 for 2050: stocks per capita ranging from 8 tons/capita to 16 tons/capita (columns), population from 325 to 452 million people (rows), lifespan scenarios ranging from a -30% decrease from average to a 30% increase from average (line color)

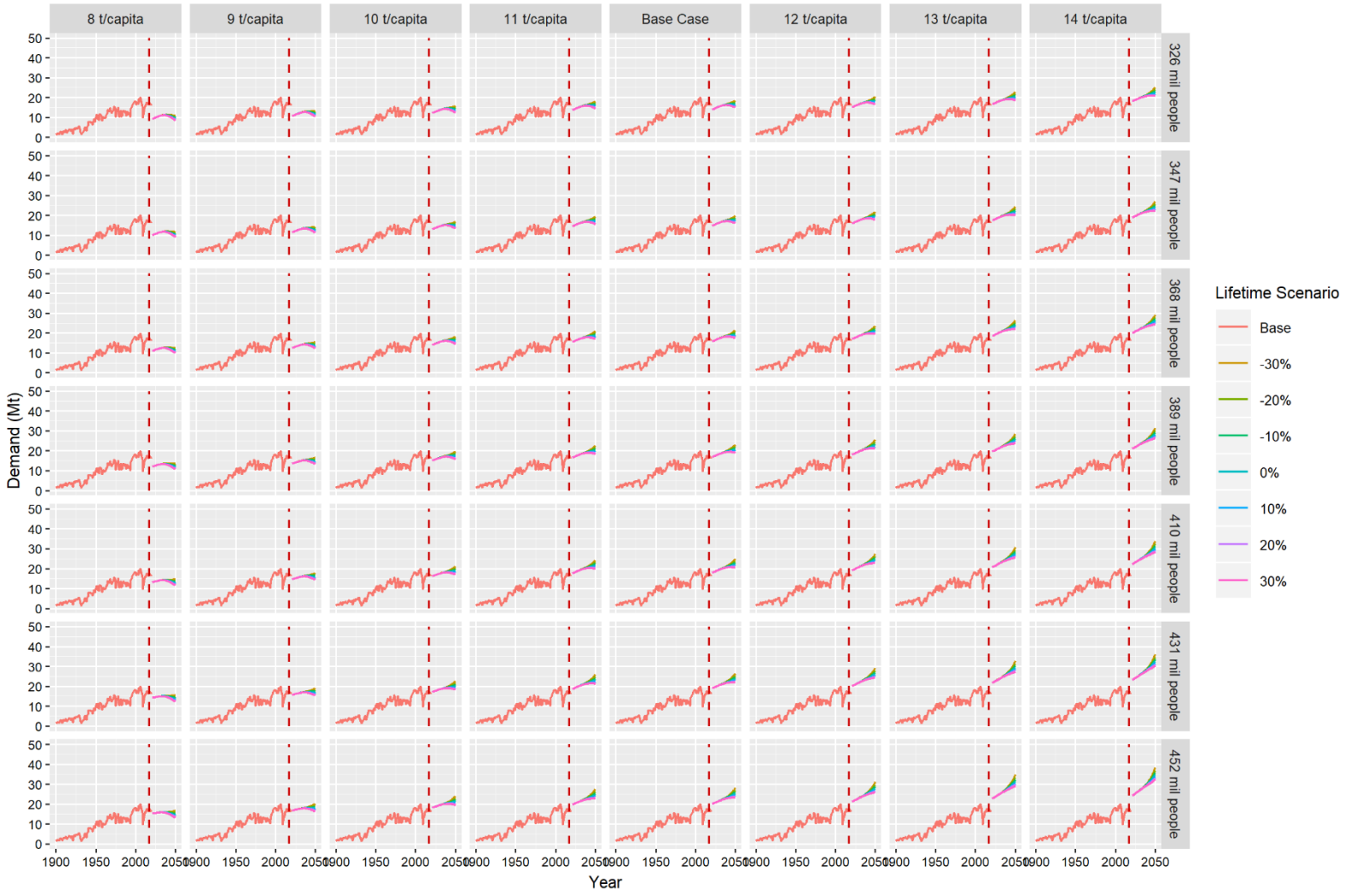

Figure C - 10, U.S. machinery steel demand 1900 to 2050 for 2050: stocks per capita ranging from 8 tons/capita to 16 tons/capita (columns), population from 325 to 452 million people (rows), lifespan scenarios ranging from a -30% decrease from average to a 30% increase from average (line color)

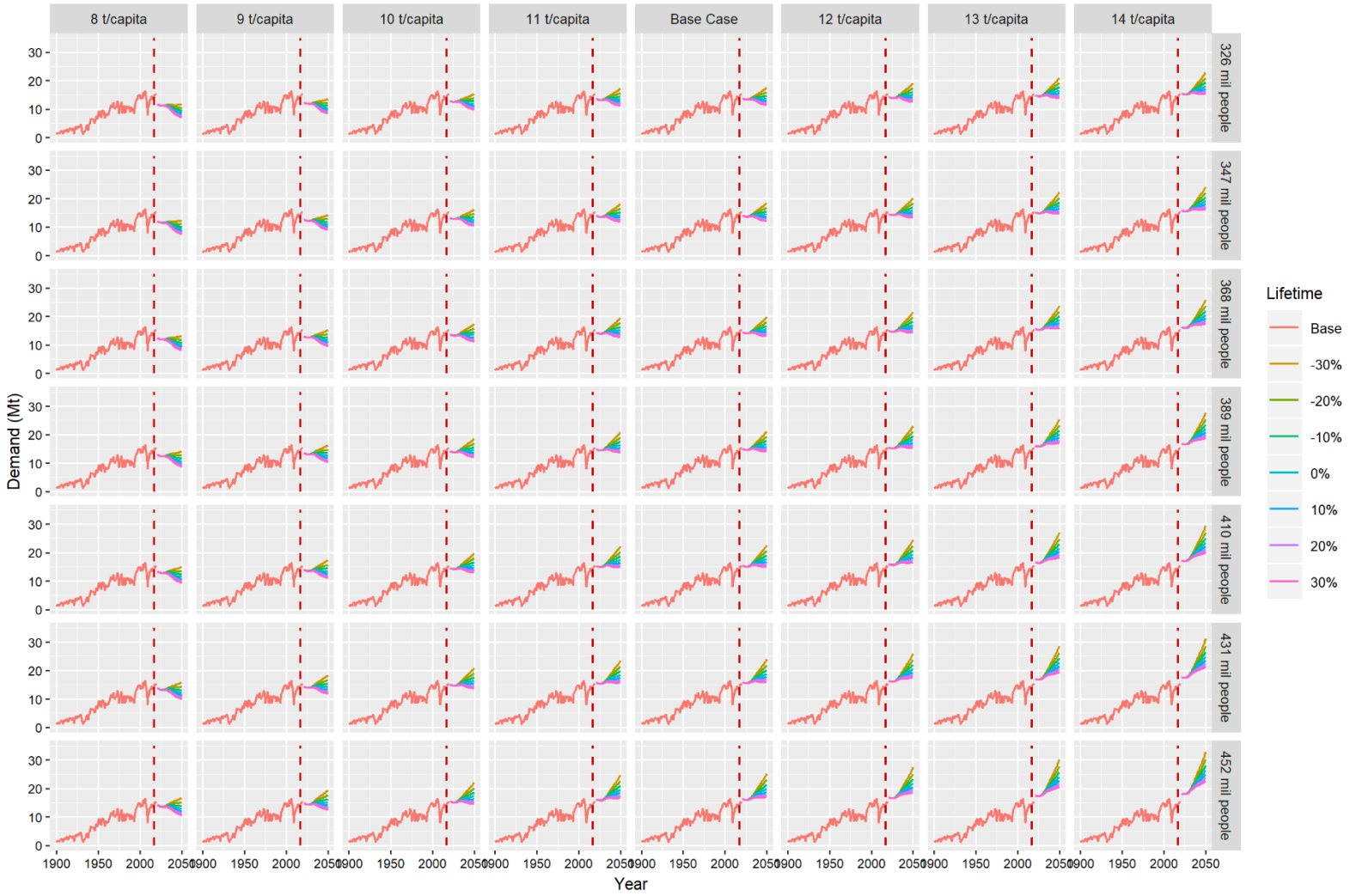

Figure C - 11, U.S. products steel demand 1900 to 2050 for 2050: stocks per capita ranging from 8 tons/capita to 16 tons/capita (columns), population from 325 to 452 million people (rows), lifespan scenarios ranging from a -30% decrease from average to a 30% increase from average (line color)

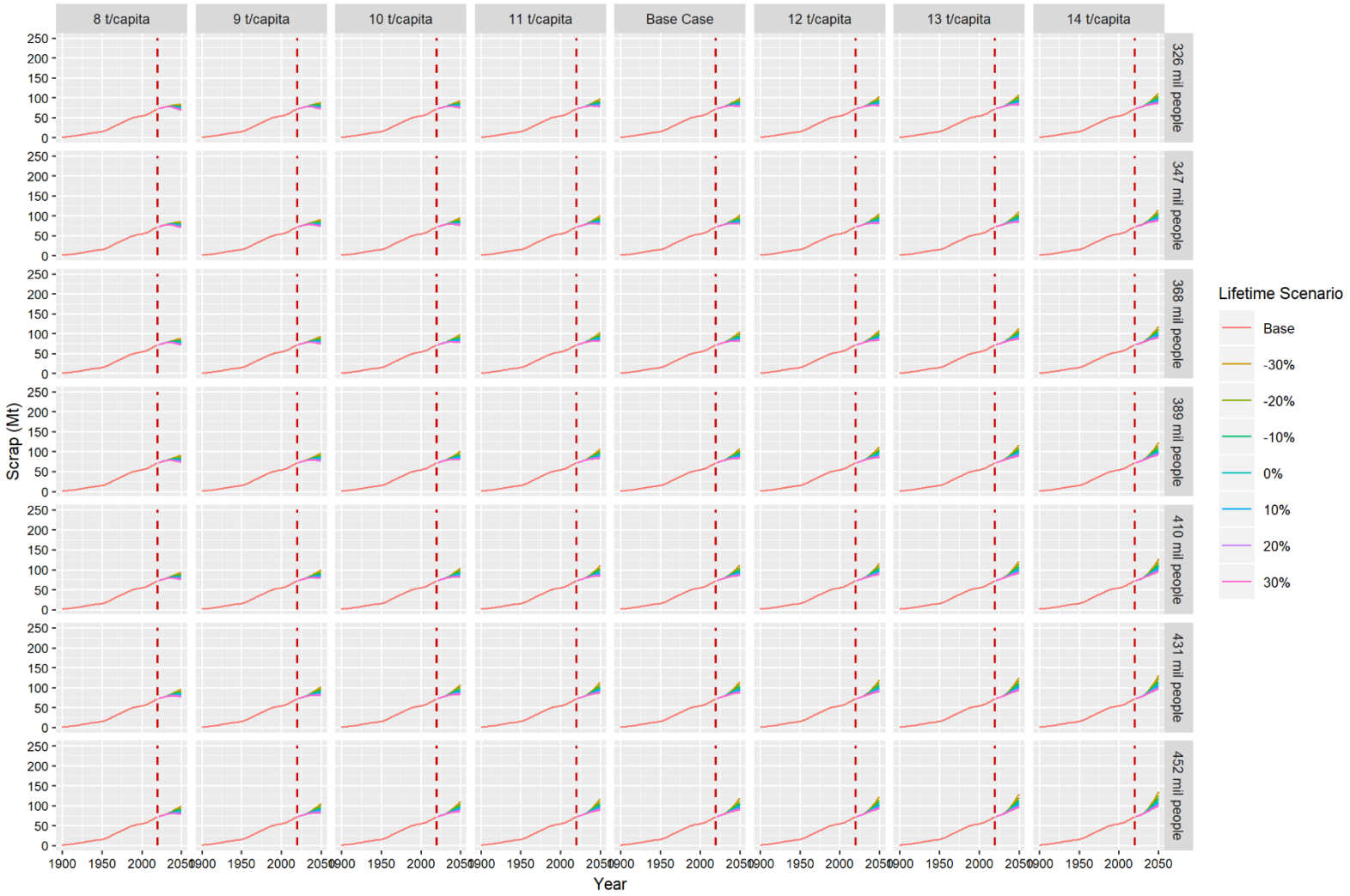

Figure C - 12, Total U.S. steel scrap 1900 to 2050 for 2050: stocks per capita ranging from 8 tons/capita to 16 tons/capita (columns), population from 325 to 452 million people (rows), lifespan scenarios ranging from a -30% decrease from average to a 30% increase from average (line color)

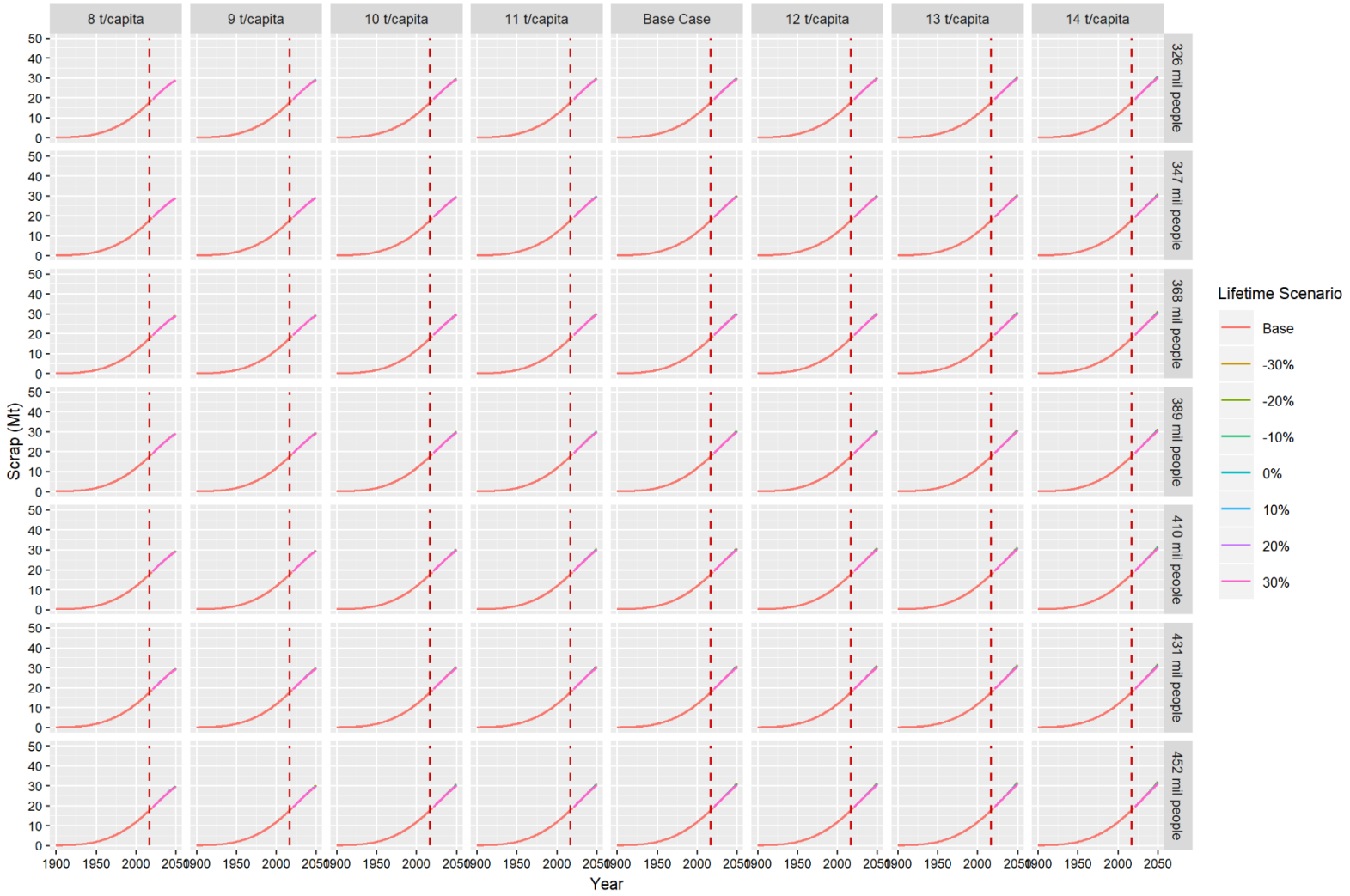

Figure C - 13, U.S. construction steel scrap 1900 to 2050 for 2050: stocks per capita ranging from 8 tons/capita to 16 tons/capita (columns), population from 325 to 452 million people (rows), lifespan scenarios ranging from a -30% decrease from average to a 30% increase from average (line color)

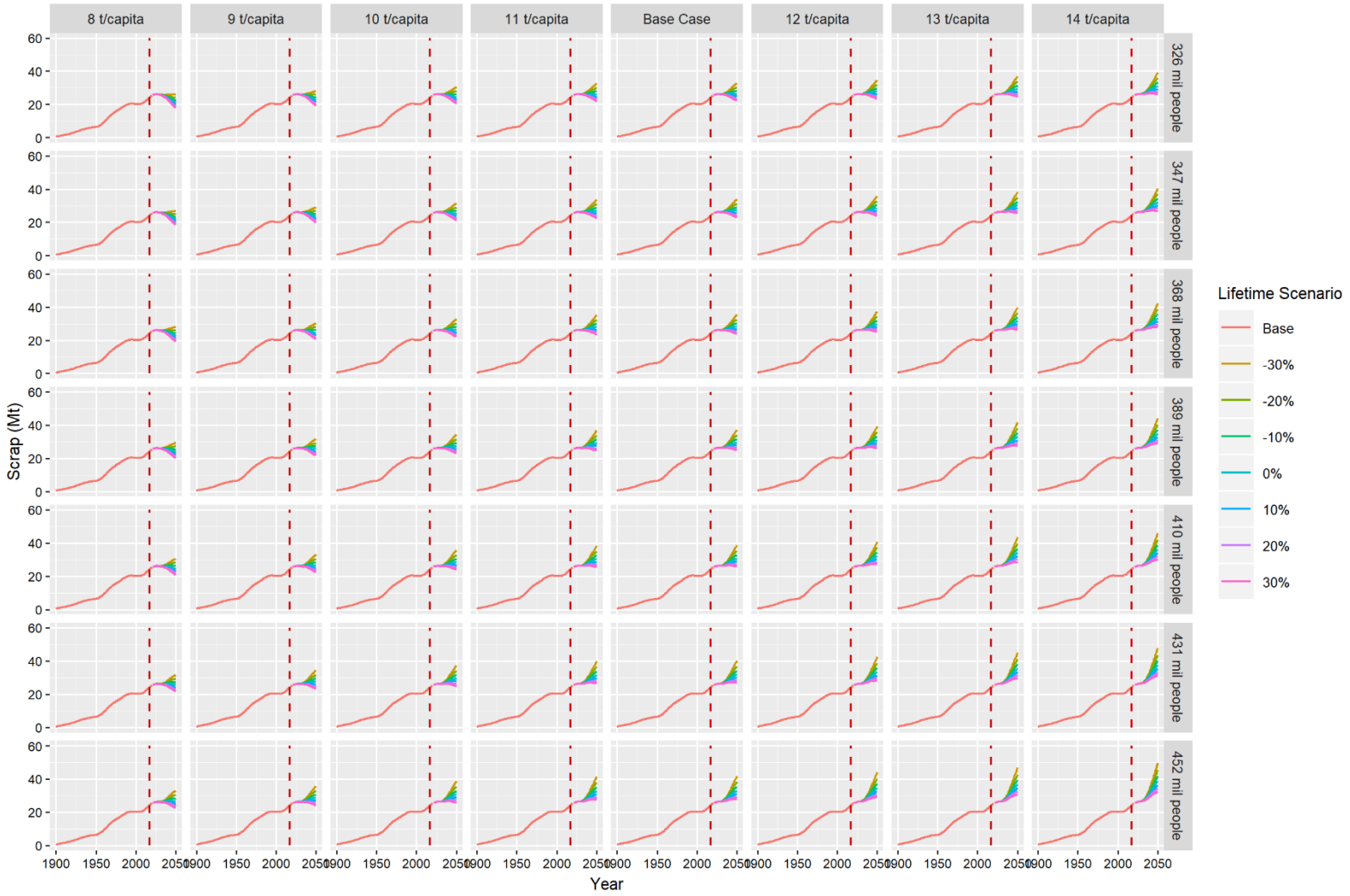

Figure C - 14, U.S. transportation steel scrap 1900 to 2050 for 2050: stocks per capita ranging from 8 tons/capita to 16 tons/capita (columns), population from 325 to 452 million people (rows), lifespan scenarios ranging from a -30% decrease from average to a 30% increase from average (line color)

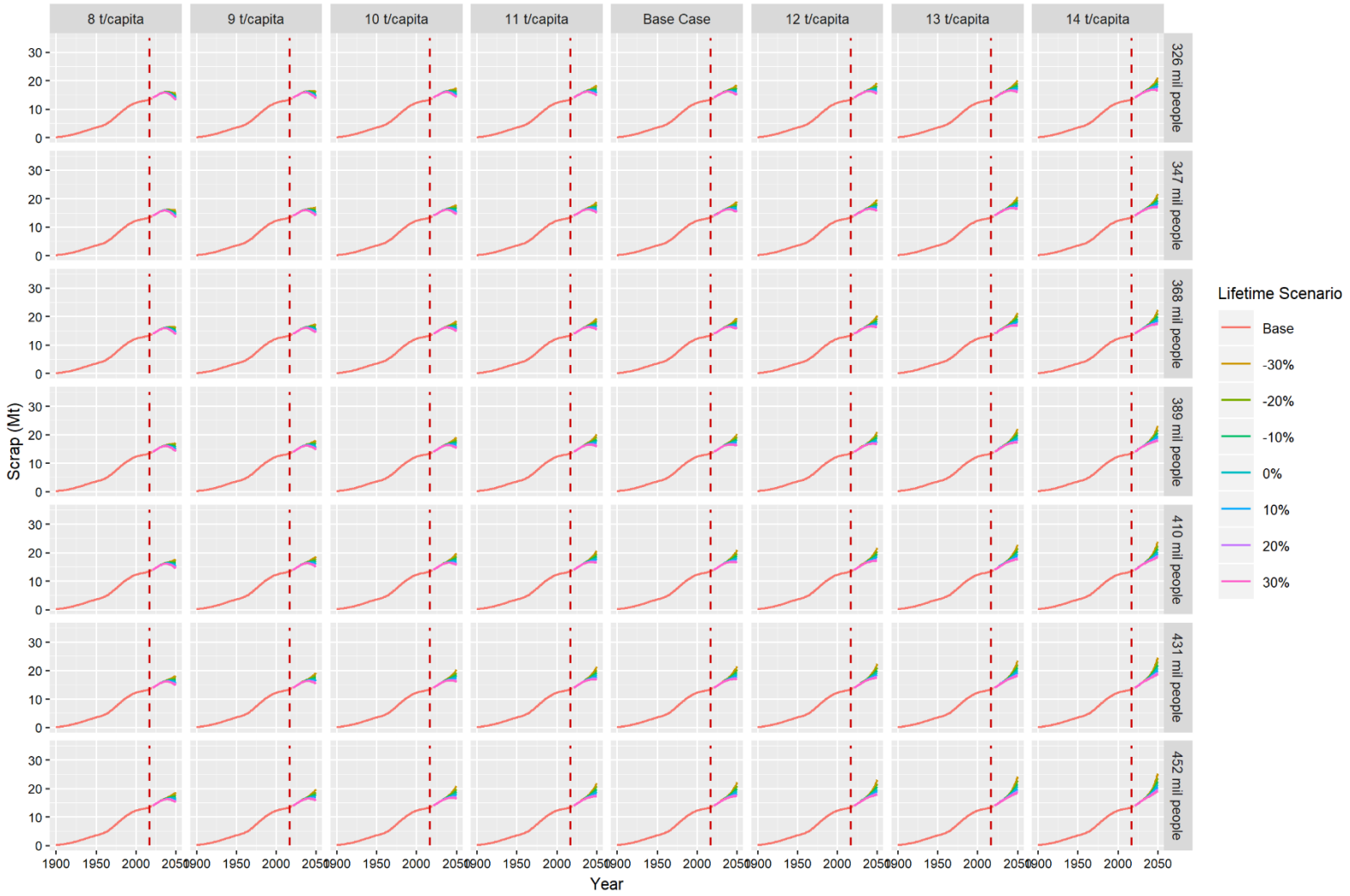

Figure C - 15, U.S. machinery steel scrap 1900 to 2050 for 2050: stocks per capita ranging from 8 tons/capita to 16 tons/capita (columns), population from 325 to 452 million people (rows), lifespan scenarios ranging from a -30% decrease from average to a 30% increase from average (line color)

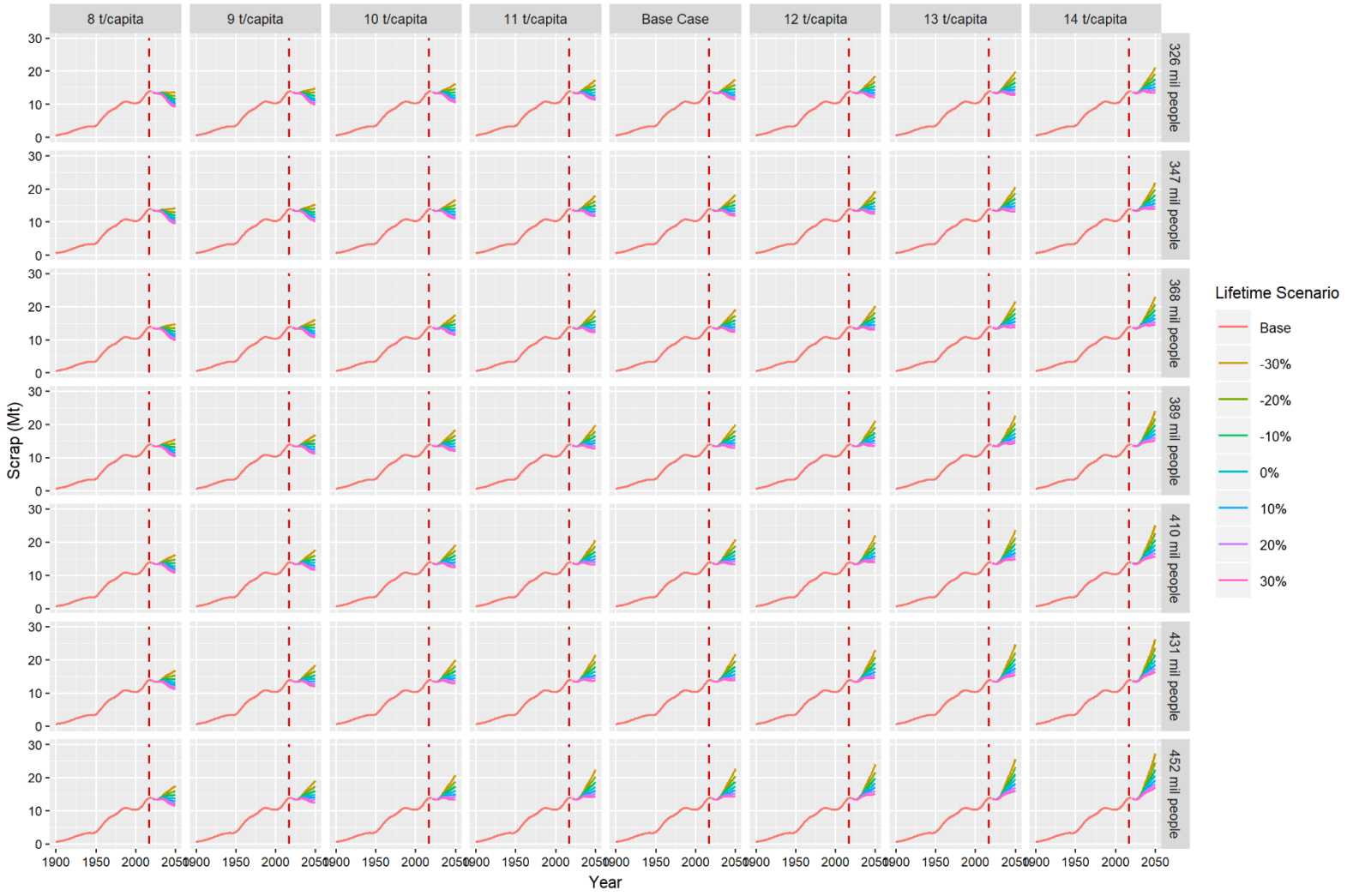

Figure C - 16, U.S. products steel scrap 1900 to 2050 for 2050: stocks per capita ranging from 8 tons/capita to 16 tons/capita (columns), population from 325 to 452 million people (rows), lifespan scenarios ranging from a -30% decrease from average to a 30% increase from average (line color)

1.4.2. Retrofit: Future demand and scrap

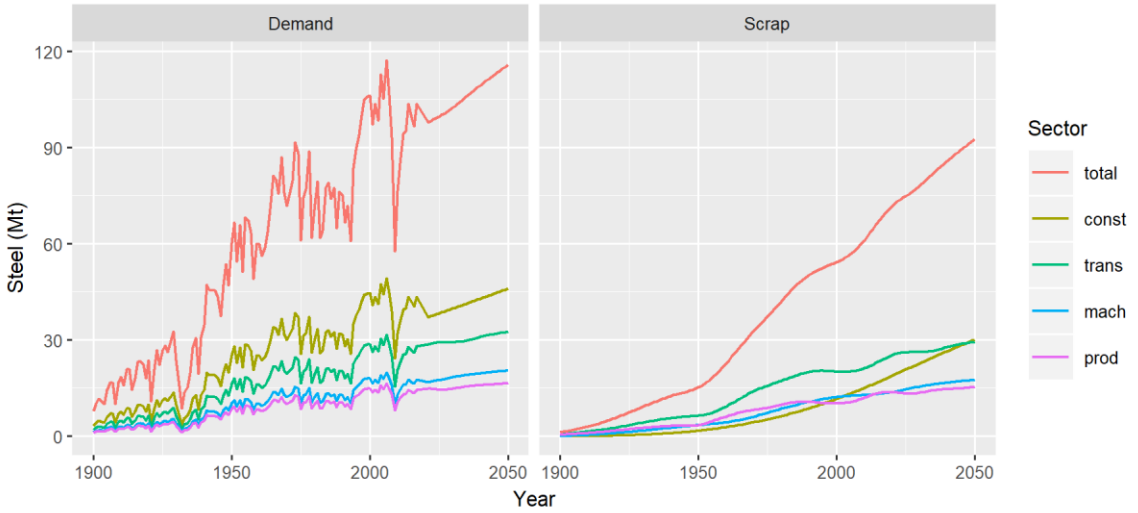

Figure C - 17, Total U.S. steel demand and scrap 1900 to 2050 for the business as usual scenario description

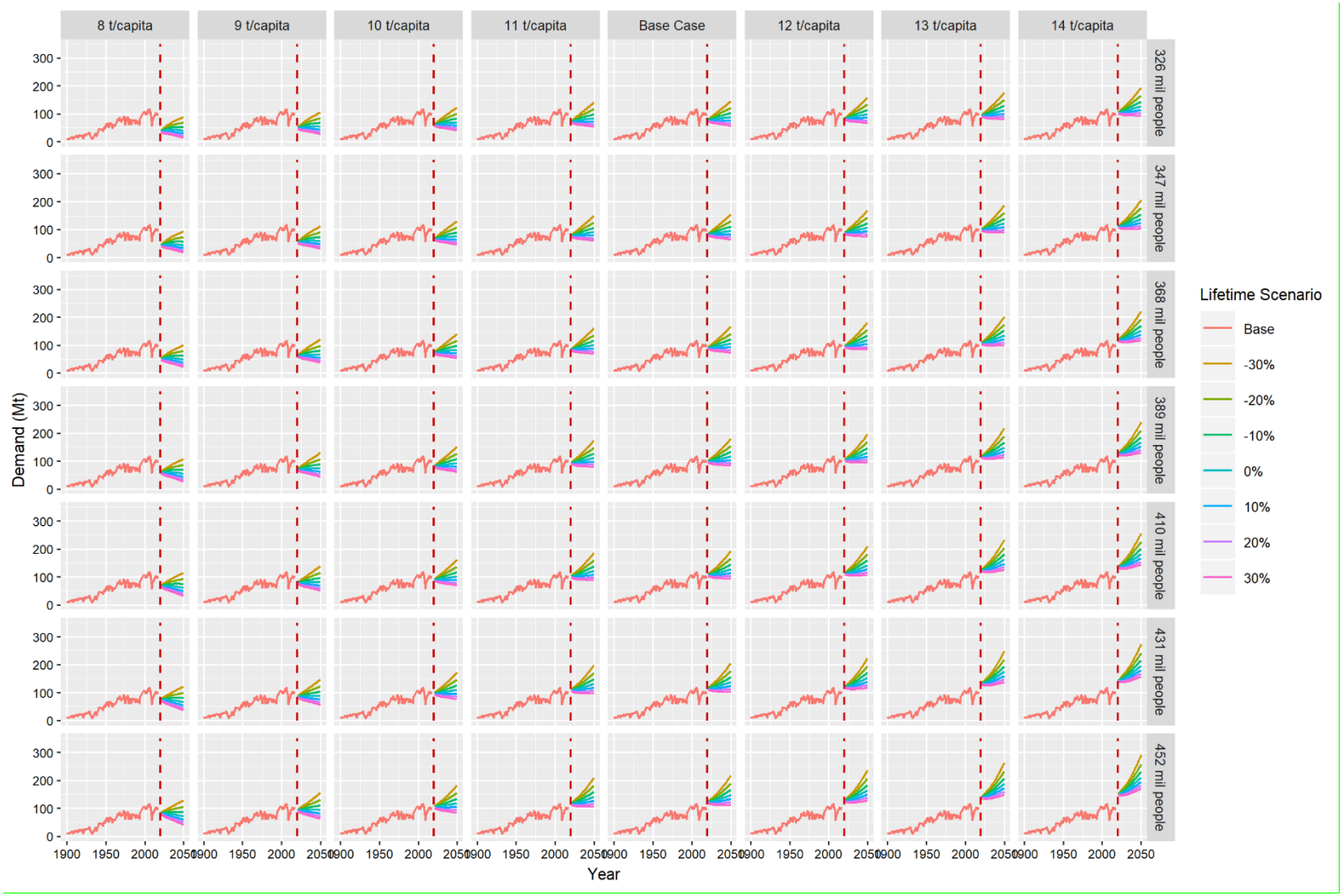

Figure C - 18, Total U.S. steel demand 1900 to 2050 for 2050: stocks per capita ranging from 8 tons/capita to 16 tons/capita (columns), population from 325 to 452 million people (rows), lifespan scenarios ranging from a -30% decrease from average to a 30% increase from average (line color)

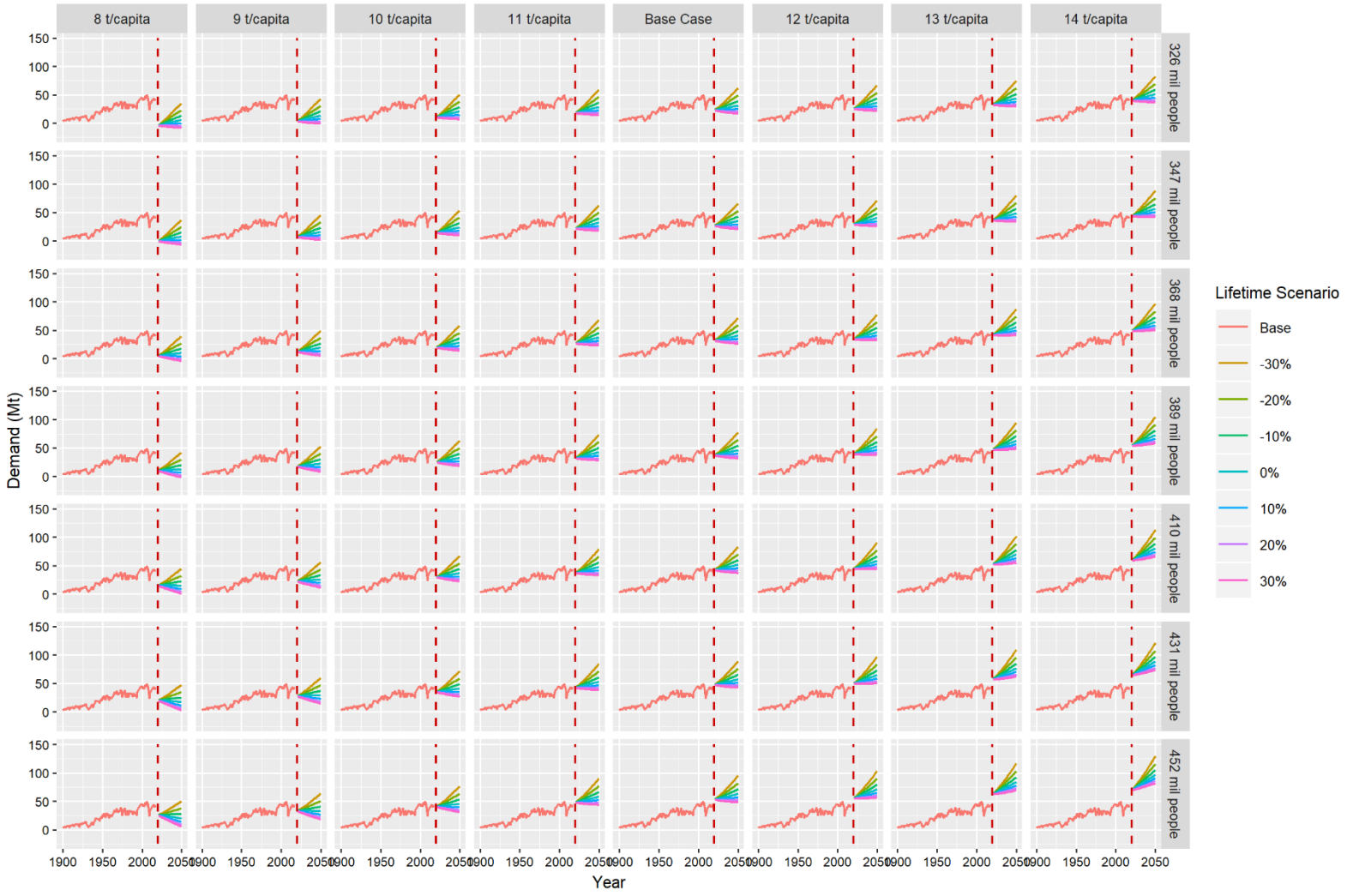

Figure C - 19, U.S. construction steel demand 1900 to 2050 for 2050: stocks per capita ranging from 8 tons/capita to 16 tons/capita (columns), population from 325 to 452 million people (rows), lifespan scenarios ranging from a -30% decrease from average to a 30% increase from average (line color)

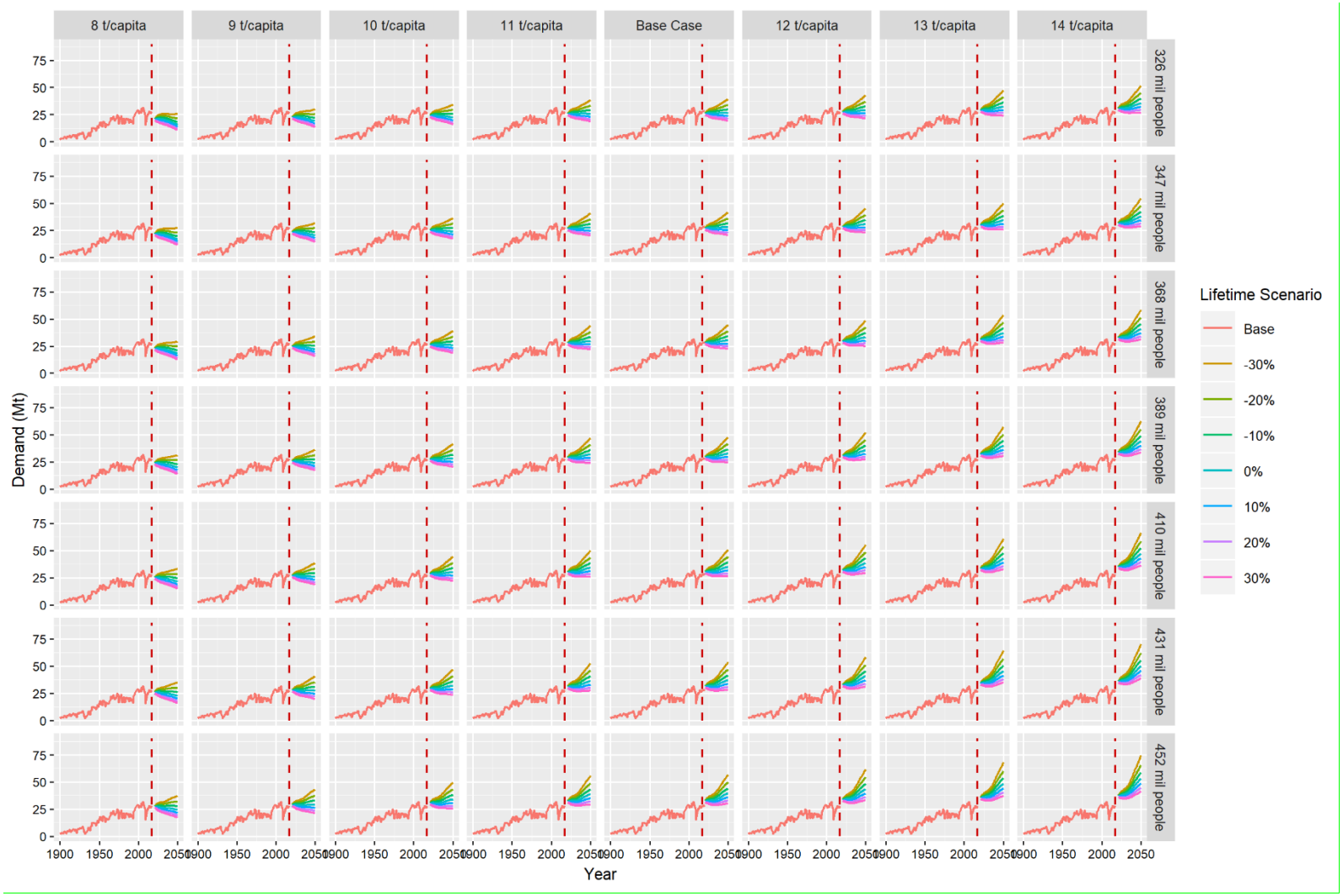

Figure C - 20, U.S. transportation steel demand 1900 to 2050 for 2050: stocks per capita ranging from 8 tons/capita to 16 tons/capita (columns), population from 325 to 452 million people (rows), lifespan scenarios ranging from a -30% decrease from average to a 30% increase from average (line color)

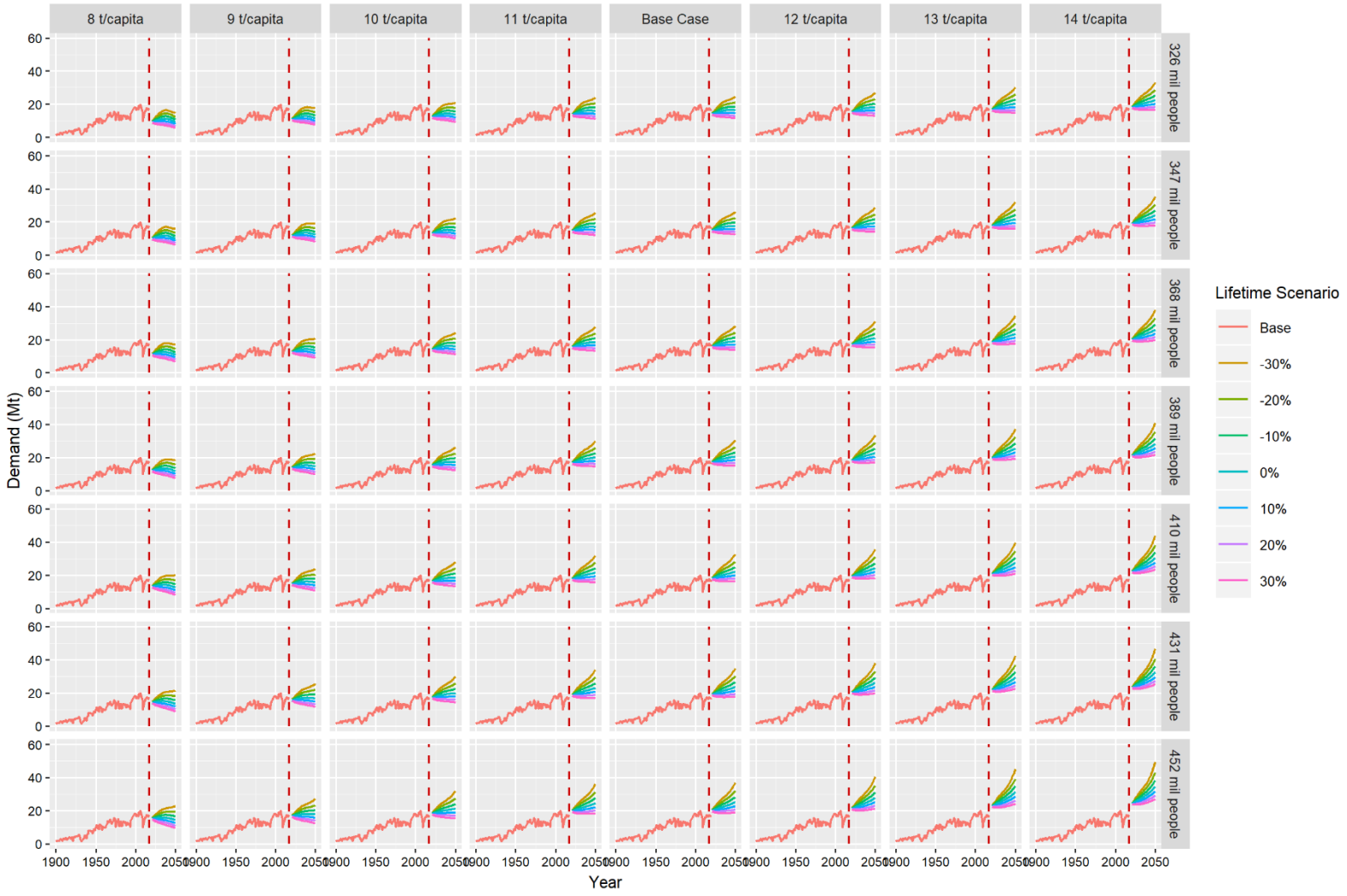

Figure C - 21, U.S. machinery steel demand 1900 to 2050 for 2050: stocks per capita ranging from 8 tons/capita to 16 tons/capita (columns), population from 325 to 452 million people (rows), lifespan scenarios ranging from a -30% decrease from average to a 30% increase from average (line color)

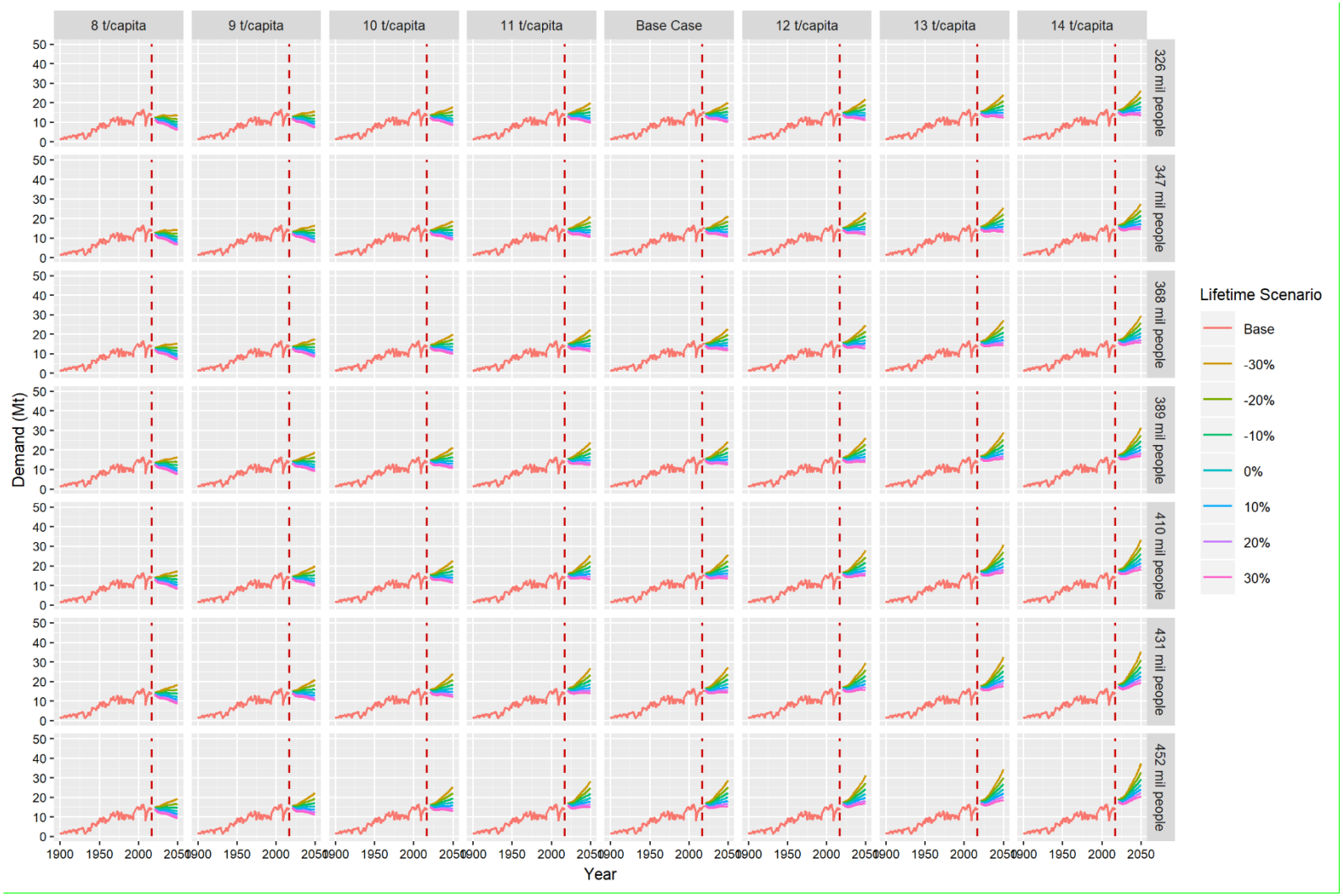

Figure C - 22, U.S. products steel demand 1900 to 2050 for 2050: stocks per capita ranging from 8 tons/capita to 16 tons/capita (columns), population from 325 to 452 million people (rows), lifespan scenarios ranging from a -30% decrease from average to a 30% increase from average (line color)

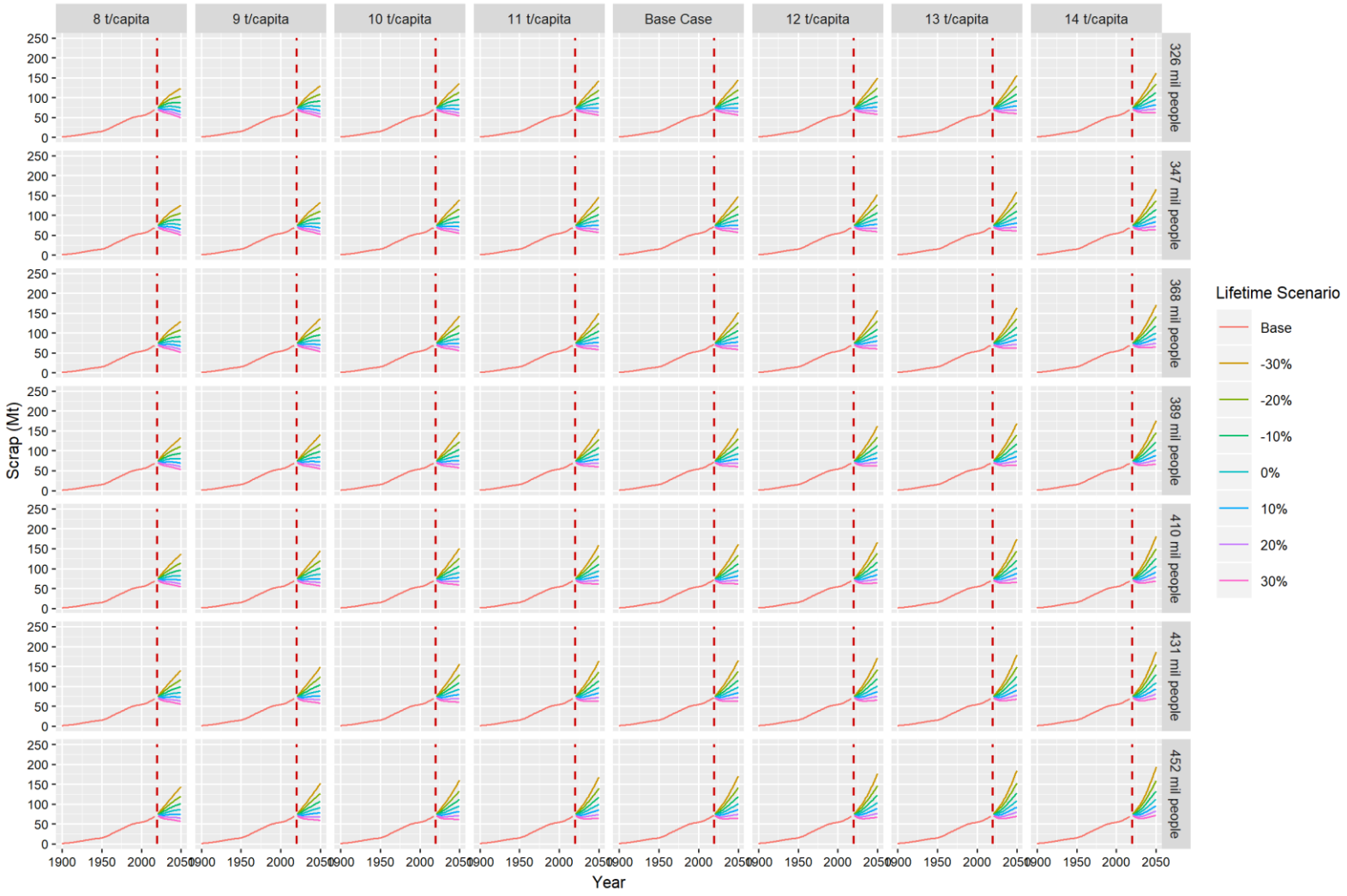

Figure C - 23, Total U.S. steel scrap 1900 to 2050 for 2050: stocks per capita ranging from 8 tons/capita to 16 tons/capita (columns), population from 325 to 452 million people (rows), lifespan scenarios ranging from a -30% decrease from average to a 30% increase from average (line color)

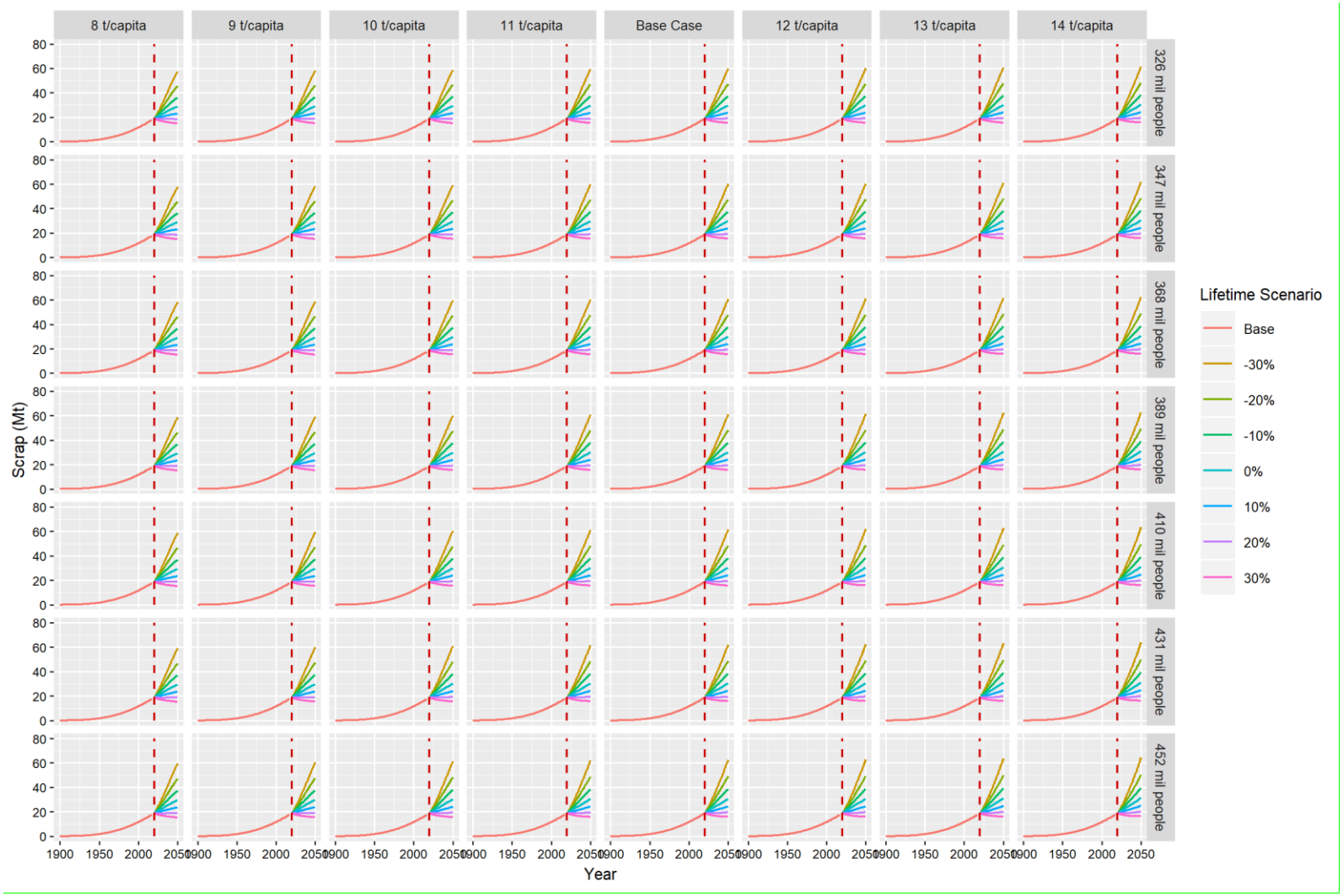

Figure C - 24, U.S. construction steel scrap 1900 to 2050 for 2050: stocks per capita ranging from 8 tons/capita to 16 tons/capita (columns), population from 325 to 452 million people (rows), lifespan scenarios ranging from a -30% decrease from average to a 30% increase from average (line color)

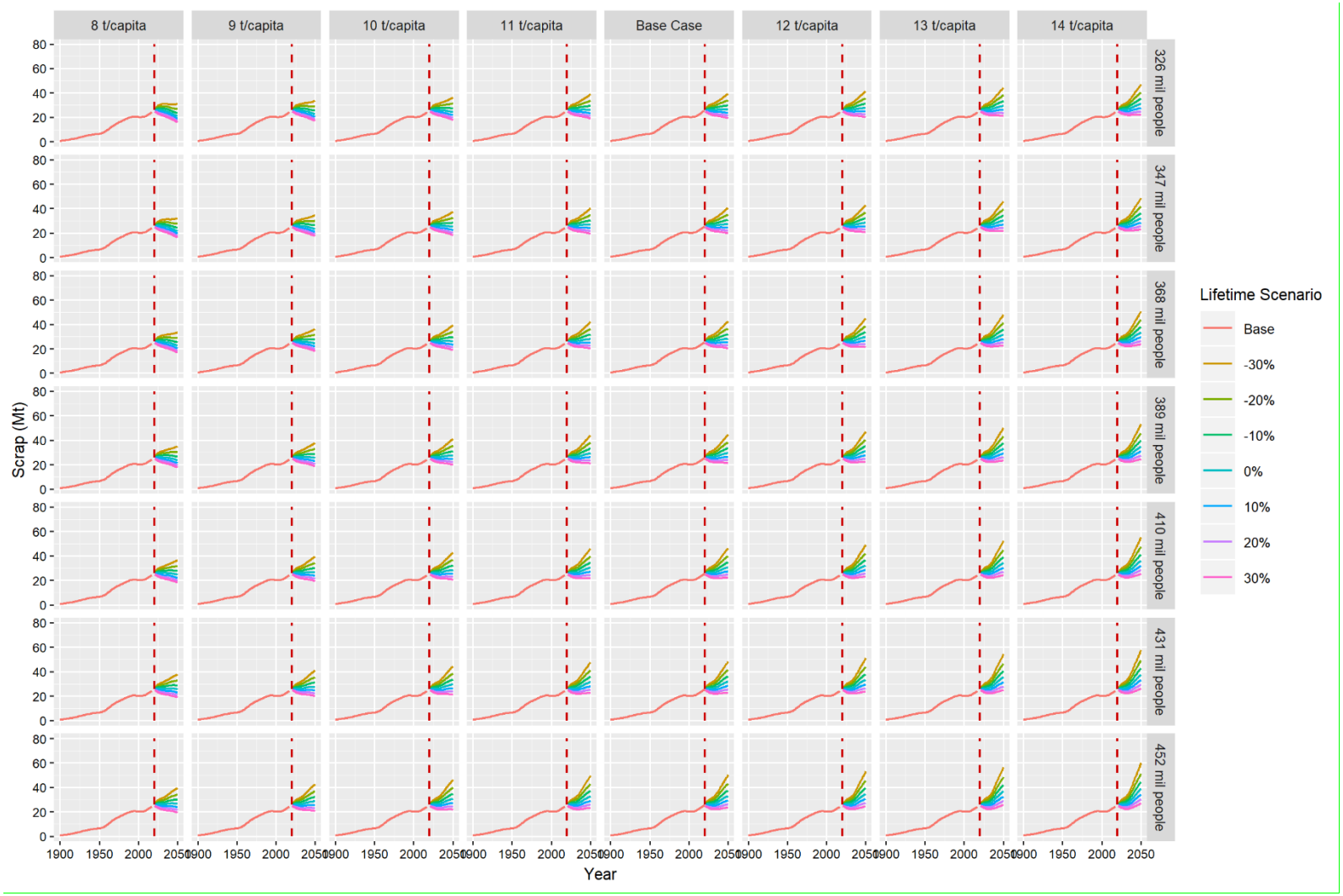

Figure C - 25, U.S. transportation steel scrap 1900 to 2050 for 2050: stocks per capita ranging from 8 tons/capita to 16 tons/capita (columns), population from 325 to 452 million people (rows), lifespan scenarios ranging from a -30% decrease from average to a 30% increase from average (line color)

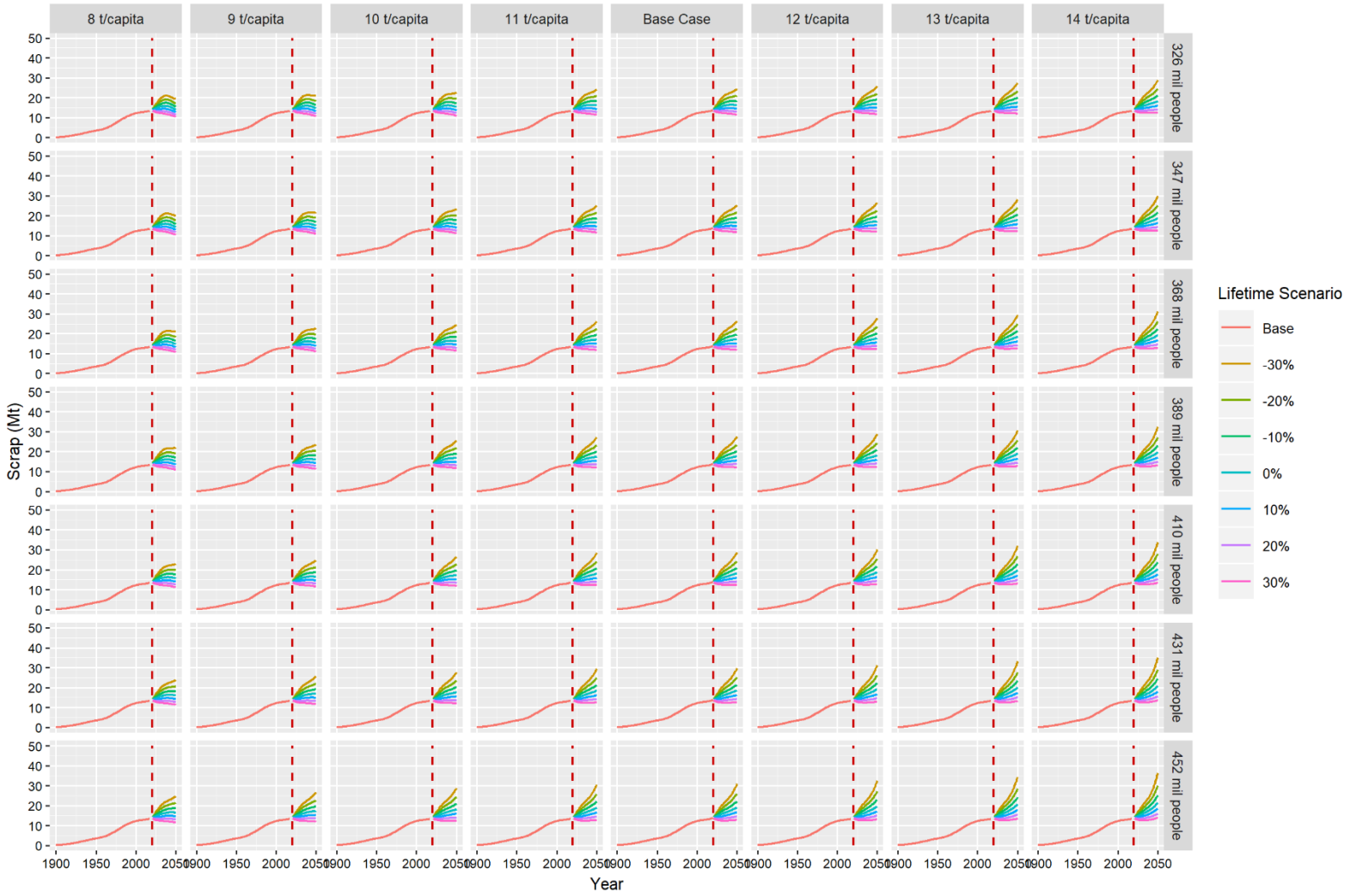

Figure C - 26, U.S. machinery steel scrap 1900 to 2050 for 2050: stocks per capita ranging from 8 tons/capita to 16 tons/capita (columns), population from 325 to 452 million people (rows), lifespan scenarios ranging from a -30% decrease from average to a 30% increase from average (line color)

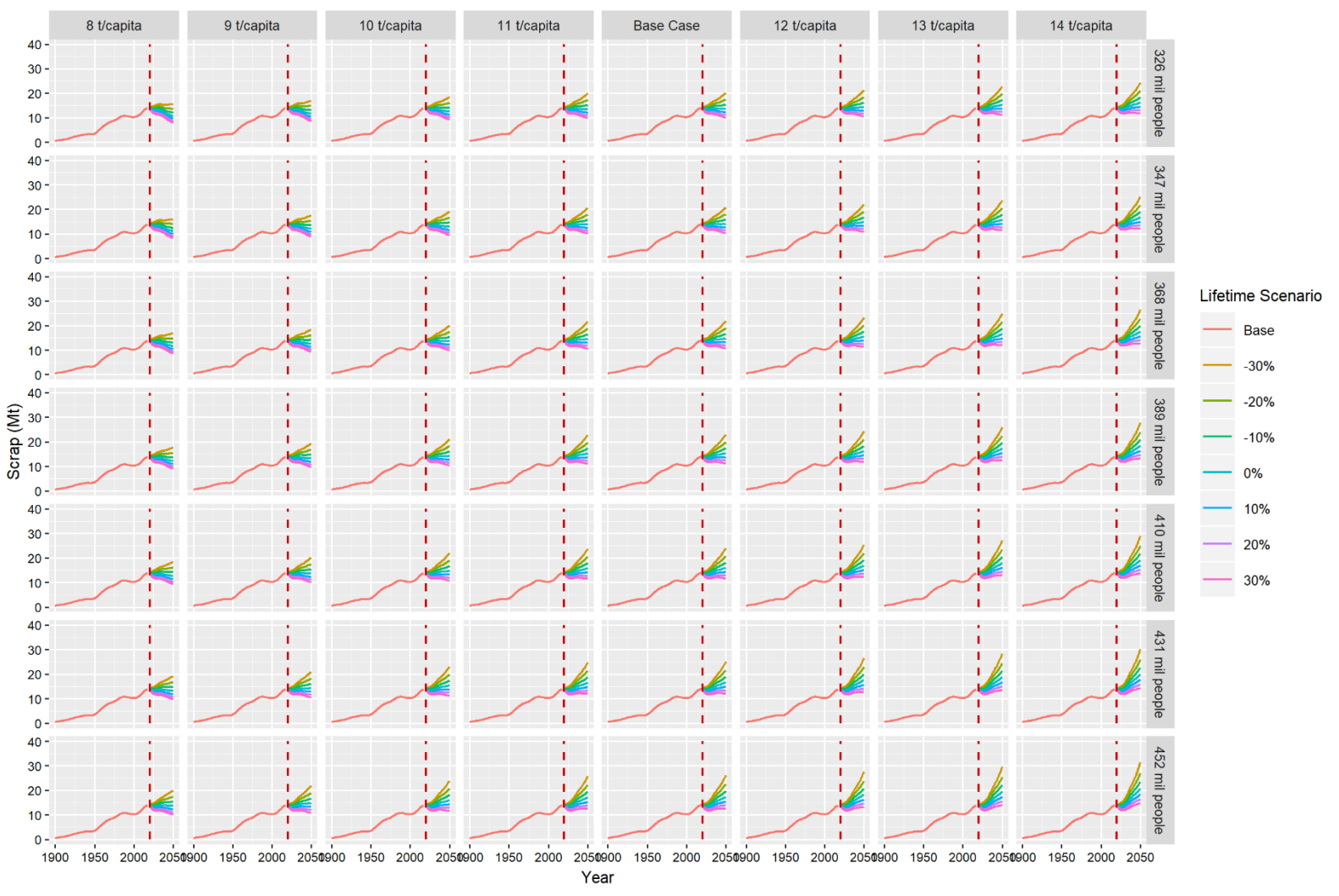

Figure C - 27, U.S. products steel scrap 1900 to 2050 for 2050: stocks per capita ranging from 8 tons/capita to 16 tons/capita (columns), population from 325 to 452 million people (rows), lifespan scenarios ranging from a -30% decrease from average to a 30% increase from average (line color)

1.5. Calculating End-of-Life Scrap

Estimates vary for the percent of available EOL scrap recycled. Therefore, we examine a range of potential values. The EOL recycling rates used here (Table C-6) are from Pauliuk et al.'s (2013) paper, also used by Elshkaki et al. (2018) and Morfeldt et al. (2015).[147,173,174] Pauliuk et al. (2013) estimates the uncertainty of these values to be +5% and -10%.[173] We used the uncertainty range of +/-10% to develop our range of allowable recycling rates for each sector. Additionally, we assume 100% of home and new scrap produced domestically is recycled. The aggregate recycling rate in 2050 ranges from 90%, as predicted by Ayres et al. (2006) and Allwood et al (2010), to 70%.[3,230]

The recycling rate in each year for each sector and scenario, $RR(T)_{s,i}$, is calculated as: for *T=2020 … 2050,* and *i=1 … N,*

$$RR(T)_{s,i} = RR_{2020,s} + \left(\frac{RR_{2050,s,i} - RR_{2020,s}}{2050-2017}\right)(T - 2020), \quad (8)$$

where $RR_{2050,s,i}$ is the recycling rate in year 2050 for theoretical value i in sector *s* and RR_{2020} is the recycling rate in year 2020 in sector *s* listed in table C-7.

Table C - 7, Base case recycling rates by scenario[173]

Product Sector	Base Case Recycle Rate
Construction	82%
Transportation	82%
Machinery	87%
Products	58%

1.6. End-of-Life Scrap and Demand

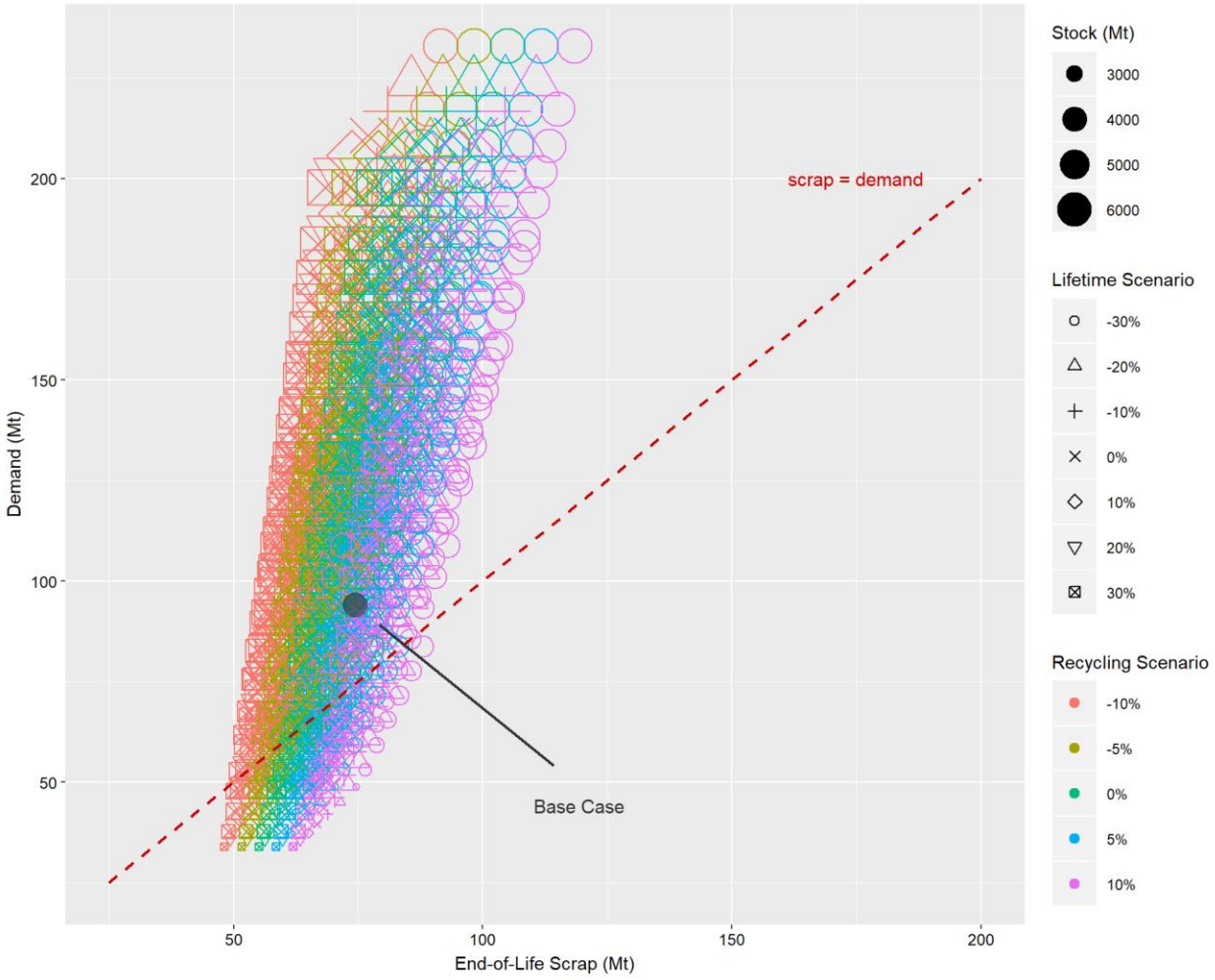

Figure C - 28, U.S. scrap versus demand in 2050. Lifespan scenarios ranging from a -30% decrease from average to a 30% increase from average (shape) and recycling scenarios range from a 10% increase from the base case to a 10% decrease from base case

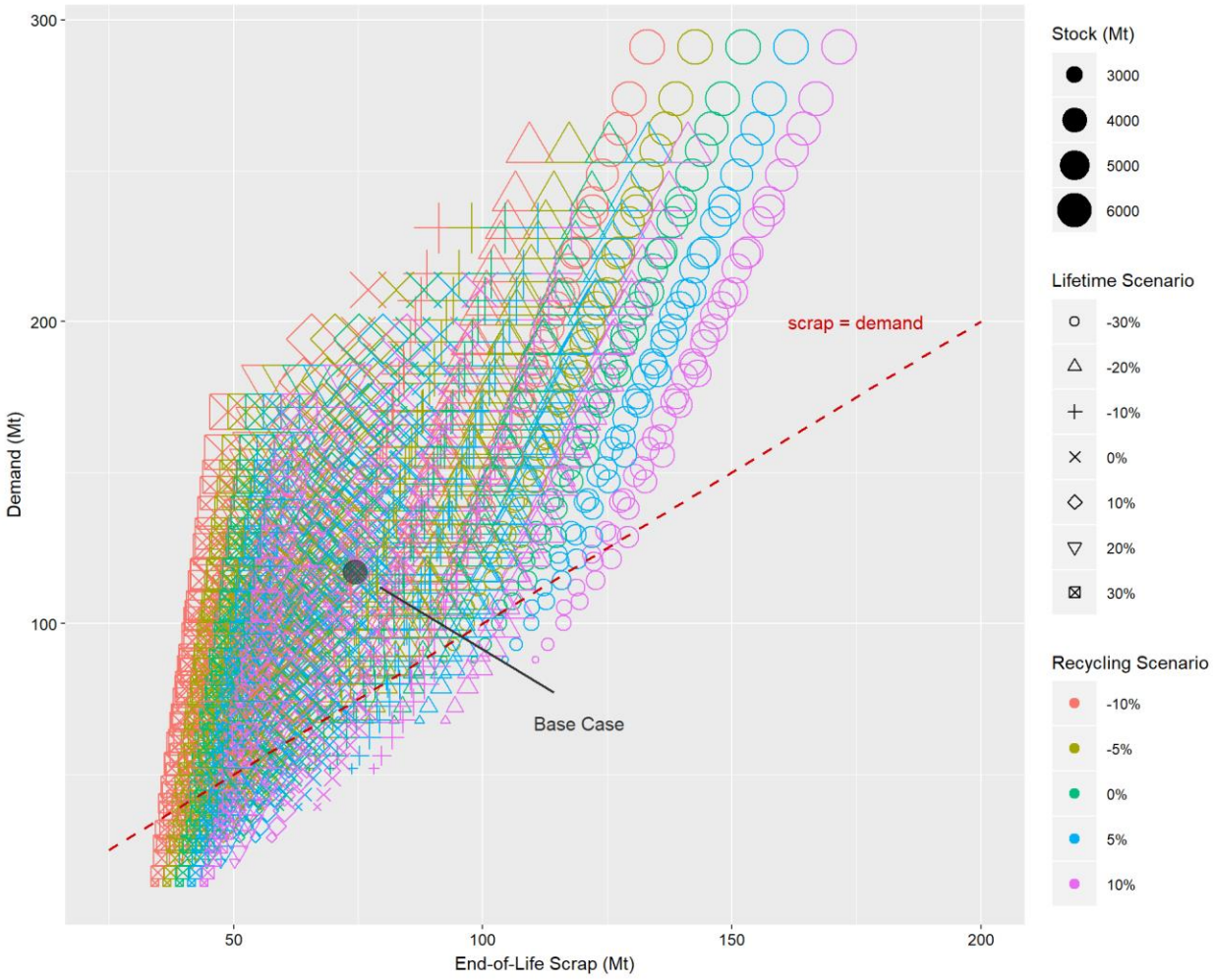

Figure C - 29, U.S. scrap versus demand in 2050 for the retrofit scenario. Lifespan scenarios ranging from a -30% decrease from average to a 30% increase from average (shape) and recycling scenarios range from a 10% increase from the base case to a 10% decrease from base case

3. Trade Scenarios

The U.S. has been a net new steel importer since about 1960[231] and the scale of recent U.S. steel imports (47% of consumption in 2015[232]) has prompted a political response to increase domestic production and cut imports through levying 25% import tariffs.[175] Given the continuing economic, security, and symbolic importance of the U.S. steel industry, it is assumed that policy interventions will prevent any further increase in the relative import reliance of U.S. steel consumption. Unlike the case of new steel, the U.S. has traditionally and continues to be a net exporter of product end of life (EOL) scrap. These exports are driven by demand in the developing world for construction products (e.g., rebar) that can be made from relatively low quality steel, such as EOL scrap with high concentrations of impurities like copper. Cooper et al. (2020) suggests

that domestic recycling of U.S. EOL steel scrap may already be limited by copper contamination and the relatively small demand for impurity tolerant construction products in the U.S. However, recycling limits due to compositional constraints are not included in this analysis. It is assumed that all manufacturing scrap generated within the U.S. is recycled domestically.

Three trade scenarios (high, medium, zero; Table C-8) are simulated in this analysis to encompass the range of possible foreign policy and economic growth effects on new and scrap steel trade. For example, the high trade scenario is based on the percentage of steel consumption that was met by imports in 2015 and the percentage of collected scrap destined to exports in 2011. More new steel (as a percentage of consumption) was imported in 2015 than in any other year recorded by the World Steel Yearbook[133] and more EOL scrap was exported (as a percentage of collected scrap) in 2011 than in any other year recorded since 2010.[133]

Table C - 8, Trade scenario import and export percentages

Scenario	Net Steel/Iron Ore Imports	Net Scrap Exports
Zero	0%	0%
Medium	25%	20%
High	50%	40%

The maximum value in Table C-9 and Table C-10 are rounded up to the nearest tens place to be used for the high trade new steel import and scrap export values respectively.

Table C - 9, Consumption, imports of steel, and imports as percent of consumption in the United States[133]

	Exports Semi-Finished & Finished (t)	Imports Semi-Finished & Finished (t)	Net Semi-Finished & Finished Import (t)	Net Indirect Imports (t)	Pig Iron Exports (t)	Pig Iron Imports (t)	Exports DRI (t)	Imports DRI (t)	Net Pig Iron/ DRI Imports (t) [a]	True Consumption (t)	% Consumption Imported [b]
2010	11791	22510	10719	11322	81	3471	9	1643	4638	91219	29%
2011	13288	26590	13302	12404	126	4190	14	1852	5448	101604	30%
2012	13561	30886	17325	16283	122	4270	8	2762	6377	112483	35%
2013	12508	29812	17304	17773	44	4118	5	2364	5942	113473	36%
2014	11961	41369	29408	16734	52	4603	4	2392	6408	123691	42%
2015	10000	36485	26485	22758	67	4534	21	1866	5825	118889	46%
2016	9247	30913	21666	23528	62	3866	178	1598	4820	115388	43%
2017	10211	35366	25155	24428	66	5127	640	1789	5725	122150	45%

Table C - 10, Percent scrap export [218]

	Purchased	Home	Import	Export	% Net Exported*
2010	66	10	4	21	30%
2011	72	10	4	24	32%
2012	70	10	4	21	28%
2013	77	8.5	3.9	18	21%
2014	62	7.1	4.2	15	20%
2015	54	6.3	3.5	13	20%
2016	53	5.9	3.9	13	19%
2017	55	5.5	4.6	15	21%
2018	56	4.4	4.8	18	26%

New steel imports fall into three categories. They can be in the form of iron (pig iron or DRI), semi-finished products (e.g., slabs), or indirect imports of finished goods (e.g., the steel contained within imported automobiles). Under each trade scenario, the quantity of steel imported belonging to each category is a fixed percentage of the overall import flow. The percentages used, Table C-10, are the average values across 2010-2018.

Table C - 11, Percent of steel imports in each production stage

	Percent of Net Imports
Net Indirect Imports (per_{ind})	41%
Net Semi-Finished & Finished Import (per_{semi})	45%
Net Pig Iron/DRI Imports (per_{prim})	14%

4. Technology Scenarios

The introduction and methods in the main body of the paper briefly outlines the novel steel production technologies modeled in this paper. This section provides more details on their development status, emissions and electricity intensity, as well as, justification for their selection.

4.4. Descriptions of Novel Production Technologies

Direct Reduction (DR)

DR is an existing technology, however, it is not wide spread. DR removes oxygen from iron ore while in its solid state, more specifically in pellets or lumps with hydrogen, natural gas or coal as the reducing agent.[151] The solid-state reduced iron, DRI, is then melted, typically in the EAF or BOF for sweetening. Traditionally using coal as the reducing agent can be more emissions intensive than the BF/BOF route. A more novel technology underdevelopment, the Paired Straight Hearth Furnace (PSH) uses coal to produce DR but operates at higher production rates and lower energy utilization due to its tall bed design, reducing emissions one third from the BOF/BF route.[153] However, it is still more emissions intensive than natural gas DR (NG-DR). In 2000 over 90% of global DRI production used natural gas.[151,154]Although NG-DR is already commercialized and has significantly lower emissions than the BF/BOF route it is more energy intensive, which has limited its market penetration to date.[150] Hydrogen direct reduction (H-DR) is not yet commercialized and is not expected to be deployed before 2030 and will likely be unprofitable until 2040,[29] but if hydrogen is produced with clean electricity, although extremely electricity intensive, it could have close to zero direct emissions. Currently, the cost of hydrogen is a major barrier to this technology.[30] Most hydrogen in the U.S. is currently produced by stream methane reforming (SMR), which produces hydrogen from natural gas, however, hydrogen can also be produced through electrolysis.[233] Electrolysis uses electricity to split water into hydrogen and oxygen.[233] Currently it is not economical and is only used when natural gas is unavailable,[233] however, electrolysis has the potential to act as a form of grid storage providing dispatchable demand capacity, and balancing services to the electricity grid (e.g., regulation up and down, and reserves).[233] These are becoming increasingly important with the addition of variable renewable generation on the grid. As the grid decarbonizes and electricity prices decrease the hydrogen production becomes cleaner, less expensive, and provides more grid services. Therefore, when discussing long-term emissions reduction scenarios with high penetrations of VG it makes sense

to assume hydrogen production through electrolysis. Advancements in electrolysis and hydrogen storage are important to the competitiveness of H-DR.[136] Another novel steel production technology is hydrogen flash smelting (FIT), which is similar to DR but does not need palletization or sintering,[233,234] the process times are able to be significantly reduced[234] and it only produces 2.5% of the direct emissions as the BF.[159] However, based on estimates from Sohn (2015) and Vogl et al. (2018) FIT requires almost twice as much hydrogen as H-DR,[136,159] and is therefore not modeled.

Smelt Reduction (DR)

SR removes the need for the coking and sintering by using pure oxygen and or the use of two vessels to achieve coal gasification, which allows better process control enabling the use of ore fines, but two vessels increases capital cost. [33] Another disadvantage is the large oxygen requirements. However, a number of SR processes are being researched and not all require two vessels or the use of pure oxygen.[33] HIsarna, although a two-vessel process, is cited as the preferred SR technology because it has been operated successfully at demonstration scale using blast air.[33,160] Although this technology has been piloted its deployment estimates range from 10 to 20 years.[152,160] Additionally, a number of SR technologies have the potential to export electricity making them net exports, greatly increasing the process efficiency however, due to the production fuel the CO_2 emissions from that electricity are greater than a natural gas.[33] Therefore, net electricity exporters, although potentially cost effective and efficient would not reduce overall emissions as other SR technologies do.[33]

Electrolysis

A technology in even earlier stages of development, electrolysis, like H-DR is theoretically zero direct emissions, if a carbon neutral electricity grid can be achieved.[154] There are two main types of electrolysis, electrowinning and pryroelectrolysis. Electrowinning uses iron ore as the cathode and electro-plated iron as the anode and operates at 110 °C in an alkaline solution electrolyte.[29] Pryoelectolysis uses dissolved iron ore in a 1600 °C molten oxide mixture as the electrolyte, liquid iron as the cathode and a material inert in relation to the oxide mixture as the anode.[150] Laboratory research is ongoing for electrolysis but it is not anticipated to reach

demonstration stage until 2030 and deployment after 2040.[29,160] Although electricity is currently not economically competitive for iron production[152] this is anticipated to change potentially making steel production another burden, along with transport we are expecting to place on a new carbon neutral grid. Finding a market for the oxygen that is produced in the electrolysis process could reduce the operating expenses.[136]

4.5. Technology electricity consumption and emissions production

Figure 4-2 compares each technology's CO_2 intensity for the different electricity emissions scenarios, using U.S. electricity intensity values. This figure clearly illustrates which technologies are able to meet the 70% emissions reduction goal, which educated the development of our technology scenarios. Table C-12 includes the material and electricity inputs for each technology as well as the direct emissions outputs. The references for each of these values are detailed in tables C-13 to C-41.

Table C - 12, Summary table of process direct emissions and electricity intensity per one ton of product out

Process	Inputs Material (type)	Inputs Material (t in /t out)	Inputs Electricity (kWh/t out)	Outputs Direct Emissions (t CO_2/t out)
Coking	*NA*	*NA*	35	0.43
Sintering	coke	0.32	32	0.17
Pellet	*NA*	*NA*	40	0.057
Blast Furnace (w/o top gas recycling)	Sinter	1.7	40	1.3
	coke	0.41		
Blast Furnace (w/ top gas recycling and fuel substitution)	Sinter	1.7	17	1.1
	coke	0.20*		
Basic Oxygen Furnace	Pig Iron, Scrap and/or DRI	1/0.92 [235]	23	0.11
Open Hearth Furnace	Pig Iron	1.19 [143]	105	0.59
Electric Arc Furnace	Scrap and/or DRI	1/0.93 [235]	508	0.10
Coal Direct Reduction	Pellet	1.3 [167]	110	2.5
Natural Gas Direct Reduction	Pellet	1.3 [167]	117	0.84
Hydrogen Direct Reduction	Pellet	1.504 [136]	3,560	0.053
Smelt Reduction	*NA*	*NA*	74	1.5
Electrolysis	*NA*	*NA*	2,690	0.026

Note: Values listed with NA mean they are not needed for the calculations in this work. All values without a direct reference were calculated in the following sections corresponding to the process type

* 50% reduction in coke[167]

Coking

Table C - 13, Coking electricity consumption

Value	Reference	Notes
31.5 kWh/t coke	Milford (2013)	SI Table 6, Calculated based on total energy and percent electricity
39.2 kWh/t coke	IISI (1998)	Table 1, Section 3.1.8, average of each facility's value (21-63 kWh/t dry coke)
35.4 kWh/t coke	*Average*	

Table C - 14, Coking direct CO_2 emissions

Value	Reference	Notes
0.794 t CO_2/t coke	Pardo & Maya (2013)	Table 1
0.412 t CO_2/t coke	Milford (2013)	SI Table 6, Calculated based on direct emissions from World Steel Association and process emissions from off-gas
0.09 t CO_2/t coke	ECOFYS (2009)	Table 16 Based on coke oven gas as fuel
0.432 t CO_2/t coke	*Average*	

Sintering

Table C - 15, Sintering electricity consumption

Value	Reference	Notes
35 kWh/t sinter	Milford (2013)	SI Table 5, Calculated based total energy and percent electricity
28.5 kWh/ t sinter	IISI (1998)	Section 3.2, Table 2, average of each facility's recent value (22.5-35 kWh/t)
32 kWh/t sinter	*Average*	

Table C - 16, Sintering direct CO_2 emissions

Value	Reference	Notes
0.2 t CO_2/t sinter	Pardo & Maya (2013)	Table 1
0.2 t CO_2/t sinter	Milford (2013)	SI Table 5, Calculated based on direct emissions from World Steel Association
0.119 t CO_2/t sintered ore	ECOFYS (2009)	Table 17
0.17 t CO_2/t sinter	*Average*	

Table C - 17, Sintering coke requirement

Value	Reference	Notes
0.42 t CO_2/t sinter	IISI (1998)	Section 3.2, Table 2, Average
0.59 t CO_2/t sinter	IISI (1998)	Chapter 2, Table 8
0.51 t CO_2/t sinter	*Average*	

Pelleting

Table C - 18, Pelleting electricity consumption

Value	Reference	Notes
40 kWh/t pellet	IISI (1998)	Section 3.2, Page 39
40 kWh/t pellet	*Average*	

Table C - 19, Pelleting direct CO_2 emissions

Value	Reference	Notes
0.057 t CO_2/t pellet	Pardo & Maya (2013)	Table 1
0.057 t CO_2/t pellet	*Average*	

Blast Furnace

Table C - 20, Blast Furnace electricity consumption

Value	Reference	Notes
53.3 kWh/t pig iron	Milford (2013)	SI Table 7, Calculated based total energy and percent electricity
27.5 kWh/thm	IISI (1998)	Section, 2.3, Table 9, Average each facility's recent electricity consumption (14-41 kWh/thm)
40 kWh/t pig iron	*Average*	

Table C - 21, Blast Furnace electricity consumption with top gas recovery

Value	Reference	Notes
17.1 kWh/thm	IISI (1998)	Section 3.3.8, Average of idealized facilities with top gas recovery (8.5-25.6 kWh/thm)
17.1 kWh/t pig iron	*Average*	

Table C - 22, Blast Furnace direct CO_2 emissions

Value	Reference	Notes
1.46 t CO_2/t pig iron	Milford (2013)	SI Table 7, Calculated based on direct emissions from World Steel Association and process emission from off-gas use
1.15 t CO_2/t pig iron	ECOFYS (2009)	Table 15
1.219 t CO_2/t pig iron	Pardo & Maya (2013)	Table 1
1.28 t CO_2/t pig iron	*Average*	

Table C - 23, Blast Furnace with top gas recycling direct CO_2 emissions

Value	Reference	Notes
1.11 t CO_2/t pig iron	Eurofer (2009)	Based on an abatement potential of 15% (Table 1)
1.11 t CO_2/t pig iron	*Average*	

Table C - 24, Blast Furnace coke consumption

Value	Reference	Notes
0.4 t coke/t pig iron	Milford (2013)	Figure 4, BF-BOF reference route
0.42 t coke/t pig iron	IISI (1998)	Section 3.1.1, the mean of the provided range (300-530 kg/thm)
0.41 kWh/t pig iron	*Average*	

Table C - 25, Blast Furnace sinter consumption

Value	Reference	Notes
1.7 t sinter/t pig iron	Milford (2013)	Figure C-4, BF-BOF reference route
1.7 kWh/t pig iron	*Average*	

Basic Oxygen Furnace

Table C - 26, Basic Oxygen Furnace (BOF) electricity consumption

Value	Reference	Notes
20 kWh/t steel	Milford (2013)	SI Table 10, Calculated based total energy and percent electricity
26 kWh/tls	IISI (1998)	Table 1, Section 3.4.6 average of plant's recent electricity consumption (14-42 kWh/tls)
23 kWh/t steel	*Average*	

Table C - 27, Basic Oxygen Furnace (BOF) direct CO_2 emissions

Value	Reference	Notes
0.112 t CO_2/t steel	Milford (2013)	SI Table 10, direct reduction plus emissions from utilization of off-gas
0.112 t CO_2/t steel	*Average*	

Open Hearth Furnace

Table C - 28, Open Hearth Furnace (OHF) electricity consumption

Value	Reference	Notes
105 kWh/t steel	Milford (2013) & Neelis (2006)	Neelis et al. (2006) energy requirements for OHF were 524% times larger than for BOF. This percentage was applied to our BOF direct electricity intensity estimate.
105 kWh/t steel	*Average*	

Table C - 29, Open Hearth Furnace (OHR) direct CO_2 emissions

Value	Reference	Notes
0.586 t CO_2/t steel	Milford (2013) & Neelis (2006)	Neelis et al. (2006) energy requirements for OHF were 524% times larger than for BOF. This percentage was applied to our BOF direct emissions intensity estimate.
0.586 t CO_2/t steel	*Average*	

Electric Arc Furnace

The electrical energy and fuel requirements of an EAF vary depending on the type of charge and grade of scrap. Haupt et al. (2016) shows that lower grade scrap requires more electrical energy.[31] Additionally, a higher ratio of DRI also requires more energy.[167,236] If it has a lower iron content then it requires more fuel energy for oxidation.[33] However, the range of potential EAF impacts are small in comparisons to the difference between EAF and primary production technologies. Therefore, for this report we use constant values for EAF electrical energy and emissions, although different scenarios vary in their percent DRI.

Table C - 30, Electric arc furnace (EAF) electricity consumption

Value	Reference	Notes
594 kWh/t liquid steel	Yellishetty (2011)	Average of their required electricity range 1584-2693 MJ/t liquid steel. Natural gas varied from 50MJ/t to 1500 MJ/t.
473 kWh/t liquid steel	Haupt (2016)	Average of provided range 386-559 kWh/ t liquid steel
568 kWh/t liquid steel	Oda (2009)	Average of provided range 513-623 kWh/t liquid steel. Heavy oil varied from 2.4 GJ/t to 3.6 GJ/t.
392 kWh/t liquid steel	Pesamosca and Patrizio (2016)	Average of electrical energy input values for twelve bucket charges from table 1. Scrap percentage varied from 87% to 100%. Chemical energy varied from 247 kWh/- 367 kWh/t.
421 kWh/t liquid steel	Kirschen et al. (2009)	Average of electrical energy input from 65 different electrical energy estimates, ranging from 91 kWh/t-580 kWh/t. Gas burners varied from 12 kWh/t-182 kWh/t with certain sources not having values and Oxide reaction varied from 85 kWh/t-446 kWh/t.
536 kWh/t liquid steel	Milford (2013)	Calculated based on electricity emissions factor from SI Table 2 and indirect emissions from SI Table 12
555 kWh/t liquid steel	Milford (2013)	Calculated based on electricity emissions factor from SI Table 2 and indirect emissions from SI Table 11
533 kWh/tls	IISI (1998)	Section 3.5.3.4, EAF average of range (335-578 kWh/tls), pollution control (12-69 kWh/tls), ladle arc furnace (20-68 kWh/tls) and others consume (12-67 kWh/tls)
504 kWh/tls liquid steel	IISI (1998)	Table 7, Chapter 3, Average electricity consumption across sites (615-392 kWh/tls)
508 kWh/t steel	*Average*	

Table C - 31, Electric arc furnace (EAF) direct CO_2 emissions

Value	Reference	Notes
0.028 t CO_2/t steel	Yellishetty (2011)	Calculated based emissions factors in Table 4 for NG and Oxygen and their 2007 values for NG and oxygen requirements (10.5 m^3/t NG and 35.6 m^3/t respectively)
0.054 t CO_2/t steel	Milford (2013)	Table 12, 100% Scrap
0.083 t CO_2/t steel	Milford (2013)	Table 11, 50% Scrap/50% DRI
0.24 t CO_2/t steel	Pardo & Mayo (2013)	Table 1
0.10 t CO_2/t steel	*Average*	

Coal Direct Reduction (Coal-DR)

Table C - 32, Coal direct reduction (DR) electricity consumption

Value	Reference	Notes
120 kWh/t DRI	Milford (2013)	Fraction of Energy from Electricity = 0.0176 = (100 kWh/t DRI * 3.6 MJ/kWh) / (20.5 GJ/t DR* 1000 MJ/GJ) Total Energy = 24.6 GJ/t = [0.63 t coal/DRI * 29.7 MJ/kg coal + 100kWh/t DRI * 3.6 MJ/kWh/1000 MJ/GJ]* 1.29 Electrical Energy = 120 kWh/t DRI = 24.6 GJ/t*0.0176*1000 MJ/GJ/3.6 MJ/kWh
100 kWh/t DRI	IISI (1998)	Section 4.5, Table 2, SL/RN
110 kWh/t DRI	*Average*	

Table C - 33, Coal direct reduction (DR) direct CO_2 emissions

Value	Reference	Notes
2.46 t CO_2/t DRI	Milford (2013)	SI Table 8 E_{DRI-C} - $E_{EAF/DRI}$ = D_{DRI-C} ($E_{EAF/DRI}$ = 0.04)
2.46 t CO_2/t DRI	*Average*	

Natural Gas Direct Reduction (NG-DR)

Table C - 34, Natural gas direct reduction (DR) electricity consumption

Value	Reference	Notes
129 kWh/t DRI	Milford (2013)	Fraction of Energy from Electricity = 0.032 = (105 kWh/t DRI * 3.6 MJ/kWh) / (11.8 GJ/t DR* 1000 MJ/GJ) Total Energy = 11.28 GJ/t = [10.9 GJ + 105kWh/t DRI * 3.6 MJ/kWh/1000 MJ/GJ]* 1.29 Electrical Energy = 129 kWh/t DRI = 11.28 GJ/t*0.032*1000 MJ/GJ/3.6 MJ/kWh
105 kWh/t DRI	IISI (1998)	Section 4.5, Midrex process (most widely commercialized)
117 kWh/t DRI	*Average*	

Table C - 35, Natural gas direct reduction (DR) direct CO_2 emissions

Value	Reference	Notes
1.06 t CO_2/t DRI	Milford (2013)	SI Table 8 $E_{DRI\text{-}NG}$ - $E_{EAF/DRI}$ = $D_{DRI\text{-}NG}$ ($E_{EAF/DRI}$ = 0.04)
0.61 t CO_2/t DRI	ECOFYS (2009)	MIDREX process
0.84 t CO_2/t DRI	*Average*	

Hydrogen Direct Reduction (H-DR)

In all cases, hydrogen is assumed to be produced with electricity. Therefore, a significant percentage of the electricity intensity of H-DR is from hydrogen production.

Table C - 36, Hydrogen direct reduction (DR) electricity consumption

Value	Reference	Notes
3,639 kWh/t steel	Fischedick (2014)	This estimate includes hydrogen production. It is the converted sum of their peak (10.6 GJ/t steel) and non-peak (2.5 GJ/t steel) electricity.
3,480 kWh/t steel	Vogl (2018)	The majority of electricity is for the electrolyser hydrogen production
3,560 kWh/t steel	*Average*	

Table C - 37, Hydrogen direct reduction (DR) direct CO_2 emissions

Value	Reference	Notes
0.053 t CO_2/t	Vogl (2018)	Emissions from carbon and lime use and consumption of graphite electrodes
0.053 t CO_2/t steel	*Average*	

Smelt Reduction

Table C - 38, Smelt reduction (SR) electricity consumption

Value	Reference	Notes
88 kWh/t steel	Milford (2013)	2% of total energy, which is estimated as total BF energy
60 kWh/t steel	IISI (1998)	Section 4.5, Table 1, HIsmelt
74 kWh/t steel	Average	

Table C - 39, Smelt reduction (SR) direct CO_2 emissions

Value	Reference	Notes
1.59 t CO_2/t steel	Milford (2013)	Based on a 20% improvement in energy efficiency
1.48 t CO_2/t steel	Junjie (2018)	Based on the HIsarna process which has a 20% reduction in primary energy and CO_2 emissions from BF/BOF process of 1,850 kg CO_2/ton steel
1.54 t CO_2/t steel	Average	

Electrolysis

Table C - 40, Electrolysis electricity consumption

Value	Reference	Notes
2,800 kWh/t	Junjie (2018)	Average of their range (2,600-3,000 kWh/t)
2,583 kWh/t	Fischedick (2014)	Listed 9.3 GJ/t for electrowining
2,692 kWh/t	*Average*	

Table C - 41, Electrolysis direct CO_2 emissions

Value	Reference	Notes
0.026 t CO_2/t steel	The European Steel Association	98% reduction with CO_2 free electricity generation, therefore assumed 2% of original emissions 1.293 t CO_2/t steel are direct emissions.
0.026 t CO_2/t steel	*Average*	

5. Calculating primary and secondary steel flows

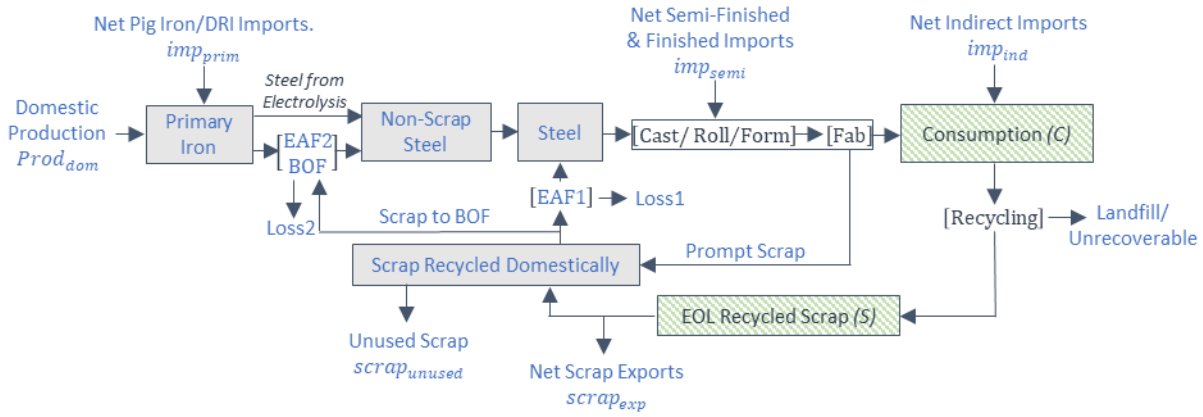

Figure C - 30, Mass flow diagram for domestic steel production and international imports and exports

The capacity of each production process domestically and internationally for each scenario is calculated using the EOL recycled scrap and consumption calculated in the DMFA in sections C-2.2 and C-2.3. Figure C-30 illustrates the process flow used to develop the linear optimization in eqn. 8-34. The optimization prioritizes domestic recycling by minimizing domestic primary production, $prod_{t,i}^{U.S.}$ eqn. 8. All variables have a lower bound of zero. Equations 8-34 are calculated for each year from 2020-2050, *t*, and each pathways, *i*.

The objective function is:

min $$f\left(prod_{t,i}^{U.S.}\right) = prod_{t,i}^{U.S.} \quad (8)$$

subject to $$trade_{t,i}^{imp} per_i^{prim}\left(Consumption_{t,i}\right) - imp_{t,i}^{prim} = 0 \quad (9)$$

$$trade_{t,i}^{imp} per_i^{semi}\left(Consumption_{t,i}\right) - imp_{t,i}^{semi} = 0 \quad (10)$$

$$trade_{t,i}^{imp} per_i^{ind}\left(Consumption_{t,i}\right) - imp_{t,i}^{ind} = 0 \quad (11)$$

$$Scrap_{t,i} - scrap_{t,i}^{exp}\left(1/trade_i^{exp}\right) = 0 \quad (12)$$

$$Consumption_{t,i} - imp_{t,i}^{ind} - fab_{i,t} = 0 \quad (13)$$

$$prompt_{i,t} - fab_{i,t}\left(1/ME_i - 1\right) = 0 \quad (14)$$

$$steel_{i,t} + imp_{t,i}^{semi} - prompt_{i,t} - fab_{i,t} = 0 \quad (15)$$

$$Scrap_{t,i} - scrap_{t,i}^{exp} + prompt_{i,t} - scrap_{t,i}^{recycled} - scrap_{t,i}^{unused} = 0 \quad (16)$$

$$scrap_{t,i}^{recycled} - EAF1_{i,t} - scrap_{t,i}^{BOF} - Loss1_{i,t} = 0 \quad (17)$$

$$(scrap_{t,i}^{recycled} - scrap_{t,i}^{BOF})(1 - \frac{1}{EAF_{loss}}) - Loss1_{i,t} = 0 \quad (18)$$

$$EAF1_{i,t} + steel_{t,i}^{nonscrap} - steel_{i,t} = 0 \quad (19)$$

$$EAF2_{i,t} + BOF_{i,t} + steel_{t,i}^{elec} - steel_{t,i}^{nonscrap} = 0 \quad (20)$$

$$EAF2_{i,t}(Loss_{EAF} - 1) + BOF_{i,t}(Loss_{BOF} - 1) - Loss2_{i,t} = 0 \quad (21)$$

$$prod_{t,i}^{U.S.} + imp_{t,i}^{prim} + scrap_{t,i}^{BOF} - Loss2_{i,t} - BOF_{i,t} - EAF2_{i,t} - steel_{t,i}^{elec} = 0 \quad (22)$$

$$prod_{t,i}^{U.S.} per_{elec,i}^{U.S.} + imp_{t,i}^{prim} per_{elec,i}^{ROW} - steel_{t,i}^{elec} = 0 \quad (23)$$

$$1.2prod_{t,i}^{U.S.}\left(per_{BF,i}^{U.S.} + per_{SR,i}^{U.S.}\right) + 1.2imp_{t,i}^{prim}\left(per_{BF,i}^{ROW} + per_{SR,i}^{ROW}\right) - BOF_{i,t} loss_{BOF} = 0 \quad (34)$$

The percent imports and exports are fixed based on the trade scenarios. Eqn. 9-12 use these percentages to calculate the mass of steel imports at each stage of production and the mass of scrap exports. The remaining equations mass flow equalities. Eqn. 13 calculates fabricated steel, fab, based on consumption, C, and net indirect imports, $imp_{t,i}^{ind}$. Eqn. 24-15 calculates prompt scrap from and the required steel inputs to fabrication, casting, rolling, and forming, based on the losses of these processes, ME. ME is dependent on the material efficiency scenario. Eqn. 16-18 determines if there is any excess scrap, $scrap_{t,i}^{unused}$, which occurs when demand for steel is less than the available scrap, as well as, the output and losses from EAF1. Eqn. 19 determines the remaining demand after scrap is processed through EAF1, $steel_{t,i}^{nonscrap}$. Eqn. 20 relates EAF2, BOF and steel produced through electrolysis$steel_{t,i}^{elec}$ to the demand remaining after EAF1, $steel_{t,i}^{nonscrap}$. Eqn. 21 determines the losses from EAF2 and the BOF. Eqn. 22 relates sources of primary iron to the processes through which they can becomes steel. Eqn. 23 calculates the mass of steel produces through electrolysis, $steel_{t,i}^{elec}$,which is required because it is the only primary production technology that directly produces steel from iron ore and therefore, its outputs do not need to be processed through the EAF or BOF. The EAF can only process DRI or scrap, but the BOF requires around 20% DRI or scrap for cooling. Equality eqn. 24 fixes the size of the BOF to 20% larger than all of the BF and SR iron produced in a given scenario. Eqn. 24 in combination with eqn. 22 ensure that each type of iron, as well as, the steel from scrap and electrolysis are processed correctly.

The only differences between EAF1 and EAF2 is that EAF1 is all scrap and EAF2 can also process DRI.

In certain scenarios, there is a greater amount of scrap available than consumption demanded. In these scenarios, there is unused scrap. It is assumed the U.S. will export this scrap and it will be recycled internationally. The emissions credits for this recycled scrap, however are not included in the emissions analysis, section C-6. In these instances the scrap trade scenario is violated, however, it would be unrealistic to assume that the additional scrap is not exported given it has a monetary value.

6. CO_2 Emissions Limits

The baseline year for this analysis is 2010. Therefore, in order to determine allowable emissions in 2050, we must first calculate 2010 CO_2 emissions attributable to U.S. steel consumption, $CO_{2,total\,2010}$. Additionally, in order to determine the remaining carbon budget we must also calculate the emission 2011-2017. These values requires calculating the flow through each production process domestically and internationally.

Based on these calculations, 112 Mt CO_2 were released in 2010 from steelmaking attributable to the 76 Mt of steel consumed in end-use products in the U.S. Subsequently, the 2050 target is annual emissions no greater than **33.6 Mt CO_2**. The 2020-2050 cumulative CO_2 emissions budget for the U.S. steel sector was estimated by assuming the budget is equivalent to a linear decrease over time in steel sector emissions from 112 Mt CO_2 in 2010 to 33.6 Mt CO_2 in 2050. The emissions already released between 2010-2020 were subtracted from the 2010-2050 budget; thus, the 2020-2050 cumulative emissions budget is **1.73 Gt CO_2**.

Equation 1 in the main text is a simplified representation of these calculations. This section shows the calculations in more detail. Table C-42 C-43 include the international and U.S. flows used in the equations in this section.

<u>Domestic Flows</u>

Domestic production, $prod_{dom,t}$, in crude steel equivalent is calculated as follows: *for t = 2010 … 2017,*

$$prod_t^{U.S.} = Apparent\ Steel_{crude,t}^{U.S.} - imp_{crude,t}^{prim} - \frac{1}{loss}\left(netimp_{crude,t}^{semi} - netimp_{crude,t}^{ind}\right), \quad (35)$$

where *loss* is the manufacturing and fabrication loss value of 0.78 from Cullen et al.'s (2012). Table C-42 includes all of the values in eqn. 32. The total domestic production is then used to calculate the production through each technology.

Domestic BF production is calculated as follows: *for t = 2010, …, 2017,*

$$BF_t^{U.S.} = \%prod_{BF,t}^{U.S.} \frac{\left(prod_t^{U.S.} - netimp_{crude,t}^{prim}\right)}{BOF_{loss}}. \quad (36)$$

The primary imports are subtracted from the total domestic production as they are an output of an international BF or DR process.

Domestic BOF production is calculated as follows: *for t = 2010, …, 2017,*

$$BOF_t^{U.S.} = \%prod_{BOF,t}^{U.S.}(prod_t^{U.S.}). \quad (37)$$

Domestic EAF production is calculated as follows: *for t = 2010, …, 2017,*

$$EAF_t^{U.S.} = \%prod_{EAF,t}^{U.S.}(prod_t^{U.S.}). \quad (38)$$

Domestic NG-DR production is calculated as follows: *for t = 2010, …, 2017,*

$$NGDRI_t^{U.S.} = \%prod_{NGDRI,t}^{U.S.}(prod_t^{U.S.}). \quad (39)$$

In 2010 to 2017 only the BF, BOF, NG-DR and the EAF were used for steel production in the U.S.

Imported Flows

Total non-primary steel imports are calculated as follows: *for t = 2010, …, 2017,*

$$imp_{steel,t} = netimp_t^{semi} + \frac{netimp_t^{ind}}{loss}. \quad (40)$$

Primary imports are not included as they are not at the steel stage.

The output of international OHFs for U.S. consumption is calculated as follows: *for t = 2010, …, 2017,*

$$OHF_t^{ROW} = imp_t^{steel}(\%prod_{OHF,t}^{ROW}). \quad (41)$$

The output of international BOFs for U.S. consumption is calculated as follows: *for t = 2010, …, 2017,*

$$BOF_t^{ROW} = imp_t^{steel}(\%prod_{BOF,t}^{ROW}). \quad (42)$$

The output of international is calculated as follows: *for t = 2010 … 2017,*

$$EAF_t^{ROW} = imp_t^{steel}\left(\frac{\%prod_{NGDRI,t}^{ROW}+\%prod_{CDR,t}^{ROW}}{EAF_{loss}} + \%prod_{EAF,t}^{ROW}\right). \quad (43)$$

We assume that all internationally produced DRI that is imported as a semi-finished or finished product is processed through an EAF.

The DRI and pig iron flows are calculated by converting all imports to pig iron or DRI equivalent as follows: *for t = 2010, …, 2017,*

$$imp_t^{primeq} = netimp_t^{prim} + \frac{netimp_t^{semi} + netimp_t^{ind}/loss}{\%prod_{BOF,t}^{ROW}BOF_{loss}+\%prod_{OHF,t}^{ROW}OHF_{loss}+EAF_{loss}(\%prod_{CDR,t}^{ROW}+\%prod_{NGDR,t}^{ROW})}. \quad (44)$$

The denominator of eqn. 44 calculates the loss factor, as the loss factors for the processes the pig iron or DRI go through internationally varies. A percent of the pig iron is processed through the BOF and a percent through the OHF internationally, and we assume all DRI is processed through the EAF internationally.

International DR-NG production for U.S. consumption is calculated as follows: *for t = 2010, …, 2017,*

$$NGDRI_t^{ROW} = imp_t^{primeq}(\%prod_{NGDR,t}^{ROW}). \quad (45)$$

International DR-C production for U.S. consumption is calculated as follows: *for t = 2010, …, 2017,*

$$CDRI_t^{ROW} = imp_t^{primeq}(\%prod_{CDR,t}^{ROW}). \quad (46)$$

International BF production for U.S. consumption is calculated as follows: *for t = 2010, …, 2017,*

$$BF_t^{ROW} = imp_t^{primeq}(1 - \%prod_{NGDR,t}^{ROW} - \%prod_{CDR,t}^{ROW}). \quad (47)$$

Exported Flows

The U.S. exports a portion of their available EOL scrap, which is assumed to be recycled internationally. The value for scrap exports, $expscrap_t$, is taken directly from World Steel Yearbook and is listed in Table C-42 to C-43 for 2010.

Emissions

The emissions from domestic production is calculated as follows: *for each technology type, tech = (BF, BOF, EAF) and for t = 2010, …, 2017,*

$$CO_{2,t}^{U.S} = \sum_{tech} \frac{tech_t^{U.S.}}{10^6} \left(\frac{EI_{tech} EI_t^{U.S.}}{1000} + EF_{tech} 1000 \right), \quad (48)$$

where $EI_{dom,t}$ is the electricity intensity of the domestic grid in year *T*. The flows through each technology type were calculated in eqn. 36-47 and table C-12 lists the electricity and emissions intensity of each technology. All *EI* values represent the electricity intensity of a process (kWh/ton steel), while all *EF* values represent the direct CO_2 emissions factor of the process (ton CO_2/ton steel).

The emissions from international production is calculated as follows: *for each technology type, tech = (BF, BOF, OHF, DRI-C, DRI-NG, EAF) and for t = 2010, …, 2017,*

$$CO_{2,t}^{ROW} = \sum_{tech} \frac{tech_t^{ROW}}{10^6} \left(\frac{EI_{tech} EI_t^{ROW}}{1000} + EF_{tech} 1000 \right). \quad (46)$$

Using the above values the total CO_2 emissions attributed to U.S. steel consumption is calculated as follows: *for t = 2010 … 2017,*

$$CO_{2,t}^{total} = CO_{2,t}^{U.S} + CO_{2,t}^{ROW} \quad . \quad (47)$$

Table C - 42, Historic international (ROW) steel flows used to calculate 2010-2017 CO_2 emissions and percent production from each technology in the 2020 base case technology scenario

	DRI[40]	OBC[40]	OHF[4] 0	Other[4] 0	Total Production [b]	C-DRI as % DRI[166,237–239]	C-DRI	NG-DRI	BF	SR [c]	Electricity EI 164,240,241
	(thousand metric tons)						Percent				(kg CO_2 /kwh)
2010	72,019	993,374	16,446	565	1,171,917	25.7%	2%	5%	94%	0%	528
2011	77,625	1,065,079	16,416	1,008	1,255,870	23.6%	1%	5%	94%	0%	537
2012	76,879	1,099,079	10,895	973	1,285,473	23.3%	1%	5%	94%	0%	531
2013	79,616	1,209,799	9,416	1,085	1,406,909	21.3%	1%	4%	94%	0%	526
2014	81,267	1,226,838	7,578	1,074	1,424,882	20.6%	1%	5%	94%	0%	519
2015	75,982	1,205,395	6,853	2,094	1,396,446	20.2%	1%	4%	94%	0%	505
2016	78,331	1,202,395	7,220	1,369	1,395,246	17.5%	1%	5%	94%	0%	490
2017	88,664	1,206,963	6,265	1,757	1,409,796	17.6%	1%	5%	94%	0%	485
2018	104,045	1,283,394	6,526	1,887	1,508,695	20.2%	1%	6%	93%	0%	485[d]
2019 [a]	104,045	1,283,394	6,526	1,887	1,508,695	20.2%	1%	6%	93%	0%	485[d]
2020 [a]	104,045	1,283,394	6,526	1,887	1,508,695	20.2%	1%	6%	93%	0%	485[d]

[a] Data for 2019 and 2020 are not published yet do values from 2018 were substituted
[b] Total Production = DRI + (OBC/0.84 + OHF/0.92 + Other), where losses represented the material lost in the BOF, Losses=0.92
[c] Other is assumed to equal SR
[d] Data for 2018-2020 are not published yet do values from 2017 were substituted
DRI = Direct Reduction Iron; OBC = Oxygen Blown Converter; OHF = Oxygen Hearth Furnace; C = Coal; NG=Natural Gas; BF = Blast Furnace; SR = Smelt Reduction

Table C - 43, Historic U.S. steel flows used to calculate 2010-2017 CO_2 emissions and percent production from each technology in the 2020 base case technology scenario

	DRI[165,166,237–239,242]	Pig Iron[40,165,242]	NG-DRI	BF	Electricity EI[164,240,241]
	(thousand metric tons)		Percent		(kg CO_2 /kwh)
2010	0	26,800	0%	100%	531
2011	0	30,200	0%	100%	511
2012	0	32,100	0%	100%	488
2013	0	30,300	0%	100%	489
2014	1,300	29,400	4%	96%	486
2015	1,100	25,400	4%	96%	456
2016	1,810	22,300	8%	92%	433
2017	2,990	22,400	12%	88%	421
2018	3,350[a]	30,113[b]	10%	90%	421[a]
2019	3,350[a]	30,113[c]	10%	90%	421[a]
2020	3,350[a]	30,113[c]	10%	90%	421[a]

[a] Data for 2018-2020 are not published yet do values from 2017 were substituted
[b] Value is based on data for oxygen blown furnace (OBF) production in 2018 from the World Steel Yearbook converted to Pig Iron using losses in the OBF equivalent to 0.92
[c] Data for 2019-2020 are not published yet do values from 2018 were substituted
DRI = Direct Reduction Iron; NG=Natural Gas; BF = Blast Furnace

7. Pathway CO_2 Emissions

The same methods are used to calculate CO_2 attributed to U.S. steel consumption for 2018 to 2050 as those used to calculate 2010 emissions. However, for 2021 to 2050, the calculations are done for each scenario and there are a larger number of primary production technologies to consider. As with the 2010 emissions calculations the first step is to calculate the steel produced by each production process domestically and internationally. The optimization, in section C-4, determines the quantity imported at each stage, the net scrap exported, the quantity of primary steel produced, as well as, the flow through the domestic EAFs and BOFs.

Domestic Flows

The international flows are less straightforward because they are imported at different stages of production therefore, they have undergone varying loss values. In order to account for these losses we shift each flow to the same stage of production. In this case, pig iron or DRI, the inputs to the BOF and EAF. Losses vary depending on if the steel has gone through the EAF or the BOF, therefore, it is calculated for both as follows: *for t = 2018 … 2050,*

$$imp_{t,i}^{BOFeq} = imp_{t,i}^{prim} + \frac{imp_{t,i}^{semi}}{BOF_{loss}} + \frac{imp_{t,i}^{ind}}{BOF_{loss}/loss_{i,t}}, \tag{48}$$

$$imp_{t,i}^{EAFeq} = imp_{t,i}^{prim} + \frac{imp_{t,i}^{semi}}{EAF_{loss}} + \frac{imp_{t,i}^{ind}}{EAF_{loss}/loss_{i,t}}. \tag{49}$$

We assume all BF and SR iron goes through the BOF. The ratio of primary to secondary production is estimated based on Pauliuk et al. (2013)'s projections for global EAF, BOF, and foundry production to 2100.[37] EAF is considered secondary, BOF primary, and foundry production 50/50. Therefore, the flows through these processes are calculated as follows: *for tech = (BF, SR) and for t = 2018,…,2050*

$$BF_{t,i}^{ROW} = imp_{t,i}^{BOFeq}(\%prim_t)(\%prod_{t,i}^{BF})(1 - \%prod_{t,i}^{BF-TG}), \tag{50}$$

$$BF-TG_{t,i}^{ROW} = imp_{t,i}^{BOFeq}(\%prim_t)(\%prod_{t,i}^{BF})(\%prod_{t,i}^{BF-TG}), \tag{51}$$

$$SR_{t,i}^{ROW} = imp_{t,i}^{BOFeq}(\%prim_t)(\%prod_{t,i}^{SR}). \tag{52}$$

We assume all DRI-C, DRI-NG, and DRI-H iron goes through the EAF. Therefore, the flows through these processes are calculated as follows: *for tech = (DRI-C, DRI-NG, DRI-H) and for t = 2018,…,2050*

$$CDRI_{t,i}^{ROW} = imp_{t,i}^{EAFeq}(\%prod_t)(\%prod_{t,i}^{CDRI}), \quad (53)$$

$$NGDRI_{t,i}^{ROW} = imp_{t,i}^{EAFeq}(\%prod_t)(\%prod_{t,i}^{NGDRI}), \quad (54)$$

$$HDRI_{t,i}^{ROW} = imp_{t,i}^{EAFeq}(\%prod_t)(\%prod_{t,i}^{HDRI}). \quad (55)$$

Electrolysis is calculated differently than the other production processes because it produces steel rather than pig iron or DRI; therefore, its process output is equivalent to the output of the BOF and EAF rather than the input. Therefore, electrolysis steel is calculated as follows, *and for t = 2018,…,2050,*

$$ELEC_{t,i}^{ROW} = (1 - \%prim_t)\left(imp_{t,i}^{prim}\frac{BOF_{loss}+EAF_{loss}}{2} + imp_{t,i}^{semi} + \frac{imp_{t,i}^{ind}}{loss_{i,t}}\right). \quad (56)$$

The flow through the EAF and the BOF is dependent on the percentage through each production process, determined by the technology scenarios. The same assumptions are made as above, in regards to which primary processes will feed into the EAF vs the BOF. However, only imports from semi-finished, finished and indirect products will have gone through the BOF or the EAF internationally before imported by the U.S., therefore, only a portion of the total flows calculated through each corresponding process above eqn. 50-56 will go through the BOF or EAF: *for t = 2018,…, 2050,*

$$BOF_{t,i}^{ROW} = (BF_{t,i}^{ROW} + BF - TG_{t,i}^{ROW} + SR_{t,i}^{ROW})\, BOF_{loss}, \quad (57)$$

$$EAF_{t,i}^{ROW} = \left(CDRI_{t,i}^{ROW} + NGDRI_{t,i}^{ROW} + HDRI_{t,i}^{ROW}\right)EAF_{loss} + imp_{t,i}^{EAFeq}(1 - \%prim_t). \quad (58)$$

Exported Flows

The U.S. exports portion of the available EOL scrap, which is assumed to be recycled internationally, and the U.S. is assumed to recycle the rest domestically. The portion exported in each scenario is the sum of the unused scrap value and the net export scrap value, which are outputs of the steel flow analysis discussed in section C-5.

Emissions

The emissions for 2018 to 2050 are calculated using the same equations as the 2010-2017 emissions (eqn. 46-47).

8. Additional Results Figures

8.1. *Impact of Parameters and Scenarios on Final Emissions*

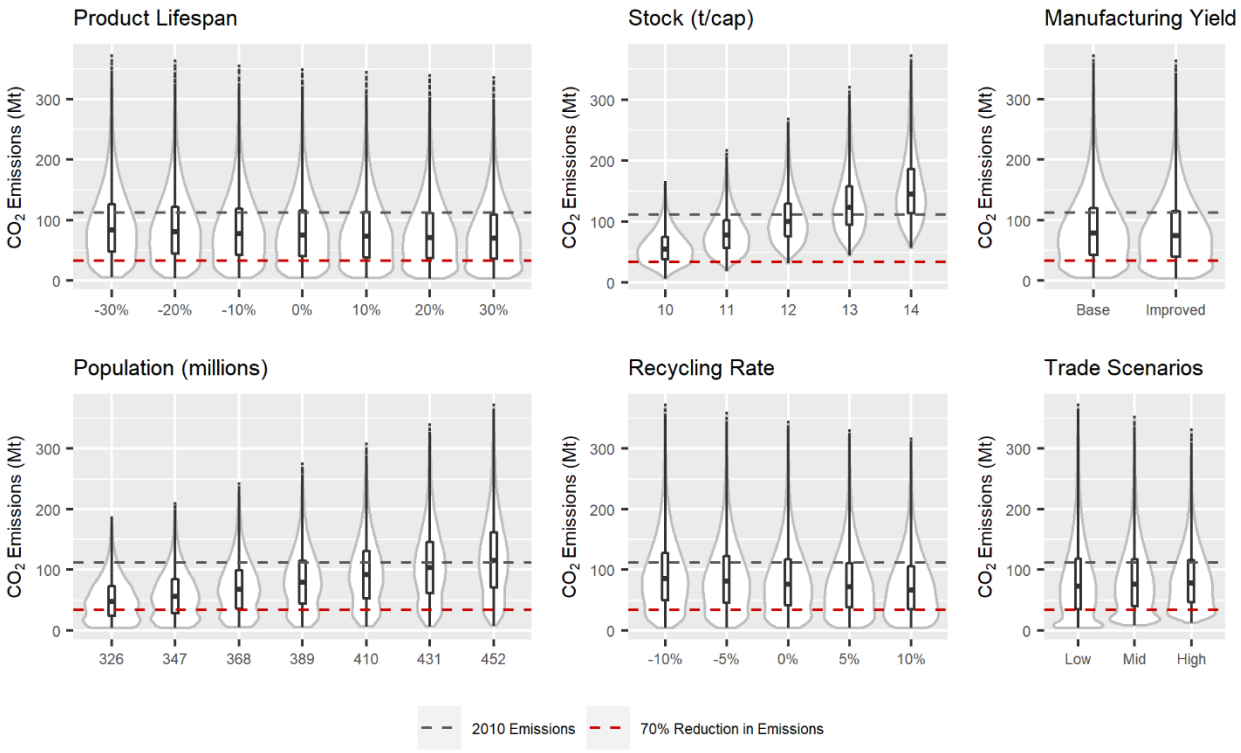

Figure C - 31, CO_2 emissions in 2050 for the case with no retrofit separated by scenario for product lifespan, stock, manufacturing yield, population, recycling rate, and trade parameters. The grey dashed line represents 2010 CO_2 emissions allocated to the steel sector and the lower dashed red line represents a 70% reduction.

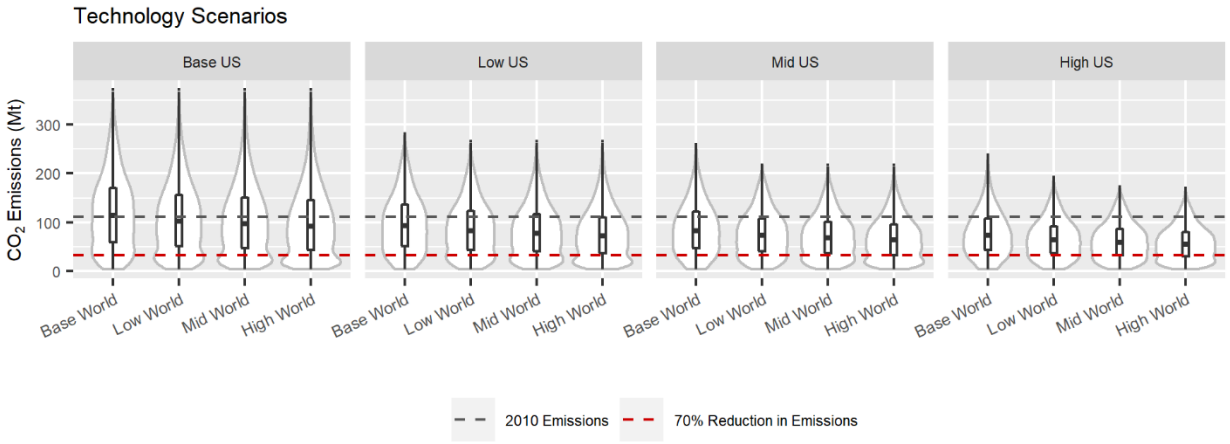

Figure C - 32, CO_2 emissions in 2050 for the case with no retrofit separated by scenarios for technology. The grey dashed line represents 2010 CO_2 emissions allocated to the steel sector and the lower dashed red line represents a 70% reduction.

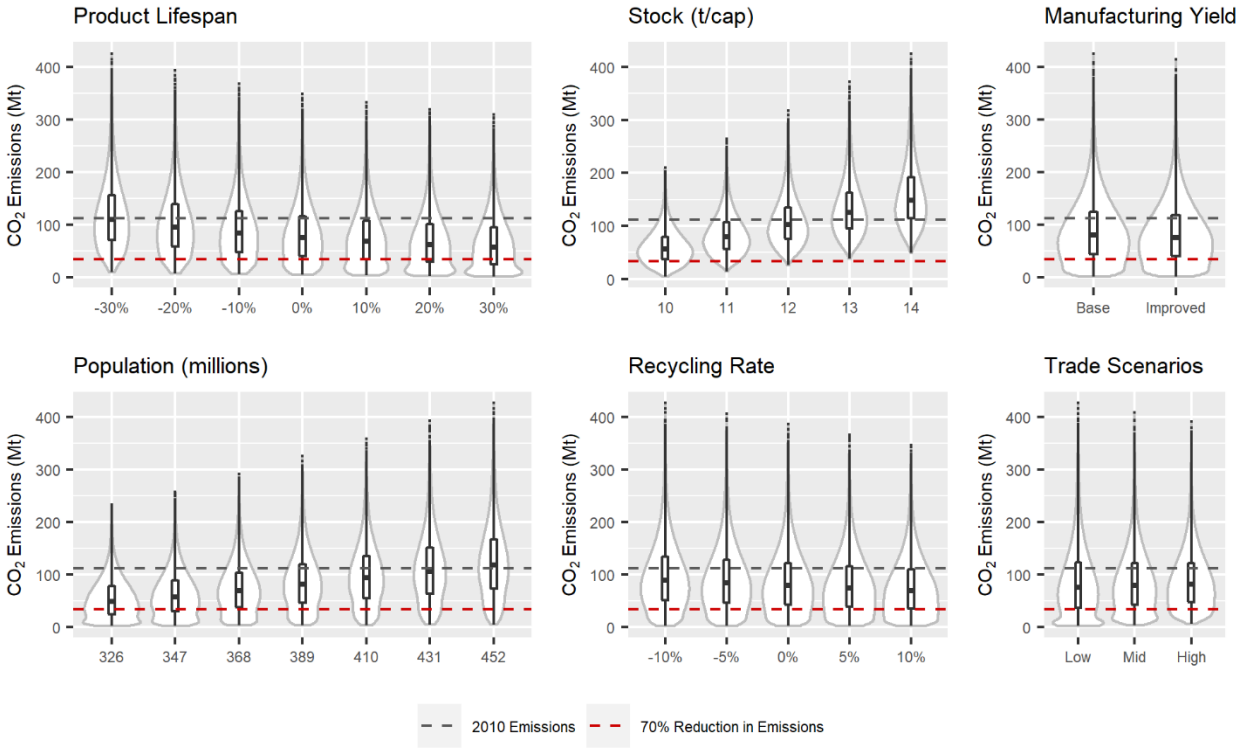

Figure C - 33, CO_2 emissions in 2050 for the case with retrofit separated by scenario for product lifespan, stock, manufacturing yield, population, recycling rate, and trade parameters The grey dashed line represents 2010 CO_2 emissions allocated to the steel sector and the lower dashed red line represents a 70% reduction.

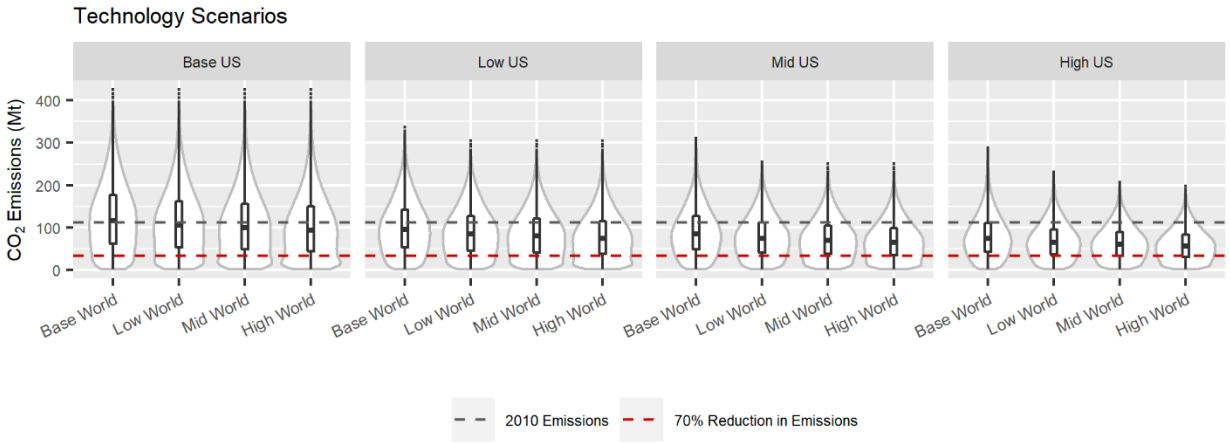

Figure C - 34, CO_2 emissions in 2050 for the case with retrofit separated by scenarios for technology. The grey dashed line represents 2010 CO_2 emissions allocated to the steel sector and the lower dashed red line represents a 70% reduction.

8.2. *Combined Scenario Parameter Impacts*

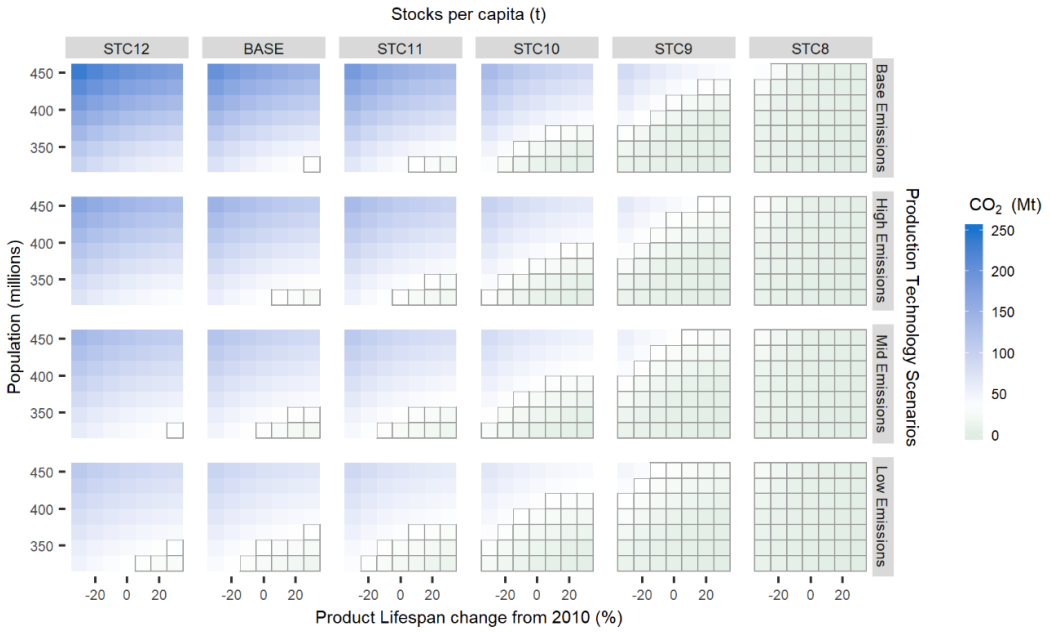

Figure C - 35, 2050 CO_2 emissions for improved manufacturing yields, low trade, 10% improvement in recycling rates, product retrofits, and cases where the US and world have equivalent emissions reduction scenarios. The bottom horizontal axis is the percent change in lifespan from average and the right vertical axis is the stocks per capita (STC). The gray boxes indicate scenarios that meet the 2050 CO_2 emissions reduction goals.

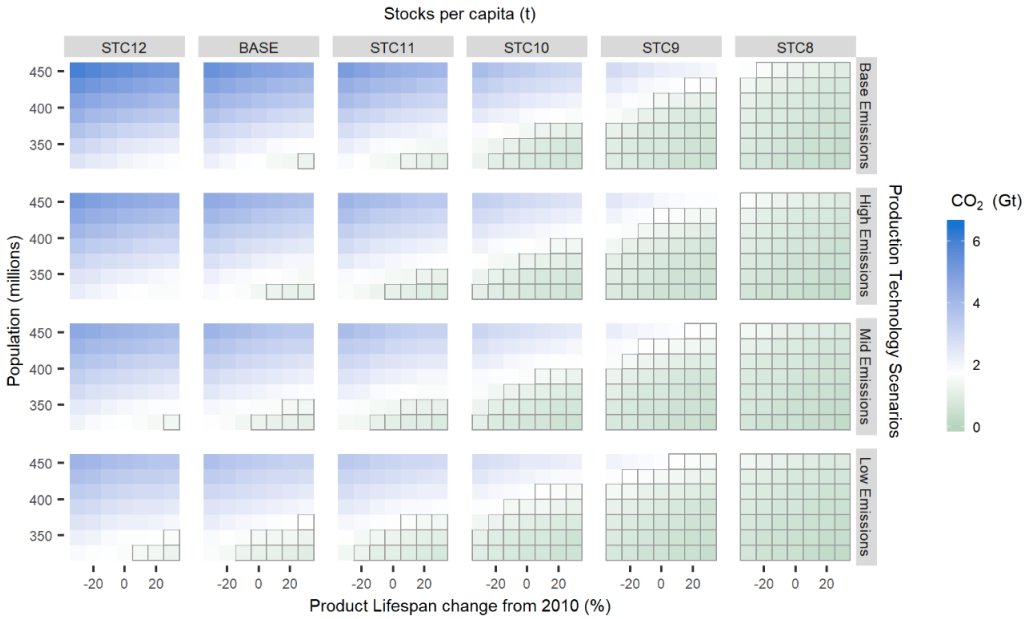

Figure C - 36, Cumulative CO_2 emissions for improved manufacturing yields, low trade, 10% improvement in recycling rates, product retrofits, and cases where the US and world have equivalent emissions reduction scenarios. The bottom horizontal axis is the percent change in lifespan from average and the right vertical axis is the stocks per capita (STC). The gray boxes indicate scenarios that meet the cumulative emissions goal

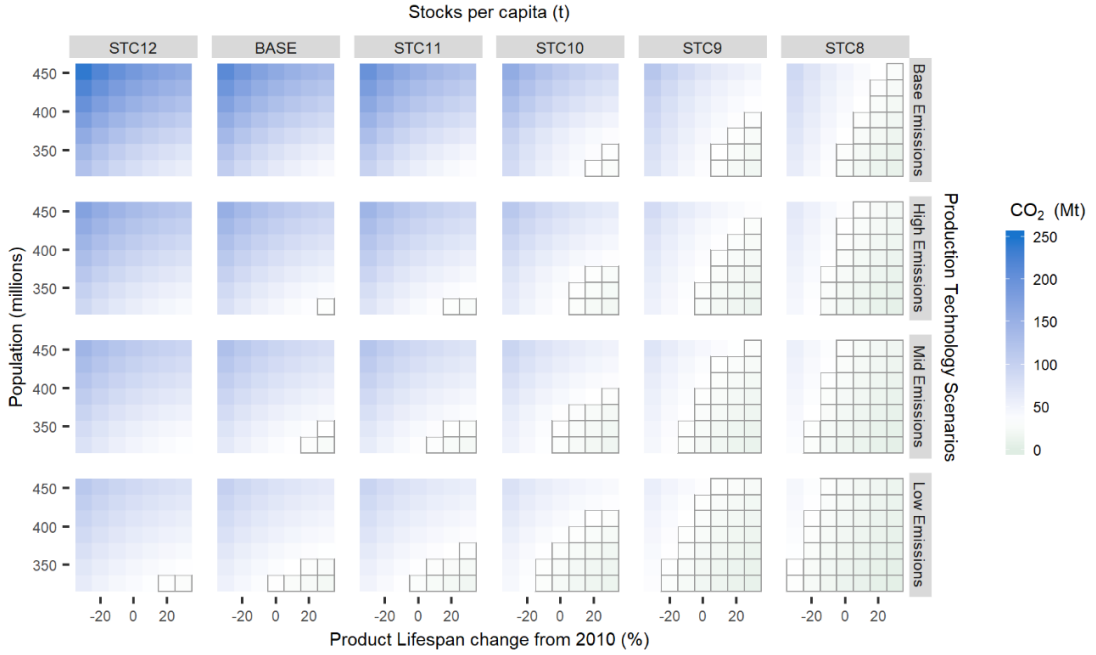

Figure C - 37, 2050 CO_2 emissions for improved manufacturing yields, high trade, 10% improvement in recycling rates, product retrofits, and cases where the US and world have equivalent emissions reduction scenarios. The bottom horizontal axis is the percent change in lifespan from average and the right vertical axis is the stocks per capita (STC). The gray boxes indicate scenarios that meet the 2050 CO_2 emissions reduction goals.

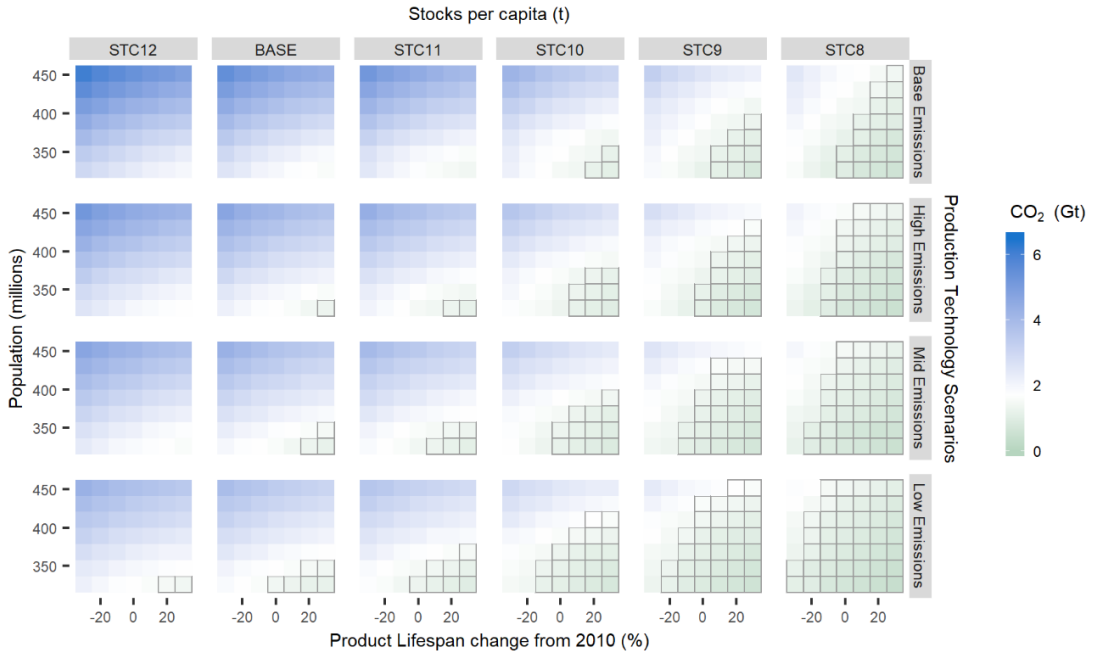

Figure C - 38, Cumulative CO_2 emissions for improved manufacturing yields, high trade, 10% improvement in recycling rates, product retrofits, and cases where the US and world have equivalent emissions reduction scenarios. The bottom horizontal axis is the percent change in lifespan from average and the right vertical axis is the stocks per capita (STC). The gray boxes indicate scenarios that meet the cumulative emissions goal

6.1. *Changes to stocks per capita*

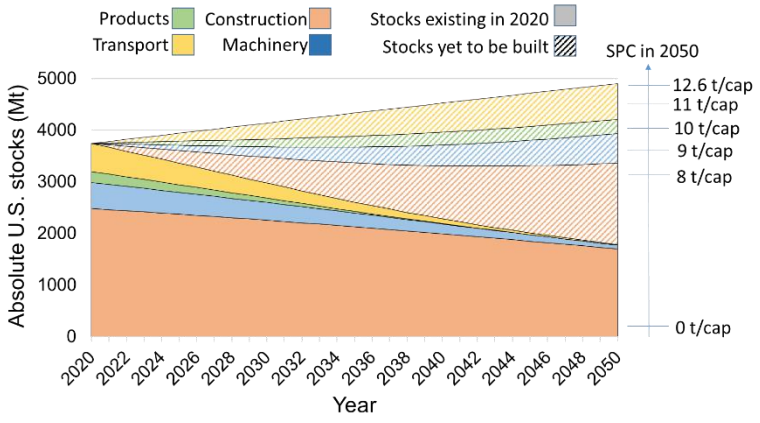

Figure C - 39, U.S. steel stocks (2020-2050) modeled for the base case steel flow parameters and split into stocks that already exist (in 2020) and have yet to be built

REFERENCES

(1) Intergovernmental Panel on Climate Change. Climate Change 2014: Mitigation of Climate Change, Summary for Policy Makers. **2014**, 1–33.

(2) United States Environmental Protection Agency. Sources of Greenhouse Gas Emissions https://www.epa.gov/ghgemissions/sources-greenhouse-gas-emissions (accessed Sep 2, 2019).

(3) Allwood, J. M.; Cullen, J. M.; Milford, R. L. Options for Achieving a 50% Cut in Industrial Carbon Emissions by 2050. *Environ. Sci. Technol.* **2010**, *44* (6), 1888–1894.

(4) Loftus, P. J.; Cohen, A. M.; Long, J. C. S.; Jenkins, J. D. A Critical Review of Global Decarbonization Scenarios: What Do They Tell Us about Feasibility? *Wiley Interdiscip. Rev. Clim. Chang.* **2015**, *6* (1), 93–112.

(5) IPCC. *Summary for Policymakers*; 2014.

(6) United States Environmental Protection Agency. Draft Inventory of U.S. Greenhouse Gase Emissions and Sinks: 1990-2018. **2020**.

(7) Jacobson, M. Z.; Delucchi, M. A. Providing All Global Energy with Wind, Water, and Solar Power, Part I: Technologies, Energy Resources, Quantities and Areas of Infrastructure, and Materials. *Energy Policy* **2011**, *39* (3), 1154–1169.

(8) Pleßmann, G.; Erdmann, M.; Hlusiak, M.; Breyer, C. Global Energy Storage Demand for a 100% Renewable Electricity Supply. *Energy Procedia* **2014**, *46*, 22–31.

(9) Connolly, D.; Lund, H.; Mathiesen, B. V.; Leahy, M. The First Step towards a 100% Renewable Energy-System for Ireland. *Appl. Energy* **2011**, *88* (2), 502–507.

(10) Allen, P.; Blake, L.; Harper, P.; Hooker-Stroud, A.; James, P.; Kellner, T. *Zero Carbon Britain: Rethinking the Future*; 2010.

(11) Clack, C. T. M.; Qvist, S. A.; Apt, J.; Bazilian, M.; Brandt, A. R.; Caldeira, K.; Davis, S.

J.; Diakov, V.; Handschy, M. A.; Hines, P. D. H.; Jaramillo, P.; Kammen, D. M.; Long, J. C. S.; Morgan, M. G.; Reed, A.; Sivaram, V.; Sweeney, J.; Tynan, G. R.; Victor, D. G.; Weyant, J. P.; Whitacre, J. F. Evaluation of a Proposal for Reliable Low-Cost Grid Power with 100% Wind, Water, and Solar. *Proc. Natl. Acad. Sci.* **2017**, 201610381.

(12) Heard, B. P.; Brook, B. W.; Wigley, T. M. L.; Bradshaw, C. J. A. Burden of Proof: A Comprehensive Review of the Feasibility of 100% Renewable-Electricity Systems. *Renew. Sustain. Energy Rev.* **2017**, *76* (April), 1122–1133.

(13) Kroposki, B.; Johnson, B.; Zhang, Y.; Gevorgian, V.; Denholm, P.; Hodge, B.-M.; Hannegan, B. Achieving a 100% Renewable Grid. **2017**, No. april, 61–73.

(14) Ela, E.; Milligan, M.; Bloom, A.; Botterud, A.; Townsend, A.; Levin, T.; Frew, B. A. Wholesale Electricity Market Design with Increasing Levels of Renewable Generation: Incentivizing Flexibility in System Operations. *Electr. J.* **2016**, *29* (4), 51–60.

(15) Davis, S. J.; Lewis, N. S.; Shaner, M.; Aggarwal, S.; Arent, D.; Azevedo, I. L.; Benson, S. M.; Bradley, T.; Brouwer, J.; Chiang, Y. M.; Clack, C. T. M.; Cohen, A.; Doig, S.; Edmonds, J.; Fennell, P.; Field, C. B.; Hannegan, B.; Hodge, B. M.; Hoffert, M. I.; Ingersoll, E.; Jaramillo, P.; Lackner, K. S.; Mach, K. J.; Mastrandrea, M.; Ogden, J.; Peterson, P. F.; Sanchez, D. L.; Sperling, D.; Stagner, J.; Trancik, J. E.; Yang, C. J.; Caldeira, K. Net-Zero Emissions Energy Systems. *Science (80-.).* **2018**, *360* (6396).

(16) Cullen, J. M.; Allwood, J. M.; Bambach, M. D. Mapping the Global Flow of Steel: From Steelmaking to End-Use Goods. *Environ. Sci. Technol.* **2012**, *46* (24), 13048–13055.

(17) NERC. Balancing and Frequency Control. **2011**, 53.

(18) PJM Interconnection. Regulation Market https://learn.pjm.com/three-priorities/buying-and-selling-energy/ancillary-services-market/regulation-market.aspx (accessed Mar 26, 2020).

(19) Teleke, S.; Baran, M. E.; Bhattacharya, S.; Huang, A. Q. Rule-Based Control of Battery Energy Storage for Dispatching Intermittent Renewable Sources. *Ieee Trans. Sustain. Energy* **2010**, *1* (3), 117–124.

(20) Swierczynski, M.; Stroe, D. I.; Stan, A. I.; Teodorescu, R.; Sauer, D. U. Selection and Performance-Degradation Modeling of LiMO2/Li4Ti5O12 and LiFePO4/C Battery Cells as Suitable Energy Storage Systems for Grid Integration with Wind Power Plants: An Example for the Primary Frequency Regulation Service. *IEEE Trans. Sustain. Energy* **2014**, *5* (1), 90–101.

(21) Stroe, D. I.; Knap, V.; Swierczynski, M.; Stroe, A. I.; Teodorescu, R. Operation of a Grid-Connected Lithium-Ion Battery Energy Storage System for Primary Frequency Regulation: A Battery Lifetime Perspective. *IEEE Trans. Ind. Appl.* **2017**, *53* (1), 430–438.

(22) Hiremath, M.; Derendorf, K.; Vogt, T. Comparative Life Cycle Assessment of Battery Storage Systems for Stationary Applications. *Environ. Sci. Technol.* **2015**, *49* (8), 4825–4833.

(23) Luo, X.; Wang, J.; Dooner, M.; Clarke, J. Overview of Current Development in Electrical Energy Storage Technologies and the Application Potential in Power System Operation. *Appl. Energy* **2015**, *137*, 511–536.

(24) Kim, T. H.; Park, J. S.; Chang, S. K.; Choi, S.; Ryu, J. H.; Song, H. K. The Current Move of Lithium Ion Batteries towards the next Phase. *Adv. Energy Mater.* **2012**, *2* (7), 860–872.

(25) Hart, D.; Sarkissian, A. Deployment of Grid-Scale Batteries in the United States. **2016**, 1–31.

(26) Swierczynski, M.; Stroe, D. I.; Stan, A. I.; Teodorescu, R.; Sauer, D. U. Selection and Performance-Degradation Modeling of Limo2/Li 4ti5o12 and Lifepo4/c Battery Cells as Suitable Energy Storage Systems for Grid Integration with Wind Power Plants: An Example for the Primary Frequency Regulation Service. *IEEE Trans. Sustain. Energy* **2014**, *5* (1), 90–101.

(27) Update, T. Wholesale Electricity Market Design Initiatives in the United States: Survey and Research Needs. **2016**.

(28) Wesseling, J. H.; Lechtenböhmer, S.; Åhman, M.; Nilsson, L. J.; Worrell, E.; Coenen, L. The Transition of Energy Intensive Processing Industries towards Deep Decarbonization: Characteristics and Implications for Future Research. *Renewable and Sustainable Energy Reviews*. 2017, pp 1303–1313.

(29) Fischedick, M.; Marzinkowski, J.; Winzer, P.; Weigel, M. Techno-Economic Evaluation of Innovative Steel Production Technologies. *J. Clean. Prod.* **2014**, *84* (1), 563–580.

(30) Wyns, T.; Axelson, M. *The Final Frontier – Decarbonising Europe's Energy Intensive Industries*; 2016.

(31) Haupt, M.; Vadenbo, C.; Zeltner, C.; Hellweg, S. Influence of Input-Scrap Quality on the Environmental Impact of Secondary Steel Production. **2016**, *2* (2), 391–401.

(32) He, H.; Guan, H.; Zhu, X.; Lee, H. Assessment on the Energy Flow and Carbon Emissions

of Integrated Steelmaking Plants. *Energy Reports* **2017**, *3*, 29–36.

(33) Cairns, C. J.; Chily, H. C. de; Smedt, E. de; Foye, C.; Hoffman, G.; Ichimiya, M.; Kim, H.-S.; Lehrman, A.; Olynyk, S.; Poblete, R. E.; Schmidt, G.; Swanepoel, P.; Tolonen, M.; Ginkel, R. M. Van; Vargas, S. *Energy Use in the Steel Industry*; International Iron and Steel Institute: Brussels, 1998.

(34) Worrell, E.; Price, L.; Neelis, M.; Galitsky, C.; Nan, Z. World Best Practice Energy Values for Selected Industrial Sectors. **2007**, No. February.

(35) Yin, X.; Chen, W. Trends and Development of Steel Demand in China: A Bottom-up Analysis. *Resour. Policy* **2013**, *38* (4), 407–415.

(36) Hatayama, H.; Daigo, I.; Matsuno, Y.; Adachi, Y. Outlook of the World Steel Cycle Based on the Stock and Flow Dynamics. *Environ. Sci. Technol.* **2010**, *44* (16), 6457–6463.

(37) Pauliuk, S.; Milford, R. L.; Mu, D. B.; Allwood, J. M. The Steel Scrap Age. *Environ. Sci. Technol.* **2013**, *47*, 3448–3454.

(38) Pauliuk, S.; Müller, D. B. The Role of In-Use Stocks in the Social Metabolism and in Climate Change Mitigation. *Glob. Environ. Chang.* **2014**, *24* (1), 132–142.

(39) International Trade Administration. *Steel Imports Report: United States*; 2018; Vol. June.

(40) World Steel Association. STEEL STATISTICAL YEARBOOK 2019 Concise Version Preface. *Worldsteel Assoc.* **2019**.

(41) Sami, S. S.; Meng Cheng; Jianzhong Wu. Modelling and Control of Multi-Type Grid-Scale Energy Storage for Power System Frequency Response. *2016 IEEE 8th Int. Power Electron. Motion Control Conf. (IPEMC-ECCE Asia)* **2016**, 269–273.

(42) Lew, D.; Brinkman, G.; Ibanez, E.; Hodge, B. M.; King, J. The Western Wind and Solar Integration Study Phase 2. *Contract* **2013**, *303*, 275–3000.

(43) Katzenstein, W.; Apt, J. Air Emissions Due to Wind and Solar Power. *Environ. Sci. Technol.* **2008**, *43* (2), 253–258.

(44) Swierczynski, M.; Stroe, D. I.; Stan, A. I.; Teodorescu, R. Primary Frequency Regulation with Li-Ion Battery Energy Storage System: A Case Study for Denmark. *ECCE Asia Downunder (ECCE Asia), 2013 IEEE* **2013**, 487–492.

(45) Matteson, S.; Williams, E. Learning Dependent Subsidies for Lithium-Ion Electric Vehicle Batteries. *Technol. Forecast. Soc. Change* **2015**, *92*, 322–331.

(46) Xu, B.; Shi, Y.; Kirschen, D. S.; Zhang, B. Optimal Battery Participation in Frequency

Regulation Markets. **2017**, No. November, 1–8.

(47) Richa, K.; Babbitt, C. W.; Nenadic, N. G.; Gaustad, G. Environmental Trade-Offs across Cascading Lithium-Ion Battery Life Cycles. *Int. J. Life Cycle Assess.* **2017**, *22* (1), 66–81.

(48) Neubauer, J.; Pesaran, A. The Ability of Battery Second Use Strategies to Impact Plug-in Electric Vehicle Prices and Serve Utility Energy Storage Applications. *J. Power Sources* **2011**, *196* (23), 10351–10358.

(49) Ambrose, H.; Gershenson, D.; Gershenson, A.; Kammen, D. Driving Rural Energy Access: A Second-Life Application for Electric-Vehicle Batteries. *Environ. Res. Lett.* **2014**, *9* (9), 094004.

(50) Sathre, R.; Scown, C. D.; Kavvada, O.; Hendrickson, T. P. Energy and Climate Effects of Second-Life Use of Electric Vehicle Batteries in California through 2050. *J. Power Sources* **2015**, *288*, 82–91.

(51) California Public Utilities Commission. *Order Instituting Rulemaking Pursuant to Assembly Bill 2514 to Consider the Adoption of Procurement Targets for Viable and Cost-Effective Energy Storage Systems*; 2013.

(52) Lin, Y.; Johnson, J. X.; Mathieu, J. L. Emissions Impacts of Using Energy Storage for Power System Reserves. *Appl. Energy* **2016**, *168*, 444–456.

(53) Hittinger, E. S.; Azevedo, I. M. L. Bulk Energy Storage Increases United States Electricity System Emissions. *Environ. Sci. Technol.* **2015**, *49* (5), 3203–3210.

(54) Fares, R. L.; Webber, M. E. The Impacts of Storing Solar Energy in the Home to Reduce Reliance on the Utility. *Nat. Energy* **2017**, *2* (2), 17001.

(55) Fisher, M. J.; Apt, J. Emissions and Economics of Behind-the-Meter Electricity Storage. *Environ. Sci. Technol.* **2017**, *51* (3), 1094–1101.

(56) Kerl, P. Y.; Zhang, W.; Moreno-Cruz, J. B.; Nenes, A.; Realff, M. J.; Russell, A. G.; Sokol, J.; Thomas, V. M. New Approach for Optimal Electricity Planning and Dispatching with Hourly Time-Scale Air Quality and Health Considerations. *Proc. Natl. Acad. Sci.* **2015**, *112* (35), 10884–10889.

(57) Gillenwater, M.; Breidenich, C. Internalizing Carbon Costs in Electricity Markets: Using Certificates in a Load-Based Emissions Trading Scheme. *Energy Policy* **2009**, *37* (1), 290–299.

(58) Arbabzadeh, M.; Johnson, J. X.; Keoleian, G. a; Rasmussen, P. G.; Thompson, L. T. Twelve

Principles for Green Energy Storage in Grid Applications. *Environ. Sci. Technol.* **2016**, *50* (2), 1046–1055.

(59) Sullivan, J. L.; Gaines, L. Status of Life Cycle Inventories for Batteries. *Energy Convers. Manag.* **2012**, *58*, 134–148.

(60) Dunn, J. B.; Gaines, L.; Sullivan, J.; Wang, M. Q. Impact of Recycling on Cradle-to-Gate Energy Consumption and Greenhouse Gas Emissions of Automotive Lithium-Ion Batteries. *Environ. Sci. Technol.* **2012**, *46* (22), 12704–12710.

(61) Notter, D. A.; Gauch, M.; Widmer, R.; Wäger, P.; Stamp, A.; Zah, R.; Althaus, H.-J. Contribution of Li-Ion Batteries to the Environmental Impact of Electric Vehicles. *Environ. Sci. Technol.* **2010**, *44* (17), 6550–6556.

(62) Ellingsen, L. A.-W.; Majeau-Bettez, G.; Singh, B.; Srivastava, A. K.; Valoen, L. O.; Stromman, A. H. Life Cycle Assessment of a Lithium-Ion Battery Vehicle Pack. *J. Ind. Ecol.* **2014**, *18* (1), 113–124.

(63) Majeau-Bettez, G.; Hawkins, T. R.; Strømman, A. H. Life Cycle Environmental Assessment of Lithium-Ion and Nickel Metal Hydride Batteries for Plug-In Hybrid and Battery Electric Vehicles. *Environ. Sci. Technol.* **2011**, *45* (10), 4548–4554.

(64) Kim, H. C.; Wallington, T. J.; Arsenault, R.; Bae, C.; Ahn, S.; Lee, J. Cradle-to-Gate Emissions from a Commercial Electric Vehicle Li-Ion Battery: A Comparative Analysis. *Environ. Sci. Technol.* **2016**, *50* (14), 7715–7722.

(65) Rydh, C. J. Environmental Assessment of Vanadium Redox and Lead-Acid Batteries for Stationary Energy Storage. *J. Power Sources* **1999**, *80* (1), 21–29.

(66) Rydh, C. J.; Sandén, B. A. Energy Analysis of Batteries in Photovoltaic Systems. Part I: Performance and Energy Requirements. *Energy Convers. Manag.* **2005**, *46* (11), 1957–1979.

(67) Denholm, P.; Kulcinski, G. L. Life Cycle Energy Requirements and Greenhouse Gas Emissions from Large Scale Energy Storage Systems. *Energy Convers. Manag.* **2004**, *45* (13), 2153–2172.

(68) Longo, S.; Antonucci, V.; Cellura, M.; Ferraro, M. Life Cycle Assessment of Storage Systems: The Case Study of a Sodium/Nickel Chloride Battery. *J. Clean. Prod.* **2014**, *85*, 337–346.

(69) Spanos, C.; Turney, D. E.; Fthenakis, V. Life-Cycle Analysis of Flow-Assisted Nickel Zinc-

, Manganese Dioxide-, and Valve-Regulated Lead-Acid Batteries Designed for Demand-Charge Reduction. *Renew. Sustain. Energy Rev.* **2015**, *43*, 478–494.

(70) Koj, J. C.; Stenzel, P.; Schreiber, A.; Hennings, W.; Zapp, P.; Wrede, G.; Hahndorf, I. Life Cycle Assessment of Primary Control Provision by Battery Storage Systems and Fossil Power Plants. *Energy Procedia* **2015**, *73*, 69–78.

(71) Oliveira, L.; Messagie, M.; Mertens, J.; Laget, H.; Coosemans, T.; Van Mierlo, J. Environmental Performance of Electricity Storage Systems for Grid Applications, a Life Cycle Approach. *Energy Convers. Manag.* **2015**, *101*, 326–335.

(72) Arbabzadeh, M.; Johnson, J. X.; De Kleine, R.; Keoleian, G. A. Vanadium Redox Flow Batteries to Reach Greenhouse Gas Emissions Targets in an Off-Grid Configuration. *Appl. Energy* **2015**, *146*, 397–408.

(73) Ryan, N. A.; Johnson, J. X.; Keoleian, G. A. Comparative Assessment of Models and Methods to Calculate Grid Electricity Emissions. *Environ. Sci. Technol.* **2016**, *50* (17).

(74) Sioshansi, R.; Denholm, P. Emissions Impacts and Benefits of Plug-In Hybrid Electric Vehicles and Vehicle-to-Grid Services. *Environ. Sci. Technol.* **2009**, *43* (4), 1199–1204.

(75) Lund, H.; Mathiesen, B. V.; Christensen, P.; Schmidt, J. H. Energy System Analysis of Marginal Electricity Supply in Consequential LCA. *Int. J. Life Cycle Assess.* **2010**, *15* (3), 260–271.

(76) Weisser, D. A Guide to Life-Cycle Greenhouse Gas (GHG) Emissions from Electric Supply Technologies. *Energy* **2007**, *32* (9), 1543–1559.

(77) Fehrenbacher, K. Tesla will use different batteries for its grid products. Here's why | Fortune.com http://fortune.com/2015/05/18/tesla-grid-batteries-chemistry/ (accessed May 28, 2017).

(78) Shahan, Z. Tesla's 2016 Deliveries = 76,230+ Vehicles, Production = 83,922 Vehicles | CleanTechnica https://cleantechnica.com/2017/01/03/teslas-2016-deliveries-production/ (accessed May 28, 2017).

(79) Dunn, J B; Gaines, L; Barnes, M; Sullivan, J; Wang, M. Material and Energy Flows in the Materials Production, Assembly, and End-of-Life Stages of the Automotive Lithium-Ion Battery Life Cycle. **2013**, *53* (9), 1689–1699.

(80) Dunn, J. B.; Gaines, L.; Kelly, J. C.; James, C.; Gallagher, K. G. The Significance of Li-Ion Batteries in Electric Vehicle Life-Cycle Energy and Emissions and Recycling's Role in Its

Reduction. *Energy Environ. Sci.* **2015**, *8* (1), 158–168.

(81) Nelson, P.; Gallagher, K.; Bloom, I.; Dees, D. *Modeling the Performance and Cost of Lithium-Ion Batteries for Electric-Drive Vehicles*; ANL-11/32; Argonne National Laboratory, 2011.

(82) Burnham, A.; Wang, M.; Wu, Y. *Development and Applications of GREET 2.7 — The Transportation Vehicle-Cycle Model*; 2006.

(83) Johnson, J. X.; Mcmillan, C. A.; Keoleian, G. A. Evaluation of Life Cycle Assessment Recycling Allocation Methods: The Case Study of Aluminum. *J. Ind. Ecol.* **2013**, *17* (5), 700–711.

(84) Mason, J. M.; Fthenakis, V. M.; Hansen, T.; Kim, H. C. Energy Pay-Back and Life Cycle CO 2 Emissions of the BOS in an Optimized 3 . 5 MW PV Installation. *Prog. Photovoltaics Res. Appl.* **2006**, *14*, 179–190.

(85) Zimmerman, R. D.; Murillo-Sánchez, C. E.; Thomas, R. J. MATPOWER: Steady-State Operations, Planning, and Analysis Tools for Power Systems Research and Education. *Power Syst. IEEE Trans.* **2011**, *26* (1), 12–19.

(86) Wang, J.; Purewal, J.; Liu, P.; Hicks-Garner, J.; Soukiazian, S.; Sherman, E.; Sorenson, A.; Vu, L.; Tataria, H.; Verbrugge, M. W. Degradation of Lithium Ion Batteries Employing Graphite Negatives and Nickel-Cobalt-Manganese Oxide + Spinel Manganese Oxide Positives: Part 1, Aging Mechanisms and Life Estimation. *J. Power Sources* **2014**, *272*, 1154–1161.

(87) Smith, K.; Shi, Y.; Santhanagopalan, S. Degradation Mechanisms and Lifetime Prediction for Lithium - Ion Batteries – A Control Perspective. *Am. Control Conf.* **2015**, No. July, 728–730.

(88) Jung, S.-K.; Gwon, H.; Hong, J.; Park, K.-Y.; Seo, D.-H.; Kim, H.; Hyun, J.; Yang, W.; Kang, K. Understanding the Degradation Mechanisms of LiNi0.5Co0.2Mn0.3O2 Cathode Material in Lithium Ion Batteries. *Adv. Energy Mater.* **2013**, *4*.

(89) Fortenbacher, P.; Mathieu, J. L.; Andersson, G. Modeling, Identification, and Optimal Control of Batteries for Power System Applications. In *2014 Power Systems Computation Conference*; 2014; pp 1–7.

(90) Cordoba-Arenas, A.; Onori, S.; Guezennec, Y.; Rizzoni, G. Capacity and Power Fade Cycle-Life Model for Plug-in Hybrid Electric Vehicle Lithium-Ion Battery Cells Containing

Blended Spinel and Layered-Oxide Positive Electrodes. *J. Power Sources* **2015**, *278*, 473–483.

(91) Xu, B.; Oudalov, A.; Ulbig, A.; Andersson, G.; Kirschen, D. Modeling of Lithium-Ion Battery Degradation for Cell Life Assessment. *IEEE Trans. Smart Grid* **2016**, *9* (2), 1131–1140.

(92) Fuller, Thomas F. Doyle, Marc. Newman, J. Simulation and Optimization of the Dual Lithium Ion Insertion Cell. *J. Electrochem. Soc.* **1994**, *141* (1), 1.

(93) PJM. Ancillary Services http://www.pjm.com/markets-and-operations/ancillary-services.aspx (accessed Nov 1, 2016).

(94) Argonne National Laboratory. GREET1 Model. UChicago Argonne, LLC 2012.

(95) Ellingsen, L. A. W.; Hung, C. R.; Strømman, A. H. Identifying Key Assumptions and Differences in Life Cycle Assessment Studies of Lithium-Ion Traction Batteries with Focus on Greenhouse Gas Emissions. *Transp. Res. Part D Transp. Environ.* **2017**, *55*, 82–90.

(96) U.S. Energy Information Administration. Table 1.2. Summary Statistics for the United States, 2004 - 2014 http://www.eia.gov/electricity/annual/html/epa_01_02.html (accessed Oct 17, 2016).

(97) U.S. Energy Information Administration. Electricity in the United States is produced with diverse energy sources and technologies https://www.eia.gov/energyexplained/index.php?page=electricity_in_the_united_states (accessed Mar 25, 2019).

(98) Wesley, C.; Frazier, W.; Donohoo-Vallett, P.; Mai, T.; Das, P. *2017 Standard Scenarios Report : A U. S. Electricity Sector Outlook*; 2018.

(99) Kirby, B.; Milligan, M.; Wan, Y. Cost-Causation-Based Tariffs for Wind Ancillary Service Impacts. *Proc. Wind.* **2006**, 1–26.

(100) Zhao, J.; Zheng, T.; Litvinov, E. A Unified Framework for Defining and Measuring Flexibility in Power System. *IEEE Trans. Power Syst.* **2016**, *31* (1), 339–347.

(101) Hodge, B. M.; Brancucci Martinez-Anido, C.; Wang, Q.; Chartan, E.; Florita, A.; Kiviluoma, J. The Combined Value of Wind and Solar Power Forecasting Improvements and Electricity Storage. *Applied Energy*. 2018, pp 1–15.

(102) U.S. Department of Energy. *Wind Vision: A New Era for Wind Power in the United States*; 2015.

(103) Deane, J. P.; Drayton, G.; O Gallachoir, B. P. The Impact of Sub-Hourly Modelling in Power Systems with Significant Levels of Renewable Generation. *Appl. Energy* **2014**, *113*, 152–158.

(104) Abujarad, S. Y.; Mustafa, M. W.; Jamian, J. J. Recent Approaches of Unit Commitment in the Presence of Intermittent Renewable Energy Resources: A Review. *Renew. Sustain. Energy Rev.* **2017**, *70* (October 2015), 215–223.

(105) Cochran, J.; Miller, M.; Zinaman, O.; Milligan, M.; Arent, D.; Palmintier, B.; Malley, M. O.; Mueller, S.; Lannoye, E.; Epri, A. T.; Kujala, B.; Power, N.; Sommer, M.; Holttinen, H.; Kiviluoma, J.; Soonee, S. K. Flexibility in 21st Century Power Systems. *21st Century Power Partnersh.* **2014**, *May*, 14.

(106) Hsieh, E.; Anderson, R. Grid Flexibility: The Quiet Revolution. *Electr. J.* **2017**, *30* (2), 1–8.

(107) Cui, M.; Zhang, J.; Feng, C.; Florita, A. R.; Sun, Y.; Hodge, B. M. Characterizing and Analyzing Ramping Events in Wind Power, Solar Power, Load, and Netload. *Renew. Energy* **2017**, *111*, 227–244.

(108) Milligan, M.; Ela, E.; Hodge, B. M.; Kirby, B.; Lew, D.; Clark, C.; DeCesaro, J.; Lynn, K. Integration of Variable Generation, Cost-Causation, and Integration Costs. *Electr. J.* **2011**, *24* (9), 51–63.

(109) Wang, Q.; Hodge, B. M. Enhancing Power System Operational Flexibility with Flexible Ramping Products: A Review. *IEEE Trans. Ind. Informatics* **2017**, *13* (4), 1652–1664.

(110) Denholm, P.; Clark, K.; O'Connell, M. *On the Path to SunShot: Emerging Issues and Challenges in Integrating Solar with the Distribution System*; 2016.

(111) Ela, E.; Kirby, B.; Lannoye, E.; Milligan, M.; Flynn, D.; Zavadil, B.; O'Malley, M. Evolution of Operating Reserve Determination in Wind Power Integration Studies. *IEEE PES Gen. Meet. PES 2010* **2010**, 1–8.

(112) Huang, B.; Member, I. S.; Krishnan, V.; Member, I.; Hodge, B.; Member, I. S. Analyzing the Impacts of Variable Renewable Resources on California Net-Load Ramp Events. **2018**, No. August, 1–5.

(113) Kamath, C. Understanding Wind Ramp Events through Analysis of Historical Data. *2010 IEEE PES Transm. Distrib. Conf. Expo. Smart Solut. a Chang. World* **2010**, 1–6.

(114) Alizadeh, M. I.; Parsa Moghaddam, M.; Amjady, N.; Siano, P.; Sheikh-El-Eslami, M. K.

Flexibility in Future Power Systems with High Renewable Penetration: A Review. *Renew. Sustain. Energy Rev.* **2016**, *57*, 1186–1193.

(115) Stoll, B.; Jain, R.; Martinez-Anido, C. B.; Ibanez, E.; Florita, A.; Hodge, B.-M. *Chapter 5: Reserve Estimation in Renewable Integration Studies*; 2017.

(116) Sevlian, R.; Rajagopal, R. Wind Power Ramps: Detection and Statistics. *IEEE Power Energy Soc. Gen. Meet.* **2012**, 1–8.

(117) Cui, M.; Zhang, J. Estimating Ramping Requirements with Solar-Friendly Flexible Ramping Product in Multi-Timescale Power System Operations. *Appl. Energy* **2018**, *225* (November 2017), 27–41.

(118) Chakraborty, P.; Baeyens, E.; Khargonekar, P. P. Cost Causation Based Allocations of Costs for Market Integration of Renewable Energy. *IEEE Trans. Power Syst.* **2018**, *33* (1), 70–83.

(119) Mays, J. Cost Allocation and Net Load Variability. *IEEE Trans. Power Syst.* **2018**, *33* (2), 2030–2039.

(120) U.S. Energy Information Adminstration. Combined wind and solar made up at least 20% of electric generation in 10 states in 2017 https://www.eia.gov/todayinenergy/detail.php?id=37233 (accessed Mar 3, 2020).

(121) Brinkman, G.; Jorgenson, J.; Ehlen, A.; Caldwell, J. H.; Brinkman, G.; Jorgenson, J.; Ehlen, A.; Caldwell, J. H. Low Carbon Grid Study: Analysis of a 50% Emission Reduction in California. **2016**, No. January.

(122) WECC. Release Notes for WECC 2024 Common Case, Version 1.1. **2014**.

(123) Martinez-anido, C. B.; Botor, B.; Florita, A. R.; Draxl, C.; Lu, S.; Hamann, H. F.; Hodge, B. The Value of Day-Ahead Solar Power Forecasting Improvement. *Sol. Energy* **2016**, *129*, 192–203.

(124) Arbabzadeh, M.; Sioshansi, R.; Johnson, J. X.; Keoleian, G. A. The Role of Energy Storage in Deep Decarbonization of Electricity Production. *Nat. Commun.* **2019**, *10* (1).

(125) GE Energy. *Western Wind and Solar Integration Study*; Schenectady, NY, 2010.

(126) Lew, D.; Brinkman, G.; Ibanex, E.; Florita, A.; Heaney, M.; Hodge, B. M.; Hummon, M.; Stark, G.; King, J.; Lefton, S. A.; Kumber, N.; Agan, D.; Jordan, G.; Venkataraman, S. *The Western Wind and Solar Integration Study Phase 2*; 2013.

(127) NREL. Eastern Renewable Generation Integration Study. **2014**, No. August 2016.

(128) CAISO. *Business Practice Manual for Market Operations*; 2020.

(129) Hastie, T.; Tibshrani, R.; Friedman, J. *The Elements of Statistical Learning: Data Mining, Inference, and Prediction*, Second Edi.; Springer, 2017.

(130) Rockström, J., Gaffney, O., Rogelj, J., Meinshausen, M., Nakicenovic, N., & Schellnhuber, H. J. A Roadmap for Rapid Decarbonization. *Science (80-.).* **2017**, *355* (6331), 1269–1271.

(131) Allwood, J. M.; Gutowski, T. G.; Serrenho, A. C.; Skelton, A. C. H.; Worrell, E. Industry 1.61803 : The Transition to an Industry with Reduced Material Demand Fit for a Low Carbon Future. *Philos. Trans. A* **2017**.

(132) Supekar, S. D.; Skerlos, S. J. Analysis of Costs and Time Frame for Reducing CO2Emissions by 70% in the U.S. Auto and Energy Sectors by 2050. *Environ. Sci. Technol.* **2017**, *51* (19), 10932–10942.

(133) World Steel Association. Steel Statistical Yearbook 2017. *World Steel Assoc.* **2017**, 1–128.

(134) Toi, A.; Sato, J. Evaluation of Material Recycling System with Logit Model. *J. IRON STEEL Inst. JAPAN* **1998**, *84* (7), 534–539.

(135) Pauliuk, S.; Wang, T.; Müller, D. B. Moving toward the Circular Economy: The Role of Stocks in the Chinese Steel Cycle. *Environ. Sci. Technol.* **2012**, *46* (1), 148–154.

(136) Vogl, V.; Åhman, M.; Nilsson, L. J. Assessment of Hydrogen Direct Reduction for Fossil-Free Steelmaking. *J. Clean. Prod.* **2018**, *203*, 736–745.

(137) Milford, R. L.; Pauliuk, S.; Allwood, J. M.; Müller, D. B. The Roles of Energy and Material Efficiency in Meeting Steel Industry CO2 Targets. *Environ. Sci. Technol.* **2013**, *47* (7), 3455–3462.

(138) Yellishetty, M.; Mudd, G. M.; Ranjith, P. G.; Tharumarajah, A. Environmental Life-Cycle Comparisons of Steel Production and Recycling: Sustainability Issues, Problems and Prospects. *Environ. Sci. Policy* **2011**, *14* (6), 650–663.

(139) Pardo, N.; Moya, J. A. Prospective Scenarios on Energy Efficiency and CO2emissions in the European Iron & Steel Industry. *Energy* **2013**, *54*, 113–128.

(140) Van Ruijven, B. J.; Van Vuuren, D. P.; Boskaljon, W.; Neelis, M. L.; Saygin, D.; Patel, M. K. Long-Term Model-Based Projections of Energy Use and CO2 Emissions from the Global Steel and Cement Industries. *Resour. Conserv. Recycl.* **2016**, *112*, 15–36.

(141) ECOFYS Netherlands; Fraunhofer ISI. Developing Benchmarking Criteria for CO2 Emissions. **2009**, No. February.

(142) Yellishetty, M.; Mudd, G.; Mason, L.; Mohr, S.; Prior, T.; Giurco, D.; Yellishetty, M.; Mudd, G. M. *Iron Resources and Production: Technology, Sustainability and Future Prospects*; 2012; Vol. 1.10.

(143) Neelis, M. L.; Patel, M. K. *Long-Term Production, Energy Use and CO2 Emission Scenarios for the Worldwide Iron and Steel Industry - Report NWS-E-2006-180*; 2006.

(144) Zhang, Q.; Xu, J.; Wang, Y.; Hasanbeigi, A.; Zhang, W.; Lu, H.; Arens, M. Comprehensive Assessment of Energy Conservation and CO2 Emissions Mitigation in China's Iron and Steel Industry Based on Dynamic Material Flows. *Appl. Energy* **2018**, *209* (October 2017), 251–265.

(145) Zhang, Q.; Hasanbeigi, A.; Price, L.; Lu, H.; Arens, M.; Lawrence, E. O. *A Bottom-up Energy Efficiency Improvement Roadmap for China's Iron and Steel Industry up to 2050*; 2016.

(146) Serrenho, A. C.; Mourão, Z. S.; Norman, J.; Cullen, J. M.; Allwood, J. M. The Influence of UK Emissions Reduction Targets on the Emissions of the Global Steel Industry. *Resour. Conserv. Recycl.* **2016**, *107*, 174–184.

(147) Morfeldt, J.; Nijs, W.; Silveira, S. The Impact of Climate Targets on Future Steel Production - An Analysis Based on a Global Energy System Model. *J. Clean. Prod.* **2015**, *103*, 469–482.

(148) Cooper, D. R.; Ryan, N. A.; Syndergaard, K.; Zhu, Y. The Potential for Material Circularity and Independence in the U.S. Steel Sector. *J. Ind. Ecol.* **2020**, No. 2007, 1–15.

(149) Wang, M. Vehicle Cycle Model: GREET 2. Argonne National Laboratory 2019.

(150) Allwood, J. M.; Kong, H.; Pole, N. *Sustainable Materials With Both Eyes Open*; 2012.

(151) Hasanbeigi, A.; Arens, M.; Price, L. Alternative Emerging Ironmaking Technologies for Energy-Efficiency and Carbon Dioxide Emissions Reduction: A Technical Review. *Renew. Sustain. Energy Rev.* **2014**, *33*, 645–658.

(152) Junjie, Y. Progress and Future of Breakthrough Low-Carbon Steelmaking Technology (ULCOS) of EU. *Int. J. Miner. Process. Extr. Metall.* **2018**, *3* (2), 15–22.

(153) Lawrence Berkeley National Laboratory. *The State – Of-the-Art Clean Technologies (SOACT) for Steelmaking Handbook*; 2010.

(154) Quader, M. A.; Ahmed, S.; Arif, R.; Ghazilla, R.; Ahmed, S.; Dahari, M. A Comprehensive Review on Energy Efficient CO2 Breakthrough Technologies for Sustainable Green Iron

and Steel Manufacturing. *Renew. Sustain. Energy Rev.* **2015**, *50*, 594–614.

(155) Pretorius, E. Phone Interview with Eugene Pretorius of Nucor Conducted by the Authors on April 27, 2018.

(156) Lindemulder, K. Phone Interview with Keith Lindemulder of Nucor Conducted by the Authors on March 26, 2018.

(157) U.S. Steel. Phone Interview with U.S. Steel Conducted by the Authors on January 31, 2020.

(158) Kirschen, M.; Risonarta, V.; Pfeifer, H. Energy Efficiency and the Influence of Gas Burners to the Energy Related Carbon Dioxide Emissions of Electric Arc Furnaces in Steel Industry. *Energy* **2009**, *34* (9), 1065–1072.

(159) Sohn, H. Y.; Mohassab, Y. Novel Flash Ironmaking Technology. *Mech. Chem. Mater. Eng.* **2015**, 336.

(160) The European Steel Association. A Steel Roadmap for A Low Carbon Europe. **2013**.

(161) Cavaliere, P. *Clean Ironmaking and Steelmaking Processes*; 2019.

(162) U.S. Energy Information Administration. *Monthly Energy Review, Table 7.2a*; 2018.

(163) U.S. Energy Information Administration. *International Energy Outlook 2016*; 2016; Vol. 0484(2016).

(164) International Energy Agency. *CO2 Emissions from Fuel Combustion 2019*; 2019.

(165) United States Geological Survey. *USGS Minerals Yearbook 2017: Advanced Data Release of the 2017 Annual Tables*; 2020.

(166) Midrex. *2018 World Direct Reduction Statistics*; 2019.

(167) Milford, R. L.; Pauliuk, S.; Allwood, J. M.; Müller, D. B. The Roles of Energy and Material Efficiency in Meeting Steel Industry CO2 Targets. *Environ. Sci. Technol.* **2013**, *47* (7), 3455–3462.

(168) Müller, D. B. Stock Dynamics for Forecasting Material Flows—Case Study for Housing in The Netherlands. *Ecol. Econ.* **2006**, *59* (February 2006), 142–156.

(169) Müller, E.; Hilty, L. M.; Widmer, R.; Schluep, M.; Faulstich, M. Modeling Metal Stocks and Flows: A Review of Dynamic Material Flow Analysis Methods. *Environ. Sci. Technol.* **2014**, *48* (4), 2102–2113.

(170) Pauliuk, S.; Wang, T. Steel All Over the World : Estimating In-Use Stocks of Iron for 200 Countries Supplementary Information. 1–51.

(171) United States Census Bureau. 2017 National Population Projections

https://www.census.gov/data/tables/2017/demo/popproj/2017-summary-tables.html (accessed Oct 15, 2019).

(172) Ortman, J. M.; Guarneri, C. E. United States Population Projections: 2000 to 2050. *United States Census Bur.* **2009**, 1–19.

(173) Pauliuk, S.; Wang, T.; Müller, D. B. Steel All over the World: Estimating in-Use Stocks of Iron for 200 Countries. *Resour. Conserv. Recycl.* **2013**, *71*, 22–30.

(174) Elshkaki, A.; Graedel, T. E.; Ciacci, L.; Reck, B. K. Resource Demand Scenarios for the Major Metals. *Environ. Sci. Technol.* **2018**, *52* (5), 2491–2497.

(175) Protection, U. S. C. and B. Section 232 Tariffs on Aluminum and Steel.

(176) Ashby, M. *Materials and the Environment: Eco-Informed Material Choice: Second Edition*; 2012.

(177) U.S. Environmental Protection Agency. Iron and Steel Foundries: National Emissions Standards for Hazardous Air Pollutants (NESHAP) https://www.epa.gov/stationary-sources-air-pollution/iron-and-steel-foundries-national-emissions-standards-hazardous-air (accessed Jun 17, 2020).

(178) Carruth, M. A.; Allwood, J. M.; Moynihan, M. C. The Technical Potential for Reducing Metal Requirements through Lightweight Product Design. *Resour. Conserv. Recycl.* **2011**, *57*, 48–60.

(179) Moynihan, M. C.; Allwood, J. M. Utilization of Structural Steel in Buildings. *Proc. R. Soc. A Math. Phys. Eng. Sci.* **2014**, *470* (2168).

(180) U.S. Green Building Council. LEED rating system https://www.usgbc.org/leed (accessed Jun 17, 2020).

(181) United States Geological Survey. Mineral Commodities Summary: Iron and Steel. **2019**.

(182) U.S. Steel. United States Steel Corporation Makes Significant Operational Adjustments to Advance “Best of Both” Strategy https://www.ussteel.com/newsroom/united-states-steel-corporation-makes-significant-operational-adjustments-advance-best-both (accessed Jun 17, 2020).

(183) Orange, R. Waste Not Want Not: Sweden to Give Tax Breaks for Repairs. *The Guardian*. Malmö September 19, 2016.

(184) Pellow, M. A.; Ambrose, H.; Mulvaney, D.; Betita, R.; Shaw, S. Research Gaps in Environmental Life Cycle Assessments of Lithium Ion Batteries for Grid-Scale Stationary

Energy Storage Systems: End-of-Life Options and Other Issues. *Sustain. Mater. Technol.* **2020**, *23* (X), e00120.

(185) Olsen, D. J.; Kirschen, D. S. Profitable Emissions-Reducing Energy Storage. **2020**, *35* (2), 1509–1519.

(186) Ziegler, M. S.; Mueller, J. M.; Pereira, G. D.; Song, J.; Ferrara, M.; Chiang, Y. M.; Trancik, J. E. Storage Requirements and Costs of Shaping Renewable Energy Toward Grid Decarbonization. *Joule* **2019**, *3* (9), 2134–2153.

(187) Mongird, K.; Fotedar, V.; Viswanathan, V.; Koritarov, V.; Balducci, P.; Hadjerioua, B.; Alam, J. Energy Storage Technology and Cost Characterization Report. *Pacific Northwest Natl. Lab.* **2019**, No. July, 1–120.

(188) Federal Energy Regulatory Commission. *Electric Storage Participation in Markets Operated by Regional Transmission Organizations and Independent System Operators. Order No. 841*; 2018.

(189) U.S. Energy Information Agency. U.S. utility-scale battery storage power capacity to grow substantially by 2023 https://www.eia.gov/todayinenergy/detail.php?id=40072#:~:text=Operating utility-scale battery storage,exceed 2%2C500 MW by 2023. (accessed Jun 3, 2020).

(190) U.S. Energy Information Administration. Short-Term Energy Outlook http://www.eia.gov/outlooks/steo/tables/pdf/2tab.pdf (accessed Oct 17, 2016).

(191) Kumar, N.; Peter, B.; Lefton, S.; Agan Dimo. *Power Plant Cycling Costs*; Golden, CO, 2012.

(192) Hummon, M.; Denholm, P.; Jorgenson, J.; Palchak, D.; Kirby, B. *Fundamental Drivers of the Cost and Price of Operating Reserves*; 2013.

(193) National Renewable Energy Laboratory. NSRDB Viewer from National Solar Radiation Database (NSRDB) http://nsrdb.nrel.gov/ (accessed Jul 11, 2016).

(194) National Renewable Energy Laboratory. Wind Integration National Dataset (WIND) Toolkit http://www.nrel.gov/electricity/transmission/wind_toolkit.html (accessed Jul 11, 2016).

(195) National Renewable Energy Laboratory. System Advisor Model (SAM) https://sam.nrel.gov/ (accessed Oct 24, 2016).

(196) Argonne National Laboratory. BatPaC: A Lithium-Ion Battery Performance and Cost

Model for Electric-Drive Vehicles http://www.cse.anl.gov/batpac/.

(197) Graedel, T. E.; Et.Al. *UNEP Recycling Rates of Metals - A Status Report, a Report of the Working Group on the Global Metal Flows to the International Resource Panel*; 2011.

(198) USGS. *Mineral Commodities Summaries*; 2016.

(199) U.S. Environmental Protection Agency. Air Markets Program Data https://ampd.epa.gov/ampd/ (accessed Nov 9, 2016).

(200) US Environmental Protection Agency. Bituminous and Subbituminous Coal Combustion. *Compil. Air Pollut. Emiss. Factors* **1995**, 52.

(201) U.S. Energy Information Administration. Carbon Dioxide Emissions Coefficients https://www.eia.gov/tools/faqs/faq.cfm?id=73&t=11 (accessed Oct 17, 2016).

(202) U.S. Environmental Protection Agency. Emission Factors for Greenhouse Gas Inventories. **2014**, No. April, 1–5.

(203) U.S. Environmental Protection Agency. *Tool for the Reduction and Assessment of Chemical and Other Environmental Impacts 2.1*; 2013.

(204) Intergovernmental Panel on Climate Change. *IPCC Fourth Assessment Report: Climate Change 2007*; 2007.

(205) U.S. Census Bureau. Population Clock https://www.census.gov/ (accessed Mar 9, 2018).

(206) U.S. Environmental Protection Agency. *DRAFT Inventory of U.S. Greenhouse Gas Emissions and Sinks: 1990-2016*; 2018.

(207) U.S. Environmental Protection Agency. Air Pollutant Emissions Trends Data https://www.epa.gov/air-emissions-inventories/air-pollutant-emissions-trends-data (accessed Mar 10, 2018).

(208) U.S. Energy Information Administration. U.S. Energy Facts Explained https://www.eia.gov/energyexplained/?page=us_energy_home (accessed Mar 10, 2018).

(209) California ISO. *California ISO Non-Generator Resource Regulation Energy Management Project Implementation Plan - Version 2.1*; 2011.

(210) Adam Nieslony. Rainflow Counting Algorithm https://www.mathworks.com/matlabcentral/fileexchange/3026-rainflow-counting-algorithm (accessed Jun 13, 2018).

(211) Palchak, D.; Denholm, P. Impact of Generator Flexibility on Electric System Costs and Integration of Renewable Energy. **2014**, No. July, 27.

(212) National Renewable Energy Laboratory. Interconnections Seams Study https://www.nrel.gov/analysis/seams.html (accessed Oct 23, 2017).
(213) National Renewable Energy Laboratory. NSRDB Viewer from National Solar Radiation Database (NSRDB) http://nsrdb.nrel.gov/ (accessed Mar 31, 2020).
(214) National Renewable Energy Laboratory. System Advisory Model (SAM) https://sam.nrel.gov/ (accessed Mar 31, 2020).
(215) National Renewable Energy Laboratory. Wind Integration National Dataset Toolkit https://www.nrel.gov/grid/wind-toolkit.html (accessed Mar 31, 2020).
(216) Ibanez, E.; Brinkman, G.; Hummon, M.; Lew, D. A Solar Reserve Methodology for Renewable Energy Integration Studies Based on Sub-Hourly Variability Analysis; 2012.
(217) American Iron and Steel Institute. *Annual Statistical Report*.
(218) United States Geological Survey. Mineral Commodity Summary. **2017**.
(219) Kelly, T. D.; Matos, G. R. *Iron and Steel Statistics*; 2017.
(220) Muller, D. B.; Wang, T.; Duval, B.; Graedel, T. E. Exploring the Engine of Anthropogenic Iron Cycles. *Proc. Natl. Acad. Sci.* **2006**, *103* (44), 16111–16116.
(221) United Nations. UN Comtrade Database https://comtrade.un.org/data/ (accessed Jul 27, 2018).
(222) Wang, T.; Müller, D. B.; Graedel, T. E. Forging the Anthropogenic Iron Cycle. *Environ. Sci. Technol.* **2007**, *41* (14), 5120–5129.
(223) Gerst, M. D.; T.E., G. Critical Review In-Use Stocks of Metals: Status and Implications. *Environ. Sci. Technol.* **2008**, *42* (19), 7038–7045.
(224) American Iron and Steel Institute. *Profile 2017*; 2017.
(225) American Iron and Steel Institute. *Profile 2015*; 2015.
(226) American Iron and Steel Institute. *Profile 2018*; 2018.
(227) American Iron and Steel Institute. *Profile 2016*; 2016.
(228) Müller, D. B.; Wang, T.; Duval, B. Patterns of Iron Use in Societal Evolution. *Environ. Sci. Technol.* **2011**, *45* (1), 182–188.
(229) United States Census Bureau. National Population Totals and Components of Change https://www.census.gov/data/tables/2017/demo/popest/nation-total.html (accessed Jul 16, 2018).
(230) Ayres, R. U. Turning Point: The End of Exponential Growth? *Technol. Forecast. Soc.*

Change **2006**, *73* (9), 1188–1203.

(231) Kelly, T. D.; Matos, G. R. *Iron and Steel Statistics U.S. Geological Suvey*; 2017.

(232) World Steel Association. *Steel Statistical Yearbook 2012*; 2012.

(233) National Renewable Energy Laboratory. *H2@Scale Workshop Report*; 2016.

(234) U.S. Department of Energy. *A Novel Flash Ironmaking Process Technology Trans Ition*; 2019.

(235) Energetics, I. *Steel Industry Technology Roadmap Barriers and Pathways for Yield Improvements*; 2003.

(236) Oda, J.; Akimoto, K.; Sano, F.; Homma, T. Diffusion of CCS and Energy Efficient Technologies in Power and Iron & Steel Sectors. *Energy Procedia* **2009**, *1* (1), 155–161.

(237) Midrex. *2016 World Direct Reduction Report*; 2016.

(238) Midrex. *2014 World Direct Reduction Report*; 2014.

(239) Midrex. *2012 World Direct Reduction Report*; 2012.

(240) International Energy Agency. *CO2 Emissions from Fuel Combustion 2016*; 2016.

(241) International Energy Agency. *CO2 Emissions from Fuel Combustion 2018*; 2018.

(242) United States Geological Survey. *2012 Minerals Yearbook: Iron and Steel*; 2016.